In vivo analysis and therapeutic targeting of calcium-mediated axonal degeneration in a multiple sclerosis model

Daniela Beckmann

December 10th, 2024

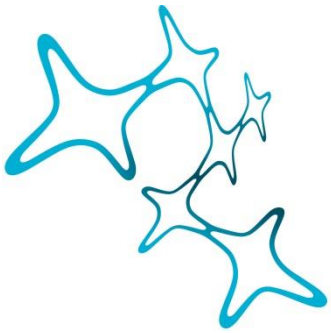

Graduate School of Systemic Neurosciences

LMU Munich

Dissertation at the
Graduate School of Systemic Neurosciences
Ludwig-Maximilians-Universität München

Supervisor
Prof. Dr. Martin Kerschensteiner
Institute of Clinical Neuroimmunology
University Hospital and Biomedical Center of the
Ludwig-Maximilians-Universität München

First Reviewer: Prof. Dr. Martin Kerschensteiner
Second Reviewer: Dr. Leanne Godinho
External Reviewer: Dr. Ivana Nikić-Spiegel

Date of Submission: 10.12.2024
Date of Defense: 15.04.2025

“ This is not entirely uninteresting! ”

Martin Kerschensteiner

Table of contents

List of abbreviations

AAPH	2,2'-azobis (2-amidinopropane)
AAV	adeno-associated virus
aCSF	artificial cerebrospinal fluid
ADPR	adenosine diphosphate ribose
AMPA	α-amino-3-hydroxy-5-methyl-4-isoxazolepropionic acid
AMPAR	AMPA receptor
ANOVA	analysis of variance
AP	action potential
APP	amyloid precursor protein
ASIC	acid-sensing ion channel
ATP	adenosine triphosphate
bp	base pairs
CaBP	calcium-binding protein
cADPR	cyclic adenosine diphosphate ribose
CaMK	calmodulin-dependent kinase
CB	calbindin-D28k
CD	cluster of differentiation
cDNA	complementary deoxyribonucleic acid
CerTN-L15	calcium sensor
CFP	cyan fluorescent protein
CIS	clinically isolated syndrome
CNS	central nervous system
CR	calretinin
CSF	cerebrospinal fluid
DMEM	Dulbecco’s Modified Eagle Medium
DMSO	dimethyl sulfoxide
DMT	disease-modifying therapy
DNA	deoxyribonucleic acid
EAE	experimental autoimmune encephalomyelitis
EBV	Epstein-Barr virus
EDSS	Expanded Disability Status Scale
ER	endoplasmic reticulum

FAD	focal axonal degeneration
FBS	fetal bovine serum
FOV	field of view
FRET	Förster resonance energy transfer
GFAP	glial fibrillary acidic protein
GFP	green fluorescent protein
GM	grey matter
GSH	glutathione
HBSS	Hanks' Balanced Salt Solution
HLA	human leukocyte antigen
i.p.	intraperitoneal
i.v.	intravenous
IMM	inner mitochondrial membrane
IP_3	inositol-1,4,5-trisphosphate
IP_3R	inositol-1,4,5-trisphosphate receptor
ITR	inverted terminal repeat
K_D	dissociation constant
KO	knockout
KOFP	Kusabira Orange fluorescent protein
LLO	lysteriolysin O
MBP	myelin basic protein
MCU	mitochondrial calcium uniporter
MD	membrane damage
MDG1	membrane damage green 1
MDG2	membrane damage green 2
MFI	mean fluorescence intensity
MOG	myelin oligodendrocyte glycoprotein
mPTP	mitochondrial permeability transition pore
MRI	magnetic resonance imaging
mRNA	messenger ribonucleic acid
MS	multiple sclerosis
NA	numerical aperture
NAA	N-acetyl aspartate

NAD	nicotinamide adenine dinucleotide
NAGM	normal appearing grey matter
NAWM	normal appearing white matter
NCLX	mitochondrial sodium calcium exchanger
NCX	sodium calcium exchanger
NfL	neurofilament light chain
NMAT2	nicotinamide mononucleotide adenylyltransferase 2
NMDA	N-methyl-D-aspartic acid
NMDAR	NMDA receptor
OCT	optical coherence tomography
OMM	outer mitochondrial membrane
OPC	oligodendrocyte precursor cell
pA	poly-adenylation sequence
PBS	phosphate buffered saline
PCR	polymerase chain reaction
PEI	polyethylenimine
PGC-1α	peroxisome proliferator-activated receptor γ coactivator 1α
PI	propidium iodide
PIRA	progression independent of relapse activity
PLC	phospholipase C
PLP	proteolipid protein
PMCA	plasma membrane calcium ATPase
PML	progressive multifocal leukoencephalopathy
PMS	progressive multiple sclerosis
PPMS	primary progressive multiple sclerosis
PV	parvalbumin α
qPCR	quantitative polymerase chain reaction
rAAV	recombinant adeno-associated virus
RCD	regulated cell death
RNFL	retinal nerve fibre layer
RNS	reactive nitrogen species
ROI	region of interest
ROS	reactive oxygen species

RRMS	relapsing-remitting multiple sclerosis
RyR	ryanodine receptor
S1P	sphingosine-1-phosphate
Sarm1	sterile-α and Toll/interleukin 1 receptor motif containing protein 1
SERCA	sarco-/endoplasmic reticulum calcium ATPase
SG	ShadowG
SPMS	secondary progressive multiple sclerosis
SR	sarcoplasmic reticulum
T2A	thosea asigna virus 2A (self-cleaving peptide)
TCA	tricarboxylic acid
TCEP	tris(2-carboxyethyl)phosphine
Thy1	thymocyte differentiation antigen 1
TNF-α	tumour necrosis factor α
TRP	transient receptor potential
VB	VectorBuilder
VDAC	voltage-dependent anion channel
vg	viral genomes
Wlds	Wallerian degeneration slow (mouse mutant)
WM	white matter
WPRE	woodchuck hepatitis virus posttranscriptional regulatory element
YFP	yellow fluorescent protein

List of figures

List of tables

Abstract

Multiple sclerosis (MS) is a chronic inflammatory, demyelinating and degenerative disease of the central nervous system (CNS), characterised by the formation of focal inflammatory lesions and additional damage due to smouldering low-grade CNS inflammation. The clinical manifestation of relapsing-remitting MS – the rapid appearance of new neurological symptoms – is likely caused by acute inflammation and demyelination. The extent of long-term, irreversible disability, however, is determined by neurodegeneration, especially loss of axons. This degeneration is observable from the earliest stages of the disease and causes progressive disability once a critical compensable threshold is passed. Currently available immunomodulatory treatments for MS suppress relapses but cannot completely halt neuroaxonal degeneration. The development of primary neuroprotective treatments is therefore an important unmet clinical need.

In vivo imaging in experimental autoimmune encephalomyelitis, an animal model of MS, is a powerful tool to study the pathogenesis of axonal degeneration. Such experiments have shown that initial axonal damage is still reversible and that the likelihood of fragmentation of damaged axons is determined by intra-axonal calcium, which enters through "nanoruptures" in the plasma membrane. As some axons can re-establish calcium homeostasis spontaneously, we hypothesised that therapeutic interventions, which support axons in regaining calcium homeostasis will shift the balance in favour of recovery and reduce axonal loss. The aim of this thesis was therefore to explore calcium modulation for axoprotective therapy by (1) exploiting endogenous calcium homeostatic pathways and (2) developing an exogenous calcium chelation approach, selectively targeted to injured axons, to prevent side effects on physiological calcium signalling.

The basis of the selective targeting approach was to deliver a prodrug calcium chelator via the membrane "nanoruptures" that characterise damaged, high-calcium axons. As a proof-of-principle we first delivered fluorogenic compounds across damaged plasma membranes, thereby developing a membrane damage sensor, that is applicable across different cell types and in different types of membrane damage. The cytosolic localisation of the biosensor also makes it useful for targeting axons, which contrasts with nuclear DNA-binding stains such as propidium iodide. First steps of translating these findings into prodrug development have also been taken. To enhance endogenous calcium buffering, we performed experiments of rAAV-mediated, neuron-specific overexpression of the cytosolic calcium-binding proteins calbindin and calretinin. Despite optimisation attempts, the axonal expression achieved with this approach was low and did not reduce intra-axonal calcium levels or the degree of axonal loss in an MS animal model. Further improvement of the overexpression approach will be necessary to assess the axoprotective potential of calcium-binding protein overexpression.

In summary, this thesis lays foundational work to address the suitability of calcium as a neuroprotective target by developing a selective targeting approach to membrane-damaged axons and by evaluating an experimental approach for rAAV-mediated axonal overexpression of calcium-binding proteins.

Zusammenfassung

Die Multiple Sklerose (MS) ist eine chronische, entzündliche, demyelinisierende und degenerative Erkrankung des zentralen Nervensystems (ZNS), welche durch die Entstehung fokaler Entzündungsherde sowie durch eine progrediente diffuse Gewebsschädigung aufgrund eines niedrig-gradig schwelenden Entzündungsprozesses charakterisiert ist. Es wird angenommen, dass die klinische Manifestation der schubförmig remittierenden MS – die akut auftretenden neurologischen Ausfälle – durch die Entzündung und Demyelinisierung ausgelöst werden. Das Ausmaß der langfristigen und irreversiblen Behinderung hingegen wird durch die Neurodegeneration bestimmt, insbesondere durch den Verlust von Axonen. Diese Degeneration ist in den frühesten Stadien der Krankheit beobachtbar und verursacht eine fortschreitende Behinderung, sobald eine kritische, kompensierbare Schwelle überschritten wird. Die derzeit verfügbaren immunmodulatorischen Therapien für MS unterdrücken Krankheitsschübe, können aber die neuroaxonale Degeneration nicht vollständig aufhalten. Die Entwicklung primär neuroprotektiver Therapien ist daher dringend notwendig.

In vivo mikroskopische Untersuchungen der experimentellen autoimmunen Enzephalomyelitis, einem Tiermodell der MS, sind ein hilfreicher Ansatz, um die Pathogenese der axonalen Degeneration zu verstehen. Experimente dieser Art haben gezeigt, dass die anfängliche Schädigung der Axone noch reversibel ist und, dass die Wahrscheinlichkeit der Fragmentierung geschädigter Axone von der Konzentration des intra-axonalen Calciums abhängt, welches durch „Nanorupturen“ in der Plasmamembran eintritt. Da manche Axone ihre Calcium-Homöostase spontan wiederherstellen können, stellten wir die Hypothese auf, dass therapeutische Interventionen, welche Axone darin unterstützen ihre Calcium-Homöostase wiederherzustellen, die Balance zugunsten einer axonalen Erholung verschieben und den Verlust von Axonen verringern können. Das Ziel dieser Arbeit war es daher die Modulierung von Calcium als mögliche axoprotektive Therapiestrategie zu untersuchen. Dies erfolgte durch zwei verschieden Ansätze: (1) Durch die Ausnutzung endogener Mechanismen der Calcium-Homöostase und (2) durch die Entwicklung eines exogenen Calcium-Komplexierungsansatzes, welcher selektiv auf geschädigte Axone abzielt. Dies sollte Nebenwirkungen auf physiologische Calcium-Signale vermeiden.

Grundlage dieses Ansatzes war es, einen Calcium Chelator als Propharmakon durch jene „Nanorupturen“ einzuschleusen, welche geschädigte Axone mit erhöhtem Calcium charakterisieren. In einer Machbarkeitsstudie schleusten wir dazu zunächst fluorogene Stoffe über die geschädigte Plasmamembran ein und entwickelten so einen Membranschädigungs-Sensor, der in verschiedenen Zelltypen und für verschiedene Arten der Membranschädigung einsetzbar ist. Die zytosolische Lokalisierung des Biosensors macht ihn auch für die Darstellung von Axonen nützlich, im Gegensatz etwa zu Propidiumiodid, einem Farbstoff, welcher lediglich die DNA im Zellkern färbt. Erste Schritte zur Übertragung dieser Erkenntnisse auf die Entwicklung eines Calcium-puffernden Propharmakons wurden ebenfalls unternommen. Um die endogene Calcium-Pufferung zu unterstützen, wurden zudem Experimente zur rAAV-vermittelten, Neuron-spezifischen Überexpression der zytosolischen Calcium-bindenden Proteine

Calbindin und Calretinin durchgeführt. Trotz mehrerer Optimierungsversuche war die so erreichte axonale Überexpression jedoch gering und konnte weder die intra-axonale Calcium-Konzentration noch den Verlust von Axonen in einem Tiermodell der MS reduzieren. Eine weitere Verbesserung des Überexpressions-Ansatzes wird notwendig sein, um das axoprotektive Potential Calcium-bindender Proteine zu untersuchen.

Zusammenfassend lässt sich sagen, dass diese Arbeit grundlegende Vorarbeiten zur Entwicklung neuroprotektiver Therapiestrategien, die an den erhöhten intraaxonalen Calciumkonzentrationen ansetzen, geleistet hat. Dies tut sie durch die Entwicklung einer selektive Zuliefe-rungsmethode in membrangeschädigte Axone sowie durch die Evaluation eines experimentellen Ansatzes für die axonale rAAV-vermittelte Überexpression Calcium-bindender Proteine.

1. Introduction

1.1. Multiple Sclerosis

Multiple sclerosis (MS) is a chronic inflammatory, demyelinating and degenerative disease of the central nervous system (CNS). The pathologic hallmarks of MS, that gave the disease its name, are CNS lesions or plaques: focal areas of inflammation, demyelination and axonal degeneration, arising in consequence of a loss of self-tolerance against CNS antigens and immune cell infiltration across the blood-brain-barrier (Dendrou *et al.*, 2015). Additionally, smouldering low-grade disease activity throughout the CNS contributes to neuroaxonal injury and accrual of disability.

MS affects around 2.8 million people worldwide, with 300 new diagnoses made every day (The Multiple Sclerosis International Federation, 2020). The disease is caused by a complex interplay of genetic and environmental risk factors, yet why some individuals develop MS and others do not is still incompletely understood (Jakimovski *et al.*, 2024). The clinical course of MS is very heterogenous, making an accurate prognosis very difficult. In most patients, MS starts with a relapsing-remitting course followed by a progressive disease stage (Baecher-Allan *et al.*, 2018). Around 50 % of patients will require a walking aid within 15 years of diagnosis (Scalfari *et al.*, 2010). With a mean age of only 32 years at diagnosis, this makes MS the most common non-traumatic cause of disability in young people (The Multiple Sclerosis International Federation, 2020).

To this day, no curative treatment exists. While disease-modifying therapies (DMTs) that dampen immune reactions can initially slow down disease progression, they do not halt neurodegeneration and eventually lose efficacy in the progressive stage of MS, where the disease process becomes mostly independent from immune cell infiltration (Scalfari *et al.*, 2024). The development of primary neuroprotective treatments for MS is therefore an important unmet clinical need.

1.1.1. Epidemiology and aetiology

With 2.8 million patients worldwide, the overall prevalence of multiple sclerosis is 36 in 100 000 people. However, the geographic distribution of the disease is very heterogenous, with higher prevalences of 100 - 300 per 100 000 in countries in Europe, North America and Australia and low prevalence in the rest of the world. The prevalence is three times higher in women than in men (The Multiple Sclerosis International Federation, 2020).

The precise aetiology of MS is yet unknown. Numerous studies on MS susceptibility have shown, that the disease is multifactorial and likely triggered by environmental factors in genetically susceptible individuals. More than 200 genetic risk variants have been defined, which can mostly be mapped to genes that affect the function of peripheral immune cells and

microglia (The Multiple Sclerosis International Federation, 2020). The strongest individual risk gene is *HLA-DRB1*15:01* with a 4-fold increased MS risk in heterozygous carriers and an 8-fold increased MS risk in homozygous carriers (Moutsianas *et al.*, 2015; The International Multiple Sclerosis Genetics Consortium, 2019). Other HLA (human leukocyte antigen) genes are also implicated in MS susceptibility or protection, suggesting that presentation of specific antigens plays a role in the development of MS (Moutsianas *et al.*, 2015). Overall, the genetic landscape of multiple sclerosis suggest that the disease originates in the immune system and argues against the concept of a primary neurodegenerative disease with secondary inflammation.

A disease concordance of 25-30 % in monozygotic twins (Hansen *et al.*, 2005; Kuusisto *et al.*, 2008; Willer *et al.*, 2003) emphasises the importance of environmental trigger factors for the development of MS. Most prominently, Epstein-Barr virus (EBV), a human herpesvirus that infects and latently persists in B cells (Thorley-Lawson, 2001), has been associated with the development of MS. Infectious mononucleosis patients, i.e. people with a symptomatic EBV infection, have an increased risk of developing MS, as have individuals with high antibody titers against EBV nuclear antigens (Levin *et al.*, 2005; Thacker *et al.*, 2006). The strongest evidence for a causative relationship between EBV infection and MS comes from a 2022 study on US military personnel in which longitudinal blood samples collected over the years of service were retrospectively analysed to unveil the temporal relationship between EBV seroconversion and MS diagnosis (Bjornevik *et al.*, 2022). The study included 35 people who developed MS and had been negative for EBV at the start of their service. Analysis of the longitudinal blood samples showed that 34 of these patients (97 %) had seroconverted before MS onset, whereas no such association was found between MS diagnosis and cytomegalovirus (CMV). Overall, the study reported a 32-fold increase in hazard ratio for multiple sclerosis diagnosis after EBV seroconversion. How EBV causes MS remains debated, yet molecular mimicry or immune dysregulation due to ineffective EBV control and/or EBV-infected B cells are the most commonly discussed hypotheses. Notably, a recent publication has described molecular mimicry between Epstein-Barr nuclear antigen 1 (EBNA-1) and the glial cell adhesion molecule glialCAM (Lanz *et al.*, 2022). Given that more than 90 % of the population has been infected with EBV by the age of 25 (Winter *et al.*, 2020), often asymptomatically, MS is still a very rare complication. Nevertheless, vaccines against EBV are under development and may one day lower MS incidence.

The gut microbiome and its composition are also known to be critical for the development of multiple sclerosis, due to interaction with the immune system. Yet again, the precise mechanisms of this complex involvement are not understood (Baecher-Allan *et al.*, 2018; Kadowaki and Quintana, 2020). Other known risk factors for MS are obesity, smoking and Vitamin D deficiency (Liu *et al.*, 2016; Poorolajal *et al.*, 2017; Duan *et al.*, 2014). The latter was often proposed to explain the geographic pattern of MS prevalence, which increases with latitudes further from the equator. However, a recent publication has challenged this view by pointing out an evolutionary explanation for increased MS risk in certain populations. According to Barrie *et al.* (2024), genetic variants that predispose to MS today arose in the Bronze Age due to lifestyle changes in the steppe pastoralis population that necessitated the co-evolution with

novel pathogens. Today's north-south gradient in European MS prevalence can be explained by different degrees of steppe pastoralis ancestry in consequence of migratory movements.

1.1.2. Clinical manifestation

1.1.2.1. Symptoms

Symptoms of MS mostly involve the motor and sensory system, however depending on lesion localisation a broad range of neurological symptoms can occur in MS patients. Early symptoms of MS can include motor weakness, sensory deficits or loss of balance. Other frequent symptoms, especially in progressive MS, are cognitive impairment, fatigue and depression (Compston and Coles, 2008; Jakimovski *et al.*, 2024). Disability progression in MS is commonly described using the EDSS (Expanded Disability Status Scale), a ten point scale which mainly assesses the patient's ability to walk (Kurtzke, 1983). Around 50 % of patients reach EDSS 6, which indicates permanent use of a walking aid, within 15 years of diagnosis (Scalfari *et al.*, 2010). In severe cases, patients may require a wheelchair, be bedridden or even die from MS.

1.1.2.2. Diagnosis

The diagnosis of MS involves a clinical assessment of the neurological symptoms, such as testing of reflexes, motor function and cognitive performance. The measurement of evoked potentials can uncover impaired nerve conduction in consequence of demyelination (Compston and Coles, 2008). Important imaging tools in the diagnosis of MS are MRI (magnetic resonance imaging) scans of brain and spinal cord which indicate the presence of neuroinflammatory lesions, responsible for the emergence of neurological symptoms. A contrast agent like gadolinium is used to distinguish new, contrast-enhancing lesions with permeable blood-brain-barrier from older, non-enhancing lesions. To diagnose MS in accordance with the 2017 McDonald criteria, the disease activity has to be disseminated in space and time, meaning that lesions have to occur in different CNS regions and new lesions have to develop over time (Thompson *et al.*, 2018). Cases in which patients do not fulfil these criteria, for example because they present with a single lesion, are classified as "clinically isolated syndrome" (CIS). The majority of CIS patients is diagnosed with MS at a later timepoint (Jakimovski *et al.*, 2024). The differential diagnosis of multiple sclerosis can also be aided by the detection of oligoclonal bands in protein electrophoresis of the cerebrospinal fluid (CSF) which indicate intrathecal antibody synthesis and are present in about 90 % of patients (Jakimovski *et al.*, 2024).

1.1.2.3. Disease course and prognosis: Relapses, progression and disability

Most patients initially experience a relapsing-remitting disease course (RRMS), which is characterised by episodes of acute neurological symptoms alternating with phases of clinical stability. With disease duration, relapse rates decline, yet recovery from relapses becomes incomplete (Jakimovski *et al.*, 2024, **Figure 1a**). Natural history studies have shown that without treatment 60 – 80 % of patients transition to secondary progressive MS (SPMS) after a median time of 15 - 20 years disease duration (Tremlett *et al.*, 2008; Tedeholm *et al.*, 2015). Progressive MS (PMS) is characterised by continuous worsening of symptoms independent of relapses and new MRI lesion activity, although superimposed relapses can still occur (Jakimovski *et al.*, 2024, **Figure 1a**). With the availability of highly efficient immunomodulatory drugs and improved diagnosis, the fraction of patients that transition from RRMS to SPMS has decreased (Cree *et al.*, 2016). In 12 % of patients however, the disease is progressive from the beginning (primary progressive MS, PPMS) (The Multiple Sclerosis International Federation, 2020).

Due to the high variance between disease courses, a prognosis for the individual patient is very difficult to make, especially at the timepoint of first diagnosis. Several studies have shown that neither relapse rate nor MRI lesion activity can predict long-term disability (Scalfari *et al.*, 2013; Cree *et al.*, 2016). Better predictors of disability progression are the steepness of EDSS increase and the degree of brain atrophy (Tur *et al.*, 2023; Rocca *et al.*, 2023, **Figure 1b**). A recent genome-wide association study on MS progression has also uncovered the first genetic risk marker for faster MS progression with genome-wide significance in the DYSF-ZNF638 locus (The International Multiple Sclerosis Genetics Consortium, 2023).

The differentiation between RRMS and PMS was classically made under the assumption that RRMS is driven by peripheral immune cell infiltration whereas PMS is driven by distinct CNS compartmentalised processes of neurodegeneration. Although this explains well, why PMS is refractive to immunomodulatory treatment, the simple binary view is challenged by the detection of ongoing neurodegeneration throughout the whole disease course, even before diagnosis und under effective treatment (Friese *et al.*, 2014; Scalfari *et al.*, 2024). Instead, RRMS and PMS may be parts of a single disease continuum, in which transition to the progressive worsening occurs when neural compensation mechanisms are exhausted, not only because of progressive neurodegeneration but also as a consequence of aging (Kuhlmann *et al.*, 2023). The importance of age is also supported by the fact that the average diagnosis ages for PPMS and SPMS are practically identical (Confavreux and Vukusic, 2006).

In summary, long-term worsening of disability in MS is largely driven by “PIRA”, progression independent of relapse activity, representing neurodegenerative processes that continue despite relapse suppression by immunomodulatory treatment (Lublin *et al.*, 2022, Woo *et al.*, 2024a, **Figure 1c**). This emphasises the need for neuroprotective drug development for the effective treatment of MS and the importance of neurodegeneration-related readouts for

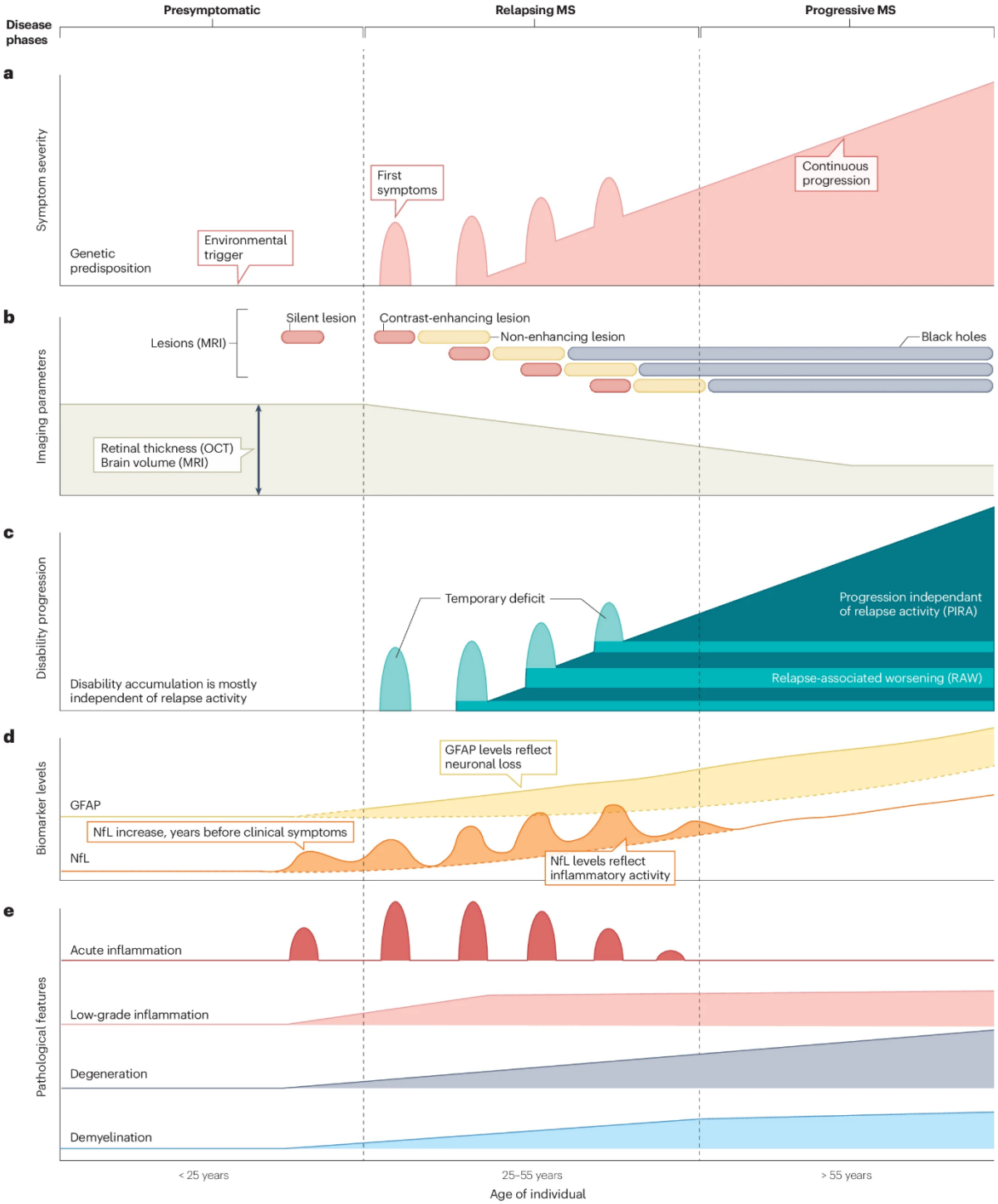

Figure 1 – Multiple sclerosis disease course and its relation to pathology.
(a) Depiction of MS symptom severity over time, defining a relapsing-remitting phenotype (RRMS) with secondary progression (SPMS). MS is believed to be caused by environmental triggers in genetically susceptible individuals. Age is a key determinant for the transition from RRMS to SPMS. **(b)** Relapses in (a) are associated with new MRI lesion activity, while retinal thickness and brain volume decline linearly. **(c**) Contribution of relapses (RAW) and relapse-independent processes (PIRA) to disability progression. **d)** The biomarkers GFAP (glial fibrillary acidic protein) and NfL (neurofilament light chain) increase with disease course, starting before onset of clinical symptoms. GFAP reflects ongoing neurodegeneration while NfL responds to acute inflammation. Dashed lines indicate levels seen in age-matched people without MS **(e)** Acute bursts of inflammation underly relapse activity, while other processes, especially degeneration, develop more continually. This has been shown in histopathological studies. (*Figure legend continues on next page)*

(Continued legend for Figure 1)

disease surveillance. These include optical coherence tomography (OCT) of the retina, which documents thinning of the retinal nerve fibre layer, as well as measurements of serum neurofilament light chain (NfL), indicative of axonal breakdown (**Figure 1b, d**). Both methods show an increase of neuroaxonal degeneration over the disease course of MS, which is apparent at or even before diagnosis and can predict future patient disability (Petzold *et al.*, 2010; Zimmermann *et al.*, 2018; Benkert *et al.*, 2022; Bjornevik *et al.*, 2022). The astrocytic structural protein GFAP (glial fibrillary acidic protein) has been suggested as an additional biomarker for neurodegeneration as it can likewise predict disease progression, yet unlike NfL is not affected by relapses (Meier *et al.*, 2023). Indeed, astrogliosis, the basis of GFAP detection in CSF and blood, is linked to neurodegeneration in both RRMS and PMS (Wheeler *et al.*, 2020; Absinta *et al.*, 2021).

1.1.3. Pathogenesis and histopathology

The diagnosis of MS is based on the detection of white matter (WM) lesions by MRI. Histologically, these focal lesions or plaques are characterised by immune cell infiltration, demyelination, axonal degeneration and astroglial scarring, varying in degree depending on lesion evolution (Baecher-Allan *et al.*, 2018). Postmortem studies also indicate more subtle pathologic changes in the non-lesioned, "normal appearing white matter" (NAWM) as well as the presence of grey matter lesions and diffuse grey matter injury, especially in PMS (Lassmann, 2018). Whereas the loss of neurons and axons is irreversible, remyelination does occur, yet is ineffective in many patients (Patrikios *et al.*, 2006). The damage to the CNS is believed to be initiated by immune cell infiltration due to loss of self-tolerance against CNS antigens. The immunopathogenesis of the disease – how and why self-tolerance is lost – remains incompletely understood (Dendrou *et al.*, 2015).

1.1.3.1. Immune cell infiltration and lesion formation

Lesion formation is initiated by tissue infiltration of activated autoreactive T cells from the bloodstream, which are reactivated in the CNS by renewed antigen presentation and recruit further immune cells to the site. The infiltrate of an acute MS lesion is eventually dominated by macrophages and CD8+ T cells with lower numbers of CD4+ T cells, B cells and plasma cells (Dendrou *et al.*, 2015). The ensuing tissue damage is mainly attributed to macrophages, which have been shown to phagocytose myelin and can be found in close apposition to damaged axons, yet also have functions in lesion resolution (Kornek *et al.*, 2000; Nikić *et al.*, 2011; Chu *et al.*, 2018). Soluble factors within the inflammatory milieu, such as antibodies, cytokines, reactive oxygen and nitrogen species can also have deleterious effects on CNS-resident cells (Woo *et al.*, 2024a). The process is illustrated in **Figure 2**.

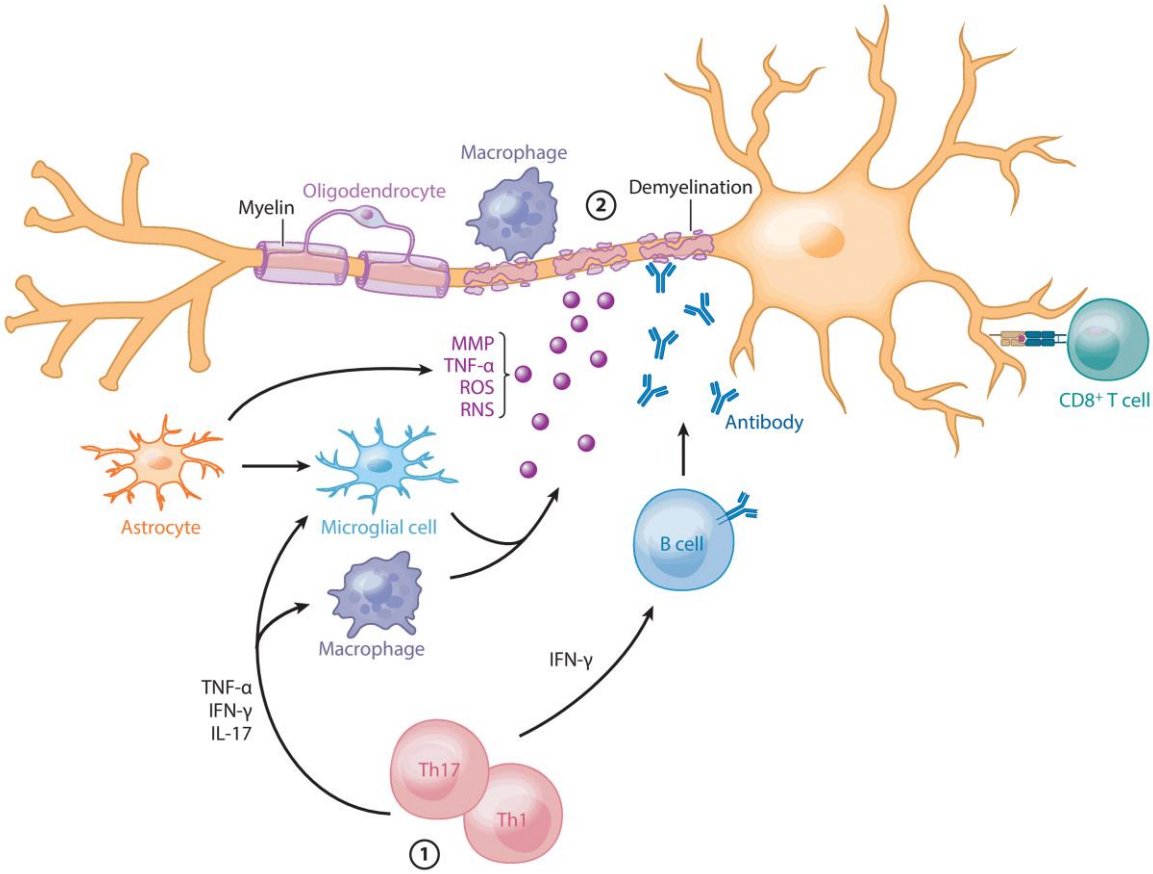

Figure 2 – CNS damage driven by immune cells.
Lesion formation is initiated by the Th1 and Th17 CD4+ T cell subsets ① which activate further cell types by secreting pro-inflammatory cytokines. The infiltrate consists of macrophages, CD8+ T cells, CD4+ T cells and B cells. Tissue destruction ② is due to macrophages, CD8+ cytotoxicity and soluble factors secreted by immune cells, astrocytes and microglia. TNF-α = tumour necrosis factor α, IFN-γ = interferon γ, IL-17 = interleukin 17, MMP = matrix metalloproteinase, ROS = reactive oxygen species, RNS = reactive nitrogen species.

No single triggering autoantigen has yet been found for MS. Autoreactive T and B cells against myelin sheath components like myelin oligodendrocyte glycoprotein (MOG), myelin basic protein (MBP) and proteolipid protein (PLP) have been detected in patients, however, autoreactive lymphocytes can also be found in healthy individuals where they do not trigger disease (Hohlfeld *et al.*, 2016a, 2016b). Thus, the question in MS immunopathogenesis is less how autoreactive cells arise but more how they evade control and become activated. A look at the genetic factors of MS susceptibility suggests, that while specific HLA variants define the epitope specificity of the autoimmune reaction, other non-HLA risk genes may lower the threshold for immune cell activation (Dendrou *et al.*, 2015). In addition, several studies have found a reduced function of regulatory T cells (Tregs) – cells responsible for peripheral control of autoimmunity – in MS patients (Viglietta *et al.*, 2004; Haas *et al.*, 2005). Whether autoreactive T cells are activated by molecular mimicry, bystander activation or by an encounter with the actual CNS antigen remains debated (Dendrou *et al.*, 2015). Despite the still evolving

knowledge, studies of MS immunopathogenesis have led to the development of numerous immunomodulatory drugs for the treatment of relapsing-remitting MS.

1.1.3.2. Lesion evolution and classification

White matter lesions can evolve over time spans of months and years. To distinguish different stages of tissue destruction, which follows a stereotypic series of events, lesions are classified as active, chronic active, smouldering or inactive (Stadelmann *et al.*, 2019).

Active lesions are characterised by dense immune cell infiltration. Foamy macrophages phagocytosing myelin are found throughout the lesion and radially expand the lesioned area, whereas lymphocytes are mainly found at the perivascular lesion core (Henderson *et al.*, 2009; Stadelmann *et al.*, 2019). Axonal degeneration is already apparent at this early lesion stage (Trapp *et al.*, 1999; Bitsch *et al.*, 2000; Frischer *et al.*, 2009).

Chronic active and smouldering lesions have a chronic, demyelinated core mostly devoid of immune cells, yet tissue destruction, mostly by activated microglia and macrophages, continues in the lesion rim and slowly expands the lesion (Ferguson *et al.*, 1997; Kuhlmann *et al.*, 2017; Dal-Bianco *et al.*, 2017; Jäckle *et al.*, 2020). Smouldering lesions are predominantly found in progressive MS and contain iron which can be visualised in MRI (Frischer *et al.*, 2015; Dal-Bianco *et al.*, 2017). Slowly expanding or smouldering lesions have recently gained attention, as they can predict transition to PMS and future disability progression (Beynon *et al.*, 2022; Preziosa *et al.*, 2022). Their study may thus help to understand the mechanisms of CNS compartmentalised inflammation, sustained by CNS-resident cells (Wheeler *et al.*, 2020; Absinta *et al.*, 2021), that are refractive to current immunomodulatory treatment.

Inactive lesions are sites of past inflammatory tissue destruction. They are characterised by an absence of peripheral immune cells and by a widespread loss of myelin, oligodendrocytes and axons (Wolswijk, 2000; Stadelmann *et al.*, 2019; Schirmer *et al.*, 2011). What determines whether an MS lesion stays chronically active or whether it turns into an inactive lesion is still unclear (Stadelmann *et al.*, 2019). The same is true for remyelination, which can be observed at all lesion stages but its efficacy has been found to be highly variable between patients (Patrikios *et al.*, 2006; Stadelmann *et al.*, 2019). The finding that axonal density is higher in remyelinated compared to chronic demyelinated plaques suggests that remyelination protects from further axonal loss (Kornek *et al.*, 2000).

1.1.3.3. Grey matter lesions and diffuse CNS damage

In addition to white matter lesions, focal areas of demyelination can also occur throughout the grey matter (GM), including the cortex, hippocampus, basal ganglia, brain stem and the grey matter of the spinal cord (Brownell and Hughes, 1962; Vercellino *et al.*, 2005; Lassmann, 2018). Compared to white matter lesions, grey matter lesions contain fewer lymphocytes and phagocytes (Peterson *et al.*, 2001). Besides neuroaxonal loss, they are also accompanied by

an extensive loss of synapses (Wegner *et al.*, 2006). Cortical lesions often have a subpial localisation, extending into deep sulci. They are associated with meningeal inflammation, including the formation of ectopic B cell follicles (Serafini *et al.*, 2004; Kutzelnigg and Lassmann, 2006; Magliozzi *et al.*, 2010; Lucchinetti *et al.*, 2011). Cortical demyelination can already be detected at the earliest stages of RRMS, but is much more prevalent in progressive MS (Lucchinetti *et al.*, 2011; Kutzelnigg *et al.*, 2005). The extent of cortical lesions has been found to correlate with cognitive impairment (Nielsen *et al.*, 2013).

Diffuse changes can also be observed outside of lesions, i.e. in the absence of dense peripheral immune infiltrates, in both normal appearing white and grey matter (NAWM, NAGM). These include diffuse microglia activation, diffuse presence of T cells, axonal injury and astrogliosis (Kutzelnigg *et al.*, 2005). Part of these changes can be attributed to anterograde and retrograde degeneration of neurons or axons damaged within focal lesions (Dziedzic *et al.*, 2010), yet diffuse damage to cortex and spinal cord also correlates with inflammation in the overlying meninges, indicating a role for soluble inflammatory mediators in the process (Androdias *et al.*, 2010; Reali *et al.*, 2020). Although NAWM and NAGM are usually defined by the absence of demyelination, a recent study has shown subtle pathologic changes to myelin even in the NAWM (van den Bosch *et al.*, 2023).

How or whether white and grey matter damage in MS are related to each other has long been debated. A recent meta-analysis demonstrated, that white matter lesion volume does correlate with grey matter atrophy, yet more in RRMS than in PMS (Lie *et al.*, 2022). This suggests that grey matter damage in RRMS may happen secondary to white matter damage, whereas in PMS primary neurodegenerative disease mechanisms dominate.

1.1.3.4. From histopathology to clinical manifestation

In relapsing-remitting MS, histopathology is dominated by focal white matter lesions. Relapse-related symptoms in RRMS patients are believed to result from inflammation and demyelination and thus slower or blocked conduction. Remission can thus be attributed to partial remyelination and adaptation of demyelinated axons, which redistribute ion channels to re-establish conduction (Reddy *et al.*, 2000; Bjartmar *et al.*, 2003). Neuroaxonal loss in contrast is irreversible and responsible for the accrual of irreversible disability in MS (Coles *et al.*, 1999; Trapp *et al.*, 1999). While axonal degeneration is clearly detectable from disease onset, progressive neuronal decline is believed to only set in once a threshold of compensable damage has been passed (Trapp *et al.*, 1999; Kuhlmann *et al.*, 2023). In progressive MS, the disease activity becomes more diffuse and independent from immune cell infiltration. Histopathologically, this is represented by low-grade inflammation in grey matter lesions and diffuse NAWM and NAGM changes, which are believed to be largely driven by tissue-resident glia and immune cells (Lassmann, 2018; Healy *et al.*, 2022). Clinically, it manifests as a loss of DMT effectiveness, as these drugs primarily target peripheral immunity (Scalfari *et al.*, 2024).

1.1.4. Treatment

No curative treatment for MS exists to date. Instead, the disease is managed using so-called disease-modifying therapy (DMT). Over the past thirty years, around twenty different DMTs with immunomodulatory and immunosuppressive effects have been approved for the treatment of relapsing forms of MS (encompassing CIS, RRMS and SPMS with relapse activity), yet only one DMT has been approved for the treatment of primary progressive MS (Jakimovski *et al.*, 2024). The molecular mechanisms of these therapies will be outlined further below.

Numerous studies have shown the benefits of early DMT initiation at the first clinical demyelinating event. DMT use in patients with clinically isolated syndrome (CIS) not only prolongs the time to confirmed RRMS diagnosis but is also associated with less disability for at least 10 years of follow-up when compared to patients with later treatment initiation (Tintore *et al.*, 2020; Kappos *et al.*, 2016). In RRMS patients, DMTs lower the relapse rate, MRI-based lesion activity and short-term disability worsening (Jakimovski *et al.*, 2024). Studies on the natural history of MS have also shown that today's fraction of patients that transition from RRMS to SPMS has decreased in comparison to the pre-DMT era (Cree *et al.*, 2016). The first DMT to be approved for PPMS, Ocrelizumab, slowed disability progression and brain volume loss in a placebo-controlled trial (Montalban *et al.*, 2017). The therapeutic effect was however only observed in PPMS patients with focal MRI activity, suggesting that Ocrelizumab like other DMTs has a peripheral mechanism of action.

In addition to DMTs, cortisol, or plasmapheresis as a second-line option, can be used for the treatment of acute relapses. Symptomatic therapy may be indicated to counteract MS symptoms like spasticity, bladder and bowel dysfunction, fatigue or depression (Jakimovski *et al.*, 2024). Patients also benefit from good management of comorbidities, especially hypertension, hyperlipidaemia, diabetes, and obesity, which are linked to MS disease activity (Salter *et al.*, 2020).

Although adequate treatment increases the health span of MS patients, currently approved therapies do not halt neurodegeneration and largely lose efficacy in older patients (Weideman *et al.*, 2017). Neuroprotective treatments may be the key to preventing MS progression, yet recent clinical trials in this regard have failed and no such medication has been approved to date (Chataway *et al.*, 2020). Another limitation of DMT use are their side effects, which range from flu-like symptoms to fatal opportunistic infections such as progressive multifocal leukoencephalopathy (PML), a consequence of viral reactivation under immunosuppression (Jakimovski *et al.*, 2024).

1.1.4.1. DMT mechanisms of action and clinical use

The first disease-modifying therapy (DMT) approved for MS was the recombinant cytokine interferon β-1b (IFNβ-1b) in the year 1993. IFNß-based formulations have various positive

immunomodulatory effects including reduced antigen presentation, reduced T cell proliferation, altered expression of cytokines and restoration of immune suppressor functions. Side effects include flu-like symptoms and increased liver enzymes (Jakimovski *et al.*, 2018).

IFNß was followed by glatiramer acetate in 1996. This DMT is a mix of synthetic polypeptides mimicking MBP (Ben-Nun *et al.*, 1996). Its immunomodulatory, tolerogenic effects are seen in an anti-inflammatory shift in T cell polarisation and cytokine profiles. Severe side effects are rare (Jakimovski *et al.*, 2024).

Mitoxantrone, approved for use in MS in the year 2000, is a cytostatic drug and exerts its immunosuppressive function by suppressing the proliferation of T cells, B cells and macrophages. Due to severe side effects that include cardiotoxicity and leukaemia, mitoxantrone is only used in highly active MS that does not respond to other treatments. Two other drugs which also act on cell proliferation but have a better safety profile, teriflunomide and cladribine (approved in 2012 and 2019 respectively) are more frequently used (Deutsche Gesellschaft für Neurologie e. V., 2022; Jakimovski *et al.*, 2024).

The year 2004 saw the approval of the first monoclonal antibody in the treatment of MS: natalizumab, directed against the endothelial adhesion molecule VLA-4 (very late antigen-4, also known as ITGA4 = integrin subunit alpha 4). Natalizumab binding blocks leukocyte adhesion and thus transendothelial migration into the CNS. It is highly effective in preventing relapses yet is also associated with the highest PML risk among all DMTs (Jakimovski *et al.*, 2024). Adhesion molecule inhibition has also been exploited as a mode of action for small molecule drugs. Fingolimod (2010), siponimod (2019), ozanimod (2020) and ponesimod (2021) all bind to and inhibit function of the sphingosine-1-phosphate (S1P) receptor on lymphocytes which regulates egress from lymph nodes. Consequently, this class of drugs prevents lymphocyte entry into the bloodstream. Common side effects are lymphopenia and increased infection risk (Jakimovski *et al.*, 2024).

The precise mode of action of dimethyl fumarate (2013) is not well understood, yet this drug has been shown to activate the Nrf2 (nuclear factor erythroid 2-related factor 2) signalling pathway thus initiating an anti-inflammatory transcriptional programme. Gastrointestinal side effects and lymphopenia can occur under this DMT (Gopal *et al.*, 2017; Jakimovski *et al.*, 2024).

Another class of DMTs consisting of alemtuzumab (2007), ocrelizumab (2017, also approved for PPMS), ofatumamab (2020), ublituximab (2022) and rituximab (off-label use) exerts its immunosuppressive effects by B cell depletion. Whereas alemtuzumab is directed against CD52, which is also present on T cells, NK cells and monocytes/macrophages, the other DMTs in this group are anti-CD20 antibodies. CD20 is present on immature and mature B cells, which are depleted by treatment, but not on plasma cells. The main side effects are lymphopenia and increased infection risk (Jakimovski *et al.*, 2024). The fact that B cell depletion is such an effective treatment for both RRMS and PPMS indicates their pivotal role in

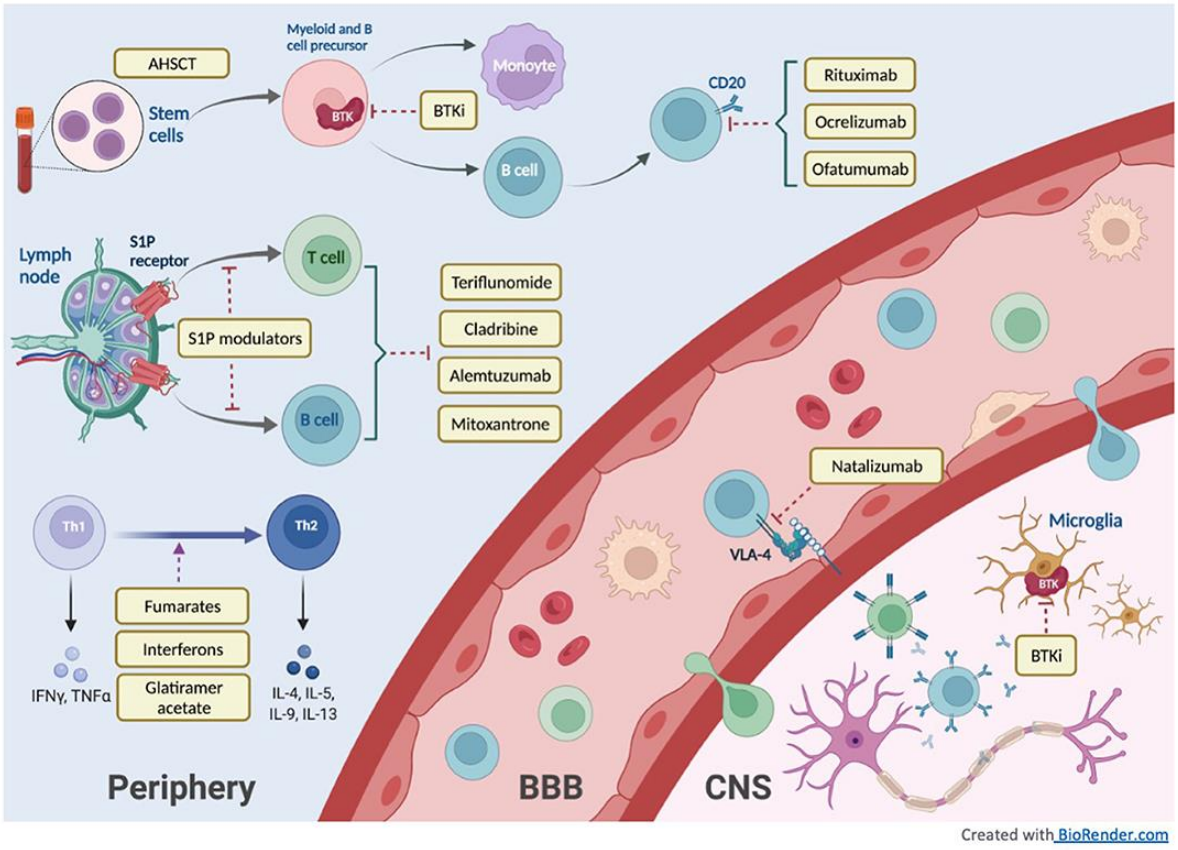

Figure 3 – DMT mechanisms of action.
Schematic depiction of the effects of DMTs on different immune cell types, their maturation (top), migration (center and BBB), proliferation (center) and polarisation (bottom). AHSCT = autologous haematopoietic stem cell transplantation; BTKi = Bruton's tyrosine kinase inhibitor (currently undergoing clinical trials); S1P = sphingosine-1-phosphate; BBB = blood-brain-barrier; CNS = central nervous system.

MS pathology, which has been underappreciated by past T cell focussed research. Indeed, the presence of oligoclonal immunoglobulins in CSF and the poor diagnosis associated with presence of ectopic B cell follicles in the meninges point to intense involvement of B cells in MS pathology. They may also provide the missing link between B cell tropic EBV and emergence of MS (Cencioni *et al.*, 2021).

Very aggressive multiple sclerosis phenotypes which do not respond to DMTs have also been successfully treated with autologous haematopoietic stem cell transplantation after near-complete immunoablation (Atkins *et al.*, 2016).

All DMT mechanisms of action are summarised in **Figure 3**. For the application in the clinic, DMTs are subdivided into different groups based on efficacy. The German Neurology Society classifies interferons, glatiramer acetate, teriflunomide and dimethyl fumarate as moderate efficacy DMTs; fingolimod, ozanimod, ponesimod, cladribine and mitoxantrone as high-effi-

cacy and the monoclonal antibodies alemtuzumab, natalizumab, ocrelizumab and ofatumumab as highest efficacy (Deutsche Gesellschaft für Neurologie e. V., 2022). Although a direct use of highest efficacy drugs has been debated, the most common approach in MS treatment is escalation therapy, in which DMTs with moderate efficacy are used as first-line treatment and only escalated to a higher efficacy group if the development of disease activity is unfavourable (Ontaneda *et al.*, 2019). This provides better risk management of side effects, which tend to be more severe in the higher efficacy groups. In any case, adequate treatment of MS requires regular supervision of disease activity. Depending on the DMT used, patients should also be regularly tested for lymphopenia, which can lead to life-threatening PML (Jordan *et al.*, 2022).

1.1.4.2. Unmet therapeutic needs and new future avenues for MS drug development

The development of DMTs has prolonged the health span of MS patients. However, shortcomings of current MS treatment strategies are the occurrence of severe adverse effects and the ongoing neurodegeneration under DMT treatment. The latter may also explain their limited effectiveness in progressive MS and in older individuals. While finding more specific DMT targets may limit adverse effects (for example reversible B cell inhibition with Bruton's tyrosine kinase inhibitors instead of B cell depletion, Reich *et al.*, 2021), the development of genuinely neuroprotective treatments is arguably the most urgent unmet clinical need in MS treatment. This may include both remyelinating drugs and primary neuroprotective approaches.

The biology of remyelination and why it often fails in MS lesions has been studied extensively, leading to the identification of druggable targets and the initiation of several clinical trials (Cunniffe and Coles, 2021). The most advanced drug candidate is clemastine, an H1 histamine receptor antagonist that stimulates oligodendrocyte precursor cell (OPC) differentiation. Clemastine has been shown to induce remyelination and improve visual acuity in patients with RRMS and evidence of chronic demyelinating optic neuropathy (Green *et al.*, 2017). Ongoing trials are also testing clemastine in combination with metformin, which aims to improve OPC responsiveness (NCT05131828).

Similarly, process has been made in characterising the mechanisms and stressors that lead to neuroaxonal degeneration in MS, such as ion dysregulation, oxidative damage and mitochondrial pathology (Woo *et al.*, 2024a). Despite these efforts, the field has seen many setbacks in the past decade, as numerous neuroprotective drug trials in progressive MS have failed to show an effect (Chataway *et al.*, 2024). This includes a phase 3 trial on high-dose biotin, proposed to boost neuronal energy production (Cree *et al.*, 2020), a phase 2 trial on the coenzyme Q10 analogue idebenone, proposed to protect mitochondria (Kosa *et al.*, 2020), the phase 2b multi-arm MS-SMART trial, investigating the effects of amiloride (blocking calcium and sodium influx), fluoxetine (improving mitochondrial metabolism by stimulation of glycogenolysis) and riluzone (inhibiting glutamate release) (Chataway *et al.*, 2020), and the phase 3 trial on simvastatin (inhibitor of the hydroxymethylglutaryl-CoA reductase, involved in cholesterol synthesis) (unpublished, presented at ECTRIMS 2024 by Jeremy Chataway).

More potentially neuroprotective drugs are currently undergoing clinical testing. A successful phase 2 trial has been reported for the antioxidant lipoic acid, achieving a reduction in brain atrophy of 68 % compared to placebo (Spain *et al.*, 2017). The phase 3 trial is currently ongoing. New drugs entering phase 2b include N-acetyl cysteine (antioxidant, NCT05122559), SAR443820 (inhibitor of receptor-interacting protein kinase 1 (RIPK1), involved in inflammatory response and cell death pathways, NCT05630547) and nicotinamide riboside (precursor of nicotinamide adenine dinucleotide (NAD), proposed to improve mitochondrial function, NCT05740722).

1.1.5. Animal models of MS

Multiple sclerosis is a complex human disease of unclear aetiology. Accordingly, animal models that encompasses all aspects of the disease, such as the immunopathogenesis, the multiple types of lesions and diffuse alterations in the CNS or the complex two-stage clinical disease course do not exists (Lassmann and Bradl, 2017). Nevertheless, several animal models have been developed to mimic and study different aspects of the disease.

The most widely used animal model for multiple sclerosis is experimental autoimmune encephalomyelitis (EAE). In active EAE, animals (mostly mice and rats for preclinical studies; but also primates for drug safety and efficacy) are immunised with myelin antigens combined with adjuvants to induce an autoimmune reaction. Freund's complete adjuvant causes an immune stimulation and phagocytosis of the antigen which in turn leads to major histocompatibility complex (MHC) class II presentation to CD4+ T cells (Billiau and Matthys, 2001). The pathogenesis of EAE is thus initiated by myelin-reactive CD4+ T cells, which cause the formation of neuroinflammatory lesions. These EAE lesions share important characteristics of MS lesions including immune infiltration, demyelination and axonal degeneration (Constantinescu *et al.*, 2011; Nikić *et al.*, 2011). In contrast to MS, EAE lesions are located almost exclusively in the spinal cord. Depending on the antigen used for immunisation and on the animal species or strain, the EAE disease course can vary: MOG immunisation in C57/BL6 mice leads to monophasic disease, whereas immunisation of SJL/J mice with PLP causes relapsing-remitting disease (Terry *et al.*, 2016).

Several other variants of EAE exist to study different aspects of MS pathology. EAE can be induced by transferring activated T cells from an immunised animal to a naive animal (Ben-Nun *et al.*, 1981). This model is called adoptive transfer EAE and is particularly useful for the study of T cell polarisation, infiltration and reactivation (Lassmann and Bradl, 2017). Both the active and passive induction model however are of limited use for the study of initiating events in immunopathogenesis. To bridge this gap, spontaneous EAE models have been developed which are based on transgenic expression of autoreactive T cell receptors (Bettelli *et al.*, 2003). Among other findings, spontaneous EAE models have helped to uncover the pivotal role of the microbiota for the development of CNS autoimmunity (Berer *et al.*, 2011). Adoptive transfer EAE with ß-synuclein-reactive T cells results in a model that recapitulates grey matter inflammation and brain atrophy (Lodygin *et al.*, 2019). Cortical inflammatory

lesions can be induced by subacute MOG immunisation followed by cortical cytokine injection (Merkler *et al.*, 2006). In addition to EAE, toxic models have been used to study demyelination and remyelination. This non-inflammatory demyelination can be induced with lysolecithin, a detergent that dissolves myelin sheaths, or the copper chelator cuprizone, which induces oligodendrocyte death (Jeffery and Blakemore, 1995; Matsushima and Morell, 2001).

Irrespective of the specific model, interspecies differences must be kept in mind when modelling disease in animals. Several differences between the immune systems of rodents and humans have been reported (Mestas and Hughes, 2004) and may have implications for the translation of model findings to human disease.

1.2. Axonal degeneration

Axons are highly specialised neuronal projections, optimised for long-distance information transfer in the form action potentials. Their unique structure – a human axon can be 20 000 times longer than the corresponding soma – also comes with unique challenges and vulnerabilities. This includes the dependence on active axonal transport for protein and organelle turnover, the high energy demands of action potential propagation and, in case of myelinated axons, the dependence on trophic support from oligodendrocytes (Guedes-Dias and Holzbaur, 2019; Howarth *et al.*, 2012; Lappe-Siefke *et al.*, 2003; Fünfschilling *et al.*, 2012).

The process of axonal degeneration is largely independent from classic somatic cell death pathways. Indeed, Wallerian degeneration, an active axon-specific self-destruction pathway, leaves the proximal axon and soma intact (Coleman and Freeman, 2010). Nevertheless, the fates of different neuronal compartments are tightly linked, and dysfunction can spread from one compartment to the other, particularly when axonal transport is affected (Woo *et al.*, 2024a; Guedes-Dias and Holzbaur, 2019).

Axonal dysfunction and degeneration can be observed in all types of MS lesions, including diffuse and smouldering lesions and from the earliest stages of pathology (Bitsch *et al.*, 2000; Frischer *et al.*, 2009; Lassmann, 2018). The loss of an axon is permanent. Even if some functionality can be restored by remodelling of axonal connections (Kerschensteiner *et al.*, 2004), the overall degree of axonal degeneration correlates with progressive disability in MS patients (Stefano *et al.*, 1998; Agosta *et al.*, 2007; Barro *et al.*, 2018). Studies in EAE however suggest, that initial axonal damage is still reversible, thus providing a therapeutic window of opportunity (Nikić *et al.*, 2011).

Stressors such as ionic imbalance, calcium overload, oxidative stress, virtual hypoxia and mitochondrial pathology have been described as contributors to axonal dysfunction and degeneration in MS (Friese *et al.*, 2014). A better understanding of these mechanism can provide a basis for the development of axoprotective therapies, which hold the promise to halt MS progression.

1.2.1. Physiological structure and function of axons

The polar neuron architecture enables unidirectional information propagation. Postsynaptic signals are received at the somatic dendrites; integration of the arriving potentials then determines whether an action potential (AP), a fast, transitory change of the membrane potential, is generated at the axon initial segment. APs are propagated along the axon to the axon terminals where they trigger synaptic neurotransmitter release. Action potential propagation is ensured by the coordinated action of voltage-gated sodium and potassium channels (Duale Reihe Physiologie - 2. Auflage, Thieme Verlag, 2010). The Na^+/K^+-ATPase in turn is responsible to restore cellular sodium and potassium concentrations, requiring a considerable energy expenditure (Howarth *et al.*, 2012).

Myelinated axons can propagate APs faster and more energy-efficiently compared to their non-myelinated counterparts due to saltatory conduction. The axonal myelin sheath consists of regularly spaced myelinated sections, called internodes, which are interrupted by nodes of Ranvier, where the axon is in direct contact with the extracellular space. Action potentials are only generated at the nodes, where voltage-gated sodium channels are clustered, and the myelin insulation enables direct AP propagation from one node to the next (Huxley A.F. and Stampfli, 1949). Ultrastructurally, myelin is a lipid-rich multi-layered membrane produced and wrapped around CNS axons by oligodendrocytes (Simons and Nave, 2015). Besides electrical insulation it also provides metabolic support from oligodendrocytes to the axon, which may make myelinated axons particularly vulnerable when myelin is damaged (Lappe-Siefke *et al.*, 2003; Fünfschilling *et al.*, 2012; Schäffner *et al.*, 2023).

To support structure and function, the axon has a highly specialised cytoskeleton. Its main constituents are an actin-spectrin membrane periodic skeleton that regulates axon diameter and anchors membrane proteins and a microtubule system that enables active transport along the axon (Leterrier *et al.*, 2017; Maday *et al.*, 2014). Neurofilaments, which serve as blood and CSF biomarkers in MS, are neuron-specific intermediate filaments which provide further structural support (Yuan *et al.*, 2017). While the role of the membrane periodic skeleton in neuropathology is only starting to be explored (Miazek *et al.*, 2021), the importance of axonal transport for neuronal health is well documented (Sleigh *et al.*, 2019). Anterograde cargos transported from the soma along microtubules include protein, mRNA and lipids, whereas retrograde transport is required for the degradation of protein and damaged organelles (Maday *et al.*, 2014). Mitochondria constantly move in both directions, to quickly respond to changing energy requirements (Plucińska and Misgeld, 2016). mRNA anterogradely transported from the nucleus can be locally translated in the axon, thus enabling quick translational responses to specific cues (Jung *et al.*, 2012). Since the axonal ER does not contain ribosomes, mRNA is translated at free ribosomes.

Taken together, the unique function of the axon requires elaborate structural and logistic adaptations. It is therefore not surprising, that axons are vulnerable to dysfunction under inflammatory attack.

1.2.2. Evidence for axonal degeneration in MS

Historically, axonal degeneration as a critical feature in MS pathology has long been overlooked in favour of the myelin-directed immune attack. However, it is becoming increasingly clear that axonal degeneration (and neurodegeneration at large) is ongoing throughout the disease course, starting even before the onset of clinical symptoms and persisting under DMT treatment (Friese *et al.*, 2014; Woo *et al.*, 2024a; Scalfari *et al.*, 2024). The following chapter will summarise the evidence for axonal degeneration in MS coming from post-mortem histological studies as well as from paraclinical studies, which also allow for longitudinal correlation with disease course.

1.2.2.1. Histological studies of axonal degeneration in MS

A systematic post-mortem study on axonal degeneration in active and chronic active white matter lesions was performed by Trapp *et al.* in 1998. This study found significant numbers of transected, i.e. irreversibly lost axons in all lesions analysed. Transected axons were characterised by end bulbs and more abundant in early, active lesions compared to older, chronic lesions. In chronic active lesions, transections were more abundant in the active rim compared to the core. Interestingly, a few of the transected axons seemed to be ensheathed by intact myelin. Other axons exhibited swellings without transection. The study also reported an increased number of transected axons in the NAWM of MS patients as compared to neurologically healthy donors, i.e. again axonal damage in the absence of myelin pathology. Although axonal loss had been reported before, the study by Trapp *et al.* was important for being one of the first to rely on immunohistochemical staining, which is more sensitive than traditional silver stains. The study corroborated findings by Ferguson *et al.* (1997) who performed similar studies using immunostaining for amyloid precursor protein (APP) a marker of impaired axonal transport. Although APP indicates axonal damage, not necessarily irreversible axon loss, the findings were highly similar with APP+ axons being most abundant in acute lesions, followed by chronic active lesions rims. In both regions, their number correlated with that of infiltrating macrophages.

One limitation of these studies was that they were performed on autopsy tissue and thus mostly included patients with a long medical history. Axonal loss and APP accumulation in early MS were therefore confirmed in a study using material from newly diagnosed patients, who had undergone MRI-guided biopsy for differential diagnosis (Bitsch *et al.*, 2000). Several studies have since confirmed the correlation between inflammation and axonal injury for all WM lesion types at all disease stages (Kuhlmann *et al.*, 2002; Frischer *et al.*, 2009; Schirmer *et al.*, 2011). Studies have also quantified the extent of axon loss in the WM. The above mentioned study by Bitsch *et al.* (2000) reported an axonal loss of 40 - 60 % within early and late demyelinating lesions respectively, yet with a high interindividual variability. A subsequent study on autopsy tissue reported an average axon loss of 65 % in chronic demyelinated lesions (Lovas *et al.*, 2000). Tract-specific post-mortem studies have reported around 20 % and 40 %

of axonal loss in sensory and corticospinal tracts respectively, as well as a 35 % reduction in the corpus callosum (DeLuca *et al.*, 2004; Evangelou *et al.*, 2000).

Transected neurites, axons as well as dendrites, can also be observed in grey matter lesions, showing again higher numbers in acute compared to chronic active and chronic lesions (Peterson *et al.*, 2001). Similar to WM findings, neurite transection is also increased in patients' NAGM compared to control tissue. Neurite damage and loss in the GM occur from the earliest stages of disease, as confirmed in biopsy material (Lucchinetti *et al.*, 2011).

Interestingly, the degree of meningeal inflammation, including the presence of ectopic B cell follicles, which are associated with fast disability progression in PMS, are associated with increased microglia activation and neurite damage in underlying cortical lesions and associated NAGM (Magliozzi *et al.*, 2007; Choi *et al.*, 2012). This suggests that toxic soluble mediators from the meningeal space may induce neurite damage either directly, or indirectly via activation of microglia.

Analogous findings have subsequently been made for diffuse axonal damage in normal appearing spinal cord white matter. Although there seems to be some correlation between axonal degeneration inside WM lesions and the periplaque WM or associated tracts, indicating that some diffuse axonal damage may be a symptom of anterograde or retrograde degeneration of axons damaged within focal lesions (Bjartmar *et al.*, 2001; Dziedzic *et al.*, 2010), most studies examining larger WM tracts have reported none or weak correlation between axonal loss and lesion load (Evangelou *et al.*, 2005; Kutzelnigg *et al.*, 2005; DeLuca *et al.*, 2006). Instead, diffuse axonal damage in spinal cord WM has been shown to correlate with inflammation in the overlying meninges and with local microglia activation (Androdias *et al.*, 2010; Reali *et al.*, 2020). Taken together, this indicates that the site at which an axon is first damaged may also lie outside of well-defined lesions.

1.2.2.2. Paraclinical studies of axonal degeneration in MS

Magnetic resonance imaging, MRI, is the most common tool to monitor disease activity in MS patients. Although overall MRI lesion activity does not predict long-term disease outcomes (Cree *et al.*, 2016), numerous cross-sectional and longitudinal studies have shown that MRI measures of brain and spinal cord atrophy do correlate with disability and can be used as prognostic tools (Losseff *et al.*, 1996; Ge *et al.*, 2000; Brownlee *et al.*, 2017; Rocca *et al.*, 2023). While measurements especially of white matter atrophy have historically been interpreted to represent axon loss, hard evidence for this correlation is lacking (Miller *et al.*, 2002; Barkhof *et al.*, 2009; Petrova *et al.*, 2018). It is therefore more useful to consider atrophy as a global marker for tissue degeneration, rather than an axon-specific one.

Diffusion MRI techniques in contrast provide higher pathologic specificity, as they can measure water molecule mobility along and perpendicular to axons. These techniques can be used to detect changes even in the normal appearing white matter of MS patients, are proven

to be sensitive to axonal damage and correlate with clinical disability (Rovaris *et al.*, 2005; DeBoy *et al.*, 2007; Agosta *et al.*, 2007).

A strong correlation between axonal degeneration and disability was also suggested by magnetic resonance spectroscopy studies looking at the metabolite N-acetyl aspartate (NAA) (Stefano *et al.*, 1998). NAA is a derivative of the amino acid aspartate and has been used as a neuronal marker due to its high abundance in neurons and their processes and absence in other CNS cell types (Simmons *et al.*, 1991). Post-mortem histological studies have confirmed that reduced NAA levels correlate with reduced axonal numbers (Bjartmar *et al.*, 2000). However, NAA levels also decrease in demyelinated axons, indicating that NAA is a marker for axonal damage, but does not necessarily indicate irreversible axon loss. Magnetic resonance spectroscopy studies in MS patients have shown that NAA decreases in acute lesions and to a lesser extent in the NAWM compared to healthy controls (Davie *et al.*, 1994). The reduction was evident from the earliest stages of disease (Filippi *et al.*, 2003). These findings are consistent with the description of axonal damage in histopathological studies. A negative correlation between NAA levels, indicative of axonal health, and disability has been seen in both cross-sectional (Lee *et al.*, 2000) and longitudinal studies (Stefano *et al.*, 1998).

Loss of axons in the retinal nerve fibre layer (RNFL) can be measured with optical coherence tomography (OCT), a method relying on infrared light reflection. Studies have found an RNFL thinning of 2 µm per year in MS patients even in the absence of optic neuritis, compared to only 0.2 µm in healthy controls. This underlines once again the presence of diffuse axonal damage in MS. Like other measures of axonal degeneration, RNFL thinning is evident from disease onset (Zimmermann *et al.*, 2018). In MS patients with optic neuritis, RNFL layer thickness correlates with visual function; in PPMS patients it was found to predict future disability (Trip *et al.*, 2005; Krämer *et al.*, 2024).

The best studied blood biomarker for MS disease progression is neurofilament light chain, an axonal structural protein that is released upon axonal degeneration. Serum neurofilament (NfL) is elevated in CIS, RRMS and PMS patients compared to age-matched controls, especially after recent relapses (Barro *et al.*, 2018; Dalla Costa *et al.*, 2019). NfL levels have also been found to correlate with current and future disability as well as with atrophy of brain and spinal cord (Barro *et al.*, 2018). Two retrospective military personnel studies, one of which uncovered the temporal relationship between EBV seroconversion and MS diagnosis, reported increased NfL levels already six years before diagnosis, yet always post seroconversion, consistent with early axonal damage in pre-diagnostic MS (Bjornevik *et al.*, 2020; Bjornevik *et al.*, 2022).

Taken together, paraclinical studies corroborate histopathological findings of early and widespread axonal degeneration in MS. They also show a clear, likely causative, association between axonal degeneration and disability. This emphasises the need for the development of axoprotective therapies for the adequate treatment of MS and prevention of long-term disability, as currently approved DMTs fail to halt neuroaxonal degeneration and lose efficacy in older patients (Weideman *et al.*, 2017; Woo *et al.*, 2024a).

1.2.2.3. Evidence of axonal degeneration in EAE

A comparative histological study of post-mortem MS and EAE tissue reported a highly similar degree and pattern of acute axonal damage in WM lesions (Kornek *et al.*, 2000). As in MS, axonal damage in EAE was associated with inflammation and thus more prominent in acute compared to chronic active or chronic lesions. Alterations in EAE NAWM have sporadically been reported (Howell *et al.*, 2010), but have not been investigated systematically. Focal axonal degeneration within white matter lesions is morphologically similar between EAE and MS. Yet whereas axonal swellings and axonal transection can be observed as "snapshots" in post-mortem MS tissue, longitudinal *in vivo* imaging in EAE revealed, that axonal degeneration is a stepwise process in which the swelling represents a reversible intermediate stage that can fully recover or proceed to fragmentation (Nikić *et al.*, 2011). An EAE model with initial relapsing-remitting and later progressive disease course has been used to show that initial disability correlates with inflammation while long-term disability is determined by axon loss, reflecting our current understanding of MS pathology (Wujek *et al.*, 2002). EAE is thus a suitable model to test whether axoprotective intervention at the reversible stage of axonal damage is feasible and can limit disability.

1.2.3. Molecular mechanisms of axonal degeneration in MS

The above chapter has outlined where and when axons degenerate in MS: most axonal damage happens acutely in the inflammatory lesion environment, whereas additional diffuse axonal damage in the NAWM may be attributable to low-grade inflammation. The following chapter will discuss how an inflammatory milieu and chronic demyelination can result in axonal energy crisis, calcium overload and, ultimately, axon disassembly. A special focus will lie on data derived from *in vivo* imaging of acute EAE lesions in the murine spinal cord. Although axonal degeneration in MS and EAE morphologically resembles Wallerian degeneration, cumulative evidence speaks against the involvement of this programmed axonal degeneration pathway (see *1.2.3.3 Axonal fragmentation pathways*). The chapter will conclude with an outlook on axoprotective treatment strategies.

1.2.3.1. Study of axonal degeneration in EAE with in vivo two-photon microscopy

In vivo imaging in animal models of disease allows for the longitudinal observation of pathological processes, as well as for genetic and pharmacologic intervention. The EAE model of multiple sclerosis can be used to study degenerative processes in neuroinflammatory lesions, which replicate key features of MS pathology such as immune cell infiltration, demyelination and axonal degeneration. Lesions in spinal cord dorsal white matter tracts are relatively easily accessible for imaging through dorsal laminectomy, i.e. the removal of the overlying vertebral arch (Nikić *et al.*, 2011). Two-photon microscopy is the method of choice for most *in vivo*

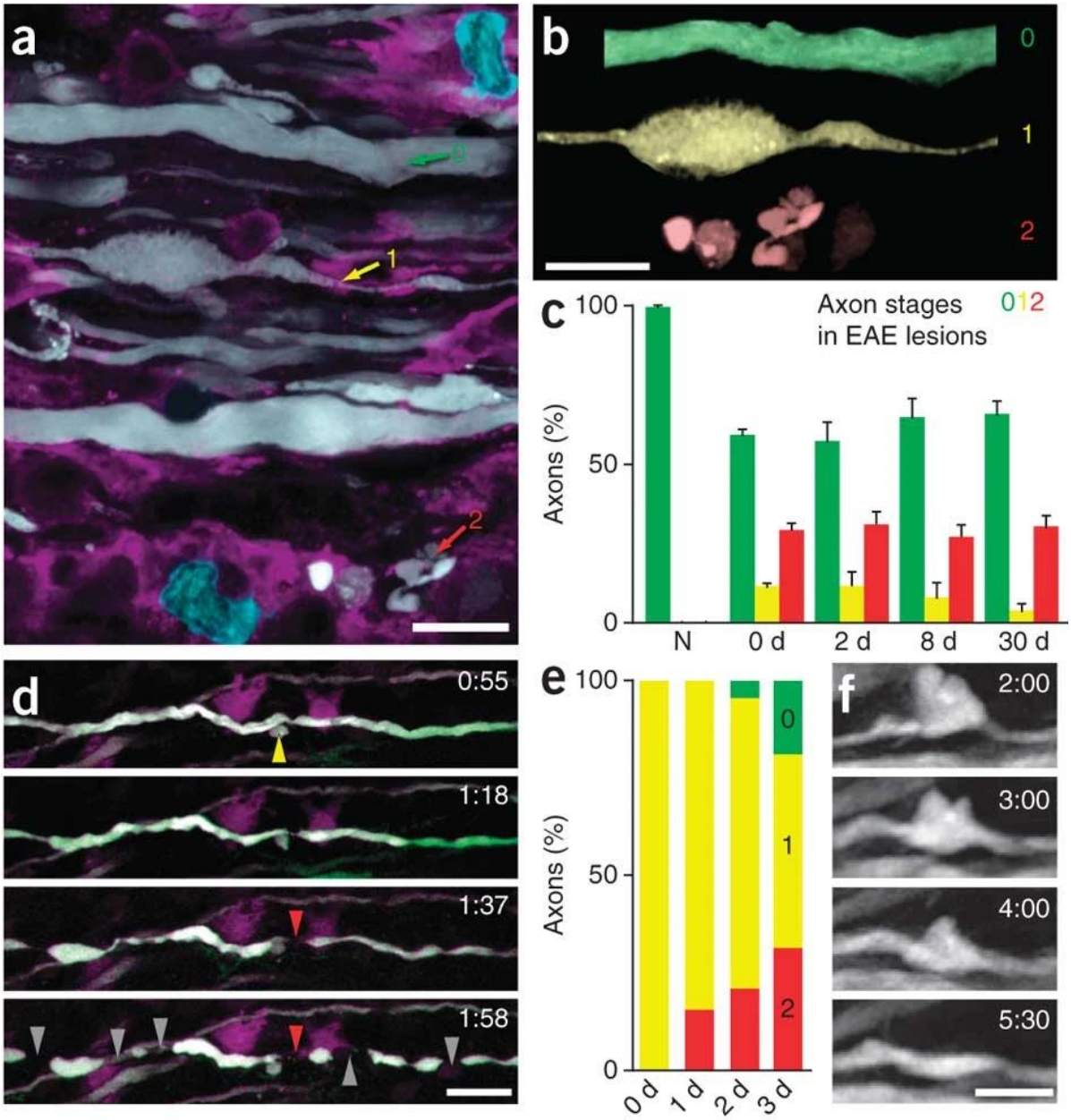

Figure 4 – Focal axonal degeneration in experimental autoimmune encephalomyelitis (EAE). **(a)** Projection image of an acute EAE lesion in spinal cord, showing axons (white), activated macrophages/microglia (magenta) and T cells (cyan). Representative axons for stage 0 ("normal"), stage 1 ("swollen") and stage 2 ("fragmented") are indicated and replicated in pseudocolour in **(b)**. **(c)** Quantification of the frequency (% ± standard error of the mean) of axon stages at different timepoints relative to EAE disease onset compared to normal spinal cord (N). **(d)** Timelapse showing an axon (white) transition from stage 1 ("swollen", yellow arrowhead) to stage 2 ("fragmented", red and grey arrowheads). Time is shown as h:min; macrophages/microglia in magenta, meningeal second harmonic scattering in green. **(e)** Fate tracking of stage 1 axons at peak of disease by daily imaging. **(f)** Timelapse showing an axon recover from stage 1. Time is shown as h:min. Scale bar 10 µm in (a, b, f), 25 µm in (d). EAE = experimental autoimmune encephalomyelitis.

imaging. It relies on fluorophore excitation by the simultaneous absorption of two long wavelength, low-energy photons instead of single high-energy photon absorption in conventional fluorescence microscopy. While this requires specialised, pulsed, high-output lasers to enable the simultaneous arrival of photons, it greatly improves imaging depth compared to single-photon microscopy, since longer wavelengths become less scattered while passing through the tissue (Xu *et al.*, 2024). Transgenic mouse lines expressing fluorescent proteins or biosensors in the Thy1 (thymocyte differentiation antigen 1) locus provide sparse neuronal labelling and thus enable fate tracking of single axons in the above described setup (Kerschensteiner *et al.*, 2005).

Nikić *et al.* (2011) have used this combination of methods to characterise the process of focal axonal degeneration (FAD) inside neuroinflammatory lesions (**Figure 4**). Axons in these lesions presented with three different morphologies: normal (stage 0), swollen (stage 1) or fragmented (stage 2) (**Figure 4a-c**). The same morphologies are observed in human MS lesions. Longitudinal imaging in mice demonstrated that FAD is a sequential process, characterised by the development of focal axonal swellings which persist for several hours or days and can progress to rapid axon fragmentation with end bulb formation (**Figure 4d, e)**. Importantly, some swellings recover spontaneously, allowing the axon to survive long-term (**Figure 4e, f**). Electron microscopy analysis of the lesioned tissue showed that axonal swelling precedes demyelination. Swollen yet myelinated axons were also found in human MS tissue. EAE lesion-spanning axons exhibited dysmorphic mitochondria, even in axons with normal morphology. This mitochondrial pathology was strictly limited to the immune infiltrated area. *In vivo* imaging suggested a detrimental role for macrophages/microglia which spend long time in close apposition with axons. Scavenging of reactive oxygen and nitrogen species (ROS, RNS), which are mainly produced by activated macrophages/microglia, induced increased recovery of swollen axons, whereas incubation with hydrogen peroxide (H_2O_2) exacerbated FAD. A related study showed that ROS/RNS-induced an axonal transport deficit that preceded mitochondrial pathology and swelling (Sorbara *et al.*, 2014). Taken together this indicates that acute, focal axonal degeneration in neuroinflammatory lesions is driven by macrophage-derived reactive species and independent of demyelination. The fact that initial damage is still reversible opens a window of opportunity for therapeutic intervention.

A follow-up study by Tai *et al.* (2023) further examined the role of mitochondria and energy metabolism in focal axonal degeneration. The study revealed a significant axonal ATP (adenosine triphosphate) deficit that was already present in morphologically normal axons, i.e. preceded irreversible damage. The ATP deficit was not due to oxidative damage of mitochondria which was only observed in stage 2 axons. Instead, proteomic analysis of axonal mitochondria, corroborated by immunostaining, demonstrated a lesion-specific depletion of the tricarboxylic acid (TCA) cycle enzymes isocitrate dehydrogenase 3 (Idh3) and malate dehydrogenase 2 (Mdh2). Overexpression of either enzyme increased axonal ATP levels but was not sufficient to prevent FAD.

Another crucial *in vivo* study by Witte *et al.* (2019) focussed on the role of calcium in FAD, as calcium plays a key role in injury-induced axonal degeneration (Yang *et al.*, 2013; Williams

et al., 2014). Calcium was found to be elevated above physiological levels in a substantial fraction of lesion-spanning axons. This was already observed in some morphologically normal, stage 0 axons, yet more frequent at stage 1 and 2. Fate tracking of individual axons demonstrated, that swollen axons with high calcium were likely to degenerate, whereas those with low calcium recovered. Importantly, some of the observed axons spontaneously returned from high to low calcium, indicating that calcium rise, much like swelling, may represent a reversible, therapeutically targetable process. Extracellular calcium chelation protected axons from FAD. Although further studies confirmed the extracellular space as the calcium source, none of the probed plasma membrane calcium channels could be associated with the influx. Instead, exclusion assays with differently sized fluorescent dyes showed an increased, unspecific permeability of the axonal membrane, indicating the existence of "nanoruptures" of approximately 10 nm diameter. The nature of these "nanoruptures" is currently unknown, however, the size is consistent with that of oligomeric protein pores which execute regulated cell death (Vandenabeele *et al.*, 2023). Likewise, lipid peroxidation induced by reactive species can alter axonal membrane permeability (Pedrera *et al.*, 2021; Mauker, Beckmann *et al.*, 2024). Increased membrane permeability clearly correlated with intra-axonal calcium levels, confirming that calcium influx via membrane nanoruptures drives axonal degeneration in neuroinflammatory lesions.

In summary, these studies give insights into the events that initiate, accompany and drive axonal degeneration in neuroinflammatory lesions. Many of the identified processes have been corroborated by findings in MS (see below) or other neurodegenerative diseases (Andreone *et al.*, 2020; Jadiya *et al.*, 2021). Understanding the molecular details of this initially reversible degenerative process is important, to identify promising targets and develop translatable treatment approaches.

1.2.3.2. Axonal stressors in MS lesions

The *in vivo* studies, summarised above, point to a role for reactive species, mitochondrial pathology, axonal transport deficit, membrane permeabilisation and calcium overload in inflammatory axonal degeneration. This chapter will briefly outline evidence for the relevance of these EAE findings to MS.

Reactive oxygen and nitrogen species are actively produced within multiple sclerosis lesions, as indicated by the upregulation of associated genes (Bagasra *et al.*, 1995; Fischer *et al.*, 2012). Oxidative damage to DNA and lipids within lesions is well documented and specifically oxidised phospholipids are believed to exacerbate neurodegeneration (Haider *et al.*, 2011; Dong *et al.*, 2021).A causative role for reactive species in axonal degeneration would explain the close correlation between the degree of immune infiltration and axonal damage in different MS lesion subtypes (Frischer *et al.*, 2009). This association can also be extended to smouldering lesions with their iron rims, as iron can further amplify oxidative stress and these lesions are associated with increased axonal damage (Lassmann *et al.*, 2012; Maggi *et al.*, 2021).

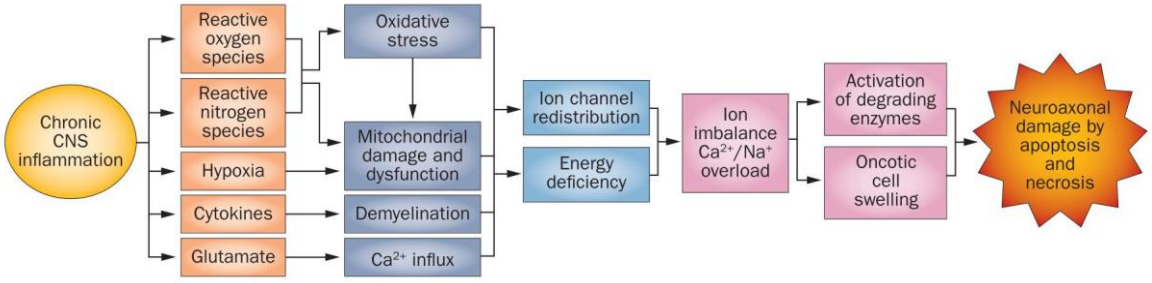

Figure 5 – Proposed cascade leading to neuroaxonal dysfunction and degeneration in MS.
The scheme illustrates a sequential yet interrelated process of how an inflammatory milieu and chronic demyelination may result in axonal energy crisis, calcium overload and eventually axon disassembly. Please note that this cascade represents the state of knowledge of 2014 and does not distinguish between neuronal (somatic) and axonal degeneration.

Multiple pathways in MS converge on mitochondrial pathology and energy deficiency (**Figure 5**). Mitochondrial DNA, due to its lack of protective histones, is particularly vulnerable to oxidative stress and mitochondrial deletions are frequently observed in MS (Campbell *et al.*, 2011). Mitochondrial function is further impaired by the reduced expression of key components of the respiratory chain, which may be due to dysregulation of the so-called "master regulator of energy metabolism" PGC-1α (peroxisome proliferator-activated receptor γ coactivator 1α) (Mahad *et al.*, 2008; Mahad *et al.*, 2009; Witte *et al.*, 2013). What is more, calcium overload (see below), when spreading to mitochondria, can reduce ATP-production and increase ROS production (Brookes *et al.*, 2004; Pandya *et al.*, 2013). The mechanisms impairing mitochondrial function are on the other side opposed by an increased energy demand in demyelinated axons which have lost their metabolic support and redistribute sodium channel to re-establish less energy-efficient, non-saltatory conduction (Craner *et al.*, 2004). This condition of mismatched energy supply and demand is also referred to as virtual hypoxia and may explain, why indeed, lesions in SPMS patients mostly form in the less perfused, watershed areas between major vessels (Holland *et al.*, 2012).

Of note, impairment of axonal transport, which is also apparent in MS lesions (Ferguson *et al.*, 1997; Bitsch *et al.*, 2000), may be both a symptom of and contributor to energy deficiency. It is dependent on ATP but also responsible for meeting energy requirements by distribution of mitochondria. Axonal transport may be further impaired by reactive species, TNFα and calcium overload, all of which are present within lesions and have been associated with microtubule destabilisation or detachment of cargo from motor proteins (van den Berg *et al.*, 2017; Kneussel and Friese, 2021).

Unspecific membrane permeabilisation through "nanoruptures", as suggested as a driver of focal axonal degeneration in EAE lesions, has not been described in MS. However, possible explanations for these "nanoruptures" are compatible with current knowledge of MS pathology. If the nanoruptures are indeed a result of lipid peroxidation, this would provide a direct

link between reactive species and axonal degeneration. Lipid peroxidation is also a central element of ferroptosis, an iron- and oxidation-dependent form of regulated cell death (RCD) and the presence of both oxidised lipids and iron in MS lesions (van San *et al.*, 2023), as well as downregulation of antioxidant genes (Hu *et al.*, 2019), has sparked interest in its contribution to MS pathology. However to date, evidence for ferroptosis involvement in MS is mostly circumstantial and mechanistic studies in EAE have not specifically assessed axonal permeabilisation or degeneration (Rothammer *et al.*, 2022; Luoqian *et al.*, 2022; van San *et al.*, 2023; Woo *et al.*, 2024b). Other RCD pathways that terminate in membrane permeabilisation are necroptosis and pyroptosis. While there are reports of necroptosis in MS (Ofengeim *et al.*, 2015; Picon *et al.*, 2021) and inflammasome assembly, a pre-requisite for pyroptosis, was observed in lesions (Barclay and Shinohara, 2017), none of these or other RCDs have been studied in axons.

In contrast, calcium overload and ionic imbalance at large are considered important contributors to neuroaxonal degeneration in MS (**Figure 5**). Yet unlike reported by Witte *et al.* (2019), the hitherto proposed mechanisms of calcium overload in MS depend on dedicated calcium channels and pumps. Glutamate excitotoxicity and reverse action of the Na^+/Ca^{2+} exchanger due to sodium overload are considered the main drivers of excessive calcium influx in MS (Craner *et al.*, 2004; Friese *et al.*, 2014). Sodium overload in turn results from demyelination, sodium channel redistribution and a disbalance between energy supply and demand at the Na^+/K^+ ATPase (Waxman, 2006). Multiple other ion channels permeable to Na^+, K^+ or Ca^{2+} have been implicated in MS and EAE pathology (Friese *et al.*, 2014), yet the overall failure of specific channel blockers in clinical trials for progressive MS has discouraged the view of MS as an acquired channelopathy (Kapoor *et al.*, 2010; Chataway *et al.*, 2020). Regarding glutamate excitotoxicity, which was experimentally excluded to contribute to FAD in EAE, different mechanisms may exist between calcium overload of axons and somata (Witte *et al.*, 2019).

1.2.3.3. Axonal fragmentation pathways

Several stressors to axonal function and integrity have been described above for both EAE and MS. However, the question remains, how these culminate in axon fragmentation and loss. In EAE, intra-axonal calcium has been identified as the key driver tipping the scale from reversible damage to irreversible axon fragmentation. Similarly, the different stressors in the MS lesion environment and maladaptive compensation strategies have been suggested to culminate in neuroaxonal calcium overload and subsequent demise (Friese *et al.*, 2014).

The sequential process of axonal swelling, followed by axon disassembly after a latent phase seen in FAD is reminiscent of Wallerian degeneration, a stereotypic process originally described after axonal transection (Waller, 1851). Wallerian degeneration leads to axonal fragmentation distal to the damage site while the proximal axon and the soma stay intact. Molecular studies have shown that much like programmed cell death, Wallerian degeneration is an active, genetically encoded self-destruction process. It is initiated when NAD (nicotinamide

adenine dinucleotide) levels in the distal axon drop following a loss of supply of the NAD synthesising enzyme NMAT2 (nicotinamide mononucleotide adenylyltransferase 2) from the soma post transection. A subsequent activation of the NADase Sarm1 (sterile-α and Toll/interleukin 1 receptor motif containing protein 1) further accelerates NAD depletion (Coleman and Höke, 2020). A Wallerian-like degeneration mechanism can also be triggered independently of axonal transection for example, when an axonal transport deficit causes insufficient NMAT2 supply (Coleman and Höke, 2020). Wallerian degeneration post damage can be slowed – or in some Wallerian-like axonopathies even completely prevented – by axonal overexpression of NMAT (Wallerian degeneration slow (Wlds) mouse mutant) or by knockout of Sarm1 (Gilley *et al.*, 2017). Small molecule Sarm1 inhibitors are currently undergoing preclinical testing for different axonopathies and have been advertised for the treatment of MS (Hughes *et al.*, 2021; Bratkowski *et al.*, 2022). The events downstream of Sarm1 are incompletely understood but seem to involve calcium mobilisation and calpain activation (Ko *et al.*, 2021; Li *et al.*, 2022; Ma *et al.*, 2013; Yang *et al.*, 2013).

Despite the obvious parallels, a role for Wallerian degeneration in MS is questionable. Axonal transection clearly occurs (Trapp *et al.*, 1998) and is followed by fragmentation of the distal stump, contributing to diffuse axonal loss in the NAWM (Dziedzic *et al.*, 2010). The degeneration process morphologically resembles Wallerian degeneration and entails an axonal transport deficit (Ferguson *et al.*, 1997; Nikić *et al.*, 2011; Sorbara *et al.*, 2014). However, EAE induction in Wlds and Sarm1 knockout (KO) mice have yielded conflicting results, overall with more negative (Singh *et al.*, 2017; Wesolowski, 2018; Viar *et al.*, 2020; Liu *et al.*, 2023b) than positive (Kaneko *et al.*, 2006) reports. Other studies show immune-mediated rather than primary axoprotective effects (Chitnis *et al.*, 2007; Zhang *et al.*, 2023). In summary, axonal degeneration in MS is likely not regulated by the NMAT2-NAD-Sarm1-axis, meaning that Sarm1 inhibitors are unlikely to prevent axonal transection and loss in MS.

In summary, this suggests that axonal fragmentation in MS and EAE is driven by a calcium-dependent, Sarm1-independent process. Two mechanisms downstream of calcium overload have been suggested to mediate axonal degeneration: opening of the mitochondrial permeability transition pore (mPTP) (Barrientos *et al.*, 2011; Villegas *et al.*, 2014) and calpain overactivation (Ma *et al.*, 2013; Yang *et al.*, 2013; Williams *et al.*, 2014). These will be briefly revisited at the end of chapter *1.3 Calcium in physiology and pathology*.

1.2.3.4. Axoprotective therapeutic approaches

As outlined above, Sarm1 inhibitors will likely not halt axonal degeneration in MS. However, the factors leading to degeneration are increasingly well understood and several promising therapeutic targets can be inferred. This includes oxidative damage which impairs axonal functions and may lead to cell death by ferroptosis. Indeed, two antioxidants, N-acetyl cysteine and lipoic acid are currently undergoing clinical trials for the treatment of progressive MS. For lipoic acid, phase 2 has already been completed and reported a 68 % reduction in brain

atrophy compared to placebo (Spain *et al.*, 2017). Mitochondrial energy supply may be another target for axoprotective intervention in MS. However, three drugs, high-dose biotin, idebenone and fluoxetine, which were proposed to have positive effects on mitochondria, failed in recent PMS clinical trials (Cree *et al.*, 2020; Kosa *et al.*, 2020; Chataway *et al.*, 2020). Another drug with proposed mitochondrial mechanism of action, nicotinamide riboside, has entered phase 2. Of note, experiments by Tai *et al.* (2023) also failed to prevent axonal degeneration despite partially restored ATP levels. In contrast, a study of PGC-1α overexpression in EAE did report increased axonal preservation (Rosenkranz *et al.*, 2021). Acute axonal degeneration in EAE seems to be independent of demyelination. Nevertheless, remyelinating drugs may have beneficial effects on long-term axonal energy homeostasis and axonal function at large by re-establishing saltatory conduction and oligodendrocytic support.

As calcium was found to be the key checkpoint of axonal degeneration in EAE, the aim of this thesis was to explore the suitability of calcium modulation as a therapeutic target (see also chapter *1.4 Aims of this thesis*). This comes with unique challenges as calcium also has numerous physiological functions, making it necessary to target "surplus" calcium specifically.

1.3. Calcium in physiology and pathology

Inorganic ions are essential for cell biology: Na^+, K^+ and Cl^- establish the membrane potential while Mg^{2+}, Zn^{2+}, Cu^{2+} and more catalyse chemical reactions as cofactors for enzymes. The function of calcium, Ca^{2+}, which acts as a messenger, is unique among inorganic ions. The ability to decode calcium signals, demands the existence of proteins that undergo conformational change upon Ca^{2+} binding as well as the maintenance of low intracellular free Ca^{2+} concentration at baseline (Schwaller, 2012). Most intracellular calcium is therefore complexed by protein. Evolutionarily, this system may have evolved due to calcium's advantageous coordination chemistry and the necessity to prevent precipitation of poorly soluble calcium phosphates (Carafoli and Krebs, 2016). The set point of intracellular Ca^{2+} concentrations around 50 - 100 nM leads to a 10 000-fold calcium gradient across the plasma membrane (Schwaller, 2012). While the membrane prevents passive diffusion, the regulated opening of plasma membrane calcium channels forces calcium into the cell, along its gradient. On the flipside, this setup also entails that a loss of membrane barrier function e.g. due to mechanical injury will inundate the cell with calcium. This leads to the persistent activation of calcium-dependent proteases and phospholipases and thus eventually to cell death (Carafoli and Krebs, 2016). Membrane repair mechanisms, that are triggered by an increase in Ca^{2+}, exist and may under some circumstances halt the calcium influx and enable a return to homeostatic levels (Zhen *et al.*, 2021).

The following chapters will provide further detail about physiological calcium signalling, homeostatic mechanisms that prevent calcium overload and the deleterious consequences of the latter.

1.3.1. Calcium signalling

The calcium signalling toolkit consists of a set of receptors, second messengers and channels, which produce the signal, calcium-binding proteins, that further shape the signal, calcium sensors that translate it into downstream effects and calcium transporters and pumps that remove calcium from the cytosol to terminate signalling.

Calcium can enter the cell either through the plasma membrane via voltage- or ligand-gated channels or be released into the cytosol from the endoplasmic and sarcoplasmic reticulum (ER, SR) (**Figure 6**, "On" reactions). Voltage-gated calcium channels are expressed in excitable cells and couple excitation to neurotransmitter release or to muscle contraction (Catterall, 2011). Ligand-gated ion channels, also called ionotropic receptors, are either anion- (Cl^-) or cation- (Na^+, K^+, Ca^{2+}) selective. Cation-selective receptors include the ionotropic glutamate receptors NMDAR and AMPAR, the nicotinic acetylcholine receptor and the serotonin receptor 5-HT_3. Their primary function is to induce depolarisation (Rao *et al.*, 2022). The extent to which they also activate calcium-sensitive processes depends on their respective calcium-permeability. While NMDAR is predominantly a calcium channel and largely responsible for strengthening synaptic connections in the calcium-mediated process of long-term potentiation, most AMPAR subtypes are impermeable to calcium (Lüscher and Malenka, 2012; Dong *et al.*, 2009). Thus, on the flipside, NMDAR is also the main channel responsible for glutamate excitotoxicity. Other cation-selective ligand-gated channels with calcium permeability are transient receptor potential (TRP) channels and acid-sensing ion channels (ASIC), which are involved in different sensory processes (Moran, 2018; Wemmie *et al.*, 2013).

Calcium signalling can also be initiated by calcium release from the ER or SR via the ryanodine receptor (RyR) or inositol-1,4,5-trisphosphate (IP_3) receptor (IP_3R). In non-muscle cells, the RyR can be activated by calcium (calcium-induced calcium release) or cADPR (cyclic adenosine diphosphate ribose) (Brini *et al.*, 2014). The IP_3R is activated by IP_3, a second messenger generated through hydrolysis of phosphatidylinositol 4,5-bisphosphate (PIP_2) in the plasma membrane by phospholipase C (PLC). PLC activation in turn is a common downstream signal of various membrane receptors, including metabotropic glutamate receptors, several growth factor receptors, Toll-like receptors and T cell receptors, to name just a few (Reiner and Levitz, 2018; Bill and Vines, 2020). While the extracellular calcium reservoir for signalling is virtually endless due to the 10.000-fold gradient, the ER/SR can become calcium depleted which induces refilling from the extracellular space by so-called store-operated calcium entry (SOCE) (Courjaret *et al.*, 2024).

Once entering the cytosol, Ca^{2+} cannot freely diffuse due to the abundance of calcium-binding species. Particularly high Ca^{2+} concentrations are thus only present in direct proximity to the channel (Naraghi and Neher, 1997). Dedicated calcium-binding proteins (CaBPs) can shape the calcium signal due to their reversible binding kinetics that favour binding when and where calcium is high and favour calcium release once calcium levels decrease, either after time (due to calcium pumps removing Ca^{2+} from the cytosol, see below) or after diffusion of the CaBPs away from the release site. Fast-acting CaBPs thus lower the calcium amplitude but stretch

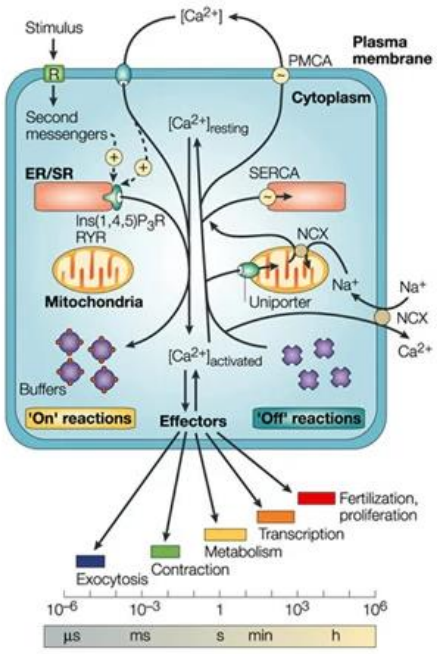

Figure 6 – Calcium signalling.
Simplified depiction of the calcium signalling toolkit, divided into "On" reactions (left) and "Off" reactions (right). Signalling is switched "On" by calcium entry via the plasma membrane or release from ER/SR signalled by a second messenger. Calcium-binding proteins – cytosolic calcium buffers – bind calcium, as do the effectors that translate the calcium signal into action. This happens on a timescale from microseconds (exocytosis) to minutes and hours (transcription, proliferation). "Off" reactions involve subcellular storage into the ER/SR and mitochondria as well as extrusion via the plasma membrane. Calcium buffers become calcium unbound at rest. ER = endoplasmic reticulum, SR = sarcoplasmic reticulum, Ins(1,4,5)P_3R = inositol-1,4,5-trisphosphate receptor (also IP_3R in the main text), NCX = sodium calcium exchanger (mitochondrial exchanger is referred to as NCLX in the main text), SERCA = sarco-/endoplasmic reticulum calcium ATPase, PMCA = plasma membrane calcium ATPase.

the signal in time and space. Slow-acting CaBPs miss the amplitude but increase the initial decay rate. This has differential effects on facilitation of subsequent calcium pulses (Sala and Hernández-Cruz, 1990; Schwaller, 2010).

In contrast to "pure" calcium-binding proteins, calcium sensors undergo a conformational change that activates their function. Some calcium sensors have very narrow functions, such as synaptotagmin for exocytosis, while others act more broadly (Brini *et al.*, 2013). This is particularly true for calmodulin, which upon calcium-binding can activate numerous downstream targets that cannot bind calcium directly. Both calcium and calmodulin act as allosteric modulators. Calmodulin's targets include several kinases (most of them called calmodulin-dependent kinases (CaMK)) as well as the phosphatase calcineurin (Brini *et al.*, 2013). The protein kinase C (PKC) in contrast is activated directly by Ca^{2+}. It goes without saying, that these kinases and phosphatase in turn have numerous downstream effects. Calcium signalling can affect mechanisms as central as transcription (e.g. via CaMK-mediated activation of the transcription factor CREB (cAMP response element-binding protein)) and energy metabolism (via calcium-regulated TCA cycle enzymes) (Hardingham *et al.*, 2001; Denton, 2009) (**Figure 6**, Effector functions). Calcium also activates the protease family of calpains. The ubiquitously expressed calpains 1 and 2 are also called µ-calpain and m-calpain, in reference to their *in vitro* calcium affinities. These names are somewhat misleading, as both calpains have physiological functions, and must thus be activatable at physiologically reachable calcium levels. Indeed, membrane localisation has been suggested to significantly lower m-calpain's calcium requirement (Leloup *et al.*, 2010). Calpains do not degrade but rather modulate their targets, which include cytoskeletal proteins, the plasma membrane calcium pump and protein kinase C (Carafoli *et al.*, 2001). Excessive calpain activation due to prolonged calcium overload has been implicated in the pathology of neurodegenerative diseases (Metwally *et al.*, 2021).

A constant removal of calcium from the cytosol is necessary to terminate the individual calcium spikes and prevent long-term calcium overload. This task is performed by calcium exchangers and pumps in the plasma membrane (sodium calcium exchanger, NCX, and plasma membrane Ca^{2+} ATPase, PMCA), in the ER/SR membrane (sarco-/endoplasmic reticulum Ca^{2+} ATPase, SERCA) and in the mitochondrial membrane (mitochondrial calcium uniporter, MCU) (Berridge *et al.*, 2003) (**Figure 6**, "Off" reactions).

1.3.2. Cellular calcium homeostasis

While the above chapter has looked at calcium handling from a signalling standpoint, many of the same mechanisms are also involved in preventing calcium overload, which would cause uncontrolled activation of calcium-dependent mechanisms, followed by cellular dysfunction or cell death and is a common observation in several neurodegenerative diseases (Jadiya *et al.*, 2021). The three main routes to clear cytosolic calcium are (1) buffering by calcium-binding proteins, (2) subcellular storage in ER and mitochondria and (3) extrusion via the plasma membrane. These mechanisms will be discussed below with an emphasis on the neuro- and axoprotective potential of their therapeutic enhancement.

1.3.2.1. Calcium buffering by calcium-binding proteins

Technically speaking, all macromolecules that bind calcium, including calcium-sensing proteins, effectively act as buffers and lower the amount of free Ca^{2+}. In practice however the term "cytosolic calcium buffer" is only applied to a small group of calcium-binding proteins whose primary function is to reversibly bind calcium. These cytosolic calcium buffers are parvalbumin α (PV) and β (oncomodulin), calbindin-D9K, calbindin-D28k (CB) and calretinin (CR) (Schwaller, 2010). Each of these proteins comprises two to six calcium-binding sites called EF hand domains. Importantly, the calcium dissociation constants of these buffers range from approximately 200 nM to 1.5 mM and thus lie above the baseline intracellular calcium concentrations of 50 - 100 nM. This means that at rest, most CaBPs are in an unbound state and available to bind calcium upon influx (Schwaller, 2010). PV, CB and CR are expressed in neurons, yet different neuronal populations express different calcium-binding proteins, and KO studies suggest that they are not functionally redundant. This is best studied in cerebellum, where Purkinje cells express both PV and CB, granule cells express CR and stellate and basket cell express PV only (Schwaller *et al.*, 2002). Each single CaBP KO has a cerebellar phenotype with no compensatory upregulation of the other CaBPs observed (Airaksinen *et al.*, 1997; Schiffmann *et al.*, 1999; Schwaller *et al.*, 2004). The buffering effect of CaBPs is furthermore concentration-dependent (Schwaller *et al.*, 2002; Airaksinen *et al.*, 1997; Hack *et al.*, 2000) and expression levels – depending on the specific protein and cell type – often reach levels as high as 30 - 150 µM (Schwaller, 2010).

Due to their potential to act as transitory calcium sinks, the question has been raised whether CaBPs can confer protection against calcium overload and neurodegeneration. Numerous descriptive studies have shown relative sparing of CaBP expressing neuronal populations in distinct neurodegenerative diseases, yet without providing evidence for causation. Indeed, studies on ischemia and excitotoxicity in the hippocampus have demonstrated that there is no clear correlation between endogenous CaBP expression patterns and vulnerability to neuronal cell death (Freund *et al.*, 1990; Freund *et al.*, 1992). What is more, CB knockout reduces neuronal cell death in a model of excitotoxicity, but exacerbates neuronal loss in an AD model, indicating that calcium regulation by CaBPs is more complex than simple removal of free calcium (Klapstein *et al.*, 1998; Kook *et al.*, 2014).

While there seems to be no infallible neuroprotective effect of endogenous CaBPs, studies of CaBP overexpression suggest that increased CaBP levels can increase neuronal resilience at least in some settings. Two very similar comparative studies suggest, that overexpression of CB or CR but not PV can protect against excitotoxicity *in vitro* (D'Orlando *et al.*, 2001; D'Orlando *et al.*, 2002). A protective effect of PV overexpression on excitotoxicity has been examined in two further studies, one confirming, one challenging these findings (Hartley *et al.*, 1996; van den Bosch *et al.*, 2002). Only one further study on CR overexpression could be found, which showed no effect of CR overexpression in ionophore-induced calcium overload (Kuźnicki *et al.*, 1996). CB overexpression has been studied more broadly and several studies have reported protective effects. This includes *in vitro* studies modelling excitotoxicity (Monje *et al.*, 2001; D'Orlando *et al.*, 2001; D'Orlando *et al.*, 2002), Alzheimer's (Guo *et al.*, 1998), Parkinson's (Sun *et al.*, 2011; Jung *et al.*, 2019) and amyotrophic lateral sclerosis (Ho *et al.*, 1996; Roy *et al.*, 1998) and notably also some *in vivo* studies in models of excitotoxicity (Phillips *et al.*, 1999), Parkinson's (Inoue *et al.*, 2019) and ischemia (Yenari *et al.*, 2001; Fan *et al.*, 2007). A study of long-term CB overexpression however found no neuroprotective effect in ischemic stroke (Freimann *et al.*, 2010) and other negative studies may have remained unreported. In summary, neuroprotective effects of CaBPs seem to be context-dependent and will have to be explored for each disease setting individually.

1.3.2.2. Calcium uptake into the ER

A second way that cells employ to lower cytosolic calcium levels is subcellular storage in the ER and in mitochondria. Uptake into the ER is mediated by the sarco-/endoplasmic reticulum Ca^{2+} ATPase (SERCA). As the calcium concentration of the ER is maintained between 200 and 800 µM (Case *et al.*, 2007), calcium has to be transported into the ER actively, against its concentration gradient. Large parts of ER calcium are bound to the ER-specific CaBP calreticulin, which increases the ER's calcium storage capacity (Nakamura *et al.*, 2001). SERCA activity is mostly regulated by cytosolic calcium levels. Due to its high calcium affinity, it becomes activated already by modest cytosolic elevations in Ca^{2+}, thus contributing to restoration of baseline calcium levels (Berridge *et al.*, 2003). At the same time, this mechanism serves to replenish ER calcium stores, which can become depleted by ER calcium release during signalling. SERCA dysfunction has been implicated in calcium dyshomeostasis

and ER stress, which can be alleviated by pharmacologic activation of SERCA (Kang *et al.*, 2016). Similarly, SERCA overexpression in models of ischemia-reperfusion injury was found to reduce cytosolic and mitochondrial calcium overload, thereby overall reducing damage (Li *et al.*, 2020; Tan *et al.*, 2020).

1.3.2.3. Calcium uptake into mitochondria

Uptake of calcium into mitochondria is mediated by the mitochondrial calcium uniporter, MCU (Baughman *et al.*, 2011). At baseline, mitochondrial calcium levels are similar to those in the cytosol, at approximately 100 nM (Szabadkai and Duchen, 2008). However, mitochondria take up calcium to levels of up to 500 nM to increase metabolism upon cytosolic calcium increase. Mitochondria also act as first responders in cases of pathological calcium overload and can temporarily store large amounts of calcium in the form of hydroxyapatite crystals (Zündorf and Reiser, 2011). Massive mitochondrial calcium uptake however impairs metabolism and can lead to opening of the mitochondrial permeability transition pore (mPTP) and cell death if calcium homeostasis is not swiftly restored (Pandya *et al.*, 2013; Bernardi *et al.*, 2023).

The outer mitochondrial membrane (OMM) is highly permeable to calcium and other ions via the voltage-dependent anion channels (VDACs). Mitochondrial matrix calcium levels are controlled at the inner mitochondrial membrane (IMM) with MCU and NCLX (mitochondrial sodium calcium exchanger) being the main routes of calcium uptake and release respectively (Rossi *et al.*, 2019). MCU's calcium affinity of approximately 20 μM is very low. It is therefore only able to take up calcium at so-called mitochondria-ER contact sites (MERCs), which are established by the physical tethering of the ER calcium release channel IP_3R to mitochondrial VDAC1 via the cytosolic chaperone Grp75 (glucose-related protein 75) (Szabadkai *et al.*, 2006). Calcium flux from the ER into the mitochondrial inter-membrane space via this structure creates calcium microdomains, which enable MCU-mediated calcium uptake into the mitochondrial matrix (Csordás *et al.*, 1999). The action of MCU is not ATP-dependent. Instead, the mitochondrial membrane potential drives the uptake of cations into the matrix. Inside mitochondria, calcium promotes ATP production by increasing the activity of three key TCA cycle enzymes, pyruvate dehydrogenase phosphatase, isocitrate dehydrogenase and oxoglutarate dehydrogenase (Denton, 2009). Particularly in neurons, the calcium link between neuronal activity (i.e. energy expenditure) and energy production is an important adaptive mechanism. This is further emphasised by the brain-specific expression of the MICU3 subunit of MCU, which enhances MCU-mediated calcium uptake (Patron *et al.*, 2019).

As mentioned above, mitochondria can act as calcium sinks in conditions of cytosolic calcium overload. However, mitochondrial calcium overload itself can also be detrimental to cells, as it leads to an impaired ATP production and increased ROS production (Brookes *et al.*, 2004; Pandya *et al.*, 2013). Calcium and ROS can furthermore activate the mitochondrial permeability transition pore (mPTP), a complex spanning both IMM and OMM, whose opening dissipates the mitochondrial membrane potential and therefore leads to an efflux of calcium

along its concentration gradient (Bernardi *et al.*, 2023). While transient mPTP opening can occur as part of physiological homeostatic processes, prolonged opening causes mitochondrial swelling and necrotic cell death.

Subcellular calcium uptake into mitochondria under conditions of cytosolic calcium overload is thus a double-edged sword. It is therefore questionable whether an intervention that would increase mitochondrial calcium uptake would be beneficial for axonal survival, due to calcium relief in the cytosol or detrimental due to mitochondrial impairment and induction of necrosis. A recent comparative study in drosophila showed, that MCU deletion or NCLX overexpression rescued neurodegenerative phenotypes in models of Alzheimer's, Parkinson's, Huntington's and frontotemporal dementia (Twyning *et al.*, 2024), indicating that in these diseases (or at least their drosophila models) mitochondrial rather than cytosolic calcium overload causes degeneration. In contrast, unpublished data from the group of Philip Williams suggests, that MCU overexpression may be beneficial for retinal ganglion cell survival after optic nerve crush injury (presented at Neuroscience 2024). Studies in EAE have shown a beneficial effect of mPTP inhibition (Forte *et al.*, 2007; Warne *et al.*, 2016), yet, *in vivo* imaging of focal axonal degeneration indicates, that mitochondrial calcium overload only happens after irreversible axonal transection (Tai *et al.*, 2023). Cytosolic calcium overload in contrast is an early event, that precedes and determines degeneration (Witte *et al.*, 2019). Indeed, MCU deficiency in EAE exacerbates axonal degeneration (Holman *et al.*, 2020), indicating that mitochondrial calcium uptake has a protective function. Whether this extends to manipulations of increased mitochondrial calcium uptake would have to be determined experimentally. On a different take, increased mitochondrial activity in consequence of PGC-1α overexpression has been suggested to improve mitochondrial calcium buffering capacity (Rosenkranz *et al.*, 2021).

1.3.2.4. Calcium extrusion via the plasma membrane

Returning calcium to the extracellular space is the task of the calcium transporters PMCA and NCX. It is the most long-term solution to counter intracellular calcium accumulation, yet energy-intensive and easily saturated.

The plasma membrane calcium ATPase (PMCA) actively extrudes calcium across the plasma membrane. Similarly to the SERCA pump, it has a high calcium affinity, i.e. is active at modest calcium elevation (Berridge *et al.*, 2003). Its quantitative contribution to calcium clearance is low compared to the more abundant transporters SERCA and NCX and it has been suggested that PMCA is not a global calcium regulator but instead modulates sub-membrane domain calcium signalling (Brini *et al.*, 2017).

The sodium calcium exchanger NCX in contrast has a lower calcium affinity but high transport capacity (Berridge *et al.*, 2003). It uses the sodium gradient generated by the Na^+/K^+ ATPase to exchange one Ca^{2+} ion for three Na^+ ions (Lytton, 2007). This transport is fully reversible, meaning that under conditions of sodium overload, as suggested in demyelination (Craner *et al.*, 2004), the NCX can function in reverse-mode, exporting sodium and importing

calcium. Consequently, whether the NCX should be blocked or activated to counteract calcium overload is context-dependent. Interestingly, pharmacological inhibition of NCX with bepridil during two-photon imaging of neuroinflammatory lesions in EAE significantly favoured axonal fragmentation over recovery, indicating that in this context, NCX action is protective, likely due to forward-mode calcium extrusion (Witte *et al.*, 2019). Neurounina-1 is a pharmacologic activator of NCX and has been shown to be neuroprotective in animal models of stroke and amyotrophic lateral sclerosis (Cerullo *et al.*, 2018; Anzilotti *et al.*, 2021). It has not yet been tested in EAE.

1.3.3. Role of calcium in cell death and axonal degeneration

Calcium is a ubiquitous messenger and one of the many signals it provides is the signal for cell death. Depending on the circumstances, calcium can act as a death switch in regulated cell death pathways or induce uncontrolled necrosis. The same is true for axonal degeneration, where calcium is an executioner in programmed Wallerian degeneration, but may also activate axonal degeneration independently of the NAD-depletion machinery in a yet unnamed destruction pathway characterised by calpain overactivation.

1.3.3.1. Role of calcium in cell death

The versatility of the calcium signal, even in cellular demise, is well exemplified by the finding that NMDA-induced excitotoxicity can lead to either apoptotic or necrotic cell death morphology, depending on the dosage (Bonfoco *et al.*, 1995).

The direct link between calcium overload and necrosis is well characterised and has been termed mitochondrial permeability transition (MPT)-driven necrosis by the Nomenclature Committee on Cell Death (Galluzzi *et al.*, 2018). As described above, mitochondrial calcium and ROS overload can induce the opening of the mitochondrial permeability transition pore (mPTP) which dissipates the mitochondrial membrane potential. The precise mechanism of mPTP opening is unclear, but is known to require cyclophilin D (Galluzzi *et al.*, 2018). Prolonged mPTP opening invariably leads to ATP depletion and necrosis. It has been debated whether mPTP opening can also release cytochrome c, mediator of intrinsic apoptosis, from the inter-membrane space into the cytosol and thus trigger apoptosis instead of necrosis under conditions of sustained energy levels (Bernardi *et al.*, 2023). Indeed, the connection between calcium and apoptosis is complex, as they interact on different levels which can further be described by (1) regulation of apoptosis initiators and effectors by calcium-regulated enzymes like calcineurin and calpain (Wang *et al.*, 1999; Liu *et al.*, 2023a), (2) mobilisation of ER calcium by pro-apoptotic proteins BAK and BAX, a mechanism that seems to be essential for apoptosis induction by at least some apoptotic stimuli (Scorrano *et al.*, 2003), and (3) indirect predisposition to apoptosis by overall cellular dyshomeostasis in calcium overload (Dhaouadi *et al.*, 2023). Calcium influx is also a late event in RCDs that execute cell death via plasma

membrane rupture, i.e. necroptosis, pyroptosis and ferroptosis (Gong *et al.*, 2017; Chen *et al.*, 2016; Pedrera *et al.*, 2021).

1.3.3.2. Role of calcium in axonal degeneration

The neuronal soma and its projections represent distinct degenerative compartments. Interestingly, calcium seems to be involved in all of these individual degenerative processes and even marks individual synapses for removal (Jafari *et al.*, 2021).The role of calcium in axonal degeneration is best defined following axonal transection, where the initial breach of the axonal membrane leads to a rise of calcium concentration into the millimolar range (Rishal and Fainzilber, 2014). This generates a calcium wave that is propagated to the soma to signal injury. At the injury site calcium elevation and calpain activation promote resealing (Howard *et al.*, 1999). Yet the prolonged time of resealing and restoration of calcium homeostasis in CNS compared to the peripheral nervous system, has been suggested to contribute to regeneration failure of the proximal stump (Ahmed *et al.*, 2001). The distal stump will fragment after a lag time, in a process called Wallerian degeneration which is signalled by NAD-metabolising enzymes (Coleman and Höke, 2020). Interestingly, a second phase of calcium influx is observed, directly preceding fragmentation (Vargas *et al.*, 2015). However, no consensus has yet been reached on how this influx is regulated and whether it is causative for fragmentation. Sarm1-mediated breakdown of NAD generates cADPR and ADPR, NAD metabolites which are known to open RyR channels in the ER and TRPM2 channels in the plasma membrane respectively, both leading to calcium influx into the cytosol (Gerdts *et al.*, 2015; Nikiforov *et al.*, 2015; Li *et al.*, 2022). Other studies point to an extracellular source of calcium (Loreto *et al.*, 2015) and involvement of voltage-gated calcium channels and NCX (George *et al.*, 1995). Reports further differ in whether calcium chelation can delay fragmentation (Vargas *et al.*, 2015) or not (Ko *et al.*, 2021) and whether mPTP opening is required (Barrientos *et al.*, 2011; Villegas *et al.*, 2014) or not (Loreto *et al.*, 2015; Ko *et al.*, 2021). A large body of evidence however implicates the calcium-dependent protease calpain in subsequent axonal cytoskeleton disassembly (George *et al.*, 1995; Ma *et al.*, 2013; Yang *et al.*, 2013).

As discussed in chapter *1.2.3.3 Axonal fragmentation pathways*, axonal degeneration in the MS model EAE is likely not mediated by Sarm1, i.e. not Wallerian. However, even though the upstream effects leading to calcium influx in EAE vs. Wallerian degeneration are different, downstream effects such as mPTP opening and calpain activation may still be shared. As mentioned earlier, the role of the mPTP in EAE is debatable, with some studies showing a protective effect upon mPTP inhibition (Forte *et al.*, 2007; Warne *et al.*, 2016), while longitudinal *in vivo* imaging suggests that axonal fragmentation precedes mitochondrial calcium overload (Tai *et al.*, 2023). Indeed, our own unpublished data suggests that focal axonal degeneration in EAE lesions is unaffected by cyclophilin D knockout, which prevents mPTP formation.

Calpain is highly expressed in MS and EAE lesions, yet predominantly by immune cells and glia (Diaz-Sanchez *et al.*, 2006; Shields *et al.*, 1998). Studies of systemic calpain inhibition in EAE therefore show strong immunosuppressive phenotypes (Hassen *et al.*, 2006; Guyton *et al.*, 2010; Trager *et al.*, 2014) which prohibit any conclusions on axon-autonomous effects. A study on mechanisms of axonal degeneration in EAE however showed increased calpain activity in lesion-spanning axons compared to control which was exacerbated by MCU KO (Holman *et al.*, 2020). These findings are corroborated by our own findings in *in vivo* imaging in which short-term calpain inhibition reduced axonal fragmentation rates (Wesolowski, 2018). However, our data also suggests that inhibition of calpain can only delay but do not prevent fragmentation (unpublished data). Axoprotective interventions should therefore target the degeneration process more upstream, for example at the level of calcium overload.

1.4. Aims of this thesis

Axonal degeneration is a critical determinant of progressive disability in MS patients, yet insufficiently prevented by the immunomodulatory drugs available for treatment. *In vivo* imaging in the EAE animal model of MS has shown that initial axonal damage is still reversible and that the likelihood of fragmentation of damaged axons is determined by intra-axonal calcium, which enters through "nanoruptures" in the plasma membrane. Importantly, we observed axons that spontaneously lowered their cytosolic calcium levels back to homeostatic baseline, indicating that calcium overload is reversible (Witte *et al.*, 2019). Our hypothesis is therefore, that therapeutic interventions, which help axons to regain calcium homeostasis will shift the balance in favour of recovery and reduce axonal loss.

The aim of this thesis was to explore the potential of calcium overload as a target of axoprotective therapy. To this end we aimed to answer the following questions:

(1) Can endogenous calcium clearance pathways be therapeutically enhanced in EAE to
    a. lower axonal calcium levels and
    b. improve axonal recovery?
(2) Can the characteristic membrane "nanoruptures" be exploited for a selective pharmacological targeting of the damaged axon subpopulation, e.g. with a prodrug calcium chelator?

Regarding question (1), we specifically studied the rAAV-mediated neuron-specific overexpression of calcium-binding proteins (CaBPs). The CaBPs calbindin and calretinin were chosen for overexpression due to their low calcium affinity (400 nM and 1.4 µM respectively, Schmidt, 2012; Schwaller, 2010) and therefore potentially low side-effects at physiological calcium levels, their fast calcium-binding kinetics, and the favourable literature review (see *1.3.2 Cellular calcium homeostasis*). The results of these experiments are described in *3.2 Therapeutic enhancement of endogenous calcium clearance pathways*.

The long-term aim with question (2) was to use exogenous calcium chelators to normalise axonal calcium levels in EAE while preventing effects on physiological calcium functions.

We thus aimed to design a prodrug that uses the characteristic plasma membrane "nanoruptures" as entry routes and needs intracellular activation to turn on its calcium-binding ability. As a proof-of-principle, we first delivered a fluorogenic probe instead of a prodrug, which has the advantage of direct fluorescent feedback on the success of delivery and turn-on. Such a membrane damage-selective fluorogenic compound can also be useful in and of itself as a biosensor for membrane damage. The screening process for the biosensor and further applications of the resulting probe are described in *3.1 Development and application of a membrane damage-selective biosensor*. The subsequent translation of this approach into a calcium chelator prodrug was in an early phase, with comprehensive data still lacking at the timepoint of thesis submission. Therefore, these experiments will only be addressed in the discussion, see *4.2 Development of a membrane damage-selective calcium chelator*.

2. Material and methods

2.1. Material

2.1.1. General laboratory equipment

Consumables		
Pipette tips and serological pipettes	ep Dualfilter T.I.P.S.® SealMax ®, 10 / 200 / 1000 µl	Eppendorf AG, Hamburg, Germany
	ep T.I.P.S.® Standard/Bulk, 10 / 200 / 1000 µl	Eppendorf AG, Hamburg, Germany
	Corning ® Costar ® Stripette ®, individually wrapped, 5 / 10 / 25 / 50 ml	Corning Inc., Corning, USA
Reaction tubes	PCR SingleCap 8er SoftStrips, 0.2 ml	Biozym Scientific GmbH, Hessisch Oldendorf, Germany
	Safe-Lock Tubes, 0.5 / 1.5 / 2.0 / 5.0 ml	Eppendorf AG, Hamburg, Germany
	Centrifugation tubes, 15 / 50 ml	Corning Inc., Corning, USA
Tools and devices		
Centrifuges	Table-top centrifuge 5417 R	Eppendorf AG, Hamburg, Germany
	Heraeus Multifuge X3R	Thermo Fisher Scientific Inc., Waltham, USA
Pipettes and pipetting aids	Research Plus pipette set	Eppendorf AG, Hamburg, Germany
	Pipetus ®	Hirschmann Laborgeräte GmbH & Co. KG, Eberstadt, Germany
Vortex	Vortex Mixer 7-2020	neoLab Migge GmbH, Heidelberg, Germany

2.1.2. Photo- and cell-free characterisation

Consumables			
Cuvettes	Single-use cuvettes UV Micro (z = 15 mm), standard, Cat. No. Y201.1		Carl Roth GmbH & Co. KG, Karlsruhe, Germany
Well plates	Cellstar ® 96 well plate, black, Cat. No. 655087		Greiner Bio-One GmbH, Kremsmünster, Austria
Buffers and media			
DMEM	Dulbecco's Modified Eagle Medium, high glucose, Cat. No. D1145		Sigma-Aldrich/Merck KGaA, Darmstadt, Germany
HBSS	Hanks' Balanced Salt Solution, modified, with sodium bicarbonate, without phenol red, calcium chloride and magnesium sulfate, Cat. No. H6648		Sigma-Aldrich/Merck KGaA, Darmstadt, Germany
PBS	Dulbecco's Phosphate Buffered Saline, modified, without calcium chloride and magnesium chloride, Cat. No. D8537		Sigma-Aldrich/Merck KGaA, Darmstadt, Germany
Chemicals, enzymes and other reagents			
Chemicals	DMSO (dimethyl sulfoxide)		Carl Roth GmbH & Co. KG, Karlsruhe, Germany
	GSH (L-glutathione, reduced)		Sigma-Aldrich/Merck KGaA, Darmstadt, Germany
	Piperidine		Sigma-Aldrich/Merck KGaA, Darmstadt, Germany
	TCEP (tris(2-carboxyethyl)phosphine)		Sigma-Aldrich/Merck KGaA, Darmstadt, Germany
Enzymes	Esterase from porcine liver, Cat. No. E3019		Sigma-Aldrich/Merck KGaA, Darmstadt, Germany
Fluorescent and fluorogenic compounds	Fluorescein	FDP	Philipp Mauker, LMU Munich, Department of Pharmacy
	H_2-FS_0	i_2-FS_0	
	H_2-FS_1	i_2-FS_1	
		a_2-FS_0	
	H-PS-FS_1	iPS-FS_1	
	H-Me-FS_1	iMe-FS_1	
	H-EM-FS_1	iEM-FS_1	
	H-PS-FS_2	iPS-FS_2 (MDG1)	
		MSS00-FS_2 (MDG2)	

Devices		
Plate reader	FluoStar Omega Plate Reader	BMG Labtech GmbH, Ortenburg, Germany
Spectrometer	Cary 60 UV-Vis Spectrophotometer	Agilent Technologies Inc., Santa Clara, USA
	Cary Eclipse Fluorescence Spectrometer	Agilent Technologies Inc., Santa Clara, USA

2.1.3. Cell culture and related methods

The following list includes material used for live cell imaging, flow cytometry of cultured cells and rAAV production.

Cell lines		
HeLa	Henrietta Lacks, Human cervical carcinoma, Cat. No. ACC57	German Collection of Microorganisms and Cell Cultures (DSMZ) GmbH, Braunschweig, Germany
HEK 293T	Human embryonic kidney, Cat. No. crl-3216	American Type Culture Collection (ATCC), Manassas, USA
PC12	Rat pheochromocytoma, Cat. No. 88022401	Sigma-Aldrich/Merck KGaA, Darmstadt, Germany
Consumables		
Cell culture dishes	Cellstar ® 14.5 cm	Greiner Bio-One GmbH, Kremsmünster, Austria
Cell culture flasks	Falcon ® Rectangular Canted Neck Cell Culture Flask with Vented Cap, 25 cm² / 75 cm²	Corning Inc., Corning, USA
Chambered coverslips	µ-Slide 8 Well Glass Bottom, Cat. No. 80827	ibidi GmbH, Gräfelfing, Germany
Filters	Millex ® PVDF Filter, Luer Lock, 0.45 µM, Cat. No. SLHV033RS	Millipore/Merck KGaA, Darmstadt, Germany
	Amicon ® Ultra-15 Centrifugal Filter Unit, 100 kDa, Cat. No. UFC910024	Millipore/Merck KGaA, Darmstadt, Germany
Needles	Sterican ® 30 G Needle	B. Braun SE, Melsungen, Germany

Reaction tubes	Protein LoBind ®, 0.5 ml	Eppendorf AG, Hamburg, Germany
Syringes	BD Plastipak™, 20 ml Luer Lock Syringe	Becton, Dickinson and Company, Franklin Lakes, USA
	BD Plastipak™, 1 ml Luer Slip Syringe	Becton, Dickinson and Company, Franklin Lakes, USA
Well plates	Costar ® Cell Culture Plate, tissue culture treated, 12 well / 48 well	Corning Inc., Corning, USA
	U-Bottom Plate, 96 well	Corning Inc., Corning, USA
Buffers and media		
Media	Dulbecco's Modified Eagle Medium (DMEM), low glucose, GlutaMAX™ supplement, pyruvate, Cat. No. 21885108	Thermo Fisher Scientific Inc., Waltham, USA
	Roswell Park Memorial Institute 1640 Medium (RPMI 1640), GlutaMAX™ supplement, Cat. No. 61870010	Thermo Fisher Scientific Inc., Waltham, USA
	Opti-MEM™ Reduced Serum Medium, no phenol red, Cat. No. 11058021	Thermo Fisher Scientific Inc., Waltham, USA
Media supplements	Fetal bovine serum (FBS) superior, Cat. No. S0615	Sigma-Aldrich/Merck KGaA, Darmstadt, Germany
	Horse serum, heat inactivated, Cat. No. H1138	Sigma-Aldrich/Merck KGaA, Darmstadt, Germany
	Penicillin/Streptomycin, Cat. No. 15140122	Thermo Fisher Scientific Inc., Waltham, USA
Buffers	Dulbecco's Phosphate Buffered Saline (PBS), with calcium chloride and magnesium chloride, Cat. No. D8662	Sigma-Aldrich/Merck KGaA, Darmstadt, Germany
	Dulbecco's Phosphate Buffered Saline (PBS), modified, without calcium chloride and magnesium chloride, Cat. No. D8537	Sigma-Aldrich/Merck KGaA, Darmstadt, Germany
	Hanks' Balanced Salt Solution (HBSS), calcium, magnesium, no phenol red, Cat. No. 14025092	Thermo Fisher Scientific Inc., Waltham, USA

Chemicals and other reagents		
Chemicals	AAPH (2,2'-azobis (2-amidinopropane) dihydrochloride)	Cayman Chemical, Ann Arbor, USA
	DMSO (dimethyl sulfoxide)	Sigma-Aldrich/Merck KGaA, Darmstadt, Germany
	PEI MAX ® (polyethylenimine hydrochloride)	Polysciences Inc., Warrington, USA
Fluorescent and fluorogenic compounds	CellTracker™ Red CMTPX, Cat. No. C34552	Thermo Fisher Scientific Inc., Waltham, USA
	Alexa Fluor™ 594 Cadaverine, Cat. No. A30678	Thermo Fisher Scientific Inc., Waltham, USA
	Fluorescein H_2-FS_0 H_2-FS_1 H-PS-FS_1 H-Me-FS_1 H-EM-FS_1 H-PS-FS_2 FDP i_2-FS_0 i_2-FS_1 a_2-FS_0 iPS-FS_1 iMe-FS_1 iEM-FS_1 iPS-FS_2 (MDG1) MSS00-FS_2 (MDG2)	Philipp Mauker, LMU Munich, Department of Pharmacy
Other reagents	ß-NGF (nerve growth factor), Cat. No. 13257-019	Thermo Fisher Scientific Inc., Waltham, USA
	Collagen IV, Cat. No. H4417	Sigma-Aldrich/Merck KGaA, Darmstadt, Germany
	Lysteriolysin O (LLO), Cat. No. ab83345	Abcam Ltd., Cambridge, UK
	Poly-D-lysine hydrobromide, Cat. No. P7280	Sigma-Aldrich/Merck KGaA, Darmstadt, Germany
	Trypsin-EDTA, 0.5 %, Cat. No. 15400054	Thermo Fisher Scientific Inc., Waltham, USA
Plasmids and viruses		
AAV helper plasmid	pAdDeltaF6 (Plasmid #112867)	Addgene, Watertown, USA
AAV capsid plasmid	pUCmini-iCAP-PHP.eB (Plasmid #103005)	Addgene, Watertown, USA
AAV transfer plasmids	*Used for rAAV production and HEK transfection for flow cytometry, see 2.1.5 Molecular cloning*	

Viruses	rAAV-PHP.eB-hSyn-CB-T2A-KOFP-WPRE-pA	Produced as part of this thesis
	rAAV-PHP.eB-hSyn-CR-T2A-KOFP-WPRE-pA	Produced as part of this thesis
	rAAV-PHP.eB-hSyn-Cre-T2A-KOFP-WPRE-pA	Produced as part of this thesis
	rAAV-PHP.eB-hSyn-CB-T2A-KOFP-WPRE-pA-VB	VectorBuilder Inc., Chicago, USA
	rAAV-PHP.eB-hSyn-CR-T2A-KOFP-WPRE-pA-VB	VectorBuilder Inc., Chicago, USA
	rAAV-PHP.eB-hSyn-ShadowG-T2A-KOFP-WPRE-pA-VB	VectorBuilder Inc., Chicago, USA
Tools and devices		
Cell counting chamber	Neubauer improved bright-line	Brand GmbH & Co. KG, Wertheim, Germany
Flow cytometer	Beckman Coulter Cytoflex S	Beckman Coulter Inc., Brea, USA
Incubator	New Brunswick Galaxy 170 S	Eppendorf AG, Hamburg, Germany
Microscopes	Leica DMi1 inverted microscope	Leica Microsystem GmbH, Wetzlar, Germany
	Leica DM IL LED inverted microscope with CoolLED pE-300	Leica Microsystem GmbH, Wetzlar, Germany CoolLED Ltd., Andover, UK
	Leica SP8X inverted confocal microscope, equipped with - heated chamber - WLL laser, Argon laser - acusto-optical beamsplitter - reflection-based adaptive focus control - HC PL APO 20x/0,75 CS2 air objective	Leica Microsystem GmbH, Wetzlar, Germany Live Imaging Services GmbH, Basel, Switzerland
Sterile work bench	Berner B-[MaxPro]²-130	Berner International GmbH, Elmshorn, Germany
Water bath	WB-4MS stirred water bath	A. Hartenstein GmbH, Würzburg, Germany

2.1.4. Imaging of axonal membrane damage in microfluidic chambers

Mice		
C57/BL6		Animal Facility, Max Planck Institute for Biological Intelligence
Consumables		
6 well glass bottom plates, Cat. No. P06-1.5H-N		Cellvis LLC, Mountain View, USA
Microfluidic chambers, Cat. No. RD450		Xona Microfluidics Inc., Chapel Hill, USA
Buffers and media		
Media	Neurobasal™ Medium, Cat. No. 21103049	Thermo Fisher Scientific Inc., Waltham, USA
Media supplements	B-27™, Cat. No. 17504044	Thermo Fisher Scientific Inc., Waltham, USA
	Penicillin-Streptomycin-Glutamine (PSG), Cat. No. 10378016	Thermo Fisher Scientific Inc., Waltham, USA
Buffers	Hanks' Balanced Salt Solution (HBSS), calcium, magnesium, no phenol red, Cat. No. 14025092	Thermo Fisher Scientific Inc., Waltham, USA
Chemicals and other reagents		
Chemicals	AAPH (2,2'-azobis (2-amidinopropane) dihydrochloride)	Cayman Chemical, Ann Arbor, USA
	Ethanol	Thermo Fisher Scientific Inc., Waltham, USA
Fluorescent and fluorogenic compounds	CellTracker™ Red CMTPX, Cat. No. C34552	Thermo Fisher Scientific Inc., Waltham, USA
	iPS-FS_2 (MDG1)	Philipp Mauker, LMU Munich, Department of Pharmacy
	Propidium iodide (PI), Cat. No. ab14083	Abcam Ltd., Cambridge, UK
Other reagents	Laminin (natural, mouse), Cat. No. 23017015	Thermo Fisher Scientific Inc., Waltham, USA
	Poly-L-lysine hydrobromide, Cat. No. P2636	Sigma-Aldrich/Merck KGaA, Darmstadt, Germany

Devices		
Microscope	Nikon Ti2 spinning disk microscope with 20x/air objective	Nikon Corp., Tokyo, Japan

2.1.5. Molecular cloning

Plasmids and cDNAs		
cDNAs	cDNA of murine calbindin-D28k	Prof. Dr. Michael Meyer, LMU Munich, Department of Cellular Physiology
	cDNA of human calretinin	Prof. Dr. Michael Meyer, LMU Munich, Department of Cellular Physiology
Plasmids, starting material	pAAV-U6-sgRNAbackbone-hSyn-Cre-T2A-KOFP-WPRE	Adinda Wens, LMU Munich, Institute of Clinical Neuroimmunology
	pAAV-hSyn-CalpainSensorV#2-WPRE-pA (derivative of Addgene #50457)	Daniela Beckmann, LMU Munich, Institute of Clinical Neuroimmunology
	pAAV-hSyn-KOFP-WPRE-pA (derivative of Addgene #50457)	Daniela Beckmann, LMU Munich, Institute of Clinical Neuroimmunology
Plasmids, products in-house	pAAV-hSyn-CB-T2A-KOFP-WPRE-pA (“CB-KOFP”)	Cloned as part of this thesis
	pAAV-hSyn-CR-T2A-KOFP-WPRE-pA (“CR-KOFP”)	Cloned as part of this thesis
	pAAV-hSyn-Cre-T2A-KOFP-WPRE-pA ("Cre-KOFP")	Cloned as part of this thesis
Plasmids, commercial	pAAV-hSyn-CB-T2A-KOFP-WPRE-pA-VB (“CB-KOFP-VB”)	VectorBuilder Inc., Chicago, USA
	pAAV-hSyn-CR-T2A-KOFP-WPRE-pA-VB (“CR-KOFP-VB”)	VectorBuilder Inc., Chicago, USA
	pAAV-hSyn-ShadowG-T2A-KOFP-WPRE-pA-VB ("SG-KOFP-VB")	VectorBuilder Inc., Chicago, USA

Oligonucleotides		
All oligonucleotides were supplied by Metabion, Planegg, Germany		
Gibson primers	DB027	5’- CGTGCCTGAGAGCGCAGTCGAGAAACCGGCTA-GAGGCCACGCCACCATGGCAGAATCCCAC-CTGCAGTCATCTCTGAT - 3’
	DB028	5’- AGCAGACTTCCTCTGCCCTCGTTGTCTCCAG-CAGAAAGAATAAGAGCA - 3’
	DB029	5’- TCTTTCTGCTGGAGACAACGAGGGCAGAG-GAAGTCTGCTAAC - 3’
	DB030	5’- TCACAAATTTTGTAATCCAGAGGTTGAT-TATCGATAATCATCAGCAATGAGCTACTGC - 3’
	DB031	5’- CCGGCTAGAGGCCACCATGGCTGGCCCGCA - 3’
	DB032	5’- CTGCCCTCCATGGGGGGCTCGCTG - 3’
	DB033	5’- CCCCATGGAGGGCAGAGGAAGTCTGCT - 3’
	DB034	5’- CAGAGGTTGATTATCGATAATCATCAG-CAATGAGCTACTGCATCTTCTACCAGC - 3’
Sequencing primers	hSyn-F	5’- GCAAGTGGGTTTTAGGACCA - 3’
	WPRE-R	5’- CATAGCGTAAAAGGAGCAACA - 3’
	DB020	5’- CGCGAAAGAAGGCTGGATT - 3’
	DB024	5’- CTCTCAGGCACGACACGA - 3’
	DB035	5’- CGACTCAGCGCTGCCT - 3’
	DB038	5’- AAATAGTCTGGTATCTCTTCTGGA - 3’
Enzymes and commercial kits		
Restriction enzymes	BglII	New England Biolabs, Ipswich, USA
	NcoI-HF	New England Biolabs, Ipswich, USA
	NdeI	New England Biolabs, Ipswich, USA
	XbaI	New England Biolabs, Ipswich, USA
	XmaI	New England Biolabs, Ipswich, USA
Restriction enzyme buffers	CutSmart^{TM} buffer	New England Biolabs, Ipswich, USA
	NEBuffer 3.1	New England Biolabs, Ipswich, USA

Other enzymes	Gibson Assembly ® Master Mix, Cat. No. E2611S	New England Biolabs, Ipswich, USA
	T4 DNA Ligase and T4 DNA Ligase Reaction Buffer, Cat. No. M0202T, B0202S	New England Biolabs, Ipswich, USA
	Q5 ® High-Fidelity DNA Polymerase and Q5 ® Reaction Buffer, Cat. No. M0491L	New England Biolabs, Ipswich, USA
Kits	QIAquick Gel Extraction Kit, Cat. No. 28706	Qiagen, Hilden, Germany
	QIAprep Spin Minprep Kit, Cat. No. 27106	Qiagen, Hilden, Germany
	QIAGEN Plasmid Maxi Kit, Cat. No. 12162	Qiagen, Hilden, Germany
Chemicals and other reagents		
Chemicals	Agarose	Sigma-Aldrich/Merck KGaA, Darmstadt, Germany
	Nuclease-free water	Qiagen, Hilden, Germany
TAE buffer	Trizma ® base (40 mM)	Sigma-Aldrich/Merck KGaA, Darmstadt, Germany
	Acetic acid (20 mM)	Sigma-Aldrich/Merck KGaA, Darmstadt, Germany
	EDTA (1 mM)	Sigma-Aldrich/Merck KGaA, Darmstadt, Germany
Other reagents	dNTP Mix, 10 mM	New England Biolabs, Ipswich, USA
	GeneRuler 1 kb DNA ladder	Thermo Fisher Scientific Inc., Waltham, USA
	peqGREEN DNA stain	PEQLAB Biotechnologie GmbH, Erlangen, Germany
Competent cells and bacterial media		
Competent cells	Stellar ® Competent Cells, Cat. No. 636763	Takara Bio Inc., Kusatsu, Japan
S.O.C. medium	Cat. No. 15544034	Thermo Fisher Scientific Inc., Waltham, USA
LB medium and agar plates	Tryptone	Merck KGaA, Darmstadt, Germany
	Yeast extract	Sigma-Aldrich/Merck KGaA, Darmstadt, Germany

	Sodium chloride	Sigma-Aldrich/Merck KGaA, Darmstadt, Germany
	Agar-agar	Merck KGaA, Darmstadt, Germany
	Ampicillin sodium salt	PanReac AppliChem GmbH, Darmstadt, Germany
Tools and devices		
Tools	Disposable scalpel	FEATHER Safety Razor Co. Ltd., Osaka, Japan
	Sterile glass beads	Zymo Research, Freiburg im Breisgau, Germany
Gel electro-phoresis	PerfectBlue Gel System	PEQLAB Biotechnologie GmbH, Erlangen, Germany
	Power PAC 200 Power Supply	Bio Rad, Hercules, USA
	Quantum Vilber Lourmat, Gel Documentation Imaging System	Vilber Lourmat, Collégien, France
	High Performance Ultraviolet Transilluminator	UVP / Analytik Jena, Jena, Germany
Other devices	NanoDrop 2000 Spectrophotometer	Thermo Fisher Scientific Inc., Waltham, USA
	PCR Thermocycler Biometra TRIO	Analytik Jena, Jena, Germany
	Thermomixer Comfort	Thermo Fisher Scientific Inc., Waltham, USA
Services		
Sequencing was performed by the LMU Biocenter Genomics Service Unit		

2.1.6. rAAV titration (qPCR)

Consumables	
Hard-Shell ® 96 Well PCR Plates	Bio Rad, Hercules, USA
Microseal 'B' PCR Plate Sealing Film	Bio Rad, Hercules, USA
Enzymes and other reagents	
DNase I recombinant, RNase-free, Cat. No. 04716728001	Roche AG, Basel, Schweiz
SsoAdvanced™ Universal SYBR® Green Supermix, Cat. No. 1725271	Bio Rad, Hercules, USA

Oligonucleotides		
All oligonucleotides were supplied by Metabion, Planegg, Germany		
fwd primer	5’- GGAACCCCTAGTGATGGAGTT - 3’	
rev primer	5’- CGGCCTCAGTGAGCGA - 3’	
Devices		
CFX Real-Time PCR instrument		Bio Rad, Hercules, USA

2.1.7. Experimental animals and related procedures

Mice		
Thy1-CerTN-L15, Heim *et al.*, 2007		Core Facility Animal Models, Biomedical Center, LMU Munich
Consumables		
Absorbent swabs	Sugi ® Sponge Points	Kettenbach GmbH & Co KG, Eschenburg, Germany
Needles	Sterican ® 23 G Needle	B. Braun SE, Melsungen, Germany
	Sterican ® 30 G Needle	B. Braun SE, Melsungen, Germany
Syringes	Inject ® 2 ml Luer Lock Syringe	B. Braun SE, Melsungen, Germany
	BD Plastipak™, 1 ml Luer Slip Syringe	Becton, Dickinson and Company, Franklin Lakes, USA
Medication		
Anaesthesia	Medetomidine hydrochloride (Dormilan)	Alfavet Tierarzneimittel GmbH, Neumünster, Germany
	Midazolam (Dormicum)	Cheplapharm Arzneimittel GmbH, Greifswald, Germany
	Fentanyl	B. Braun SE, Melsungen, Germany

Antagonist	Atipamezole hydrochloride	Prodivet Pharmaceuticals S.A., Raeren, Belgium
	Flumazenil	Hameln GmbH, Hameln, Germany
	Naloxone hydrochloride	B. Braun SE, Melsungen, Germany
Antiseptic cream	Braunovidon Salbe 10 %	B. Braun SE, Melsungen, Germany
Eye cream	Bepanthen ® Augen- und Nasensalbe	Bayer AG, Leverkusen, Germany
Reagents		
Agarose		Sigma-Aldrich/Merck KGaA, Darmstadt, Germany
Artificial cerebrospinal fluid (aCSF)	Solution A (500 ml)	
	8.660 g NaCl 0.224 g KCl	Merck KGaA, Darmstadt, Germany
	0.206 g $CaCl_2 \cdot 2\ H_2O$ 0.163 g $MgCl_2 \cdot 6\ H_2O$	Sigma-Aldrich/Merck KGaA, Darmstadt, Germany
	+ Solution B (500 ml)	
	0.214 g $Na_2HPO_4 \cdot 7\ H_2O$ 0.027 g $NaH_2PO_4 \cdot H_2O$	Merck KGaA, Darmstadt, Germany
EAE immunisation	Purified recombinant MOG (N1-125, from E.coli)	in-house production
	Freund's incomplete adjuvant, Cat. No. F5506	Sigma-Aldrich/Merck KGaA, Darmstadt, Germany
	Mycobacterium tuberculosis, H37 RA, Cat. No. 231141	Becton, Dickinson and Company, Franklin Lakes, USA
	Pertussis toxin, inactivated, Cat. No. P7208	Sigma-Aldrich/Merck KGaA, Darmstadt, Germany
Tools and devices		
i.v. injection	Mouse restrainer	Braintree Scientific Inc., Braintree, USA
Immunisation	Hamilton 1 ml syringe	Hamilton, Reno, USA
Surgery	Mouse heating pad	Ugo Basile, Gemonio, Italy
	Disposable scalpel	FEATHER Safety Razor Co. Ltd., Osaka, Japan
	Noyes Spring Scissors, straight	Fine Science Tools GmbH, Heidelberg, Germany

	Noyes Spring Scissors, angled up	Fine Science Tools GmbH, Heidelberg, Germany
	Vannas-Tübingen Spring Scissors, straight	Fine Science Tools GmbH, Heidelberg, Germany
	Dumont Mini Forceps – Style 5	Fine Science Tools GmbH, Heidelberg, Germany
	Potts-Smith Forceps, straight, serrated	Fine Science Tools GmbH, Heidelberg, Germany
	FST 250 Hot Bead Sterilizer, surgical instrument sterilizer	Fine Science Tools GmbH, Heidelberg, Germany
	Spinal clamping device	Narishige Inc., NY, USA
Microscopes	SZ51 Stereomicroscope with KL 1500 LCD cold light source	Olympus, Tokio, Japan
	FV1200 MPE multiphoton microscope, equipped with - MaiTai ® HP-DeepSee™ Titanium:sapphire laser - 25x/1.25 NA water immersion objective - FVMPE-RS filter cubes: o SDM560 o cyan/yellow 472/30 |505| 520/35 o orange 580/40	Olympus, Tokio, Japan Newport / Spectra-Physics, Irvine, USA

2.1.8. Tissue harvest, staining and microscopy

Consumables		
Butterfly needle	Safety-Multifly ® 21 G	Sarstedt AG & Co, Nümbrecht, Germany
Cryomolds	Tissue-Tek ® Cryomold ® Biopsy	Sakura Finetek Ltd., Tokyo, Japan
	Tissue-Tek ® Cryomold ® Intermediate	Sakura Finetek Ltd., Tokyo, Japan
Slides and cover slips	SuperFrost ® Plus Microscope Slides	Gerhard Menzel Glasbearbeitungswerk GmbH, Braunschweig, Germany
	Epredia™ SuperFrost Ultra Plus™ GOLD Microscope Slides	Epredia Ltd., Portsmouth, USA

	Coverslips 24 x 60 mm	Gerhard Menzel Glasbearbeitungswerk GmbH, Braunschweig, Germany
Well plates	Costar ® Multi-well plate, untreated, 48 well	Corning Inc., Corning, USA
Buffers and media		
PBS, non-sterile	Sodium chloride (137 mM)	Sigma-Aldrich/Merck KGaA, Darmstadt, Germany
	Potassium chloride (27 mM)	Sigma-Aldrich/Merck KGaA, Darmstadt, Germany
	Sodium phosphate dibasic (10 mM)	Sigma-Aldrich/Merck KGaA, Darmstadt, Germany
	Potassium phosphate monobasic (1.8 mM)	Sigma-Aldrich/Merck KGaA, Darmstadt, Germany
Antibodies and fluorescent dyes		
Primary antibodies	anti-calbindin, rabbit recombinant monoclonal antibody, Cat. No. ab108404	Abcam Ltd., Cambridge, UK
	anti-calretinin, rabbit polyclonal antiserum, Cat. No. SYSY214102	Synaptic Systems GmbH, Göttingen, Germany
Secondary antibodies	donkey anti-rabbit IgG (H+L), Highly Cross-Adsorbed Secondary Antibody, Alexa Fluor™ Plus 647 Cat. No. A32795	Thermo Fisher Scientific Inc., Waltham, USA
Fluorescent dyes	NeuroTrace™ 640/660 Deep-Red Fluorescent Nissl Stain, Cat. No. N21483	Thermo Fisher Scientific Inc., Waltham, USA
Chemicals and other reagents		
Chemicals	Paraformaldehyde	Sigma-Aldrich/Merck KGaA, Darmstadt, Germany
	Sodium azide	Sigma-Aldrich/Merck KGaA, Darmstadt, Germany
	Sucrose	Sigma-Aldrich/Merck KGaA, Darmstadt, Germany
	Triton-X	Sigma-Aldrich/Merck KGaA, Darmstadt, Germany
Embedding media	Tissue-Tek ® O.C.T. Compound, Cat. No. 12351753	Sakura Finetek Ltd., Tokyo, Japan
	Epredia™ M-1 Embedding Matrix, Cat. No. 1310	Epredia Ltd., Portsmouth, USA

Mounting media	VECTASHIELD ® Antifade Mounting Medium, Cat. No. H-1000-10	Vector Laboratories Inc., Burlingame, USA
	Fluoromount-G™ Mounting Medium, Cat. No. 00-4958-02	Thermo Fisher Scientific Inc., Waltham, USA
Other reagents	Heparin-Natrium 25.000 IE	Ratiopharm GmbH, Ulm, Germany
	Bovine Serum Albumin (BSA), Cat. No. A7030	Sigma-Aldrich/Merck KGaA, Darmstadt, Germany
Tools and devices		
Tools	Mouse precision brain slicer	Braintree Scientific Inc., Braintree, USA
	Dumont Mini Forceps – Style 5	Fine Science Tools GmbH, Heidelberg, Germany
	Noyes Spring Scissors, straight	Fine Science Tools GmbH, Heidelberg, Germany
	StainTray™	Simport Scientific Inc., Beloeil, Canada
	ImmEdge ® Hydrophobic Barrier (PAP) Pen	Vector Laboratories Inc., Burlingame, USA
Microscope	Leica TCS SP8 upright DMI6000 confocal microscope, equipped with - Diode, Argon, DPSS and HeNe lasers - HC PL Apo 40x/1.30 oil immersion objective	Leica Microsystem GmbH, Wetzlar, Germany
Other devices	Cryostat Leica CM1950	Leica Microsystem GmbH, Wetzlar, Germany
	Ismatec IP High Precision Multichannel Pump	ISMATEC SA, Labortechnik-Analytik, Glattbrugg, Switzerland
	Orbital Shaker	neoLab Migge GmbH, Heidelberg, Germany
	Tilting Shaker	A. Hartenstein GmbH, Würzburg, Germany

2.1.9. Software

Software		
Image processing	Fiji/ImageJ, version 2.3.0/1.53q	Open Source, General Public License
Flow cytometry	FlowJo, version 10.10.0	Becton, Dickinson and Company, Franklin Lakes, USA
Plasmid maps and cloning	SnapGene, version 4.3.11	GSL Biotech LLC, Boston, USA
General data processing and plotting	Excel, Microsoft Office Professional Plus 2016	Microsoft Corporation, Redmond, USA
	Python, version 3.9.7	Open Source, General Public License
	GraphPad Prism, version 7.05	GraphPad Software, La Jolla, USA
Figure design	ChemDraw, version 22.2.0	Revvity Signals Software Inc., Waltham, USA
	Affinity Designer, version 2.3.1	Serif (Europe) Ltd., Nottingham, UK
	Inkscape, version 1.3	Open Source, General Public License
Browser tools		
Protein BLAST	https://blast.ncbi.nlm.nih.gov/Blast.cgi	National Institutes of Health, Bethesda, USA
NEB T_m calculator	https://tmcalculator.neb.com/#!/main	New England Biolabs, Ipswich, USA
Promega Biomath Calculators	https://www.promega.de/resources/tools/biomath/	Promega Corp., Madison, USA

2.2. Methods

2.2.1. Photocharacterisation of novel fluorophores

Absorption spectra of the newly synthesised fluorophores were acquired with a Cary 60 UV-Vis Spectrophotometer with a scan rate of to 600 nm/min and slit width of 2.5 nm. Emission spectra were acquired with a Cary Eclipse Fluorescence Spectrometer with a scan rate of 120 nm/min and slit width of 5 nm. The excitation wavelength was 480 nm and emission spectra were recorded from 490 to 620 nm. For both applications, fluorophores were dissolved in PBS (pH 7.4, 1 % DMSO) at a concentration of 10 µM. Quantum yields of the novel fluorophores were calculated with an equation by Würth *et al.* (2013), using fluorescein ($\Phi f,st$ = 0.85) as a reference fluorophore:

$$\Phi_{f,x} = \Phi_{f,st} \cdot \frac{F_x}{F_{st}} \cdot \frac{1 - 10^{-A_{st}(\lambda_{ex})}}{1 - 10^{-A_x(\lambda_{ex})}} \cdot \frac{n_x(\lambda_{em})^2}{n_{st}(\lambda_{em})^2}$$

Fluorescence readout of fluorophore photostability was performed in black 96 well plates on a FluoStar Omega Plate Reader heated to 37°C with excitation set to 485 nm (bandpass 10 nm) and a 520 nm long-pass emission filter. Fluorophores were excited and emission recorded ten times over a total duration of 6 h.

2.2.2. Cell-free characterisation of probe stability and activation

Fluorescence readout of probe stability and activation was performed in black 96 well plates on a FluoStar Omega Plate Reader heated to 37°C with excitation set to 485 nm (bandpass 10 nm) and a 520 nm long-pass emission filter.

For stability testing, 10 µl of water was placed in the wells and 1 µl of probes from a 1 mM stock in DMSO (or 1 mM stock in water for H-PS-FS_2 and iPS-FS_2 = MDG1) added on top. Finally, 89 µl of the different media (PBS, HBSS or DMEM without FBS supplementation) were added to all probes simultaneously using a multipipette. The final probe concentration was 10 µM. All samples were tested in technical duplicates. Fluorescence intensity per well was measured at 0, 15, 30, 60, 120, 180, 240, 300 and 360 min. To determine maximum intensity, 100 µl of a 50 mM piperidine solution were added to each well at the end of the experiment. For maximum activation of MSS00-FS_2 (= MDG2), tris(2-carboxyethyl)phosphine (TCEP, 200 µM, 100 µl) was used instead of piperidine. To obtain stability curves over time, all measured values were corrected for background by subtracting fluorescence at 0 min and normalised to maximum fluorescence after 2 h piperidine or TCEP incubation.

For cell-free activation of probes, 49 µl of PBS were placed in wells and 1 µl of probe from a 1 mM stock in DMSO (or 1 mM stock in water for H-PS-FS_2 and iPS-FS_2 = MDG1) added on top. Finally, 50 µl of porcine liver esterase in PBS (500 ng/ml, > 15 units/mg) were added

to all wells simultaneously using a multipipette. The final probe concentration was 10 µM and final esterase concentration 250 ng/ml. For activation of MDG2, a PBS solution containing glutathione (GSH) instead of esterase was used, with final GSH concentrations being 0.1 mM, 0.3 mM, 1 mM or 3 mM. All samples were tested in technical duplicates. Fluorescence intensity per well was measured every two minutes for a total duration of 90 min. To determine maximum intensity, 100 µl of a 50 mM piperidine solution were added to each well at the end of the experiment. For maximum activation of MDG2, TCEP (200 µM, 100 µl) was used instead of piperidine. To obtain activation curves over time, all measured values were corrected for background by subtracting fluorescence at 0 min and normalised to maximum fluorescence after 2 h piperidine or TCEP incubation.

To assess stability of the stocks, the non-fluorescent probes were also succumbed to absorption spectroscopy as outlined above for fluorophores.

2.2.3. Cell culture

HEK 293T cells and HeLa cells were grown in DMEM, supplemented with 10 % fetal bovine serum (FBS) and 1 % Penicillin/Streptomycin. HEK cells were split at a 1:5 ratio and HeLa cells at 1:20 two times per week. PC12 cells were grown in RPMI, supplemented with 10 % horse serum, 5 % FBS and 1 % Penicillin/Streptomycin. PC12 cells were split weekly at a ratio of 1:20 with two additional media changes in between. All cells were grown at 37°C and 5 % CO_2. A Leica DMi1 inverted microscope was used to monitor cell growth.

2.2.4. Live cell imaging for fluorogenic probe characterisation

2.2.4.1. Sample preparation

8 well glass bottom chambered coverslips were used to grow cells for live cell imaging. For HEK cell assays, wells were coated with 0.1 mg/mL poly-D-lysine for 2 h at 37°C, cells seeded at a density of 30.000 cells per cm^2 and live cell imaging performed the next day. For PC12 cell assays, coating with 0.1 mg/ml poly-D-lysine solution for 2 h at 37°C, followed by 0.1 µg / cm^2 collagen IV overnight at 37°C was started six days before live cell imaging experiments, to allow for PC12 cell differentiation. PC12 cells were seeded at a density of 10.000 cells per cm^2. Proper separation of PC12 cell clumps was assured by drawing the cells through a 30 G needle ten times. Cells were seeded in standard PC12 growth medium (RPMI, 10 % horse serum, 5 % FBS, 1 % Penicillin/Streptomycin) which was changed to PC12 differentiation medium (RPMI, 1 % horse serum, 1 % Penicillin/Streptomycin, 100 ng/ml β-NGF) after 2 h, once cells had attached. Another medium change to fresh differentiation medium was performed 48 - 72 h after seeding.

2.2.4.2. LLO and AAPH damage assay procedures

All steps of the damage assays and subsequent imaging were performed in Hanks' Balanced Salt Solution (HBSS) and without CO_2 incubation (pH buffering ensured by HBSS).

The following timeline applies for HEK-LLO live cell assays: HEK cells were incubated with 0.5 µM CellTracker™ Red CMTPX for 15 min to stain all cells irrespective of damage. Afterwards, medium was changed to ice cold HBSS with 0.2 µg/ml lysteriolysin O (LLO) or to ice cold HBSS only for negative control wells. After a 5 min incubation on ice, the medium was removed and cells subsequently incubated with 5 µM compound solutions prepared in 37°C warm HBSS. Chambered coverslips were transferred onto the microscope stage (37°C) and imaging started after 10 min of compound incubation without prior washing (see below).

The following timeline applies for PC12-AAPH live cell assays: PC12 cells were incubated with 0.5 µM CellTracker™ Red CMTPX for 15 min to stain all cells irrespective of damage. Afterwards, medium was changed to 37°C warm HBSS with 300 mM 2,2'-azobis(2-amidinopropane) dihydrochloride (AAPH) and 100 ng/ml β-NGF or to HBSS with β-NGF only for control wells. Cells were incubated for 90 min on the microscope stage (37°C), followed by one HBSS wash and subsequent medium change to 5 µM compound solutions. Imaging was started after 10 min of compound incubation without prior washing (see below).

For post-wash retention assays, an HBSS wash step was performed after image acquisition of the 10 min compound incubation ("pre-wash") timepoint. The complete medium was removed and replaced by fresh 37°C HBSS twice. The timeline was also altered for resealing assays: Here, after LLO-/AAPH incubation (and additional HBSS wash for AAPH as described above), medium was not directly changed to compound solutions but instead first to HBSS. The medium change to 5 µM compound solutions was then performed individually for each well after the indicated recovery times (0, 10, 20, 40, 60, 90, 120 min) relative to the end of damage treatment.

2.2.4.3. Instrumentation and image acquisition

All live cell imaging experiments were performed at the Core Facility Bioimaging of the LMU Biomedical Center using an inverted Leica SP8X confocal microscope equipped with a heated chamber, Argon laser, WLL2 laser (470 - 670 nm) and acusto-optical beam splitter.

A 20x/0.75 NA air objective and additional optical zoom of 2x were used to acquire images with a pixel size of 284 x 284 nm. Light path settings were as follows: compound excitation 488 nm (Argon), emission 500 - 540 nm (unless stated otherwise); CellTracker excitation 594 nm (WLL2), emission 605 - 645 nm. Both channels were recorded with hybrid photo detectors and acquired sequentially to avoid crosstalk. Transmitted light images were generated with a conventional photomultiplier tube. Three different fields of view (FOVs) were recorded per well. These were selected based on cell density before the start of the experiment.

During the experiment, navigation to the FOVs and focus were automated using a programmable stage and reflection-based adaptive focus control.

Due to massive differences in the brightness of different compounds which exceeded the dynamic range of the detectors, brighter compounds were detected with narrower, red-shifted detection windows and resulting fluorescence intensities normalised afterwards. The exact dimensions of the detection windows are listed in **Table 1**. A sequential scan of both the original 500 - 540 nm window and the red-shifted window was taken at low 488 nm Argon laser power at the end of each experiment to determine the normalisation factor.

Table 1 – Red-shifted, narrowed detection windows for bright compounds.

Compounds	Detection window HEK-LLO	Detection window PC12-AAPH
H_2-FS_1 i_2-FS_1 a_2-FS_1	580 - 585 nm	560 - 565 nm
H_2-FS_0 i_2-FS_0 fluorescein FDP	545 - 570 nm	550 - 565 nm
all other compounds	500 - 540 nm	500 - 540 nm

For compound screening, the scan was started after 10 min of compound incubation. To prevent bias introduced by time delays between compounds imaged in different wells, we permutated the positioning of compounds between replicates. There was a constant time delay of 2.5 min between imaging of the LLO- or AAPH-treated cells and their respective sham-treated controls, ensured by the setup of the plate. For long-term wash-free imaging, additional scans of the same FOVs were started after 15, 25, 35, 55, 75, 105 and 135 min of compound incubation.

In post-wash retention experiments, the pre-wash scan was likewise started after 10 min of compound incubation. Washing was performed as described above and scans of the same FOVs started 0, 10, 20, 40, 60, 90 and 120 min post-wash. For resealing assays, images of each individual well were taken after 10 min of compound incubation in the respective well.

2.2.4.4. Image analysis

Fiji/ImageJ was used for image analysis. All images were segmented into two regions of interest (ROIs), cells and background, based on the CellTracker channel (staining all cells irrespective of damage) using the “Trainable Weka Segmentation” plugin. For reasons further outlined below, the segmentation for the resealing assay was performed on the compound channel. The classifier was trained individually for every image. The generated intracellular ROI was then eroded by 10 pixels. This served to exclude the thin periphery of cells from the analysis, since both CellTracker and compound signal are very low there. The eroded mask

was then applied to the compound channel to obtain mean fluorescence intensity values for cells and background, which were exported to Excel. If these values resulted from detection with red-shifted emission windows, they were subsequently multiplied with a normalisation factor, obtained by measuring and averaging mean fluorescence intensity of ten cells in the original divided by the red-shifted detection window.

All values were normalised to a reference: for compound screening, values were normalised to mean intracellular value of undamaged DMSO-treated cells. For long-term wash-free imaging, values were normalised to mean at 10 min incubation time. For post-wash retention, values were normalised to mean pre-wash. For resealing experiments, values were normalised to mean at 0 min recovery time.

Images that were out of focus, showed less than three cells or overgrown cells (> 2/3 of area covered by cells) as well as images with an intolerable amount of dead cells or debris were excluded from analysis. The complete replicate (damaged and undamaged condition) was repeated for the affected compound, if more than one of three FOVs had to be excluded. GraphPad Prism was used for plotting. Each data point represents one replicate (mean over three fields of view).

Note on the altered segmentation for the resealing assay: Unlike in other experiments, segmentation for the resealing assay was performed not on the CellTracker channel but on the compound channel. This was necessary to exclude cells from analysis that had never been damaged (in the following referred to as “undamaged cells”). While in all HEK-LLO assays a small fraction of cells remains undamaged, as seen by lack of compound uptake, this is no problem as long as this fraction is constant. In the resealing assay however, the delayed medium change increasingly favours detachment of damaged cells towards later timepoints, while undamaged cells remain attached. This introduces bias, as later analysis timepoints will have increased proportions of undamaged cells as compared to earlier timepoints. The bias can be circumvented by segmenting on the compound channel, which only encompasses damaged cells. This approach will however also exclude completely resealed cells from analysis, which despite being initially damaged do not appear in the compound channel once probed. Yet, our data show that this factor is negligible. Using a two-dye approach in which we incubated cells at 0 min recovery time with Alexa Fluor™ 594 Cadaverine and additionally, after up to 2 h recovery time, with MDG1, we could estimate, that less than 3 % of damaged cells completely reseal (data not shown). Although damaged cell detachment mainly happens in the HEK-LLO assay, images from PC12-AAPH resealing experiments were segmented in the same way for reasons of comparability.

2.2.5. Imaging of axonal membrane damage in microfluidic chambers

Preparation of microfluidic chambers and isolation of primary neurons have been described previously (Ashrafi *et al.*, 2014; Harbauer *et al.*, 2022). In brief, 6 well glass bottom plates were washed 3x with distilled water, dried, then coated with 20 mg/ml poly-L-lysine and

3.5 mg/ml laminin overnight. Microfluidic chambers were sterilised with 70 % ethanol, dried and then assembled into the prepared 6 well plates. Hippocampal neurons were dissected at E16.5, pelleted at 4000 g for 4 min and resuspended in primary neuron medium (Neurobasal™ Medium supplemented with Penicillin-Streptomycin-Glutamine (PSG) and B-27™) at a final concentration of 400.000 cells/ml. 10 µl of cell solution were applied to the somal compartments of the microfluidic chambers and incubated at 37°C and 5 % CO_2. After 15 min, wells were completely filled up with medium. Every 2 - 3 days, 50 % of the medium was replaced with fresh primary neuron medium and experiments were performed at 8 or 9 DIV (days *in vitro*). Initial steps were performed in primary neuron medium at 37°C and 5 % CO_2; only the compound incubation was performed in HBSS at 37°C and without CO_2 incubation (pH buffering ensured by HBSS). For MDG1 experiments, 5 µM CellTracker™ Red CMTPX solutions were prepared in medium, added to the top somal and axonal well of the chambers and incubated for 15 min, then rinsed off 2x with medium. This step was skipped for propidium iodide (PI) experiments due to spectral overlap. Next, 300 mM AAPH was prepared in medium, 150 µl added to the top axonal well only and incubated for 90 min. Negative controls received 150 µl of medium only. To ensure proper osmotic pressure, 120 µl of medium (without AAPH) were applied to both somal wells. Microfluidic chambers were then transferred to the microscope, all four wells washed 3x with HBSS and pre-dye images of multiple FOVs acquired using a Nikon Ti2 spinning disk microscope with a 20x air objective. This was directly followed by incubation with either 25 µM MDG1 or 3.3 µg/ml PI. Images of the same FOVs were taken at 15 min incubation time without prior washing.

Fiji/ImageJ was used for images analysis. Mander's co-localisation coefficient between CellTracker and MDG1 was calculated using the JACoP plugin. Five FOVs were chosen for analysis in each condition. Values were exported to Excel; plotting and statistical analysis were performed with GraphPad Prism. Each data point represents one independent experiment (mean of all 5 ROIs). Statistical significance was assessed with ANOVA (analysis of variance).

2.2.6. Experimental animals

All animal experiments were performed in accordance with regulations of the relevant animal welfare acts and protocols approved by the local animal ethics committee of the state of Bavaria (Regierung von Oberbayern) in accordance with European guidelines. Mice were housed at the Core Facility Animal Models of the LMU Biomedical Center under standardised conditions, including 12 hour light / 12 hour dark cycle, individually ventilated cages, social housing with up to 5 mice per cage, standardised cage enrichment and ad libitum access to water and food pellets. All experiments were performed in 8- to 16-week-old transgenic Thy1-CerTN-L15 mice with sparse neuronal expression of a Förster resonance energy transfer (FRET)-based calcium sensor on C57/BL6 background, first described by Heim *et al.* (2007). Male and female mice were equally distributed across the different experimental and control groups.

2.2.7. rAAV-mediated overexpression

2.2.7.1. Molecular cloning of AAV plasmids

Cloning for experimental cohorts 1 and 2 was performed in-house, whereas plasmids for cohort 3 were ordered from a commercial supplier.

For in-house cloning, cDNAs of murine calbindin-D28k (CB) and human calretinin (CR) were kindly provided by Professor Michael Meyer. A plasmid encoding Cre-T2A-KOFP (KOFP = Kusabira Orange fluorescent protein, full plasmid name pAAV-U6-sgRNAbackbone-hSyn-Cre-T2A-KOFP-WPRE) was kindly provided by Adinda Wens. The pAAV backbone for viral packaging of the DNA, also including human synapsin 1 (hSyn) promoter and the mRNA regulatory elements WPRE (woodchuck hepatitis virus posttranscriptional regulatory element) and hGH poly(A) (= pA, poly-adenylation sequence from human growth hormone) were taken from derivatives of the Addgene plasmid #50457, pAAV-hSyn-DIO-EGFP.

The plasmids pAAV-hSyn-CB-T2A-KOFP-WPRE-pA ("CB-KOFP") and pAAV-hSyn-CR-T2A-KOFP-WPRE-pA ("CR-KOFP") were generated by three-fragment Gibson assembly. The first fragment was obtained by digestion of an AAV plasmid (pAAV-hSyn-CalpainSensorV#2-WPRE-pA) with NcoI-HF, cutting directly downstream of the hSyn promoter and NdeI, cutting directly upstream of WPRE. For restriction digest, 4 µg of AAV plasmid were mixed with 2 µl per restriction enzyme and 6 µl of CutSmart^{TM} buffer, filled up with nuclease-free water to 50 µl and incubated at 37°C for 1 h. The other two fragments were obtained by PCR (polymerase chain reaction). Calbindin or calretinin were amplified from the corresponding cDNAs without including the stop codon. T2A-KOFP was amplified from plasmid pAAV-U6-sgRNAbackbone-hSyn-Cre-T2A-KOFP-WPRE. Overlaps between the fragments were generated by adding them to the primer sequence, which was designed using the Gibson assembly tool of the SnapGene software. **Table 2** lists the primers used for each amplification with 5' overlaps highlighted in blue, including Kozak sequence in bold print. PCRs were performed as follows: 0.5 µl of plasmid DNA (25 ng/µl) was mixed with 2.5 µl per primer (10 µM) and 44.5 µl of master mix containing 10 µl Q5 ® High-Fidelity DNA Polymerase Buffer, 1 µl dNTPs (10 mM), 33 µl nuclease-free water and 0.5 µl Q5 ® High-Fidelity DNA Polymerase per sample. The PCR was run in a thermocycler using the following programme: Initial denaturation at 98°C for 30 sec, 30 cycles of denaturation, annealing and elongation (98°C – 5 sec, 70°C – 10 sec, 72°C – 30 sec), final elongation at 72°C for 2 min; except for amplification of KOFP for pAAV-hSyn-CB-T2A-KOFP-WPRE-pA assembly, where annealing temperature was 63°C, as calculated with the NEB T_m calculator browser tool. Restriction digest and PCR products were then loaded onto a 1.2 % agarose gel with peqGREEN DNA stain in TAE buffer and gel electrophoresis run for 45 - 60 min at 110 V. Correct band size was verified using GeneRuler 1 kb DNA ladder as size reference and visualisation under UV. Bands were excised from the gel with a scalpel and DNA purified using the QIAquick Gel Extraction Kit, following manufacturer's instructions. Elution volume was reduced to 15 µl to maximise eluate concentration, which was measured with NanoDrop. For

Table 2 – Gibson assembly primers.

Assembly and amplification of		Primer name	Primer sequence
pAAV-hSyn-CB-T2A-KOFP-WPRE-pA	CB	DB027	5'- CGTGCCTGAGAGCGCAGTCGAGAAACCGGCTA-GAGGCCAC**GCCACC**ATGGCAGAATCCCAC-CTGCAGTCATCTCTGAT - 3'
		DB028	5'- AGCAGACTTCCTCTGCCCTCGTTGTCTCCAGCAGAAA-GAATAAGAGCA - 3'
	KOFP	DB029	5'- TTCTTTCTGCTGGAGACAACGAGGGCAGAG-GAAGTCTGCTAAC - 3'
		DB030	5'- TCACAAATTTTGTAATCCAGAGGTTGATTATCGA-TAATCATCAGCAATGAGCTACTGC - 3'
pAAV-hSyn-CR-T2A-KOFP-WPRE-pA	CR	DB031	5'- CCGGCTAGAG**GCCACC**ATGGCTGGCCCGCA - 3'
		DB032	5'- CTGCCCTCCATGGGGGGCTCGCTG - 3'
	KOFP	DB033	5'- CCCCATGGAGGGCAGAGGAAGTCTGCT - 3'
		DB034	5'- CAGAGGTTGATTATCGATAATCATCAGCAATGAGC-TACTGCATCTTCTACCAGC - 3'

Gibson assembly, digest and PCR products were combined at a molar ratio of 1:3:3 (threefold excess of PCR products), using 100 ng of digested backbone. All three fragments were mixed with 10 µl of Gibson Assembly ® Master Mix, filled to 20 µl with nuclease-free water and incubated at 50°C for 15 min for the three-enzymatic reaction to take place.

The plasmid pAAV-hSyn-Cre-T2A-KOFP-WPRE-pA ("Cre-KOFP") was not obtained by Gibson assembly but by restriction cloning. An AAV plasmid (pAAV-hSyn-KOFP-WPRE-pA) was digested with XbaI, cutting directly upstream of the hSyn promoter and BglII cutting directly downstream of WPRE. The same restriction enzymes were used to excise hSyn-Cre-T2A-KOFP-WPRE from pAAV-U6-sgRNAbackbone-hSyn-Cre-T2A-KOFP-WPRE. Restriction digests were performed as described above, except for use of NEBuffer 3.1 instead of CutSmart™. Gel electrophoresis and band purification from gel were performed as described above. The digestion products were then combined at a molar backbone to insert ratio of 1:3, using 50 ng of backbone. The DNA fragments were mixed with 2 µl T4 DNA Ligase Buffer and 1 µl T4 DNA Ligase, filled to 20 µl with nuclease-free water and incubated at room temperature for 10 min.

For transformation, 1 µl of Gibson assembly or ligation product was added to 20 µl of Stellar ® Competent Cells. The mixture was incubated on ice for 30 min, heat shocked at 42°C for 45 seconds, then put on ice for additional 2 min before 200 µl of S.O.C. medium were added and cultures incubated for 1 h on a thermoshaker set to 37°C and 600 rpm. Agar

plates (10 g tryptone, 5 g yeast extract, 10 g NaCl, 15 g Agar, 1 l H_2O) containing 100 mg/ml ampicillin for antibiotic selection of transformed clones, were pre-heated to 37°C, the bacterial culture added on top and distributed evenly using sterile glass beads. Agar plates were incubated at 37°C overnight and single colonies picked for miniprep into 3 ml LB-Ampicillin (10 g tryptone, 5 g yeast, 10 g NaCl, 1 l H_2O, 100 mg/ml ampicillin) the following day. Minipreps were performed on overnight cultures using the QIAprep Spin Minprep Kit, following the manufacturer's instructions. The isolated DNA was thoroughly sequenced and the integrity of the ITRs (inverted terminal repeats) confirmed by digestion with XmaI. Maxipreps were performed on overnight cultures (500 ml LB-Ampicillin, inoculated with the mini cultures), using the QIAGEN Plasmid Maxi Kit in accordance with the manufacturer's instructions. Sequencing and ITR digests were repeated for the maxi DNA.

Cloning for cohort 3 was outsourced to the commercial contractor VectorBuilder. Plasmids were designed with the "Design My Vector" tool on the company website, using the following building blocks: Vector Type: Mammalian Gene Expression AAV Vector; Promoter: SYN1 (human synapsin 1 promoter); ORF: ["Calbindin" (mCalb1[NM_009788.4]) OR "Calretinin" (mCalb2[NM_007586.2]) OR "ShadowG" (sequence copied from Addgene plasmid #104620)] AND "Kusabira Orange" (sequence copied from plasmid maps of cohorts 1/2); Linker: T2A; Regulatory Elements: WPRE, BGH pA; Antibiotic Resistance: Ampicillin.

2.2.7.2. rAAV production

rAAVs for experimental cohorts 1 and 2 were produced in-house, whereas virus for cohort 3 was ordered from a commercial supplier.

For in-house virus production, eight 14.5 cm cell culture dishes per virus were coated with poly-D-lysine (0.01 mg/ml, 2 h at 37°C), washed with PBS twice and approximately 10 x 10^6 HEK cells seeded per plate to achieve ~ 80 % confluence for transfection on the next day. Per plate, a transfection mix of 16 µg AAV transfer plasmid, 10 µg of PHP.eB AAV capsid plasmid, 20 µg pAdDeltaF6 AAV helper plasmid and 100 µg polyethylenimine (PEI) in 4 ml Opti-MEM™ Reduced Serum Medium was prepared, allowed to rest for 20 - 30 minutes at room temperature, then added to the cells dropwise and evenly distributed across the complete plate area. A medium change to fresh DMEM with Penicillin-Streptomycin but without FBS was performed 24 h later. Expression of the fluorescent reporter became visible under the microscope (Leica DM IL LED) 1 - 2 days post transfection. rAAV-containing supernatant was harvested on day 3 and cells replenished with fresh medium without FBS to allow for another harvest on day 6. Directly after each harvest, the supernatant was centrifuged at 1500 rpm, 5 min, 4°C, filtered through a 0.45 µm filter, then stored at 4°C. After completing the second harvest, the combined filtered supernatant was concentrated using 100 kDa Amicon ® Ultra-15 Centrifugal Filter Units. These were equilibrated by adding 15 ml PBS and centrifugation at 4200 rpm, 2 min, 4°C and then repeatedly loaded and centrifuged (4200 rpm, 30 min, 4°C) with viral supernatant, until the complete volume had been reduced to 300 µl per virus. The concentrated supernatant was used for i.v. injection (see below) without further purification.

2.2.7.3. rAAV titration (qPCR)

The titer of the viral concentrates was assessed by qPCR (quantitative polymerase chain reaction), using Addgene's "AAV Titration by qPCR Using SYBR Green Technology" protocol (https://www.addgene.org/protocols/aav-titration-qpcr-using-sybr-green-technology/). In brief, 5 µl per rAAV were treated with DNase (1 µl DNase, 5 µl DNase buffer, total volume 50 µl) for 30 min at 37°C to remove DNA outside viral capsids. For titering, 10-, 200-, 1000-, 5000-, 25 000-, 125 000-, 625 000- and 3 135 000-fold dilutions of the digested rAAV were prepared by serial dilution. In parallel, a 10x dilution series of the AAV plasmid ranging from 2×10^8 to 2×10^4 molecules per µl was prepared as well. Per well, 5 µl of DNA (AAV dilutions and plasmid standards) were combined with 15 µl of master mix (10 µl Universal SYBR mix, 0.15 µl fwd primer (100 µM), 0.15 µl rev primer (100 µM), 4.7 µl nuclease-free water). The same fwd and rev primers, recognising the viral ITR region up- and downstream of the recombinant viral genome, were used for all viruses. All samples were prepared in technical duplicates. The 96 well qPCR plate was closed with film, briefly centrifuged at 1000 g to collect liquid at the bottom and then ran on a Bio-Rad CFX Real-Time PCR instrument. The following programme was run: 39 cycles, 98°C – 3 min, 98°C – 5 sec, 58°C – 30 sec. Acquired cycle threshold (c_t) values and log10 of known plasmid concentrations were plotted against each other to generate a standard curve. This allowed the deduction of viral copy numbers (viral genomes (vg) / ml) from respective c_t values. Vg/ml values were normalised to dilution and then averaged across all measurements to calculate the vg/ml concentration of the initial concentrate. For cohort 1, virus was aliquoted into Protein LoBind ® tubes and stored at - 80°C. For cohort 2, virus was not aliquoted and stored at 4°C until use.

Virus production for cohort 3 was outsourced to the commercial contractor VectorBuilder. Viruses were ordered ultra-purified (by caesium chloride density gradient) and qPCR-titered. Cohort 3 viruses were shipped on dry ice and upon arrival stored at - 80°C.

2.2.7.4. i.v. injections and experimental timeline

For i.v. injection, viruses were diluted in sterile PBS to a final concentration of 1×10^{13} vg/ml (cohort 1), 2×10^{13} vg/ml (cohort 2) or 1×10^{12} vg/ml (cohort 3), assuring the necessary final dosage within 100 µl injection volume. 8- to16-week-old Thy1-CerTN-L15 mice were randomly assigned to the different viruses, ensuring that males and females were evenly distributed across groups. Mice were then placed in a restrainer and tail vein dilation induced by dipping the tail into hand-warm water. The injection site was disinfected with ethanol and 100 µl of the viral dilution injected intravenously, using a 30 G needle. The mice were checked for adverse effects of i.v. injection on the day after. Their weight was recorded and mice were monitored for behavioural changes, motor symptoms, incontinence and dermatitis. In the absence of symptoms, check-up frequency was reduced to twice weekly. The experiment was timed to allow for approximately 5 weeks between virus injection and imaging readout. To this end, EAE (see below) was induced 21 days after virus injection.

2.2.8. Induction of acute experimental autoimmune encephalitis (EAE)

Mice were anaesthetised with medetomidine (0.5 mg/kg), midazolam (5.0 mg/kg), and fentanyl (0.05 mg/kg), which were applied intraperitoneally (i.p.) using a 30 G needle. They were then immunised with 250 µl of an emulsion containing 200 µg of purified recombinant MOG (N1-125) in complete Freund's adjuvant with 650 µg mycobacterium tuberculosis. The mixture was emulsified by passing it between two connected syringes, then transferred to a Hamilton syringe for subcutaneous injection with a 23 G needle. The injection volume was split between three injection sites: 100 µl were injected per flank and 50 µl at the tail base. The mice also received an i.p. injection of 200 ng pertussis toxin and subsequently, on the contralateral site, an anaesthesia antagonising cocktail (atipamezole: 2.5 mg/kg; flumazenil: 0.5 mg/kg; naloxone: 1.2 mg/kg). The pertussis toxin injection was repeated on day 2 post immunisation. The scoring described above (weight, behavioural changes, motor symptoms, incontinence and dermatitis at the injection site) was performed daily after immunisation. Motor symptoms (= EAE score) were recorded on a 5 point scale as follows: 0, no clinical signs; 0.5, partial tail weakness; 1, tail paralysis; 1.5, gait instability or impaired righting ability; 2, hind limb paresis; 2.5, hind limb paresis with dragging of one foot; 3, total hind limb paralysis; 3.5, hind limb paralysis and forelimb paresis; 4, hind limb and forelimb paralysis; 5, death. Onset of EAE was defined as the first day of EAE score ≥ 0.5.

2.2.9. *in vivo* two-photon imaging of spinal cord

2.2.9.1. Surgery and imaging procedure

Mice were prepared for *in vivo* imaging when reaching peak of disease, which was defined as day 2 - 3 post EAE symptom onset and an EAE score of ≥ 2.5. Mice that had only reached score 2.0 by day 3 post onset were also included.

Mice were anaesthetised with i.p. medetomidine (0.5 mg/kg), midazolam (5.0 mg/kg), and fentanyl (0.05 mg/kg) and placed on a heating pad. Eyes were covered with Bepanthen cream to prevent drying. The dorsal surface of the lumbar spinal cord was surgically exposed by laminectomy as described previously (Nikić *et al.*, 2011). In brief, the back of the mouse was shaved, the skin disinfected with ethanol and a longitudinal skin incision made with a scalpel. Surgery was aided by magnification with a stereomicroscope. The lumbar spinal column was exposed by severing muscle tissue laterally of the spinal column followed by removal of muscle tissue dorsal of vertebrae. To expose the spinal cord, scissors were carefully inserted into the spinal canal to cut the bone and lift off the dorsal roof of the spinal canal. This procedure was performed for vertebrae L3 and L4. The exposed spinal cord was constantly superfused with artificial cerebrospinal fluid (aCSF) to avoid drying. A clamping device was used to position-fix the spinal column and fix it onto the microscope stage to control x, y, z movement during imaging. To allow objective immersion, a 3.5 % agarose well was built up around the surgical opening and filled with aCSF. Breathing and reflexes were checked every 30 min

throughout the surgery and imaging procedures and anaesthesia deepened by re-injection if necessary.

Mice were imaged with an Olympus FV1200 MPE multiphoton microscope equipped with a motorised stage, a 25x/1.25 NA water immersion objective and a spectrally tuneable titanium:sapphire laser emitting femtosecond pulses with a maximum power of 30 mW at the back focal plane. For detection of CerTN-L15 (Cerulean, variant of cyan fluorescent protein (CFP) / Citrine, variant of yellow fluorescent protein (YFP)) and KOFP, the following light path settings were used: Emission light was split by a 560 nm beamsplitter. Shorter wavelengths were reflected onto a cyan-yellow filter cube (cyan 472/30 |505| yellow 520/35) with a shortened yellow bandpass to prevent concomitant detection of KOFP. The cyan-yellow filter cube was positioned in front of two gallium arsenide phosphide detectors. The long-pass of the 560 nm beamsplitter was forwarded to a 580/40 nm bandpass filter for the detection of KOFP on a non-descanned detector photomultiplier tube. The CFP donor of the CerTN-L15 FRET-based sensor was excited at 840 nm and both CFP (donor) and YFP (acceptor) emission recorded simultaneously. Reproducibility of the YFP/CFP ratio between experiments was ensured by running both detectors at the same amplification voltage. KOFP was excited at a wavelength of 1100 nm. Since the setup only possesses one tuneable laser, CerTN-L15 and KOFP images of the same field of view had to be acquired one after another, with a time delay of 2 - 3 min in between. Starting from cohort 3, KOFP images were acquired with 5x averaging to improve image quality. Regions of interest for imaging (usually 5 - 10 per mouse) were selected based on the presence of stage 1 (swollen) and stage 2 (fragmented) axons. Pixel size was 281 x 281 nm with a z-step size of 1 µm. After *in vivo* microscopy and out of deep anaesthesia, mice were transcardially perfused with 4 % paraformaldehyde (PFA) for tissue preservation (see below).

2.2.9.2. Image analysis

In vivo two-photon images of the spinal cord were analysed with Fiji/ImageJ. The evaluator was blinded to the group identity of analysed images. Individual axons were traced in z-stacks and morphological stages (stage 0 “normal”, stage 1 “swollen, stage 2 “fragmented”) assigned as described previously (Nikić *et al.*, 2011). An overlay of the CerTN-L15 and KOFP images was used to identify individual axons as CerTN-L15+/KOFP–, CerTN-L15+/KOFP+ or CerTN-L15–/KOFP+. For CerTN-L15+ axons, three intra-axonal and three adjacent background ROIs were defined and CFP- and YFP intensities measured within to calculate a mean background-subtracted YFP/CFP ratio. The same ROIs were used to estimate axon diameter (= minor axis of elliptic ROI). Staging and fluorescent measurement data of all analysed images was imported into Python and unblinded. Very dim axons (YFP value < 285 on a 12-bit scale), were removed from the analysis as they are prone to tracing and staging errors and can yield inaccurate calcium measurements. The filtered dataset was used to calculate the ratio of KOFP+ per CerTN-L15+ axons per lesion as a proxy for virus efficacy, to plot axon diameter histograms for the different axon subpopulations and to summarise morphological and calcium (YFP/CFP ratio) data. GraphPad Prism was used for plotting and statistics, with

the exception of the diameter histograms which were made with Python's Matplotlib library. For statistical analysis in GraphPad Prism, a Shapiro-Wilk test for normality was first performed for all data sets. Where normality was confirmed, this was followed by parametric analysis of variance (ANOVA) with Bonferroni's multiple comparisons test. Where normality could not be confirmed, a non-parametric test, Kruskal-Wallis test with Dunn's multiple comparisons test, was performed instead. Each data points represents an axon, a lesion or a mouse, as indicated in the figure legend.

2.2.10. Stainings and confocal microscopy of cortex and spinal cord

2.2.10.1. Tissue harvest procedure

Mice were transcardially perfused first with PBS-Heparin (10 U/ml), then with 4 % paraformaldehyde (PFA) for tissue preservation, using a Ismatec IP High Precision Multichannel Pump and a butterfly needle. Skull and vertebral column were isolated and postfixed in 4 % PFA overnight, then transferred to PBS with 0.1 % sodium azide for storage. For staining, brains were carefully removed from the skull and for each mouse a 1 mm thick slice containing motor cortex was prepared with a mouse precision brain slicer. The spinal cord was carefully removed from the vertebral column and a 3 mm long piece of lower thoracic spinal cord isolated from each mouse. Tissue was dehydrated by incubation in 30 % sucrose for 2 - 4 days.

2.2.10.2. NeuroTrace staining of cortex

Brain slices were placed into cryomolds and frozen in Tissue-Tek ® O.C.T. Compound. Frozen blocks were cut into 40 µm thick coronal sections on a cryostat and sections placed into PBS-filled wells of a 48 well plate for free-floating staining. Three sections were cut per brain, spaced by 120 µm. Sections were washed three times with PBS on a tilting shaker before incubation with NeuroTrace™ 640/660 Deep-Red Fluorescent Nissl Stain, diluted 1:1000 in PBS with 0.5 % Triton-X at 7°C overnight. Sections were washed three times with PBS, then transferred onto SuperFrost ® Plus Microscope Slides with a brush. Sections were dried, covered with VECTASHIELD ® Antifade Mounting Medium, coverslipped and sealed with nail polish.

2.2.10.3. Calbindin and calretinin immunostainings of spinal cord

Spinal cord pieces were placed into cryomolds and frozen in Epredia™ M-1 Embedding Matrix. Frozen blocks were cut into 20 µm thick transverse sections, which were directly picked up onto Epredia™ SuperFrost Ultra Plus™ GOLD Microscope Slides for on-slide staining. Slides were dried at room temperature for 40 min, outlined with a ImmEdge ® Hydrophobic

Barrier (PAP) Pen, then rinsed with PBS twice. All incubation and washing steps were performed at room temperature and under slight agitation on an orbital shaker. For blocking, slides were incubated for 1 h with 5 % bovine serum albumin (BSA) in PBS with 0.2 % Triton-X. All subsequent incubations and washes were performed using PBS with 0.2 % Triton-X and 2.5 % BSA unless specified otherwise. Primary antibodies against calbindin (Cat. No. ab108404) or calretinin (Cat. No. SYSY214102) were diluted 1:500 and incubated on-slide overnight. The next day slides were washed three times for 10 min then incubated for 2 h with a donkey anti-rabbit-Alexa Fluor™ Plus 647 secondary antibody, diluted 1:500. Slides were again washed three times for 10 min and a final 1 min wash step was performed with deionised water to remove residual salt. Liquid was shaken off, 80 µl Fluoromount-G™ Mounting Medium added, slides coverslipped and the medium allowed to harden overnight.

2.2.10.4. Confocal microscopy of stained tissue sections

Stained tissue sections were recorded with a Leica SP8 confocal microscope using a 40x/1.30 NA oil immersion objective. For imaging of cortex, light path settings were as follows: KOFP excitation 561 nm (DPSS), emission 575 - 615 nm; NeuroTrace excitation 633 nm (HeNe), emission 645 - 685 nm. Both channels were recorded with hybrid photo detectors and acquired sequentially to avoid crosstalk. Pixel size was 1.1 x 1.1 µm with a z-step size of 3 µm. For imaging of spinal cord, light path settings were as follows: CerTN-L15 excitation 488 nm (Argon), emission 498 - 538 nm; KOFP excitation 561 nm (DPSS), emission 571 - 611 nm; Alexa Fluor™ Plus 647 excitation 633 nm (HeNe), emission 643 - 683 nm (for CR) or 643 - 703 nm (for CB). All three channels were recorded with hybrid photo detectors and acquired sequentially to avoid crosstalk. Pixel size was 284 x 284 nm with a z-step size of 3 µm.

2.2.10.5. Image analysis

Confocal images were analysed with Fiji/ImageJ. All plotting and statistical analysis was performed using GraphPad Prism.

For analysis of viral transduction in cortex, in each image a small area with the same anatomical location, 280 µm wide and encompassing all cortical layers was defined. Within one z-slice of this area, all NeuroTrace positive cells were manually outlined. This ROI set was then overlaid onto the KOFP channel and mean grey value measurements made for each identified cell. ROIs with an area below 20 μm^2 were excluded from analysis as they likely do not represent neurons. A KOFP fluorescence background measurement was made for each image by defining, measuring and averaging over three areas without KOFP+ cells. Cells were defined as KOFP+ when the cellular KOFP measurement was at least 1.5-fold brighter than the background measurement of the same image. Based on this data, number of KOFP+ cells per NeuroTrace+ cells and mean fluorescence intensity of KOFP+ cells were calculated for each image. A Shapiro-Wilk test for normality was performed for both data sets. Where normality

was confirmed, this was followed by ANOVA with Bonferroni's multiple comparisons test. Where normality could not be confirmed, a non-parametric test, Kruskal-Wallis test with Dunn's multiple comparisons test, was performed instead.

For analysis of calbindin and calretinin overexpression, one representative image per mouse and staining was selected for analysis. For these images, CerTN-L15+ or KOFP+ cells in the grey matter were manually outlined throughout the complete z-stack (each cell defined in the z-slice where it was best in focus). To prevent bias, both CerTN-L15 and KOFP were indistinguishably displayed in greyscale and the calbindin/calretinin channel completely removed for cell definition. Subsequently, an adjacent background ROI was defined for each cell, displaying all channels to ensure that the ROIs actually represent tissue background. Measurements of mean grey values were made for all cells and channels and corresponding background subtracted for each. For correlation, KOFP measurements were plotted against calbindin or calretinin staining intensity. A linear regression curve was added, and Spearman r calculated as a rank-based measure of correlation, as normality, assessed with Shapiro-Wilk test, could not be confirmed. To visualise the degree of overexpression, calbindin or calretinin staining intensity was compared between KOFP– and KOFP+ cells. A cell was defined as KOFP+, when the KOFP measurement of the cell was at least 1.5-fold brighter than for the corresponding background ROI. Since Shapiro-Wilk test did not confirm normality, groups were compared by non-parametric Kruskal-Wallis with Dunn's multiple comparisons test.

2.2.11. Flow cytometry-based analysis of viral expression efficacy *in vitro*

2.2.11.1. Flow cytometry of transfected HEK cells

HEK cells were seeded into cell culture treated 12 well plates at a density of 100.000 cells per well and transfected 3 h later. For transfection, 320 ng of plasmid per well were combined with 2 µl PEI and 80 µl Opti-MEM™ Reduced Serum Medium, left to rest at room temperature for 30 min, then added dropwise to the well. Four days later, cells were detached with trypsin, pelleted, then resuspended in PBS and transferred to U-bottom 96 well plates. KOFP fluorescence in transfected cells was analysed with a Beckman Coulter Cytoflex S and with FlowJo.

2.2.11.2. Flow cytometry of infected HeLa cells

HeLa cells were seeded into cell culture treated 48 well plates at a density of 8.000 cells per well and infected one day later. For infection, 10^{13} viral particles were added per well. Three days later, cells were detached with trypsin, pelleted, then resuspended in PBS and transferred to U-bottom 96 well plates. KOFP fluorescence in infected cells was analysed with a Beckman Coulter Cytoflex S and with FlowJo.

2.2.12. Statistical analysis

GraphPad Prism was used for all statistical analyses. Descriptions of statistical approaches can be found in the figure legends and are described above for each image analysis individually. In brief, error bars represent standard deviation (SD) unless noted otherwise. Shapiro-Wilk test was used to test samples for normal distribution. ANOVA with Bonferroni multiple comparison test was used for variance testing in normally distributed samples. Kruskal-Vallis test with Dunn's multiple comparison test was used instead, where normality could not be confirmed. Spearman rank correlation test was used to test for correlation in non-normally distributed samples.

3. Results

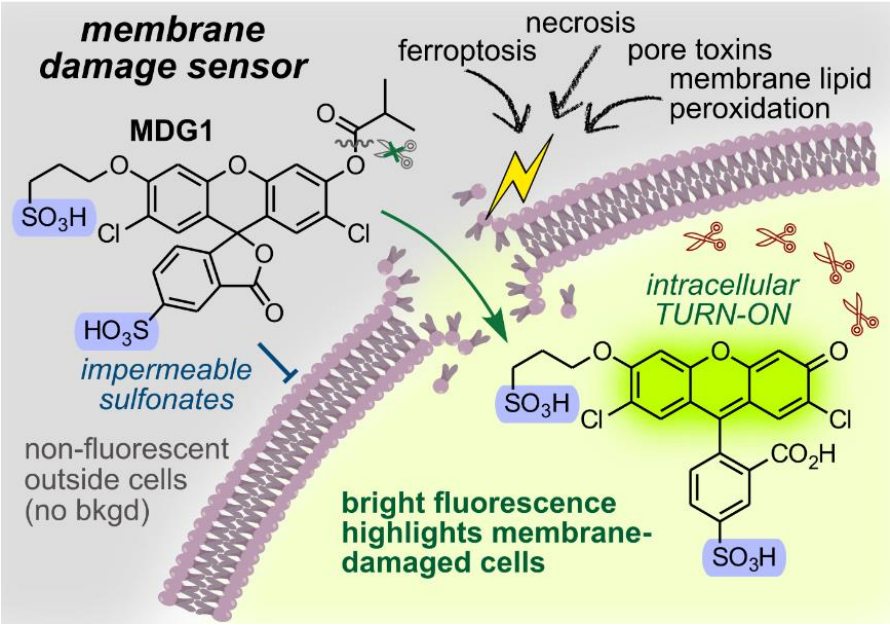

Figure 7 – Selective fluorescent labelling of membrane-damaged cells using polar, ester-capped dichlorofluorescein derivatives.
Membranes can be damaged by various mechanisms including ferroptosis, necrosis, pore-forming toxins and lipid peroxidation. Damage to the membrane impairs its barrier function so that it can become permeable to compounds that would otherwise be excluded. We have exploited this system to develop a fluorogenic probe termed MDG1 (membrane damage green 1, see top left), which by origin is non-fluorescent due to chemical capping and membrane-impermeable due to two permanently charged sulfonate groups (-SO_3H, shaded in blue). Upon membrane damage MDG1 can enter cells, and its fluorescence is released by uncapping. The necessary ester cleavage is performed by esterases (red scissors), which are only present inside but not outside the cell. This results in bright cytosolic fluorescent labelling of membrane-damaged cells with no fluorescent background extracellularly. Reprinted with permission from J. Am. Chem. Soc. 2024, 146, 11072−11082. Copyright © 2024 American Chemical Society. Probe design and figure design by Philipp Mauker.

3.1. Development and application of a membrane damage-selective biosensor

As outlined in the aims of this thesis, the long-term purpose of this project was to establish a selective targeting approach to deliver potential axoprotective drugs, such as calcium chelators, directly to damaged axons using their characteristic membrane nanoruptures as an entry path. As a proof-of-principle study, we first delivered fluorogenic compounds ("turn-on fluorophores") to membrane-damaged cells *in vitro*. Beyond its purpose to guide prodrug development, the selective fluorogenic compound can also act in and of itself as a biosensor for membrane damage and aid the study of compromised cells or axons that find themselves at the crossroads between degeneration and repair/survival. This project was carried out in collaboration with Philipp Mauker and Oliver Thorn-Seshold, Department of Pharmacy, LMU Munich.

We based our compounds on dichlorofluorescein, a small, bright organic fluorophore, which can be trapped in a non-fluorescent state, disabling π-conjugation, by chemical capping. When

using esters for capping, the fluorophore can be rapidly released by intracellular esterases (Rotman and Papermaster, 1966). This approach to fluorogenicity has been widely used for dichlorofluorescein and other compounds and prevents background fluorescence in the extracellular space. In the following chapters, capped non-fluorescent compounds will be referred to as "probes" and the uncapped fluorescent compounds as "fluorophores".

Due to the lipophilic nature of the plasma membrane, small apolar molecules can freely cross it, while larger or more polar molecules cannot. One way to impermeabilise molecules is therefore, to attach permanently charged groups, such as sulfonates (Guthrie, 1978). In order to find a compound that selectively labels membrane-damaged cells, i.e. a compound that is excluded from healthy cells but taken up by and activated in damaged cells, we synthesised a range of polar dichlorofluorescein derivatives. These were then screened for their performance in *in vitro* assays of plasma membrane damage. A graphic summary of the chemical approach can be found in **Figure 7**.

3.1.1. Compound screening identifies membrane damage green 1 (MDG1), a disulfonated probe reliably acting as membrane damage sensor

As described previously, we based our biosensor approach on dichlorofluorescein (new nomenclature: H_2-FS_0), to which we attached different impermeabilising and capping groups to obtain a range of differently polar candidates (see **Figure 8** for structures and nomenclature). With the exception of i_2-FS_0 and FDP, which were included as reference to existing work in the field (Chyan *et al.*, 2017; Rotman *et al.*, 1963), these are novel probes and have first been described by us. A more thorough explanation of the rationale for single candidate design and of the synthesis routes can be found elsewhere (Mauker, Beckmann *et al.*, 2024). Candidate design and chemical synthesis were performed by Philipp Mauker at LMU Munich, Department of Pharmacy.

We measured absorption and emission spectra of the novel fluorophores (**Supplementary Figure 1a, b**) and used these to calculate quantum yields (**Supplementary Table 1**). Compared to dichlorofluorescein (H_2-FS_0), peak absorption of H_2-FS_1 was slightly red-shifted (from 502 to 507 nm) whereas the asymmetric mono-capped fluorophores (H-Me-FS_1, H-EM-FS_1, H-PS-FS_1 and H-PS-FS_2) showed two absorption maxima at around 460 and 485 nm. Their absorbance at 485 nm is 4-fold lower than for H_2-FS_0 and H_2-FS_1 leading also to a 4-fold lower quantum yield. Emission spectra were not notably different between fluorophores (emission maximum ~ 525 nm). All fluorophores were photostable (**Supplementary Figure 1c**) and stocks of the capped non-fluorescent probes were sufficiently stable in handling (< 5 % ester cleavage into active fluorophores), as concluded from their low absorption and emission (**Supplementary Figure 1d, e**). To enable wash-free imaging without background, a probe must fulfil two additional criteria: (1) It has to remain non-fluorescent outside cells, i.e. spontaneous non-enzymatic hydrolysis has to be avoided, and (2) enzymatic processing inside the cell has to be rapid to generate detectable fluorescence. We tested probe

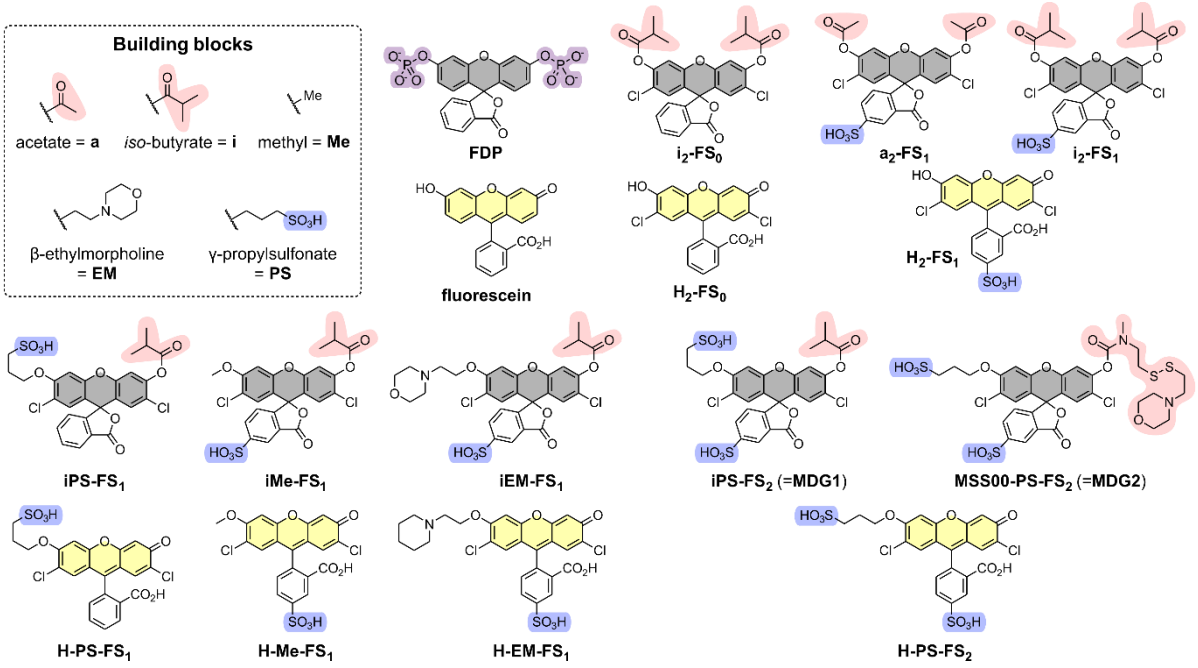

Figure 8 – Structure overview of all probes and fluorophores and their naming rationale. Non-fluorescent probes (capped structure before cleavage) are shaded in grey. The corresponding fluorophores they release upon cleavage are placed directly below (centred, if two probes release the same fluorophore) and shaded in yellow. Capping groups are shaded in pink and impermeabilising groups in blue. Capping groups of FDP are shaded in purple as they are at the same time impermeabilising. FDP = fluorescein-diphosphate. For all other compounds nomenclature was defined as follows: Groups attached to the xanthene (three-ring system with central oxygen) are listed before the hyphen. H, a hydrogen atom, indicates absence (past cleavage) of other chemical groups. "F" denotes the dichlorofluorescein core. S_n indicates the total number of sulfonates. Accordingly, dichlorofluorescein itself becomes H_2-FS_0 using this nomenclature. For ease of name use, our star compound iPS-FS_2 is also referred to as MDG1 (membrane damage green 1) and its derivative MSS00-PS-FS_2 as MDG2. Adapted and reprinted with permission from J. Am. Chem. Soc. 2024, 146, 11072−11082. Copyright © 2024 American Chemical Society. Chemical synthesis and figure by Philipp Mauker.

stability in three different media, PBS, HBSS and DMEM. As expected from the media composition, spontaneous hydrolysis was lowest in PBS, somewhat higher in HBSS and very pronounced in DMEM (**Supplementary Figure 1g, h**). Likewise expected (Chyan *et al.*, 2017), isobutyrates (i) were more hydrolytically stable than acetates (a). As a compromise between probe stability and cell viability, we decided to perform live cell imaging experiments in HBSS. Probe activation by esterases was measured cell-free by incubation with porcine liver esterase, which clearly activated probes above spontaneous hydrolysis (**Supplementary Figure 1f**). Activation of single-capped probes (i) was considerably quicker than activation of double-capped probes (i_2, a_2). Photocharacterisation, cell-free stability measurements, and esterase activation assays were performed by Philipp Mauker.

To act as a membrane damage biosensor, a probe must be excluded from healthy cells while crossing damaged plasma membranes. To find out which of our probes fulfils these criteria, we modelled plasma membrane damage *in vitro* and performed confocal live cell imaging (**Figure 9a**). Different stressors can induce different types of membrane damage. We decided to first induce a very simple and well-defined form of damage, using the bacterial

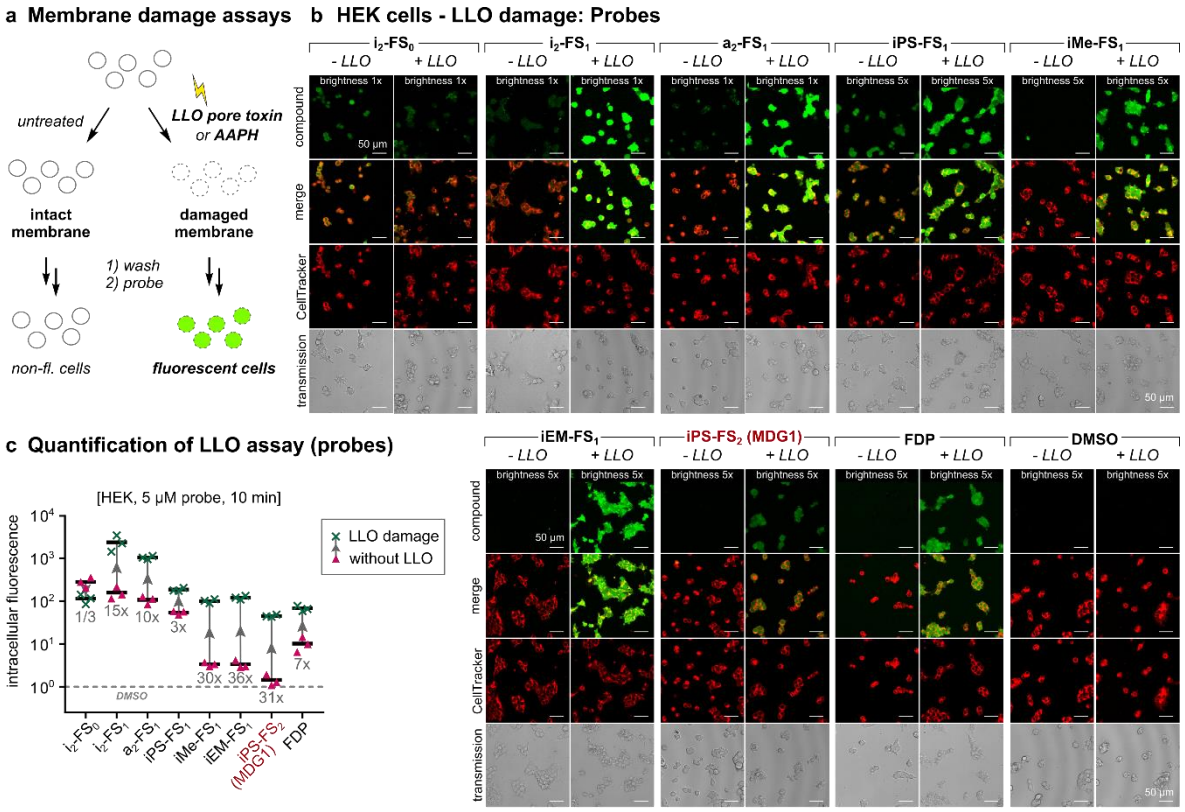

Figure 9 – Uptake of probes into LLO-damaged HEK cells.
(a) Schematic representation of membrane damage assays: membranes are damaged by incubating cells with either lysteriolysin O (LLO, bacterial pore-forming toxin) or 2,2'-azobis(2-amidinopropane) dihydrochloride (AAPH, free radical donor), while control cells remain untreated. The damaging agent is then washed off and cells are subsequently incubated with the fluorogenic probes. A successful probe will label cells in the damaged condition only. **(b)** Confocal microscopy images of live HEK cells incubated with LLO (or sham) for 5 min followed by 5 µM probe treatment. Images taken after 10 min of probe incubation without prior washing. **(c)** Quantification of intracellular fluorescence, normalised to DMSO, for damaged vs. undamaged cells. n = 3, each data point represents an independent experiment, horizontal lines indicate means. The factor below each dataset denotes the ratio between damaged and undamaged cell fluorescence. Scale bars 50 µm. To enable visualisation across the vast range of fluorescence intensities, dim compounds are displayed with enhanced brightness (5x); 1x in this figure equals 1x in Figure 10 and Figure 15c. Dotted vertical line in (c) denotes intracellular fluorescence of DMSO-treated undamaged HEK cells, DMSO = dimethyl sulfoxide. Adapted and reprinted with permission from J. Am. Chem. Soc. 2024, 146, 11072−11082. Copyright © 2024 American Chemical Society.

pore-forming toxin lysteriolysin O (LLO). This toxic protein oligomerises in the plasma membrane, thereby forming a non-selective channel that is permeable to ions and small molecules. Due to these characteristics, LLO has been exploited previously to deliver otherwise impermeable small molecules into cells (Murakami *et al.*, 2018). We treated HEK cells with 0.2 µg/ml LLO for 5 min, washed off LLO and incubated LLO-damaged and undamaged control cells with 5 µM of the different probes for 10 min until image acquisition (**Figure 9b**).

All probes showed turn-on from zero extracellular background, indicating that spontaneous hydrolysis in HBSS was indeed minimal and washing off probes is not required. Due to the intensity differences between the released fluorophores, which result from their different

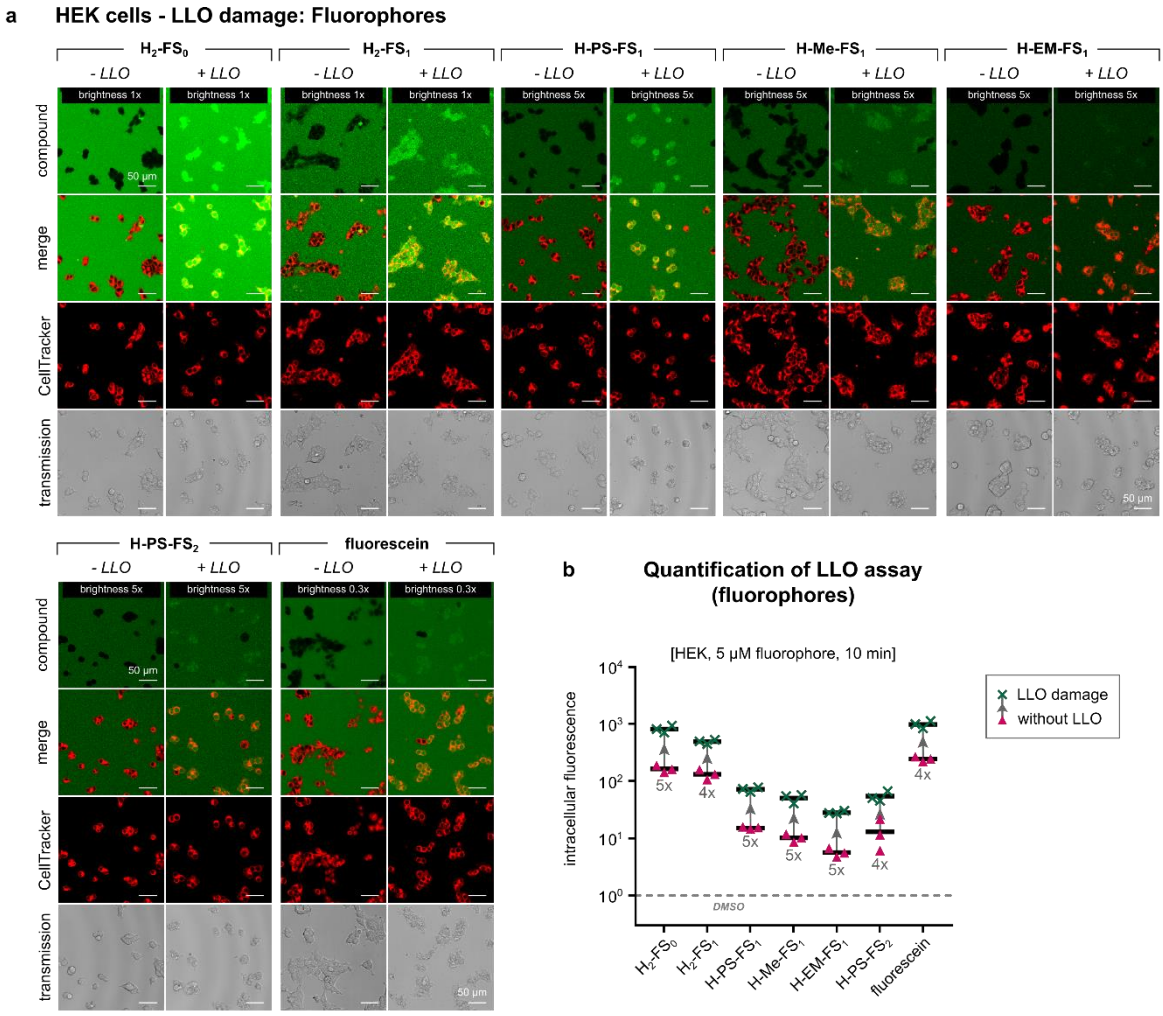

Figure 10 – Uptake of fluorophores into LLO-damaged HEK cells.
(a) Confocal microscopy images of live HEK cells incubated with LLO (or sham) for 5 min followed by 5 µM fluorophore treatment. Images taken after 10 min of fluorophore incubation without prior washing. **(b)** Quantification of intracellular fluorescence, normalised to DMSO, for damaged vs. undamaged cells. n = 3, each data point represents an independent experiment, horizontal lines indicate means. The factor below each dataset denotes the ratio between damaged and undamaged cell fluorescence. Scale bars 50 µm. To enable visualisation across the vast range of fluorescence intensities, dim compounds are displayed with enhanced brightness (5x) while very bright compounds are dimmed down (0.3x); 1x in this figure equals 1x in Figure 9 and Figure 15c. Dotted vertical line in (b) denotes intracellular fluorescence of DMSO-treated undamaged HEK cells. DMSO = dimethyl sulfoxide. Adapted and reprinted with permission from J. Am. Chem. Soc. 2024, 146, 11072−11082. Copyright © 2024 American Chemical Society.

quantum yields, microscopy images are displayed at different brightness levels to keep the focus on compound localisation rather than intensity. As reported previously, i_2-FS_0, which bears no impermeabilising groups, can enter and label undamaged cells (Chyan *et al.*, 2017). It is the only probe that generates less signal in permeabilised compared to healthy cells, which might be explained by severe leak-out from damaged cells after activation. Interestingly, addition of just one sulfonate group was not enough to exclude probes from healthy cells: i_2-FS_1, a_2-FS_1 and iPS-FS_1 show a stronger signal in LLO-damaged compared to undamaged cells, yet the fluorescent signal in undamaged cells remains considerably high, which is undesirable for a membrane damage sensor (**Figure 9b, c**). We did observe an exclusion from

healthy cells for iMe-FS_1 and iEM-FS_1, which are modifications of i_2-FS_1, in which one capping group is replaced by a more polar moiety, as well as for the disulfonated probe iPS-FS_2 (**Figure 9b, c**). All three show around 30-fold signal increase in damaged over healthy cells, thereby outcompeting the commercially available compound FDP, which shows poorer cell exclusion and only 7-fold increase upon damage. Of note, FDP was originally developed as a fluorogenic phosphatase substrate and not intended as a membrane damage sensor (Rotman *et al.*, 1963), explaining the mediocre performance in this setting. Overall, iPS-FS_2 achieves the best performance as it has the lowest fluorescence in undamaged cells and can thus detect damage with the highest specificity. For ease of name use, lead compound iPS-FS_2 will also be referred to as MDG1 (membrane damage green 1).

We also incubated LLO-damaged and healthy HEK cells with the permanently fluorescent fluorophores (**Figure 10a, b**). In contrast to the turn-on probes, these show high extracellular fluorescence and can only enter permeabilised cells, while healthy cells appear as "shadow images". This experiment emphasises the elegance of the turn-on approach, which greatly increases the contrast between cells and extracellular background. The intracellular fluorescence measurements for fluorophore-excluding healthy cells are likely overestimated due to inclusion of a few very bright background pixels in the intracellular measurements, emphasising again the advantages of zero background when using turn-on mechanisms.

We next turned our attention to a different type of membrane damage: lipid peroxidation. Radical damage to the plasma membrane occurs at ROS- and RNS-laden sites of inflammation or in ferroptosis and can alter membrane lipids, resulting in increased membrane permeability (Haider *et al.*, 2011; Stockwell, 2022; Pedrera *et al.*, 2021). Since our main interest lies in targeting membrane-damaged axons, we decided to use a neuronal cell line, PC12, for these experiments. Although the cause of membrane damage in axons in inflammatory lesions is currently unknown, such lesions have high loads of ROS and RNS, making permeabilisation due to lipid peroxidation a plausible hypothesis. To induce lipid peroxidation *in vitro*, we incubated PC12 cells with the radical-generating initiator 2,2'-azobis(2-amidinopropane) (AAPH) (Miki *et al.*, 1987) **(Figure 11**). In this membrane damage assay, only MDG1 turned out as a reliable damage sensor: it is excluded by healthy PC12 cells but enters upon AAPH damage (**Figure 11a,b**). The difference between the two conditions is 8-fold, i.e. lower than the 31-fold change seen in the simpler membrane damage assay. iMe-FS_1 and iEM-FS_1, which had reported well on LLO damage in HEK cells did show residual uptake into healthy PC12 cells and small to no signal increase in AAPH damage. They were therefore not further pursued. FDP was at the limit of detection in this setup and although excluded from healthy PC12 cells, its signal did increase only very slightly (3-fold) in AAPH damage. We think that the fold change between the damaged and undamaged condition may be overall lower with AAPH compared to LLO (**Figure 9c and Figure 11b**) because lipid peroxidation unlike LLO does not create large organised voids to permeate through but much smaller "creases" that compounds need to "wriggle" through.

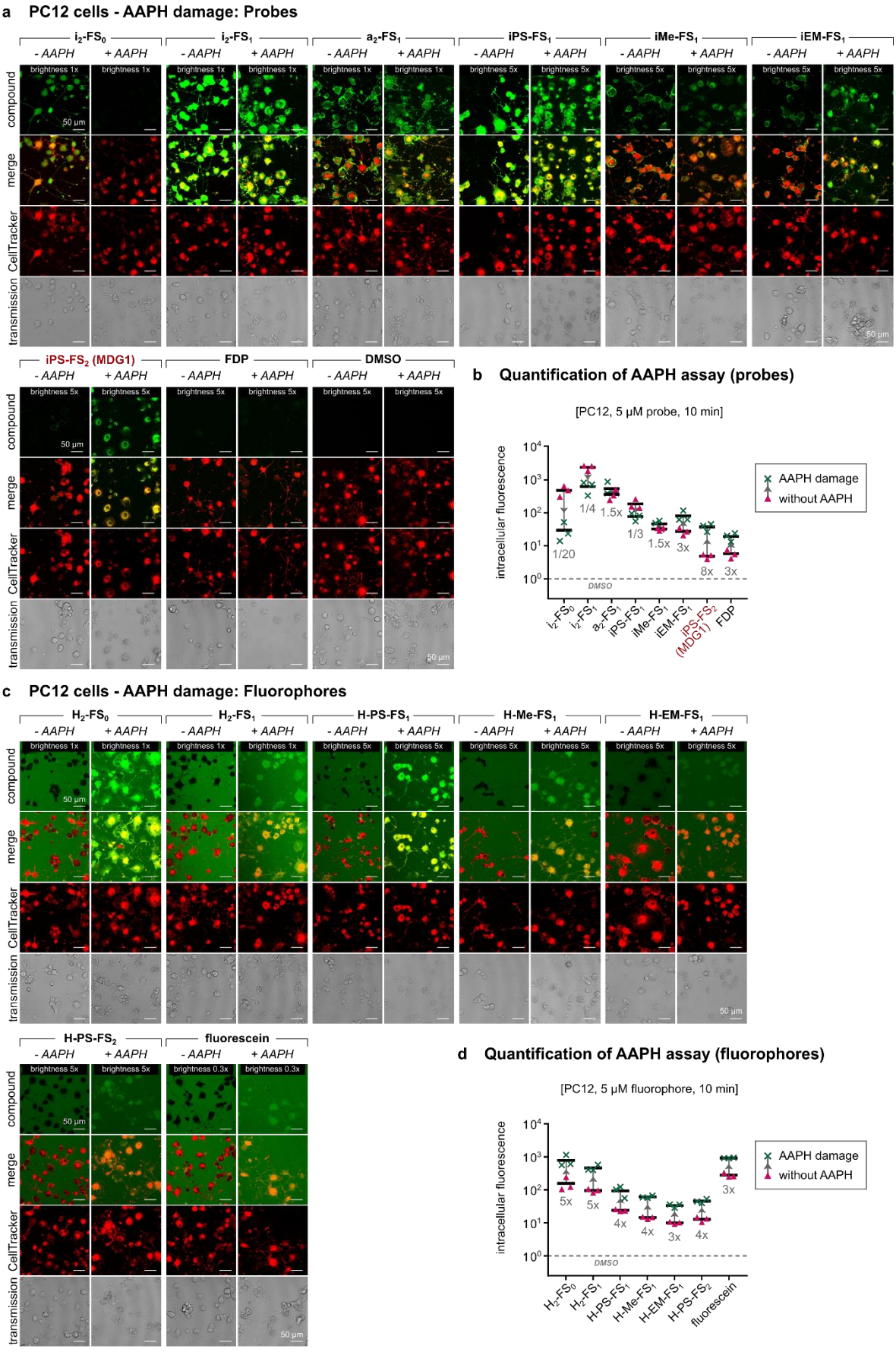

Figure 11 – Uptake into AAPH-damaged PC12 cells.
(Figure legend on next page)

(Legend for Figure 11) **(a, c)** Confocal microscopy images of live PC12 cells incubated with AAPH (or sham) for 90 min followed by 5 µM probe (a) or fluorophore (c) treatment. Images taken after 10 min of probe/fluorophore incubation without prior washing. **(b, d)** Quantification of intracellular fluorescence, normalised to DMSO, for damaged vs. undamaged cells. n = 3, each data point represents an independent experiment, horizontal lines indicate means. The factor below each dataset denotes the ratio between damaged and undamaged cell fluorescence. Scale bars 50 µm. To enable visualisation across the vast range of fluorescence intensities, dim compounds are displayed with enhanced brightness (5x) while very bright compounds are dimmed down (0.3x); 1x in this figure equals 1x in Figure 15e. Dotted vertical line in (b, d) denotes intracellular fluorescence of DMSO-treated undamaged PC12 cells. DMSO = dimethyl sulfoxide. Adapted and reprinted with permission from J. Am. Chem. Soc. 2024, 146, 11072−11082. Copyright © 2024 American Chemical Society.

We also tested the permanently fluorescent fluorophores on AAPH-damaged PC12 cells and found that analogous to findings with LLO, they could only penetrate AAPH-damaged PC12 cells (**Figure 11c, d**).

In summary, the disulfonate MDG1 resulted to be our best probe for charge-based discrimination of membrane damage, as it was the only probe that was excluded by healthy HEK and PC12 cells and taken up after LLO- and AAPH-induced membrane damage. Its broad applicability across different cell types and membrane stressors was confirmed by two additional experiments: MDG1 successfully reported on ferroptosis induced by inhibition of glutathione peroxidase 4 (GPX4) and on the extent of a laser-induced necrotic lesion. These experiments were performed in T cells isolated from murine lung and drosophila embryo epithelium respectively (data not shown, experiments performed by Chantal Wientjens and Andrew J. Davidson, see Mauker, Beckmann *et al.*, 2024).

3.1.2. MDG1-labelling is stable long-term in non-washed cells but poorly retained post-wash

After confirming that MDG1 reliably acts as membrane damage sensor across different cell types and membrane stressors, we next addressed practical aspects of MDG1 application. Only 10 minutes are necessary for effective loading of MDG1 into membrane-damaged cells (**Figure 9b, c, Figure 11a, b**), however some research questions may require longer tracking of MDG1-labelled cells. We therefore followed up on MDG1-treated cells and found that they remain clearly labelled for at least 2 h if MDG1 is not removed from the medium (**Figure 12a, b**). This comes however at the cost of diminished contrast, as the extracellular signal slowly increases. Importantly though, the background remains much lower than the cellular signal, which for LLO-damaged HEK cells plateaus at 75% of the initial signal and for AAPH-treated PC12 cells even continues to rise over the complete 2 h time window studied. The results are markedly different, when MDG1 is washed off after 10 min of loading time and cells observed afterwards (**Figure 13a, b**). Since H-PS-FS_2, the fluorophore released by uncapping of MDG1, is not designed to interact with any cellular components, it can freely diffuse out into the medium. Indeed, LLO-damaged HEK cells lose more than 90 % of their initial signal within 40 minutes, when there is no extracellular MDG1 to compensate for the loss.

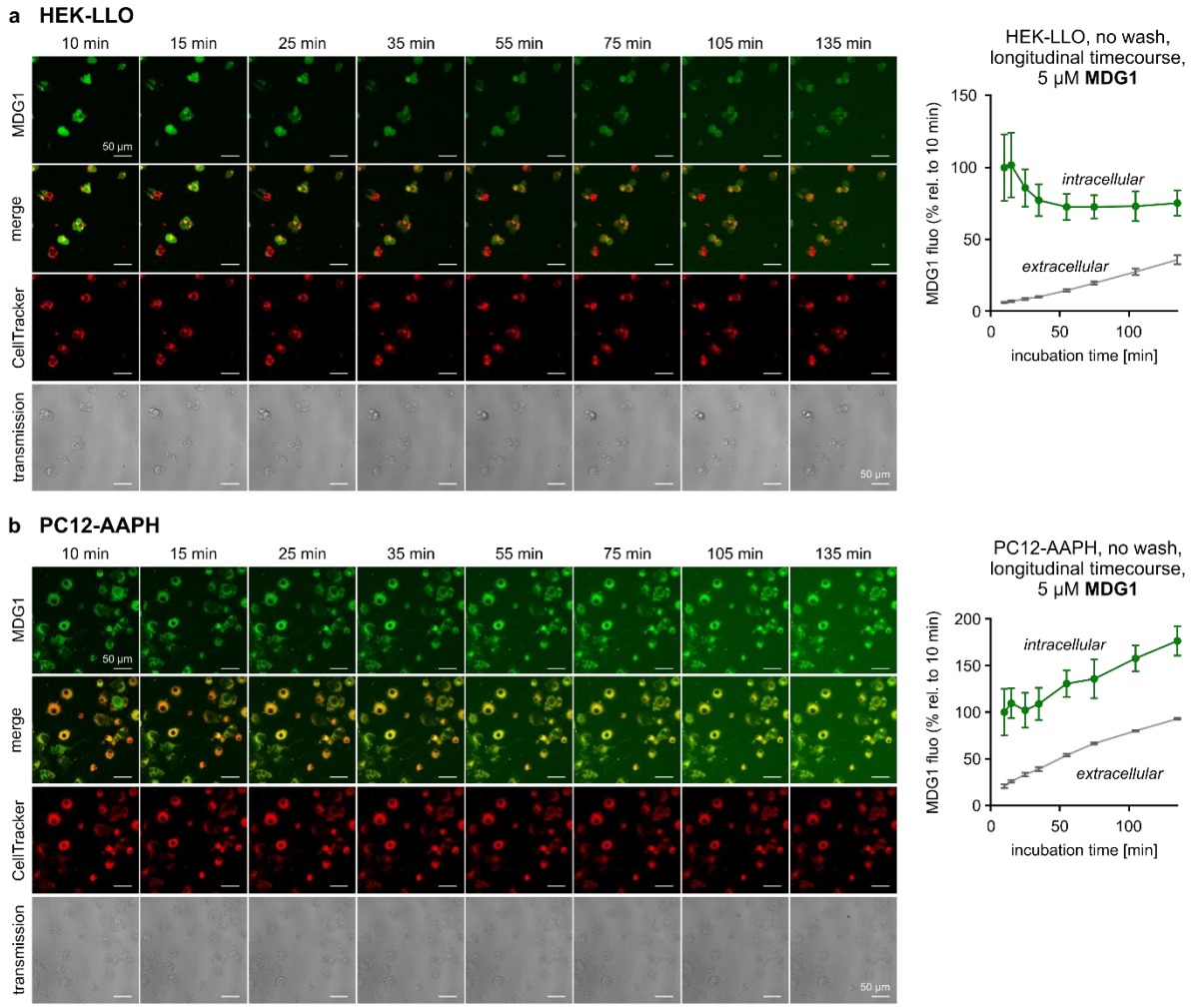

Figure 12 – Long-term incubation with MDG1.
(a) *left:* Confocal microscopy images of live HEK cells damaged with LLO, then incubated with 5 µM MDG1. Images were taken longitudinally at the indicated timepoints post addition of MDG1, which was not washed off at any time. *right:* Quantification of intra- and extracellular MDG1 fluorescent signal over the time course of the experiment, normalised to intracellular signal at 10 min. n = 3 independent experiments, mean ± standard deviation. **(b)** *left:* Confocal microscopy images of live PC12 cells damaged with AAPH, then incubated with 5 µM MDG1. Images were taken longitudinally at the indicated timepoints post addition of MDG1, which was not washed off at any time. *right:* Quantification of intra- and extracellular MDG1 fluorescent signal over the time course of the experiment, normalised to intracellular signal at 10 min. n = 3 independent experiments, mean ± standard deviation. Scale bars 50 µm. Adapted and reprinted with permission from J. Am. Chem. Soc. 2024, 146, 11072−11082. Copyright © 2024 American Chemical Society.

AAPH-damaged PC12 cells retain the signal much better, they quickly reach a plateau of one third of the pre-wash fluorescence intensity, which is significantly higher than autofluorescence of non-labelled cells. Although this indicates that these cells can be distinguished from undamaged cells even post-wash, we generally advise to use MDG1 in wash-free setups. The difference in long-term retention between the HEK-LLO and PC12-AAPH assays caught our attention, and we speculated, that it might be due to more efficient membrane repair in the AAPH condition, which prevents further leak-out. We therefore set out to test this hypothesis by repurposing our membrane damage sensor MDG1 as a resealing sensor. More precisely,

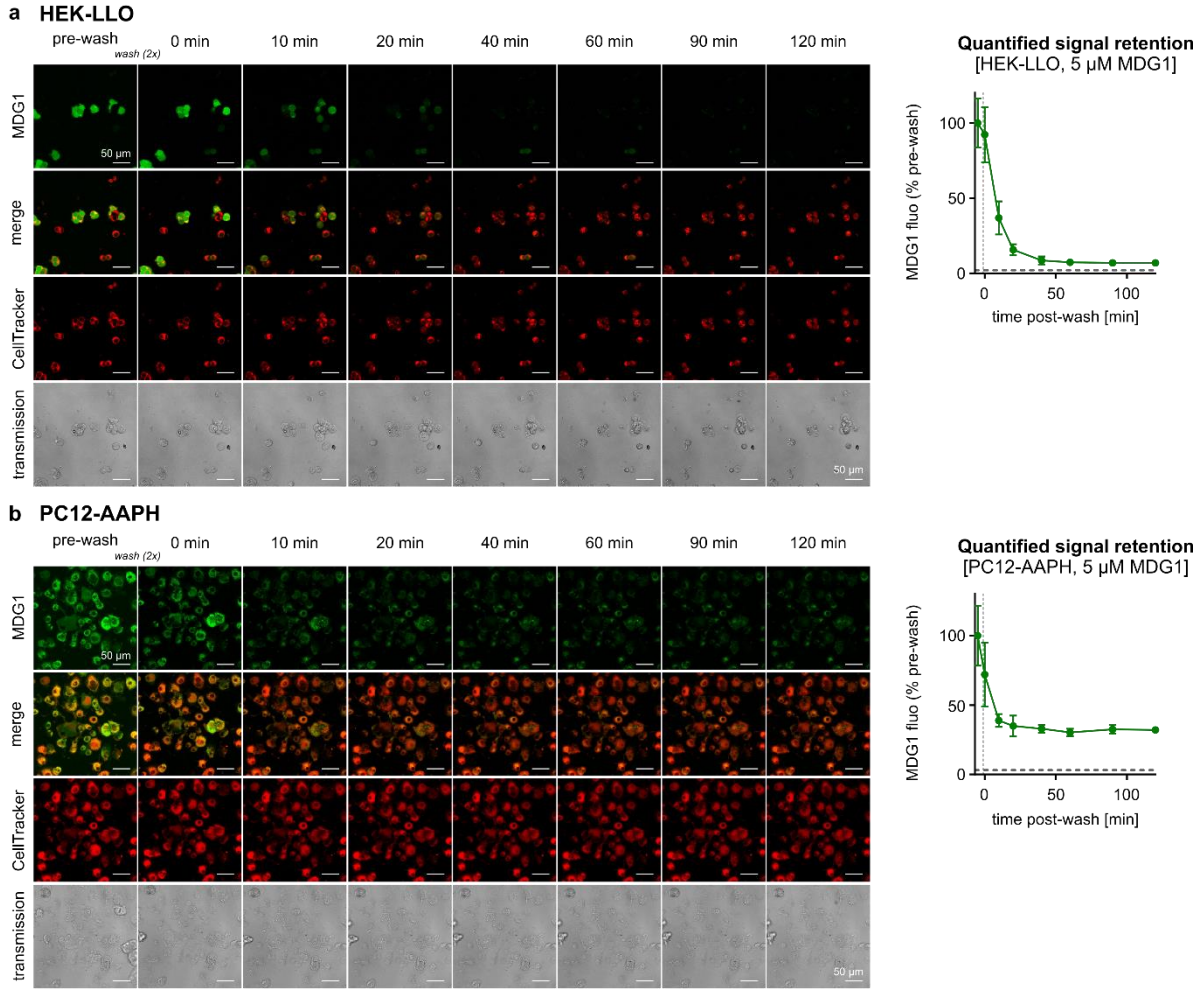

Figure 13 – Post-wash signal retention of MDG1.
(a) *left:* Confocal microscopy images of live HEK cells damaged with LLO, then incubated with 5 µM MDG1 for 10 min, afterwards washed and incubated in fresh HBSS. Images were acquired longitudinally, once pre-wash and at the indicated timepoints post-wash. *right:* Quantification of intracellular MDG1 fluorescent signal over the time course of the experiment, normalised to signal pre-wash. n = 3 independent experiments, mean ± standard deviation. **(b)** *left:* Confocal microscopy images of live PC12 cells damaged with AAPH, then incubated with 5 µM MDG1 for 10 min, afterwards washed and incubated in fresh HBSS. Images were acquired longitudinally, once pre-wash and at the indicated timepoints post-wash. *right:* Quantification of intracellular MDG1 fluorescent signal over the time course of the experiment, normalised to signal pre-wash. n = 3 independent experiments, mean ± standard deviation. Scale bars 50 µm. Dashed lines in (a, b) indicate level of autofluorescence in damaged cells without MDG1. Adapted and reprinted with permission from J. Am. Chem. Soc. 2024, 146, 11072−11082. Copyright © 2024 American Chemical Society

we added MDG1 to cells after different post-stress recovery times of up to 2 h. Indeed, in the PC12-AAPH assay we did observe a linear decline in MDG1 uptake when the probe was added after increasing recovery times, indicating that PC12 cells do repair the AAPH-induced damage to their plasma membrane and slowly reseal (**Figure 14b**). LLO-damaged HEK cells also showed an initial signal decrease, indicative of resealing but then plateaued at around 40 % of the original non-recovery signal (**Figure 14a**). While this is in itself an interesting finding that exemplifies the types of studies our membrane damage sensor facilitates, it does not fully explain the long-term difference in dye retention between the two assay types, since

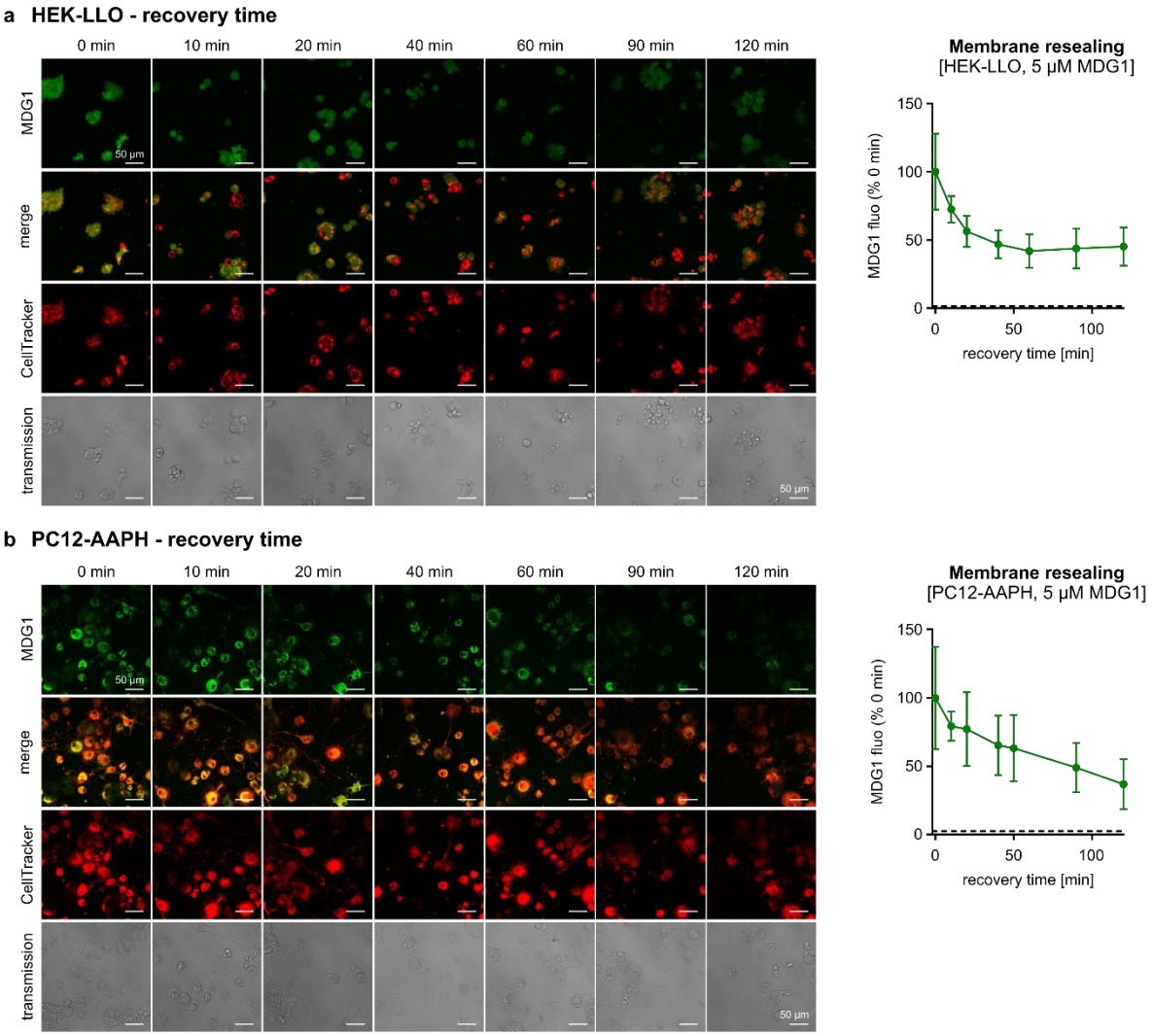

Figure 14 – Resealing of plasma membrane after LLO- or AAPH-mediated damage.
(a) *left:* Confocal microscopy images of live HEK cells damaged with LLO. Cells were allowed to recover for the indicated amount of time, then incubated with 5 µM MDG1 and the image acquired after 10 min of loading. *right:* Quantification of intracellular MDG1 fluorescent signal when probing after x min of recovery from damage. Normalised to signal at 0 min recovery time. n = 3 independent experiments, mean ± standard deviation. **(b)** *left:* Confocal microscopy images of live PC12 cells damaged with AAPH. Cells were allowed to recover for the indicated amount of time, then incubated with 5 µM MDG1 and the image acquired after 10 min of loading. *right:* Quantification of intracellular MDG1 fluorescent signal when probing after x min of recovery from damage. Normalised to signal at 0 min recovery time. n = 3 independent experiments, mean ± standard deviation. Scale bars 50 µm. Dashed lines in (a, b) indicate level of autofluorescence in damaged cells without MDG1. Adapted and reprinted with permission from J. Am. Chem. Soc. 2024, 146, 11072−11082. Copyright © 2024 American Chemical Society.

AAPH-damaged cells reach the 40 % signal mark noticeably later than LLO-damaged HEK cells. In addition to resealing, the differences between the assays may also be influenced by different baseline rates of probe entry and dye exit in the different cell- and damage types.

In summary, MDG1 can be used to track damaged cells for at least 2 h in wash-free imaging and can also function to detect recovery from membrane damage. Its applicability is somewhat

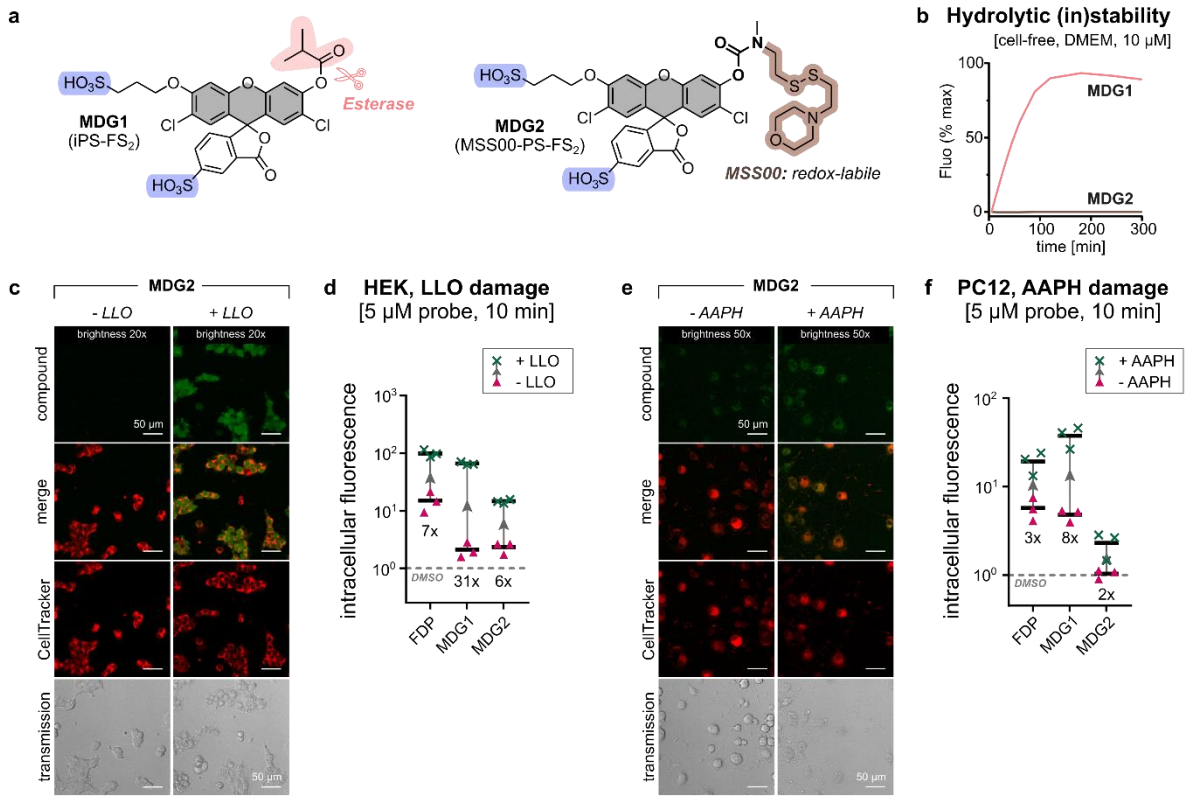

Figure 15 – Hydrolytic stability and membrane damage selectivity of MDG2 (MSS00-PS-FS$_2$). **(a)** Structural formulas of MDG1 (iPS-FS$_2$) and MDG2 (MSS00-PS-FS$_2$) which share the disulfonated fluorophore scaffold (sulfonates shaded in blue) but differ in the turn-on trigger (isobutyrate shaded in pink, disulphide group shaded in brown). **(b)** Spontaneous hydrolysis in DMEM of the ester probe MDG1 compared to redox probe MDG2. **(c)** Confocal microscopy images of live HEK cells incubated with LLO (or sham) for 5 min followed by 5 µM MSS00-PS-FS$_2$ treatment. Images taken after 10 min of probe incubation without prior washing. **(e)** Confocal microscopy images of live PC12 cells incubated with AAPH (or sham) for 90 min followed by 5 µM MSS00-PS-FS$_2$ treatment. Images taken after 10 min of probe incubation without prior washing. **(d, f)** Quantification of intracellular fluorescence, normalised to DMSO, for damaged vs. undamaged cells. Data for FDP and MDG1 re-plotted from Figure 9 and Figure 11. n = 3, each data point represents an independent experiment, horizontal lines indicate means. The factor below each dataset denotes the ratio between damaged and undamaged cell fluorescence. Scale bars 50 µm. To enable visualisation across the vast range of fluorescence intensities, dim compounds are displayed with enhanced brightness (20x / 50x); 1x in (c) equals 1x in Figure 9 and Figure 10; 1x in (e) equals 1x in Figure 11. Dotted vertical line in (d, f) denotes intracellular fluorescence of DMSO-treated undamaged HEK or PC12 cells respectively. DMSO = dimethyl sulfoxide. Adapted and reprinted with permission from J. Am. Chem. Soc. 2024, 146, 11072−11082. Copyright © 2024 American Chemical Society. Data in (b) collected by Philipp Mauker.

limited by its propensity to hydrolyse and by the lack of active retention inside a damaged cell. While introducing an active retention mechanism into our probes is beyond the scope of this work, we did take steps to improve the hydrolytic stability. The probe design is inherently modular: different chemical groups mediate either capping or impermeabilisation. This means, that the turn-on trigger can be exchanged without a major influence on probe (im-)permeability. We thus replaced the hydrolysis-prone esterified isobutyrate capping group of MDG1 with a redox labile disulphide trigger (MSS00), yielding the probe MSS00-PS-FS$_2$ or MDG2 for short (**Figure 15a**). This probe can be activated by thiols, such as glutathione (GSH), which just like esterases will only be available inside the cell. In a cell-free setting, no undesired MDG2 activation was found across media, even in DMEM, which in contrast

quickly hydrolyses MDG1 (**Figure 15b and Supplementary Figure 1i**). In turn, MDG2 was readily activated by GSH concentrations as low as 0.1 mM (**Supplementary Figure 1j**, experiment performed by Philipp Mauker), i.e. markedly below the usual intracellular concentration pf GSH of 1 - 5 mM (Hwang *et al.*, 1992). In direct comparison to MDG1, MDG2 showed equally good exclusion from healthy cells (even better exclusion from PC12) but a lower fold change in damaged cells (LLO: 8-fold; AAPH: 3-fold; **Figure 15c-f**). Since MDG1 and MDG2 release the same fluorophore, this must be due to probe characteristics such as slower uptake or activation. Since extracellular hydrolysis is not an issue with MDG2, it should be possible to overcome these shortcomings by increasing MDG2 concentration or incubation time.

To sum up, the "MDG" platform of mono-capped, disulfonated fluorogens is a biochemically flexible tool, which allows modifications of the turn-on mechanism without compromising membrane damage selectivity.

3.1.3. MDG1 visualises membrane damage in the axonal compartment

The previous chapters have outlined how the membrane damage sensor MDG1 was developed and characterised. Since MDG1 is not the first compound to make use of permeabilised membranes for the detection of dead cells or such at risk of dying, we next sought to demonstrate a use case in which MDG1 is clearly superior to existing "live-dead stains" or "cell viability assays". Broadly, the commercially available products can be classified into two groups: (1) dyes that forgo any activation mechanism (e.g. Trypan Blue or amine-reactive viability dyes) (Strober, 2001; Perfetto *et al.*, 2006). These either require washing, which is ineffective *in vivo* and detaches damaged cells *in vitro*, or have poor contrast when utilised wash-free (see damaged cell labelling with permanently fluorescent fluorophores, **Figure 10a and Figure 11c**). Product group (2) subsumes compounds that turn on fluorescence by intercalation with DNA (e.g. propidium iodide (PI) and Sytox) (Arndt-Jovin and Jovin, 1989; Molecular Probes, Thermo Fisher Scientific). These nuclear stains, however, can only uncover membrane damage close to the nucleus (i.e. in the soma) but not in remote subcellular compartments such as neuronal axons or dendrites. Since we aim to use the MDG1 biosensor and eventually MDG1-inspired prodrugs to investigate and treat axonal pathology, we tested the performance of MDG1 in comparison to PI in detecting axonal membrane damage. To this end, we isolated primary mouse neurons from hippocampus and cultured them in microfluidic chambers, which model the physical separation of neuronal cell bodies and their axons and allow for manipulation of one compartment independently of the other (**Figure 16**). These experiments were performed by Simone Wanderoy at the Max Planck Institute for Biological Intelligence. Axons were damaged with the radical donor AAPH and the membrane damage indicators MDG1 or PI were applied thereafter. For PI, we observed labelled nuclei in the somatic compartment but no labelling in the axonal compartment, which is devoid of DNA (**Figure 16a**). After MDG1-treatment in contrast, the cytosol of damaged axons lit up, while undamaged control axons showed little to no fluorescence (**Figure 16b, c**).

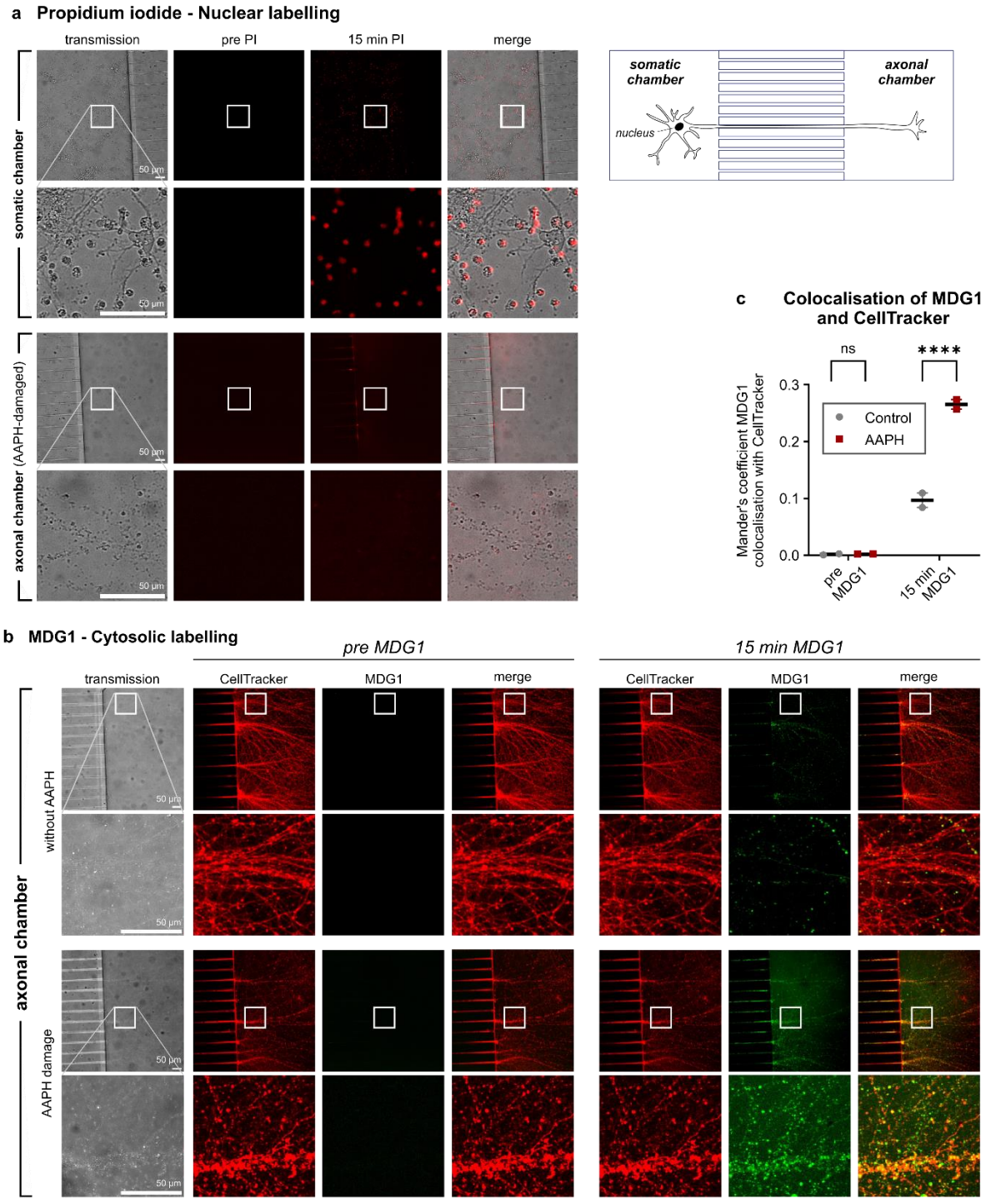

Figure 16 – Cytosolic MDG1 visualises membrane damage in the axonal compartment while PI stains nuclei only.

a) *right:* Schematic representation of neuronal culture growing in a microfluidic chamber that models physiologic separation of soma and axon terminals. The device allows manipulation of one compartment independently of the other. *left:* Microscopy images of neuronal culture growing in microfluidic chambers. Neurons were damaged by AAPH treatment of the axonal compartment only. This was followed by incubation with PI (3.3 µg/ml) in both somatic and axonal chamber. Images were acquired before addition of PI and 15 min after. The top and bottom panel show the somatic and axonal compartment respectively to emphasise the nuclear location of PI. Within both panels, the lower row images have been zoomed in from the row above. *(Figure legend continues on next page)*

(Continued legend for Figure 16) **(b)** Microscopy images of neuronal culture growing in microfluidic chambers. Neurons were damaged by AAPH (or sham) treatment of the axonal compartment only. This was followed by incubation with MDG1 (25 µM). Images were acquired before addition of MDG1 and 15 min after. The top and bottom panel both show the axonal compartment, but for the damaged and undamaged condition respectively. Within both panels, the lower row images have been zoomed in from the row above. **(c)** Co-localisation of CellTracker (all axons) and MDG1 (membrane damage sensor) quantified using Mander's coefficient. n = 2, each data point represents an independent experiment, horizontal lines indicate means, ANOVA. Scale bar 50 µm. ns = not significant ($p > 0.05$), **** $p > 0.0001$. Adapted and reprinted with permission from J. Am. Chem. Soc. 2024, 146, 11072−11082. Copyright © 2024 American Chemical Society. Data collected by Simone Wanderoy.

We conclude that MDG1 is a reliable membrane damage sensor and the first compound to combine healthy cell impermeabilisation with enzymatic turn-on to provide cytosolic labelling. It is therefore the first tool, to enable wash-free fluorogenic imaging of damaged distal cellular processes such as neuronal axons making it a valuable tool in the study of neuropathology.

3.2. Therapeutic enhancement of endogenous calcium clearance pathways

Focal axonal degeneration in neuroinflammatory lesions is an initially reversible process: damaged axons first develop swellings, which can proceed to fragmentation or be resolved, enabling the axon to survive long-term. When investigating checkpoints that control whether a swollen axon will fragment or recover, it was found that degeneration is driven by calcium influx via a permeabilised plasma membrane (Witte *et al.*, 2019). Axons with low calcium recovered and some high-calcium axons were able to spontaneously return to homeostatic low calcium levels. In the previous chapter, the development of a selective targeting mechanism for membrane-damaged axons, which may in the future be used to deliver calcium chelator prodrugs into the axons at need, was outlined. An alternative therapeutic approach to tip the balance in favour of calcium homeostasis and thus axonal survival is to boost endogenous calcium clearance pathways.

In essence, cells employ three mechanisms to lower free cytosolic calcium: sequestration by calcium-binding proteins, uptake of calcium into membrane-bounded organelles or extrusion by plasma membrane calcium pumps and exchangers. We reasoned that overexpression of low affinity calcium-binding proteins, which due to this low affinity will only bind substantial amounts of calcium at times of calcium overload, should have lower side effects on physiological calcium handling than the manipulation of calcium transport across membranes and also provides the most extensive literature. We therefore decided to explore the axoprotective potential of neuron-specific overexpression of the calcium-binding proteins calbindin and calretinin.

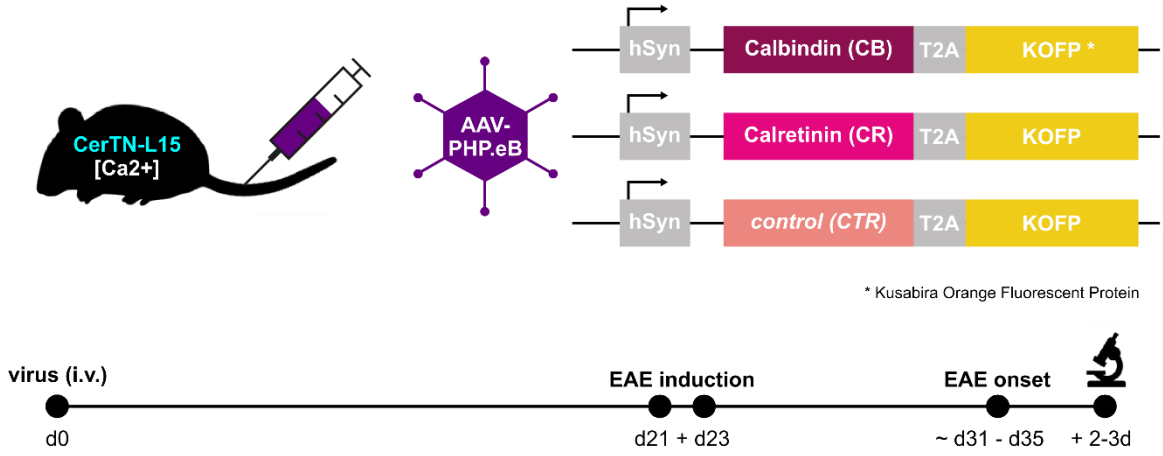

Figure 17 – Schematic representation and timeline of rAAV-mediated calcium-binding protein overexpression in transgenic calcium sensor mouse line CerTN-L15.
Three different recombinant adeno-associated viruses (rAAVs) were produced with the PHP.eB capsid variant and injected intravenously into three groups of mice with transgenic expression of the calcium sensor "CerTN-L15". The three viruses encoded either calbindin, calretinin or a control gene of same size, which were coupled to the expression of Kusabira Orange fluorescent protein (KOFP) with a T2A self-cleaving peptide. The gene construct was under control of the human synapsin promotor (hSyn) to limit expression to neurons. A timeline of the experiment is depicted below. Virus was injected three weeks prior to EAE induction which comprises immunisation with myelin oligodendrocyte glycoprotein (MOG) and pertussis toxin (PTX) on day 21 and a second injection of PTX on day 23. Mice were scored daily for motor symptoms, which were assessed on a 5-point scale. First motor symptoms usually occur on day 10 - 14 relative to EAE induction which equals day 31 - 35 relative to virus injection. The motor symptoms peak after 2 - 3 days, which was chosen as the timepoint for *in vivo* two-photon imaging. EAE = experimental autoimmune encephalomyelitis

3.2.1. Rationale and approach for overexpression of calcium-binding proteins

Calbindin (CB) and calretinin (CR) are two calcium-binding proteins (CaBPs) which are endogenously expressed in the central nervous system and have low calcium affinity (calbindin: K_D = 400 nM, calretinin: K_D = 1.4 µM) (Schmidt, 2012; Schwaller, 2010). These low affinity buffers flatten calcium transients by efficiently binding calcium at high concentrations while calcium release from the protein is favoured once cytosolic calcium levels return to low baseline levels (Sala and Hernández-Cruz, 1990; Schwaller, 2010). Such buffering may therefore buy axons time to recover from damage before irreversible destruction pathways are activated.

In order to test this hypothesis, we produced recombinant adeno-associated viruses (rAAVs) for the neuron-specific overexpression of calbindin, calretinin or a negative control gene (**Figure 17**). We initially used Cre recombinase as a control gene, which we expected to be without its DNA-cutting function in the absence of any loxP sites. Since the Cre-expressing virus showed unexpected toxicity, we switched to ShadowG, a mutated non-fluorescent variant of GFP (green fluorescent protein) as the control gene. Mice receiving the Cre-virus developed weight loss, but no neurological symptoms, indicating a systemic rather than neuron-specific toxicity of the virus. The expression of calbindin, calretinin or the control gene was linked to expression of a fluorescent reporter, Kusabira Orange fluorescent protein (KOFP), by the self-

cleaving peptide T2A, meaning that both genes are transcribed as a single mRNA and cleaved into two proteins during translation (Liu *et al.*, 2017). The genes were placed downstream of a human synapsin promoter to limit expression to neurons. We used the PHP.eB capsid variant of AAV9, which efficiently infects neurons, and which can be injected intravenously due to its ability to cross the blood-brain-barrier (Chan *et al.*, 2017). The rAAVs were injected into the transgenic mouse line CerTN-L15 that expresses a FRET-based calcium sensor in the Thy1 locus, yielding a sparse neuronal labelling. The rAAVs were injected three weeks before EAE induction (**Figure 17**). *In vivo* calcium imaging of EAE lesions in spinal cord white matter tracts was performed at peak of disease which is reached 2 - 3 days after first onset of EAE motor symptoms. This experimental setup enables a readout of axon morphology (normal/swollen/fragmented) in all fluorescently labelled axons as well as a measurement of axonal calcium levels in the CerTN-L15+ axons and controls for differences in disease severity between mice since virus-transduced (i.e. KOFP+) and non-transduced control axons are sampled from the same lesion.

3.2.2. Characterisation of rAAV-PHP.eB-mediated transduction

To enable identification of virus-transduced axons, all three viruses carry the same reporter gene encoding Kusabira Orange fluorescent protein (KOFP). The number and fluorescence intensity of KOFP-labelled axons therefore also provides feedback on the efficacy of viral transduction and viral overexpression. To our regret, the number of KOFP+ axons and the intensity of the KOFP signal in *in vivo* two-photon imaging were not as good as seen previously in our laboratory (Tai *et al.*, 2023). Since the KOFP recording is only used to identify transduced axons, not for quantitative measurements, the imaging settings were optimised for each individual mouse and lesion. The images in **Figure 18a** therefore cannot be used to compare absolute KOFP intensities. However, the contrast between axons and background and the number of identifiable axons in the KOFP channel compared to CerTN-L15 channel can provide an estimate of virus efficacy.

We performed this experiment in three independent cohorts and made various adjustments to the protocol in between, which aimed to improve the axonal labelling. These changes included using freshly produced virus, i.e. avoiding - 80°C storage, increasing the number of injected particles and switching from in-house to commercial virus production. We also exchanged the control gene from Cre recombinase to ShadowG as mentioned above. The in-house produced CR-KOFP and CB-KOFP viruses were based on cDNAs of murine calbindin and human calretinin respectively, which were kindly provided by Professor Michael Meyer. Since the AAV plasmids were newly constructed for the commercial virus production, we decided to request the murine orthologues for both CB and CR for these. This is a minor change, since the human and mouse orthologue of calretinin are 98 % identical on protein level (result obtained using NCBI protein BLAST, accession numbers NP_031612 and CAA39991.1). The details of all changes between cohorts are comprehensively listed in **Table 3**.

Table 3 – Differences between experimental cohorts of rAAV-mediated calcium-binding protein over-expression.

	Cohort 1	**Cohort 2**	**Cohort 3**
Group size (n mice per virus)	2	6	5
AAV plasmid production	in-house	in-house	commercial
rAAV production	in-house	in-house	commercial
Expressed genes	CB = mCalbindin CR = hCalretinin CTR = Cre recombinase	CB = mCalbindin CR = hCalretinin CTR = Cre recombinase	CB = mCalbindin CR = mCalretinin CTR = ShadowG
Number of injected particles	1 x 10^{12}	2 x 10^{12}	1 x 10^{11}
Virus storage (production to injection)	2-5 months at - 80°C	1-3 weeks at 4°C	2 months at - 80°C (shipped on dry ice)

As mentioned before, the number of KOFP+ axons and the intensity of the KOFP signal in *in vivo* two-photon imaging were not as good as we had seen in previous rAAV-mediated over-expression experiments in our laboratory. What is more, there were noticeable differences in the efficacies of the three different viruses that persisted across cohorts, despite our optimisation efforts (**Figure 18a, b**). CB-KOFP consistently showed poor contrast between axons and background (**Figure 18a**), and significantly less KOFP+ axons were identified for the CB-KOFP group compared to the control virus (**Figure 18b**, pooled cohorts). These observations could not be explained by differences in virus production since viruses yielded comparable titers. Also, the gene size, which is known to negatively influence viral packaging (Ibreljic *et al.*, 2024) was similar for all genes (murine calbindin 783 bp, human calretinin 813 bp, murine calretinin 813 bp, Cre recombinase 1026 bp, ShadowG 717 bp); if anything, calbindin should be better expressed than calretinin and Cre due to smaller size. This indicates that the degree of success of the viral overexpression approach is highly dependent on the gene to be overexpressed, including factors other than gene size.

We next sought to untangle, whether the reduced number of KOFP+ axons for CB-KOFP compared to CTR-KOFP was due to less cells being infected by the virus or due to infected cells having lower expression levels of the delivered genes. This would result in false negatives: axons that express KOFP, but so lowly that they are below the detection limit. As outlined before, the two-photon images of spinal cord axons are not useful to answer this question because the way they were taken forbids quantitative comparison. We instead used fixed tissue from the same mice for confocal imaging of cortex cryosections. NeuroTrace™ 640/660 Deep-Red Fluorescent Nissl Stain was used to label all neurons, allowing for the quantification of the KOFP+ neuron fraction. This experiment revealed, that indeed, CTR-KOFP

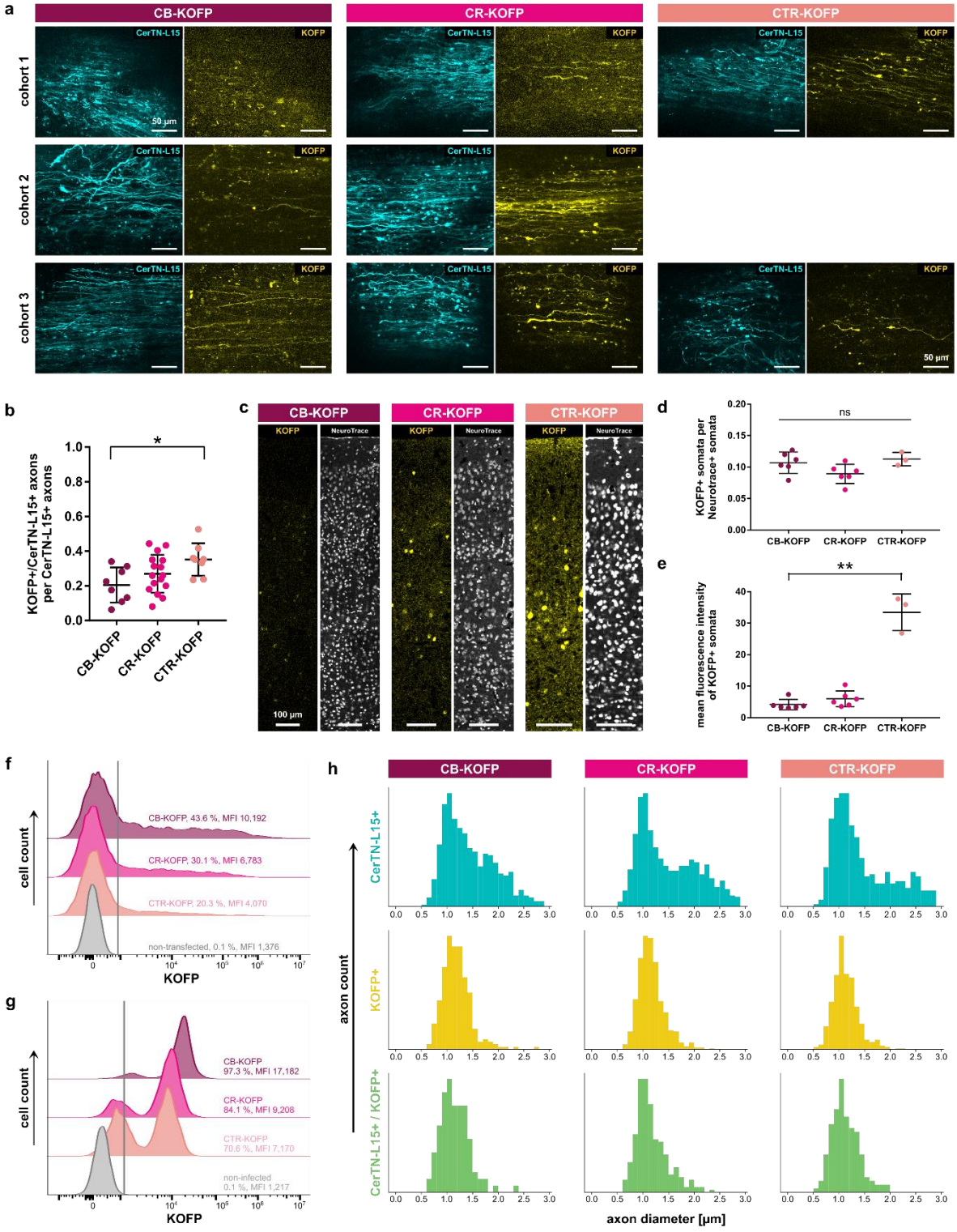

Figure 18 – Analysis of viral transduction and overexpression efficacies.
(a) Maximum projection images from *in vivo* two-photon imaging of spinal cord white matter EAE lesions for all three viruses (CB-KOFP / CR-KOFP / CTR-KOFP) and the three different experimental cohorts. CTR-KOFP cohort 2 image missing due to virus toxicity. All images were taken with individually optimised settings and absolute intensities are not comparable between images. *(Figure legend continues on next page)*

(Continued legend for Figure 18) . **(b)** Quantification of the fraction of CerTN-L15+ axons that are also KOFP+. Each data point represents one lesion. Data pooled from all cohorts. CB-KOFP n = 8, CR-KOFP n = 16, CTR-KOFP n = 8; mean ± standard deviation; ANOVA with Bonferroni's multiple comparisons test. **(c)** Single plane images of cortex of virus-injected mice counterstained with NeuroTrace. Narrow regions of interest (ROIs) like these, spanning all cortical layers, are the basis of the quantification in (d, e). **(d)** Number of KOFP+ cells normalised to the number of NeuroTrace+ cells in cortex. Each data point represents one ROI. All data stems from cohort 1. CB-KOFP n = 6 (from 2 mice), CR-KOFP n = 6 (from 2 mice), CTR-KOFP n = 3 (from 1 mouse); mean ± standard deviation; ANOVA with Bonferroni's multiple comparisons test. **(e)** Mean fluorescence intensity of KOFP+ cortical cells. Each data point represents one ROI. All data stems from cohort 1. CB-KOFP n = 6 (from 2 mice), CR-KOFP n = 6 (from 2 mice), CTR-KOFP n = 3 (from 1 mouse); mean ± standard deviation; Kruskal-Wallis with Dunn's multiple comparisons test. **(f)** Flow cytometry histogram of KOFP intensity in AAV plasmid transfected HEK cells. Vertical line indicates the cut-off used to define KOFP+ cells. % indicates percentage of KOFP+ cells. MFI refers to KOFP+ cells only. **(g)** Flow cytometry histogram of KOFP intensity in rAAV-infected HeLa cells. Vertical line indicates the cut-off used to define KOFP+ cells. % indicates percentage of KOFP+ cells. MFI refers to KOFP+ cells only. **(h)** Histogram of axon diameters in *in vivo* two-photon imaging. Double positive axons are plotted individually at the bottom but are also included in both the CerTN-L15+ and KOFP+ plots. Data pooled from all cohorts. Panels top to bottom CB-KOFP n = 565 / 261 / 106, CR-KOFP n = 856 / 619 / 256, CTR-KOFP n = 463 / 424 / 160. CB = calbindin, CR = calretinin, CTR = negative control gene, KOFP = Kusabira Orange fluorescent protein, CerTN-L15 = name of the transgenic calcium sensor, MFI = mean fluorescence intensity. Scale bar 50 µm in (a), 100 µm in (c). ns = not significant ($p > 0.05$), * $p < 0.05$, ** $p < 0.01$. Flow cytometry acquisition in (f, g) by Clara de la Rosa del Val.

achieved significantly brighter cellular labelling than CB-KOFP, while the result for CR-KOFP was intermediate between the two (**Figure 18c, e**). However, when adjusting the cut-off for defining KOFP+ cells to these vast brightness differences, the number of KOFP+ cells was not significantly different between the three viruses tested (**Figure 18c, d**). This indicates that the observed inter-virus disparities are not based on differences in transduction but on differences in expression of the virally delivered genes. This may explain, why an increased viral dose had limited effects on the labelling quality (**Figure 18a, Table 3**) since this approach can increase the number of transduced neurons but will not influence transcription or translation within these (unless in case of multiple infection, which is however statistically rare at low multiplicity of infection).

Collectively, the analysis of viral overexpression efficacy suggests that the success of the approach depends on the gene to be overexpressed and is mediated by the efficacy of its expression, which is independent of gene size. Since mouse experiments of this kind are challenging and time-consuming, we aimed to find out whether it is possible to predict viral overexpression performance using *in vitro* experiments. We first tested whether the observed differences in KOFP intensity would be reproduced when transfecting HEK cells with the transfer plasmids used for rAAV production. We assessed the number and mean fluorescence intensity (MFI) of KOFP expressing cells for each of the three transfected plasmids using flow cytometry four days after transfection. Surprisingly, transfected HEK cells showed the opposite trend compared to transduced neurons *in vivo*: in HEK cells, both percentage of KOFP+ cells and their MFI was highest for CB-KOFP, intermediate for CR-KOFP and lowest for CTR-KOFP (= Cre-KOFP) (**Figure 18f**). We thus reasoned that viral delivery of the genes

may be necessary to replicate the effect seen *in vivo*. PHP.eB-AAVs did not infect HEK cells (data not shown) but did infect HeLa cells. We therefore assessed the number and MFI of KOFP expressing HeLa cells incubated with the single viruses. The results mirrored those seen with transfected HEK cells, again contradicting the *in vivo* findings (**Figure 18g**). These experiments were aided by Clara de la Rosa del Val who performed the flow cytometry. In conclusion, we were not able to replicate the viral overexpression differences observed *in vivo* by using simple *in vitro* systems. It is possible that transfection or infection of neuronal cell lines or primary neuron cultures would bridge this gap, however this was not tested as part of this thesis.

Another relevant observation that we made when imaging CerTN-L15– and KOFP-labelled axons was a difference in axon diameters: while CerTN-L15+ axons can have a wide range of different calibres, KOFP+ axons were mostly of small calibre, below 2 µm diameter (**Figure 18a, h**). This means that the comparison between KOFP+ and KOFP– axons within the same lesion is biased because two inherently different axon populations are being compared. The calibre effect was however consistent for all three viruses, meaning that KOFP+ axons in CB- or CR-KOFP-injected mice are comparable to KOFP+ axons in CTR-KOFP-injected mice.

3.2.3. Analysis of overexpression of calcium-binding proteins and their effects on axonal calcium levels and degeneration

In the previous chapter, efficacy of the viral overexpression approach was assessed by looking at signals from the fluorescent reporter KOFP. Although the T2A system should link KOFP expression to that of CB, CR or control respectively, we wanted to confirm this experimentally in the injected mice. We therefore performed immunostaining for calbindin and calretinin on spinal cord sections and measured the KOFP and calbindin/calretinin signals of individual cells. As expected for successful implementation of the T2A system, calbindin staining was highly correlated to KOFP intensity in CB-KOFP-injected mice, whereas there was no correlation between calbindin staining and KOFP intensity in control mice (**Figure 19a, c**). Likewise, calretinin signal correlated with KOFP in CR-KOFP-injected mice but not in controls (**Figure 19b, d**). Notably, we also detected endogenous expression of calbindin and calretinin in KOFP– cells. To better understand how much compared to endogenous levels CB and CR are overexpressed in transduced cells, we defined a binary cut-off to separate KOFP+ from KOFP– cells and compared these groups to each other **Figure 19e, f**). This way of analysis replicated the results of the correlation: the calbindin and calretinin signals were significantly higher in KOFP+ compared to KOFP– cells of CB-KOFP– and CR-KOFP-injected mice respectively whereas no such difference between KOFP+ and KOFP– was observed in cells from CTR-KOFP-injected control mice. The mean calbindin signal in calbindin overexpressing mice was 2.2 times higher in KOFP+ compared to KOFP– cells. For calretinin, the increase was 2.7-fold. **Figure 19e and f** also illustrate that the complete cell population shifts

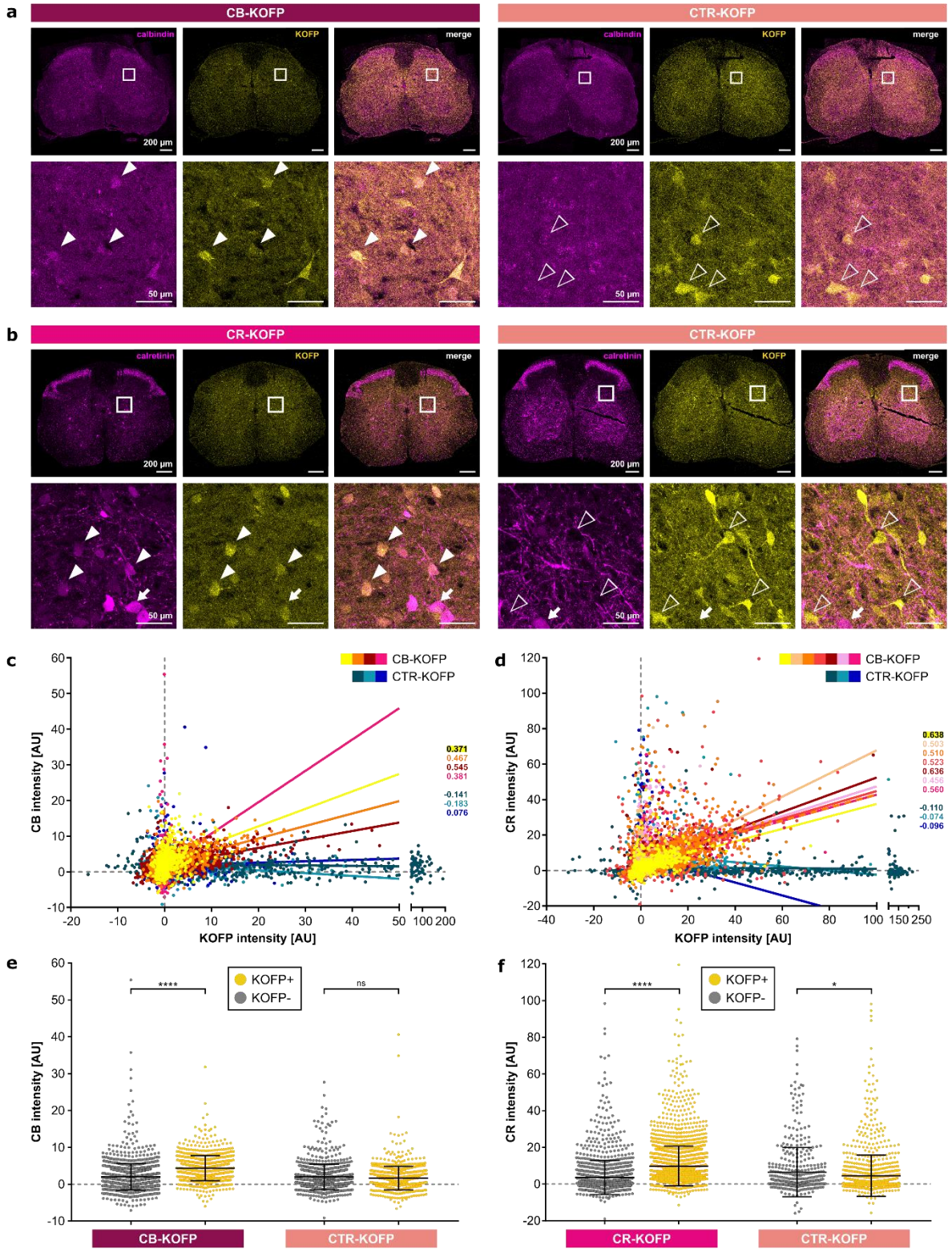

Figure 19 – Confirmation of calbindin and calretinin overexpression.
(a, b) Maximum projection images of spinal cord immunostained for calbindin (a) or calretinin (b). Panel below is zoomed into the window outlined in white. Filled arrowheads indicate KOFP+ cells with CB/CR expression; empty arrowheads indicate KOFP+ cells without CB/CR expression. Arrows indicate KOFP- cells with endogenous calretinin expression **(c, d)** Correlation between KOFP signal and CB (c) or CR (d) staining intensity in virus-injected mice. *(Figure legend continues on next page)*

(Continued legend for Figure 19) Colours represent individual mice which were pooled from all cohorts, with warm colours representing CB-KOFP (c) or CR-KOFP (d) injected mice and blue shades representing CTR-KOFP-injected control mice. Each data point represents one cell. Lines are linear regressions of the corresponding dataset. Values on the right are Spearman's rank correlation coefficients for the corresponding dataset. n ≥ 475 for each single mouse. Note that x- and y-axis do not intersect at 0/0, instead horizontal and vertical dashed lines mark the zero position on both axes. **(e, f)** Comparison of calbindin (e) or calretinin (f) staining intensity between KOFP+ (yellow) and KOFP- (grey) cells. Each data point represents one cell. CB-KOFP: 4 mice pooled from all cohorts, n = 1591 / 873 KOFP-/+ cells. CTR-KOFP in (e): 3 mice pooled from all cohorts, n = 960 / 881 KOFP-/+ cells. CR-KOFP: 7 mice pooled from all cohorts, n = 1509 / 2802 KOFP-/+ cells. CTR-KOFP in (f): 3 mice pooled from all cohorts, n = 465 / 1116 KOFP-/+ cells. Mean ± standard deviation; Kruskal-Wallis with Dunn's multiple comparisons test. Note that the y-axis does not start at zero, instead a horizontal dashed line marks staining intensity of zero. Scale bar 200 µm in upper panels of (a, b), 50 µm in lower panels of (a, b). CB = calbindin, CR = calretinin, CTR = negative control gene, KOFP = Kusabira Orange fluorescent protein, AU = arbitrary units, ns = not significant ($p > 0.05$), * $p < 0.05$, **** $p < 0.0001$. Staining intensities were background-subtracted and can therefore be negative.

towards higher calbindin/calretinin expression upon overexpression. However, for both of these proteins, the shift is relatively small compared to the range of endogenously occurring calbindin and calretinin levels (as seen in KOFP– cells). This means that overexpressing CB and CR in cells without endogenous expression yields low expression compared to endogenously expressing cells and overexpression in cells with endogenous expression only gives a small expression boost.

To investigate whether the degree of calbindin- or calretinin overexpression achieved in this AAV-based experiment was axoprotective, we assessed the morphology of axons within EAE lesions. We decided to analyse a subset of mice spanning all three experimental cohorts. For this analysis subset, mice with the most severe lesions and highest density of KOFP+ axons were selected. In total, we analysed 8 lesions from 4 CB-KOFP mice, 16 lesions from 7 CR-KOFP mice and 8 lesions from 3 CTR-KOFP mice. The same mice were used to confirm overexpression (see **Figure 19**). We have previously established the classification of axonal morphologies as stage 0, "normal"; stage 1, "swollen" and stage 2, "fragmented" to describe axonal degeneration processes in EAE lesions (Nikić *et al.*, 2011). Examples for this classification can be found in **Figure 20a**. We counted the number of axons per stage, subdivided into KOFP+ and KOFP– axons, for each of the three experimental groups and represented them as percentage of total axons (**Figure 20b-d**). An axoprotective intervention should prevent irreversible axon loss, i.e. reduce the frequency of stage 2 axons. In the present dataset however, both stage 1 and 2 are more frequent in virus-transduced (KOFP+) compared to non-transduced axons. Concluding from the fact that this is seen for all three viruses (**Figure 20b-d**), including the negative control virus, this pattern can be attributed not to the intervention but to the axonal subpopulation that is transduced by the rAAVs. Indeed, we had already described that KOFP+ axons across all three viruses are of small calibre (**Figure 18h**) and in our experience with axonal degeneration in EAE, small calibre axons are more prone to fragmentation (Nikić *et al.*, 2011). To untangle, whether there are differences between CB/CR overexpression and control that may be masked by the population effect, we calculated for each axon stage the ratio between its frequency in the KOFP+ and KOFP– axon subsets

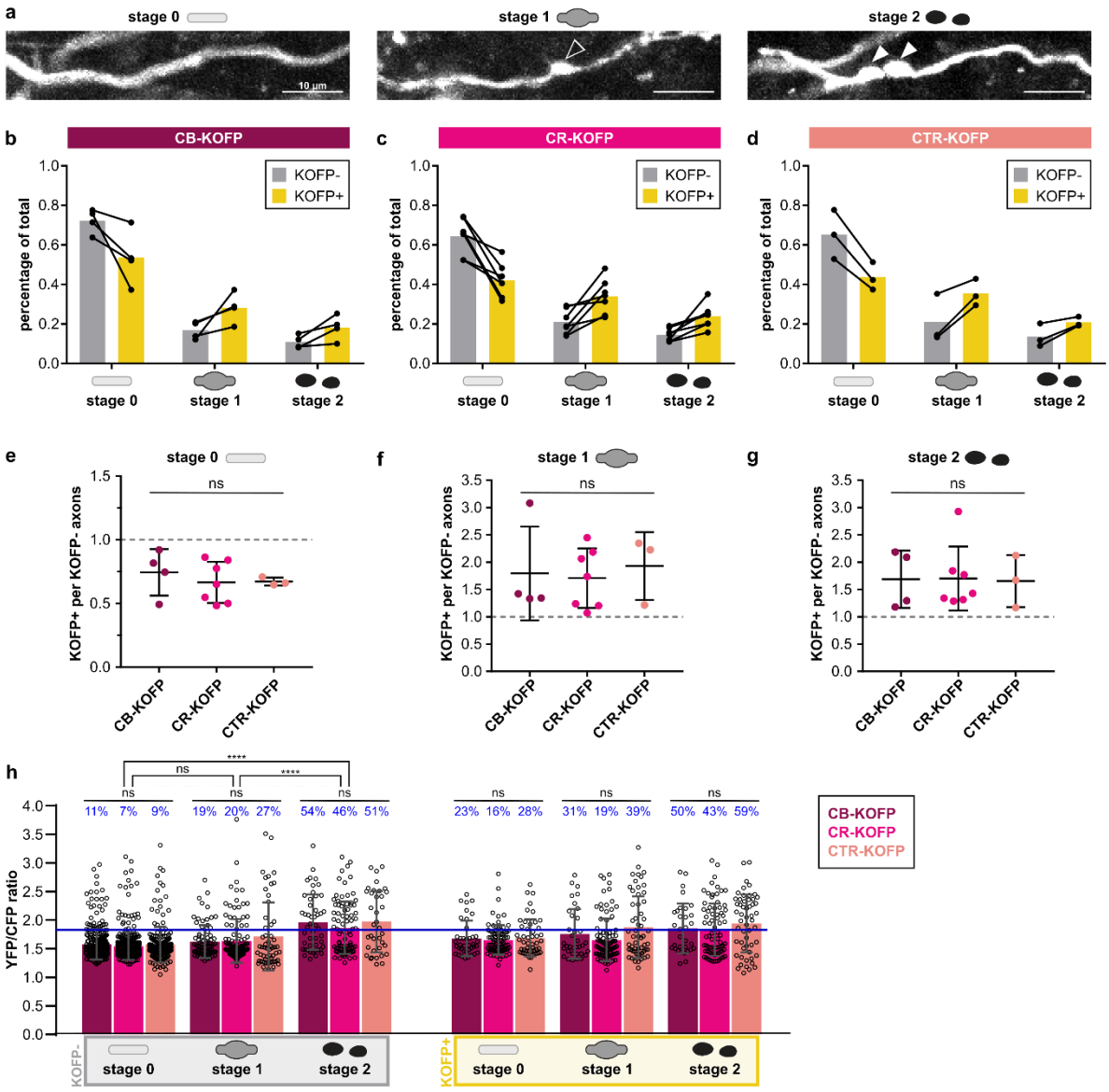

Figure 20 – Calcium-binding protein overexpression is not axoprotective.
(a) Example images for the different morphological stages of axonal degeneration: stage 0 "normal", stage 1 "swollen" (indicated by empty arrowhead), stage 2 "fragmented" (indicated by filled arrowheads). **(b, c, d)** Relative frequency of axon stages 0/1/2 within the KOFP+ or KOFP- axon population of CB-KOFP (b), CR-KOFP (c) and CTR-KOFP (d) mice. Data pooled from all cohorts. Each data point represents one mouse. Data points from the same mouse are connected by a line. Bar height represents the mean. CB-KOFP n = 4, CR-KOFP n = 7, CTR-KOFP n = 3. **(e, f, g)** Number of KOFP+ axons normalised to KOFP- axons of stage 0 (e) stage 1 (f) and stage 2 (g). Dashed lines mark a ratio of 1 (same number of KOFP+ and KOFP- axons). Data pooled from all cohorts. Each data point represents one mouse. CB-KOFP n = 4, CR-KOFP n = 7, CTR-KOFP n = 3; mean ± standard deviation; Kruskal-Wallis with Dunn's multiple comparisons test. (**h**) YFP/CFP ratios of transgenic CerTN-L15 calcium sensor. Higher ratio indicates higher calcium. Each data point represents one axon. Data pooled from all cohorts. Left half (grey): KOFP- axons, sorted by stage and within stage subplotted for all three viral groups. Right half (yellow): KOFP+ axons, sorted by stage and within stage subplotted for all three viral groups. KOFP- stage 0 n ≥ 210, stage 1 n ≥ 56, stage 2 n ≥ 37 per group; KOFP+ stage 0 n ≥ 39, stage 1 n ≥ 35, stage 2 n ≥ 32 per group. Mean ± standard deviation; Kruskal-Wallis with Dunn's multiple comparisons test performed once for complete dataset and separately to compare KOFP- axons pooled by stage. *(Figure legend continues on next page)*

(Continued legend for Figure 20) The dashed line indicates a YFP/CFP ratio of mean + 1 standard deviation of pooled KOFP- stage 0 axons, which was used as a threshold between low and high calcium. Percentages in blue indicate the fraction of axons above threshold. Scale bar 10 µm. CB = calbindin, CR = calretinin, CTR = negative control gene, KOFP = Kusabira Orange fluorescent protein, YFP/CFP = yellow/cyan fluorescent protein, ns = not significant ($p > 0.05$), **** $p < 0.0001$.

(**Figure 20e-g**). These ratios were not different between overexpressing mice and those injected with the control virus. The data was checked for systematic bias introduced by sex, final EAE score or cohort and no such distortions were detected (data not shown). In summary, we conclude that calbindin- and calretinin overexpression, at least at the moderate levels achieved with this experimental setup, cannot improve axonal recovery in EAE lesions.

To corroborate this finding, we also looked at the calcium levels of KOFP+ compared to KOFP– axons. The ratio between YFP- and CFP emission of the FRET-based calcium sensor CerTN-L15 serves as a proxy for relative cytosolic calcium levels. Within our dataset of KOFP– axons, we could replicate the results of Witte *et al.* (2019), who observed elevated calcium in a fraction of stage 0 axons, in an even larger fraction of stage 1 axons and in a majority of stage 2 axons (**Figure 20h**). KOFP+ axons generally had higher YFP/CFP ratios than KOFP– axons, even at stage 0 and also in negative control mice. This may again be an axonal subpopulation effect or, more likely, is the result of crosstalk between the calcium sensor and KOFP fluorescence. For an unbiased comparison, it is therefore again necessary to compare KOFP+ axons between the experimental groups rather than comparing KOFP+ to KOFP– axons within the same experimental group. The calcium levels of KOFP+ axons at any stage were not different between overexpressing and control mice (**Figure 20h**).

Taken together we have achieved a mild overexpression of the calcium-binding proteins calbindin and calretinin in neurons. This mild overexpression did not have any effect on morphological readouts of axonal degeneration nor on axonal calcium levels. More studies are needed to assess the axoprotective potential of substantial calcium-binding protein overexpression.

4. Discussion

Progression of irreversible disability in multiple sclerosis is driven by neuroaxonal degeneration, which can progress partially independent of immune cell infiltration. Despite recent advances in the treatment of MS, all currently approved drugs target acute inflammation and are mainly effective in reducing MS relapses. These drugs can thus dampen but not halt neurodegeneration (Scalfari *et al.*, 2024) and the development of drugs that are primarily neuroprotective is an important unmet clinical need. Recent clinical trials for neuroprotective agents in MS have not met their endpoints (Cree *et al.*, 2020; Kosa *et al.*, 2020; Chataway *et al.*, 2020), highlighting our insufficient understanding of the degeneration process and neuroprotective targets.

To identify novel neuroprotective targets, we study axonal degeneration in the MS mouse model EAE. In this model, degeneration is driven by calcium influx via nanopores that arise in the axolemma at sites of inflammation. Interestingly, in previous studies we observed, that some axons survive initial damage by spontaneously recovering calcium homeostasis. We also showed that chelation of extracellular calcium is beneficial, allowing more damaged axons to recover. The aim of this thesis was therefore to further explore calcium modulation as a therapeutic target in EAE. In a two-winged approach we exploited endogenous mechanisms of lowering cytosolic calcium by overexpressing calcium-binding proteins and, in parallel, developed an exogenous delivery mechanism selectively targeting damaged axons. As a proof-of-principle, we developed a fluorogenic membrane damage sensor that selectively labels the cytosol of damaged cells or axons. The same design principle may in the future be used to deliver prodrug calcium chelators to axons in need while preventing side effects on physiological functions of calcium in healthy, non-permeabilised axons. This and other aspects of the two approaches will be discussed below.

4.1. Development of a fluorogenic membrane damage sensor

Axons in inflammatory lesions, which are damaged and at risk of degeneration, are characterised by increased plasma membrane permeability. As a proof-of-principle approach for selective delivery to this metastable, therapeutically interesting axon population via their damaged plasma membranes, we developed fluorogenic membrane damage biosensors. These require intracellular turn-on of fluorescence while being permeable to damaged cells and axons only. They therefore provide direct fluorescent feedback on the success of delivery.

Chemically, this was achieved by – for the first time – combining two otherwise well-established mechanisms: charge-based impermeabilisation and intracellular turn-on by removal of capping groups (**Figure 7**). Since we did not know how much charge would be necessary to reach the sweet spot of exclusion by healthy cells but uptake into plasma membrane-damaged cells, we synthesised a range of differently polar dichlorofluorescein-based compounds and screened them in *in vitro* assays of membrane damage. All probes were ester-capped for intracellular activation by esterases. A subset of probes that had asymmetric modifications on

the xanthene ring system had a decreased quantum yield; however, we found them sufficiently bright to be imaged at reasonable probe concentrations and laser power.

We modelled two different membrane permeabilisation scenarios. First, we performed application of a bacterial pore-forming toxin, LLO, to the widely used HEK cell line. The second scenario was chosen to be more relevant to MS. We differentiated PC12 cells into neurons and induced oxidative damage by challenging them with the radical initiator AAPH. The two screens resulted in the identification of the probe iPS-FS_2, which we also termed MDG1 (membrane damage green 1) for short, as a reliable membrane damage sensor. MDG1 performed well in both settings, meaning that unlike other probes it was efficiently excluded by both healthy HEK and healthy PC12 cells but taken up by their damaged counterparts. LLO-damaged HEK cells showed a 31-fold increase in MDG1 signal compared to healthy HEK cells. The difference between AAPH-damaged and healthy PC12 cells was somewhat lower at 7-fold. MDG1 clearly outperformed the commercially available probe FDP, by being both better excluded from healthy cells and having a higher signal fold change in damaged cells (**Figure 9b, c, Figure 11a, b**).

The lower fold change in AAPH- compared to LLO damage may result from the different kinds of membrane damage. The bacterial toxin LLO oligomerises into a tunnel-like structure in the membrane that allows free diffusion of ions and small molecules. Peroxidation of membrane lipids in contrast causes more subtle changes to the lipid bilayer: less efficient packing of altered lipids creates some wriggle room, which small molecules may permeate through. A lower fold change in the AAPH- compared to the LLO assay was also observed for all other probes, strengthening this interpretation. Interestingly, we also noticed a correlation between MDG1 and BODIPY-11 signal in T cells undergoing lipid peroxidation / ferroptosis (data not shown, see Mauker, Beckmann *et al.*, 2024). This is interesting because the two probes report on two different aspects: MDG1 signal depends on membrane permeability, whereas BODIPY-11 reports on oxidation status of membrane lipids. The observation, that more lipid peroxidation goes hand in hand with increased permeability is not a trivial one, as there is an ongoing debate in the field, whether lipid alteration alone leads to membrane permeabilisation in ferroptosis or whether this requires secondary protein pore formation (Ramos *et al.*, 2024). Although our findings do not exclude an additional role for protein pore formation mediating the complete plasma membrane rupture, they do support the view that peroxidative lipid alterations are sufficient to initiate barrier loss. This is further backed by our findings in resealing experiments, in which MDG1 signal linearly declined when the probe was added after increasing recovery times post oxidative stress (**Figure 14b**). This is consistent with a linear enzymatic detoxification process for oxidised membrane lipids.

The broad applicability of MDG1 as a universal membrane damage sensor has been shown by testing it on different cell types (HEK, PC12, ex vivo T cells) and in different damage scenarios (pore-forming toxins, lipid peroxidation/ferroptosis induced by external membrane stressors or by GPX4 inhibition). These experiments were completed by an experiment in drosophila embryos, where MDG1 revealed the full volume of a laser-induced necrotic lesion,

whereas the commercial live-dead stain Sytox-labelled nuclei of necrotic cells only (data not shown, see Mauker, Beckmann *et al.*, 2024).

Although we here use the term “membrane damage sensor”, the concept is similar to that of commercially available live-dead stains or cell viability assays, as both make use of increased membrane permeability to label their target cells. However, there are some major differences between the two approaches: First of all, live-dead stains assume that labelled cells are dead, therefore there is no concern for toxicity. In fact, many live-dead stains, including Sytox and propidium iodide (PI) turn on fluorescence by DNA intercalation which is potentially mutagenic. Fixable live-dead stains are amine-reactive, i.e. attach to proteins, which if used in live cells could impair function. MDG1 in contrast is not designed to interact with any cellular components. Our interest in membrane compromised axons is based on the fact, that they are not unequivocally destined to degenerate, but can survive long-term if the membrane is resealed and physiologically low calcium levels are restored. The fact that membrane resealing mechanisms exist, also in non-neuronal cells (Zhen *et al.*, 2021), indicates that there may be other contexts in which a non-toxic biosensor can provide added benefit for following transiently permeabilised cells for longer time frames.

We infer low toxicity of MDG1 from its assumed lack of interactions, yet we were not able to show this experimentally. We performed long-term observation experiments on LLO- or AAPH-damaged HEK cells and on AAPH-damaged PC12 cells (PC12 cells are not susceptible to LLO damage), however these were not conclusive. Our initial plan was to assess proliferative capacity in MDG1 vs. PI loaded HEK cells, but damaged cells mostly died, and the few survivors stopped dividing irrespective of MDG1 or PI treatment (data not shown). AAPH-treated PC12 cells mostly survived (> 90 %) but are post-mitotic, forcing us to choose a different readout. We thus performed bulk RNA sequencing 6 and 24 h post damage to detect potential effects of MDG1 and PI. Although we did see changes in transcription in damaged compared to control PC12 cells, these transcriptional changes did not follow a consistent pattern between replicates. It was therefore not possible to derive any PI- or MDG1-induced signature from these samples (data not shown). The observed variability of the transcriptional changes may be explained by the fact, that peroxidation cannot only impact membrane lipids but also DNA and protein and as such the complete transcriptional machinery. To experimentally assess the toxicity of MDG1 compared to commercial live-dead stains, it will therefore be necessary to use a milder model of membrane damage than the ones used for biosensor screening for example replicating experiments of Murakami *et al.* (2018), who permeabilised cells with LLO to deliver membrane-impermeable drugs and then resealed cells after delivery, by applying an ATP-regenerating system, GTP (guanosine triphosphate) and glucose. Another alternative for toxicity testing would be not to damage cells at all but instead deliver intracellular MDG1 or PI by microinjection.

A second unique feature of MDG1 that sets it apart from live-dead stains, beside its assumed low toxicity, is the combination of membrane impermeabilisation with cytosolic enzymatic turn-on. Commercial products either turn on fluorescence by DNA intercalation i.e. have a

nuclear localisation or they are cytosolic but permanently on (e.g. Trypan blue or amine-reactive live-dead stains). The latter group requires washing to achieve good contrast between cells and the extracellular space. This was also seen in our set of experiments in which we directly applied the permanently fluorescent fluorophores rather than the capped probes to damaged cells (**Figure 10, Figure 11c, d**). This resulted in intracellular labelling, but it was difficult to distinguish cells from likewise fluorescent background. The ester-capped probes in contrast provide turn-on from zero background, which enables wash-free imaging. This is particularly advantageous when considering *in vivo* settings, where washing may be less effective. The turn-on mechanism will also be of importance for the translation of findings to a calcium chelator prodrug, whose very purpose is to remain in an "off", non-calcium-binding state until reaching its destination: the damaged axon's cytosol.

While for applications like flow cytometry it does not matter whether a dye is located in the nucleus or in the cytosol, there can be various microscopy approaches in which cytosolic labelling by MDG1 is preferred. As mentioned above, MDG1 revealed the full volume of a laser-induced necrotic lesion, rather than just the damaged cell's nuclei like Sytox. The case is even stronger for cells with long processes, where it is impossible to detect damage to a process by staining the faraway nucleus. Indeed, we compared performance of MDG1 versus PI in revealing damage to the axonal compartment of neurons growing in microfluidic chambers. Whereas MDG1 clearly labelled the cytosol of damaged axons, but not control axons, PI signal was only visible in nuclei (**Figure 16**). This finding holds promise for the translation of the approach for prodrug delivery into membrane-damaged axons.

Despite its promises, MDG1 also has various shortcomings and limitations. The fact that it is not designed to interact with any components inside cells prevents toxicity, but this also means that the activated fluorophore can leave the cell the same way it entered. Indeed, when we washed off MDG1 after 10 min of loading and followed up on cells afterwards, we observed a quick decline in intracellular MDG1 levels (**Figure 13**). We therefore strongly advise to only use MDG1 in a wash-free setup. When not washed off, damaged cells remain clearly MDG1-labelled for at least 2 h (**Figure 12**). This prolonged incubation comes at the cost of some increase in background fluorescence, resulting from spontaneous probe hydrolysis in the medium. It is important to note though, that fluorophores that were activated inside cells and then leaked back to the extracellular medium or fluorophores that were released by spontaneous hydrolysis do stain the extracellular space but are still excluded from healthy cells. This means that with prolonged incubation and imaging one loses contrast but not specificity. Nevertheless, improved retention remains one of the top priorities in advancing our membrane damage probes and potential designs of next generation MD probes with active retention mechanisms will be discussed below.

A strength of the MDG1 designs is that is inherently modular. Other than in the commercially available probe FDP, where the phosphonate esters provide both impermeabilisation and capping, these functions are completely independent from each other in MDG1 where the sulfonate groups ensure impermeabilisation and the isobutyrate ester serves as cap. This also means that the capping group and thus the activation trigger can be exchanged without a major

impact on probe permeability. We confirmed this by exchanging the isobutyrate ester of MDG1 with a redox-labile MSS00 group, yielding the probe MDG2. In cell-free settings, this probe was readily activated even below physiologic GSH levels, yet showed no spontaneous hydrolysis in PBS, HBBS or DMEM (**Figure 15a, b, Supplementary Figure 1**). It selectively labelled damaged cells but appeared to be less bright than MDG1 in cellular experiments (**Figure 15c-f**). Since both compounds eventually release the same fluorophore, the difference in brightness must result from less fluorophore being generated, either because plasma membrane crossing or uncapping is less efficient. We are therefore currently working on the development of brighter redox-activated MD probes (design discussed in more detail below), that would combine MDG1's good labelling characteristics with MDG2's hydrolytic stability. While MDG1 performs very well in short-term imaging of cells kept in HBSS buffer, an equally bright, but more hydrolytically stable probe will be useful for prolonged imaging, preventing the rise of fluorescent background, as well as in *in vivo* settings where the probe encounters a more hydrolytically active extracellular environment.

In summary, intracellular retention and probe stability have been identified as the main limitations of the MDG1 membrane damage sensor for application beyond simplified *in vitro* experiments. While hydrolytic stability was improved by changing the trigger from esterase- to redox activation, the applicability of our redox probe MDG2 was in turn limited by its reduced brightness. In the future, the fluorescent signal generation of MDG2 may be improved, by replacing the linear disulfide redox trigger with a bicyclic system. This cyclic pre-organisation should enable a faster reaction with GSH and thus more fluorophore release per unit of time (Zeisel *et al.*, 2024). Another option is to change the core of the biosensor from fluorescein to rhodol, a structural hybrid between fluorescein and rhodamine. As mentioned above, asymmetric mono-capped fluoresceins like the fluorophore released by MDG1 and MDG2 suffer from a reduced brightness. Rhodols are inherently asymmetric and their quantum yield is less affected by further asymmetric functionalisation (Peng and Yang, 2010; Liu *et al.*, 2011). We estimate that a rhodol-based variant of MDG2 could be 6- to 8-fold brighter compared to the fluorescein-based variant. The second limitation, poor intracellular retention of biosensor signal, can be addressed in parallel, for example by making a SPiDER- (spiro-based immobilisable diethylrhodol) probe. Upon trigger cleavage, these probes simultaneously activate fluorescence and produce a quinone methide intermediate (Doura *et al.*, 2016). This intermediate can covalently react with protein, thus immobilising the probe. Instead of arbitrarily targeting all protein, which in long-term experiments may cause unwanted side effects, it is also conceivable to make a membrane damage sensor that is a HaloTag ligand. The HaloTag method is a modular protein tagging system, which relies on the covalent linkage between a modified haloalkane dehalogenase (HaloTag) and a chloroalkane linker on a synthetic HaloTag ligand (Los *et al.*, 2008). Although this system requires extra preparation, since transgenic expression of HaloTag is required, its advantages lie not only in probe retention. The HaloTag system also offers increased specificity of the biosensor signal as HaloTag can be expressed in a cell type-specific manner and, when fused to different proteins, can further guide subcellular probe localisation. A fluorogenic silicon rhodamine dye with chloroalkane linker, which is activated by HaloTag binding, already exists (Lukinavičius

et al., 2013) and it will be interesting to see whether a disulfonated derivative would act as a fluorogenic membrane damage sensor HaloTag ligand.

4.2. Development of a membrane damage-selective calcium chelator

The initial motivation behind the development of a membrane damage biosensor was to translate these findings to a calcium chelator prodrug. Just like the MDG1 biosensor, this prodrug would be permeable to damaged cells or axons only and require intracellular esterase activation of its calcium-binding ability. This translation effort, synthesis and testing of the prodrug, is in an early phase and comprehensive data still lacking. Therefore, this was not included in the results part of this thesis but shall briefly be discussed here.

An intracellular-only, cell-permeable calcium chelator, BAPTA-AM, is widely used and commercially available. In this molecule, the four organic acid groups of BAPTA (1,2-bis(o-aminophenoxy)ethane-N,N,N′,N′-tetraacetic acid), that are responsible for calcium coordination, are capped with acetoxymethylesters (AM), which can be cleaved off by intracellular esterases. Analogous to the disulfonated probe MDG1, my collaborator Philipp Mauker therefore synthesised a disulfonated version of BAPTA-AM, which will be referred to as BAPTA-S_2-AM. One limitation in this project was the complicated, low yield synthesis route for BAPTA-S_2-AM, which meant that only very limited amounts of the prodrug were available for testing.

In contrast to the fluorogenic compound screening, prodrug testing requires indirect assessment of its action, using calcium imaging. Although this is a commonly used method and many small molecule and protein-based calcium indicators exist, most applications such as detection of neuronal firing, require high affinity calcium indictors that detect minute alterations of calcium to levels slightly above baseline. Membrane permeabilisation in contrast can potentially lead to a massive elevation of intracellular calcium due to the 10 000-fold calcium concentration gradient across the membrane (1 - 2 mM extracellular, 50 - 100 nM intracellular, Schwaller, 2010). As a reference, intracellular calcium can reach 5 - 10 µM in excitotoxicity and even millimolar levels after axonal transection (Hyrc *et al.*, 1997; Stout and Reynolds, 1999; Rishal and Fainzilber, 2014). To assess pathological calcium overload in axons in inflammatory lesions, we are using a mouse line expressing the medium affinity calcium sensor CerTN-L15, that has a calcium dissociation constant (K_D) of 1.2 µM and a detection range of roughly 0.2 to 10 µM (Witte *et al.*, 2019; Heim *et al.*, 2007). Even though this is a good sensor to distinguish normal from elevated calcium in a binary way, the sensor is potentially saturated in high-calcium axons and thus does not allow us to approximate absolute calcium concentrations. We have therefore recently started a series of experiments of rAAV-mediated overexpression of low affinity protein-based calcium sensors (Twitch-4, K_D = 2.8 µM; Twitch-5, K_D = 9.3 µM; Twitch-2B-54S+, K_D = 174 µM and GreenT-EC.b, K_D = 800 µM, Thestrup *et al.*, 2014; Valiente-Gabioud *et al.*, 2023), followed by EAE induction and two-photon imaging at peak of disease. Knowing the detection ranges of theses sensors and seeing which of them still show a reaction to axonal calcium influx in EAE lesions will enable us to eventually estimate the axonal calcium concentration of degenerating axons.

This approach exemplifies well, how each calcium indicator only provides a narrow window on a limited range of calcium concentrations around its dissociation constant and how it is blind to calcium levels below or above. This also means that effects of calcium buffering, as we wish to see with the prodrug, first in *in vitro* testing and later in EAE, can only be detected when using an appropriate calcium indicator, as buffering effects outside a sensor's detection limits cannot be seen.

To prove that our prodrug chelator lowers cytosolic calcium, but only in membrane-damaged cells, we are aiming to compare BAPTA-S_2-AM to the healthy cell-permeable version BAPTA-AM in two different settings: calcium influx due to generalised plasma membrane permeabilisation (using LLO) and calcium influx without further membrane permeabilisation (using the calcium ionophore ionomycin). If our assumptions hold true, then BAPTA-AM that can cross any membrane, should be able to buffer calcium in both scenarios. BAPTA-S_2-AM in contrast should require the LLO pore for cellular entry and should not buffer ionomycin-mediated calcium influx. For simplicity, we perform these experiments in HEK cells, which are easy to transfect with the calcium indicator plasmids.

As mentioned above, these experiments are in an early phase, and we have not yet tested every calcium chelator with all experimental conditions. What can be said already, is that Twitch-5 provides a good detection range to detect a buffering effect of BAPTA-AM on LLO-mediated calcium influx, whereas ionomycin-mediated influx is more severe and will require titration of the ionomycin concentration or use of a lower affinity indicator. What troubles us at the moment, is the fact that we were not able to replicate the effect of BAPTA-AM on LLO-mediated influx using equimolar amounts of BAPTA-S_2-AM. Future experiments will have to show whether BAPTA-S_2, post cleavage, is able to bind calcium with similar affinity as BAPTA or whether the observation is due to slower membrane crossing or slower activation of BAPTA-S_2-AM compared to BAPTA-AM. Depending on the outcome, modifications to the prodrug may be necessary before *in vivo* testing is a sensible next step.

Regarding *in vivo* testing it remains to be said, that the most important readout for axonal degeneration is not lower calcium, but improved recovery, as assessed by axon morphology. In our experimental setup, we will be able to apply the pro-chelator directly to the spinal cord exposed for *in vivo* imaging. However, as a long-term therapy in mice or as a human therapy this is no available delivery route. Instead, we may have to experiment with intrathecal delivery.

To sum up, important foundations for the development of prodrug calcium chelators have been laid by the development of the fluorogenic probe MDG1 and by experimenting with different calcium indicators. Yet, a lot of work still lies ahead, most importantly the confirmation of prodrug function and its use in EAE.

4.3. rAAV-mediated overexpression in the axonal compartment

The second branch of my thesis was dependent on rAAV-mediated overexpression of calcium-binding proteins in axons. rAAVs have recently gained momentum in the field of neuroscience, due to the development of AAV9 capsid variants that can cross the blood-brain-barrier (Chan *et al.*, 2017). Before, AAVs had to be injected locally, which causes local injury and only achieves a limited spread around the injection site. With the new serotypes, including PHP.eB which is used in this thesis, AAVs can be injected intravenously and achieve wide-spread CNS transduction. We therefore produced and injected three different viruses, carrying either calbindin, calretinin or a control gene, whose expression was linked to that of the fluorescent reporter Kusabira Orange fluorescent protein (KOFP) (**Figure 17**).

Despite the promises of the method, we encountered several problems using this approach. First of all, we utilised Cre recombinase as a length-matched negative control gene for calbindin and calretinin overexpression. Due to the absence of loxP sites, which guide Cre's recombinant action, we believed the enzyme to be without any function and were surprised to see that the Cre virus was toxic to mice. Indeed, Cre toxicity has previously been described in the literature, including toxicity to neurons (Forni *et al.*, 2006) and may be mediated by DNA damage due to recombination at naturally occurring pseudo *lox*P sites (Schmidt-Supprian and Rajewsky, 2007). Several of our mice which had received the Cre-KOFP virus developed progressive weight loss; we did however not observe any neurological symptoms. Likewise, no overt neuronal damage or death was seen in Cre-KOFP receiver mice that had undergone *in vivo* imaging (**Figure 18a**) or NeuroTrace staining of the cortex (**Figure 18c**), although it has to be noted that we did not proactively search for these signs at the time. Cumulatively, these observations indicate a systemic rather than neuron-specific toxicity of the virus, which may have been mediated for example by AAV-PHP.eB infection of liver cells (Deverman *et al.*, 2016) and ensuing dysfunction. We did not investigate this further but instead replaced the control gene for the third cohort with ShadowG, a mutated, non-fluorescent GFP variant. The reason why we need a control gene and cannot use a control virus that only expresses the reporter Kusabira Orange fluorescent protein (KOFP), is that transcript size is relevant to transcription efficiency, and we want our control to be as similar as possible to the therapeutic viruses.

A second problem that we encountered, was that viral overexpression efficacy varied depending on the transgene expressed and especially calbindin had a poor performance with many images having too low quality to be analysed (**Figure 18a-e**). In contrast, for calretinin and control mice, the majority of images was analysable. This means that the data shown underrepresents the full extent of the problem. In *in vivo* imaging, poor performance of the calbindin virus was mostly visible as less axons labelled, however more in-depth analysis in fixed tissue revealed that all viruses transduced a comparable number of cells, yet the expression levels of the reporter, which is directly linked to expression of the overexpressed gene, were very different between viruses. Thus, low axon count in two-photon imaging was most probably due to low-expressing axons falling below the detection threshold.

We conclude that this effect is linked to the transgene itself and not to mere transgene size, viral preparation or viral injection for numerous reasons: First, transgene size could be ruled out, because calbindin, which had the poorest performance, is encoded by a shorter gene than calretinin and Cre recombinase. Second, all viral productions yielded similar titers and differences between calbindin virus and other viruses persisted even when all viruses were produced freshly again (cohort 1 vs. cohort 2). This argues against viral assembly problems, which would result in a lower titer and against other problems in the production process since it was seen in two independent productions. Indeed, the differences even persisted when we had the same genes expressed from new plasmids and virus made by a commercial manufacturer (cohort 3). Although intravenous injection quality may differ between mice it is unlikely with the large group sizes that by chance all mice in the calbindin group received less injection volume.

We then tested *in vitro* whether we could predict *in vivo* expression, thereby allowing a better matching of expression level of the gene of interest to control genes. However, we found that cells transfected with the viral plasmid as well as cells infected with the virus expressed calbindin very well, better even than calretinin and Cre recombinase (**Figure 18f, g**). Other than *in vivo*, expression levels *in vitro* as assessed by KOFP fluorescence intensity were proportional to gene size. It is theoretically conceivable that the differences between viruses result from a step not encompassed by the *in vitro* setups, such as viral stability in blood or blood-brain-barrier crossing. However, it is difficult to rationalise how the viral transgene should influence these steps. Another explanation for different expression levels is different neuron-specific regulation of the transgenes, which we would miss by testing on non-neuronal cell lines. Such regulation would have to be at the level of transcription, post-transcriptional mRNA stability or at the level of mRNA trafficking. Post-translational regulation such as proteasome degradation can be ruled out since we detect the differences by looking at the fluorescent reporter. Due to the T2A system, reporter and gene of interest are transcribed on the same mRNA (i.e. likely co-regulated) but then cleaved off during translation, yielding two independent proteins. Indeed, there is tentative evidence for different regulation of calbindin and calretinin: according to a database of neuronal compartment-specific transcriptomes and translatomes (https://public.brain.mpg.de/dashapps/localseq/) accompanying a publication by Glock *et al.* (2021), which is based on hippocampus, calbindin is preferentially found in the soma compared to neuropil. Calretinin in contrast was enriched in neuropil compared to soma, although the filtering options of the database suggest that in case of calretinin this may also be a glial contamination. In summary, our data suggests, that viruses carrying different transgenes infect similar numbers of cells when produced in parallel and injected at the same titer. The expression level in infected cells however depends on the transgene and is likely due to neuron-specific transcriptional or post-transcriptional regulation. This means that qPCR-based titering is helpful in calibrating the number of infected cells yet neither qPCR-based nor infectious titering can predict transgene expression levels at least if performed in non-neuronal cells.

The unexpected finding, that calbindin expression may repressed in neurons raises the question of why this circumstance was not described in earlier studies of neuroprotective calbindin overexpression. A closer inspection of the studies summarised in *1.3.2.1 Calcium*

buffering by calcium-binding proteins reveals two main differences in comparison to the work in this thesis: first, with the exception of one study, which however did not report a neuroprotective effect (Freimann *et al.*, 2010), strong ubiquitous promoters instead of weaker neuron-specific promoters were used. It is conceivable that these promoters yielded sufficient expression to outcompete negative regulation, yielding satisfactory expression levels. Second, the conclusion that calbindin is negatively regulated by neurons in the *in vivo* setup presented in this thesis, was drawn from an experiment in which the expression of an invariable reporter was quantified while T2A-coupled to variable transgenes (**Figure 18c**). This experiment showed transgene-dependent changes in reporter expression. The studies cited above, in contrast, confirmed successful overexpression either by comparing overexpressing to untreated cells or to cells treated with vectors containing reporter only. No size-matched control transgenes were used, meaning that transgene-dependent regulatory mechanisms, if present, could not be detected. It is also possible that the presence of negative regulation of calbindin is dependent on the specific neuronal subtype being studied.

Another observation that we made, is that all of our viruses labelled preferentially small calibre axons (**Figure 18h**). This may be due to the tropism of the virus, having a predilection for the corresponding neuronal subtypes. However, keeping in mind that we observe relatively low expression of the virally delivered transgenes, this may also be a dilution effect: a small calibre axon needs less copy numbers of KOFP to be detected in microscopy, because they are confined to a smaller space. A doubling in axon diameter will quadruple the axonal volume and the required copy number for fluorescent detection. Since axons of different calibres have different degeneration characteristics, the fact that virus-labelled axons are mainly small calibre has implications for the interpretation of our experiments and we cannot exclude that the intervention would have had protective effects on larger calibre axons.

The problems that we encountered and discussed here do not necessarily put the overall method of intravenous rAAV-mediated overexpression into question. Rather it seems that the employment of the method for overexpression in axons uncovers some of its limitations. Overexpression in the axon means, that either the mRNA or the protein has to travel large distances from the soma throughout the axon. Also, the axon can make up 95 % of a neurons volume, exemplifying well how heavily diluted a low-expressed protein will become. Here, longer time frames for expression may be helpful, although in the case of calcium-binding proteins, this may lead to adaptation of the calcium regulatory network (Freimann *et al.*, 2010). It has to be noted, that we have successfully achieved good axonal expression in our lab previously (Tai *et al.*, 2023) and also the Cre control used in my experiments provided satisfactory labelling. However, as long as we do not understand why some other transgenes, most notably calbindin, are not well expressed, this method has its limitations.

Several steps can be taken to help overcome these limitations. First of all, the *in vitro* transduction experiments that were aimed to characterise transgene expression should be repeated in cultured neurons. If these replicate the expression differences observed in neurons *in vivo*, this can be used as a pre-screening tool to predict successful overexpression before starting laborious mouse experiments. Second, it should be rigorously ruled out, that differences in viral overexpression are after all dependent on viral plasmids or virus production. To do this,

CB-KOFP, CR-KOFP and CTR-KOFP should be re-cloned to resemble the viral plasmids employed by Tai *et al.* (2023) as closely as possible. This would imply using the same fluorescent reporter (switch from KOFP to TdTomato) and the same self-cleaving peptide (P2A instead of T2A). The backbone, promoter and regulatory elements (WPRE and poly-adenylation sequence) are already identical between the viruses. The viruses should then be reproduced in parallel, also using the same purification protocol, and parallelly injected into mice. This would tell whether expression differences between the different transgenes persist. Third, if calbindin is indeed the target of transcriptional or post-transcriptional repression in neurons, this must be encoded in its base sequence. It would therefore be interesting to see whether a codon-optimised version of calbindin, where different codons are used to encode the same amino acid sequence, would be better expressed. If it is in contrast trafficking of calbindin mRNA to axons that is the bottleneck, addition of an axonal mRNA localisation motif may improve axonal expression.

Another possibility to increase expression more generally, is the use of stronger promoters. When using PHP.eB, it is advisable to use neuron-specific promoters, since the capsid also has a strong tropism for astrocytes (Chan *et al.*, 2017). In this thesis, I have been using the hSyn promoter. However, another study using PHP.eB has shown, that neuron-specific enolase promoter (NSE) achieves higher expression levels than hSyn (Radhiyanti *et al.*, 2021). Furthermore, a derivative of the PHP.eB capsid, CAP-B10, has been published recently, which has improved neuron-specific tropism with roughly 75 % of infected cells being neuronal, compared to only 40 % in PHP.eB (Brown *et al.*, 2021; Chan *et al.*, 2017). Due to its higher specificity, this capsid variant could potentially be used with a ubiquitous promoter such as CMV or CAG promoter which can achieve much stronger expression than hSyn or NSE. Other studies have also made use of a transposon system to achieve better expression upon AAV integration into host DNA (Zheng *et al.*, 2024). As a last resort it would also be conceivable to forgo intravenous delivery and instead employ either local injection or neonatal intraventricular injection of rAAVs.

In summary, low expression of some transgenes is a limitation for rAAV-mediated overexpression in axons. This may be overcome by interfering with mRNA regulation or more generally by employing stronger promoters.

4.4. Axoprotective potential of calcium-binding proteins

Calcium-binding proteins, especially those with low calcium affinity such as calbindin and calretinin, bind calcium when concentrations are high and gradually release it as concentrations return to baseline. Hypothesising that such a buffering effect may buy axons time to recover from damage without activation of irrevocable degeneration mechanisms, we performed experiments of rAAV-mediated overexpression of calbindin and calretinin in neurons and their axons. However, our data suggests no axoprotective effect: the morphology, representing different stages of degeneration, was unaltered between axons overexpressing calbindin, calretinin or a control gene. Likewise, intra-axonal calcium levels were unaltered between these groups (**Figure 20**).

Our study has however three main limitations: Firstly, the calcium sensor employed, CerTN-L15, has a K_D of 1.2 µM, which, as already discussed above, makes it suitable to distinguish calcium overload from physiological calcium but unsuitable to detect smaller changes within calcium overloaded axons. It is therefore possible that calbindin or calretinin exert an effect on calcium levels but that this effect is too small to desaturate the sensor. Secondly, all virus-positive axons were of small calibre, meaning that we lack data on potential protective effects in large calibre axons. Thirdly and most importantly, although we did confirm that calbindin and calretinin were indeed overexpressed, as shown by correlation between calbindin/calretinin IHC with KOFP fluorescence, the extent of the overexpression was relatively small (**Figure 19**). When looking at mean expression, we see around 2.5-fold increase of both calbindin and calretinin levels compared to control virus. However, the control mean is very low, because it encompasses many cells with no detectable calbindin and calretinin expression and a 2.5-fold increase may therefore, though statistically significant, not necessarily be meaningful. In particular, the increase in expression is very small when compared to the range of endogenous expression levels which can be much higher than mean plus standard deviation in overexpressing cells. Given that the intra-axonal calcium increase post membrane barrier permeabilisation must be massive, following the 1000-fold concentration gradient across the membrane, the overexpression achieved here may well be just a drop in the ocean.

It is therefore possible, that the absence of an axoprotective effect in our study of calcium-binding overexpression is not due to the unsuitability of the therapeutic approach but due to underdosing. Indeed, the effects of CaBPs are known to be highly dose-dependent (Schwaller *et al.*, 2002; Airaksinen *et al.*, 1997; Hack *et al.*, 2000). The experiments should therefore be repeated in an experimental setting that allows for more pronounced axonal overexpression. For troubleshooting, it might also be helpful to employ less sensitive calcium indicators to detect smaller calcium buffering effects.

4.5. Future perspectives of calcium targeting in axons

The aim of this thesis was to explore the potential of calcium as a therapeutic target to rescue axonal degeneration in neuroinflammatory lesions. In two different approaches, we therefore aimed to make use of exogenous and endogenous calcium buffers respectively.

Neurons and other cell types endogenously express calcium-binding proteins that can flatten calcium spikes. With the aim of increasing neuronal resilience to calcium influx after membrane barrier loss, we performed experiments of rAAV-mediated overexpression of the calcium-binding proteins calbindin and calretinin. Unfortunately, the levels of overexpression that we achieved with this delivery method were low and we could not observe any effect on the frequency of axonal degeneration or on intracellular calcium levels. I therefore propose that the method is refined to achieve higher overexpression and these experiments then repeated. The following steps can be taken to increase our understanding of the rAAV delivery method and increase overexpression levels: (1) Standardising cloning and virus production procedures. This will limit all variation between viruses to the transgene expressed and thus

simplify troubleshooting. (2) Establishing *in vitro* testing of viruses in neuronal cultures. This may serve to discover low expression early and start the troubleshooting process before going *in vivo*. (3) Testing stronger neuronal promoters in PHP.eB or utilising more neuron-specific capsids like CAP-B10 with ubiquitous promoters. (4) Experimenting with codon optimisation or addition of axonal mRNA targeting sequences to prevent repression and support mRNA trafficking to the axon. (5) If these measures are not enough to achieve satisfactory overexpression, I propose to fall back on other rAAV delivery mechanisms such as local injection or neonatal intrathecal injection.

There are also other ways, beyond calcium-binding protein overexpression, to modulate endogenous calcium handling to improve axonal resilience. Apart from buffering, cells also employ mechanisms of calcium storage in ER and mitochondria and calcium extrusion via the plasma membrane to lower cytosolic calcium levels. Pharmacologic activators exist for many of the involved membrane channels and pumps, such as CDN1163, activator of SERCA, neurounina, activator of NCX and methylene blue, activator of PMCA. Evidence for their protective potential in other disease models exists (Kang *et al.*, 2016; Cerullo *et al.*, 2018; Anzilotti *et al.*, 2021; Berrocal *et al.*, 2018) and they are blood-brain-barrier-permeable, thus allowing for simple experiments with daily i.p. or i.v. dosing in EAE mice. Indeed, I have already started pharmacological experiments with the NCX-activator neurounina, yet analysis of axonal morphology and calcium levels in treated vs. vehicle mice is still outstanding.

The disadvantage of these pharmacologic experiments is that potential protective effects observed are not necessarily genuinely neuroprotective but may also be mediated by drug action on infiltrating immune cells. This means, that findings need to be corroborated by genetic studies, ensuring neuron-specificity. Also, to my knowledge, there is to this date no pharmacologic activator of the mitochondrial calcium uniporter (MCU), meaning that only genetic options are available to study increased calcium storage in mitochondria. Neuron-specific overexpression of the calcium pumps outlined here would make for very relevant experiments. However, this puts us back at the bottleneck of unreliable axonal expression achieved with intravenous rAAV-PHP.eB. This emphasises again, that this crucial method has to be better understood and optimised for axonal overexpression before it can aid our exploration of calcium as a neuroprotective target.

Regarding exogenous calcium buffering, our long-term aim was to develop a prodrug calcium chelator that would only be able to enter and then be activated within membrane-damaged axons to prevent side effects on physiological calcium functions. In this thesis, we took an important first step towards this goal by performing a proof-of-principle study of selective delivery to membrane-damaged cells and axons, which resulted in the development and scientific publication of the membrane damage sensor MDG1(Mauker, Beckmann *et al.*, 2024). Several important steps have to be taken to get from here to prodrug treatment in EAE mice. First of all, we want to make some improvements on the biosensor regarding its retention inside cells and its resistance to hydrolysis. Especially the latter will be relevant for taking the biosensor from cells and axons growing *in vitro* to the white matter tracts within the murine spinal cord. In parallel we have synthesised a first prototype of the prodrug chelator and have started establishment of an *in vitro* testing setup by employing different calcium sensors and

different calcium insults that are dependent on or independent of membrane permeabilisation. Our latest findings suggest however, that the prodrug prototype is not efficiently entering into and/or activated within damaged cells. It is therefore likely, that much like for the biosensor, we will have to test several variations of the prodrug chelator to find one that has the desired function.

4.6. Concluding remarks

This thesis has laid foundational work to address the suitability of calcium as a neuroprotective target for the prevention of axonal degeneration in neuroinflammatory lesions.

The contribution of this thesis lies mainly in the development of a selective targeting approach to membrane-damaged axons, in the development of an experimental pipeline for the overexpression of potentially neuroprotective proteins in axons and in the extensive troubleshooting performed to map out the limitations of the rAAV delivery approach. Future studies are needed to translate biosensor findings into a workable prodrug calcium chelator and to test its benefits *in vivo*. Successful manipulation of endogenous calcium-handling pathways will require an optimisation of the rAAV delivery approach, for which I have made various suggestions. In the meantime, pharmacologic experiments of calcium pump activation can provide a way to map out which of these pumps are worth performing more rigorous genetic experiments.

References

Absinta, M., Maric, D., Gharagozloo, M., Garton, T., Smith, M.D., Jin, J., Fitzgerald, K.C., Song, A., Liu, P., Lin, J.-P., Wu, T., Johnson, K.R., McGavern, D.B., Schafer, D.P., Calabresi, P.A. and Reich, D.S. (2021), "A lymphocyte-microglia-astrocyte axis in chronic active multiple sclerosis", *Nature*, Vol. 597 No. 7878, pp. 709–714.

Agosta, F., Absinta, M., Sormani, M.P., Ghezzi, A., Bertolotto, A., Montanari, E., Comi, G. and Filippi, M. (2007), "In vivo assessment of cervical cord damage in MS patients: a longitudinal diffusion tensor MRI study", *Brain a journal of neurology*, Vol. 130 No. Pt 8, pp. 2211–2219.

Ahmed, F.A., Ingoglia, N.A. and Sharma, S.C. (2001), "Axon resealing following transection takes longer in central axons than in peripheral axons: implications for axonal regeneration", *Experimental neurology*, Vol. 167 No. 2, pp. 451–455.

Airaksinen, M.S., Eilers, J., Garaschuk, O., Thoenen, H., Konnerth, A. and Meyer, M. (1997), "Ataxia and altered dendritic calcium signaling in mice carrying a targeted null mutation of the calbindin D28k gene", *Proceedings of the National Academy of Sciences*, Vol. 94 No. 4, pp. 1488–1493.

Andreone, B.J., Larhammar, M. and Lewcock, J.W. (2020), "Cell Death and Neurodegeneration", *Cold Spring Harbor perspectives in biology*, Vol. 12 No. 2.

Androdias, G., Reynolds, R., Chanal, M., Ritleng, C., Confavreux, C. and Nataf, S. (2010), "Meningeal T cells associate with diffuse axonal loss in multiple sclerosis spinal cords", *Annals of neurology*, Vol. 68 No. 4, pp. 465–476.

Anzilotti, S., Valsecchi, V., Brancaccio, P., Guida, N., Laudati, G., Tedeschi, V., Petrozziello, T., Frecentese, F., Magli, E., Hassler, B., Cuomo, O., Formisano, L., Secondo, A., Annunziato, L. and Pignataro, G. (2021), "Prolonged NCX activation prevents SOD1 accumulation, reduces neuroinflammation, ameliorates motor behavior and prolongs survival in a ALS mouse model", *Neurobiology of disease*, Vol. 159, p. 105480.

Arndt-Jovin, D.J. and Jovin, T.M. (1989), "Fluorescence labeling and microscopy of DNA", *Methods in cell biology*, Vol. 30, pp. 417–448.

Ashrafi, G., Schlehe, J.S., LaVoie, M.J. and Schwarz, T.L. (2014), "Mitophagy of damaged mitochondria occurs locally in distal neuronal axons and requires PINK1 and Parkin", *The Journal of cell biology*, Vol. 206 No. 5, pp. 655–670.

Atkins, H.L., Bowman, M., Allan, D., Anstee, G., Arnold, D.L., Bar-Or, A., Bence-Bruckler, I., Birch, P., Bredeson, C., Chen, J., Fergusson, D., Halpenny, M., Hamelin, L., Huebsch, L., Hutton, B., Laneuville, P., Lapierre, Y., Lee, H., Martin, L., McDiarmid, S., O'Connor, P., Ramsay, T., Sabloff, M., Walker, L. and Freedman, M.S. (2016), "Immunoablation and autologous haemopoietic stem-cell transplantation for aggressive multiple sclerosis: a multicentre single-group phase 2 trial", *Lancet (London, England)*, Vol. 388 No. 10044, pp. 576–585.

Baecher-Allan, C., Kaskow, B.J. and Weiner, H.L. (2018), "Multiple Sclerosis. Mechanisms and Immunotherapy", *Neuron*, Vol. 97 No. 4, pp. 742–768.

Bagasra, O., Michaels, F.H., Zheng, Y.M., Bobroski, L.E., Spitsin, S.V., Fu, Z.F., Tawadros, R. and Koprowski, H. (1995), "Activation of the inducible form of nitric oxide synthase in the brains of patients with multiple sclerosis", *Proceedings of the National Academy of Sciences of the United States of America*, Vol. 92 No. 26, pp. 12041–12045.

Barclay, W. and Shinohara, M.L. (2017), "Inflammasome activation in multiple sclerosis and experimental autoimmune encephalomyelitis (EAE)", *Brain pathology (Zurich, Switzerland)*, Vol. 27 No. 2, pp. 213–219.

Barkhof, F., Calabresi, P.A., Miller, D.H. and Reingold, S.C. (2009), "Imaging outcomes for neuroprotection and repair in multiple sclerosis trials", *Nature reviews. Neurology*, Vol. 5 No. 5, pp. 256–266.

Barrie, W., Yang, Y., Irving-Pease, E.K., Attfield, K.E., Scorrano, G., Jensen, L.T., Armen, A.P., Dimopoulos, E.A., Stern, A., Refoyo-Martinez, A., Pearson, A., Ramsøe, A., Gaunitz, C., Demeter, F., Jørkov, M.L.S., Møller, S.B., Springborg, B., Klassen, L., Hyldgård, I.M., Wickmann, N., Vinner, L., Korneliussen, T.S.,

Allentoft, M.E., Sikora, M., Kristiansen, K., Rodriguez, S., Nielsen, R., Iversen, A.K.N., Lawson, D.J., Fugger, L. and Willerslev, E. (2024), "Elevated genetic risk for multiple sclerosis emerged in steppe pastoralist populations", *Nature*, Vol. 625 No. 7994, pp. 321–328.

Barrientos, S.A., Martinez, N.W., Yoo, S., Jara, J.S., Zamorano, S., Hetz, C., Twiss, J.L., Alvarez, J. and Court, F.A. (2011), "Axonal degeneration is mediated by the mitochondrial permeability transition pore", *The Journal of neuroscience the official journal of the Society for Neuroscience*, Vol. 31 No. 3, pp. 966–978.

Barro, C., Benkert, P., Disanto, G., Tsagkas, C., Amann, M., Naegelin, Y., Leppert, D., Gobbi, C., Granziera, C., Yaldizli, Ö., Michalak, Z., Wuerfel, J., Kappos, L., Parmar, K. and Kuhle, J. (2018), "Serum neurofilament as a predictor of disease worsening and brain and spinal cord atrophy in multiple sclerosis", *Brain a journal of neurology*, Vol. 141 No. 8, pp. 2382–2391.

Baughman, J.M., Perocchi, F., Girgis, H.S., Plovanich, M., Belcher-Timme, C.A., Sancak, Y., Bao, X.R., Strittmatter, L., Goldberger, O., Bogorad, R.L., Koteliansky, V. and Mootha, V.K. (2011), "Integrative genomics identifies MCU as an essential component of the mitochondrial calcium uniporter", *Nature*, Vol. 476 No. 7360, pp. 341–345.

Benkert, P., Meier, S., Schaedelin, S., Manouchehrinia, A., Yaldizli, Ö., Maceski, A., Oechtering, J., Achtnichts, L., Conen, D., Derfuss, T., Lalive, P.H., Mueller, C., Müller, S., Naegelin, Y., Oksenberg, J.R., Pot, C., Salmen, A., Willemse, E., Kockum, I., Blennow, K., Zetterberg, H., Gobbi, C., Kappos, L., Wiendl, H., Berger, K., Sormani, M.P., Granziera, C., Piehl, F., Leppert, D. and Kuhle, J. (2022), "Serum neurofilament light chain for individual prognostication of disease activity in people with multiple sclerosis: a retrospective modelling and validation study", *The Lancet. Neurology*, Vol. 21 No. 3, pp. 246–257.

Ben-Nun, A., Mendel, I., Bakimer, R., Fridkis-Hareli, M., Teitelbaum, D., Arnon, R., Sela, M. and Kerlero de Rosbo, N. (1996), "The autoimmune reactivity to myelin oligodendrocyte glycoprotein (MOG) in multiple sclerosis is potentially pathogenic: effect of copolymer 1 on MOG-induced disease", *Journal of neurology*, Vol. 243 No. 4 Suppl 1, S14-22.

Ben-Nun, A., Wekerle, H. and Cohen, I.R. (1981), "The rapid isolation of clonable antigen-specific T lymphocyte lines capable of mediating autoimmune encephalomyelitis", *European journal of immunology*, Vol. 11 No. 3, pp. 195–199.

Berer, K., Mues, M., Koutrolos, M., Rasbi, Z.A., Boziki, M., Johner, C., Wekerle, H. and Krishnamoorthy, G. (2011), "Commensal microbiota and myelin autoantigen cooperate to trigger autoimmune demyelination", *Nature*, Vol. 479 No. 7374, pp. 538–541.

Bernardi, P., Gerle, C., Halestrap, A.P., Jonas, E.A., Karch, J., Mnatsakanyan, N., Pavlov, E., Sheu, S.-S. and Soukas, A.A. (2023), "Identity, structure, and function of the mitochondrial permeability transition pore: controversies, consensus, recent advances, and future directions", *Cell death and differentiation*, Vol. 30 No. 8, pp. 1869–1885.

Berridge, M.J., Bootman, M.D. and Roderick, H.L. (2003), "Calcium signalling: dynamics, homeostasis and remodelling", *Nature reviews. Molecular cell biology*, Vol. 4 No. 7, pp. 517–529.

Berrocal, M., Corbacho, I., Gutierrez-Merino, C. and Mata, A.M. (2018), "Methylene blue activates the PMCA activity and cross-interacts with amyloid β-peptide, blocking Aβ-mediated PMCA inhibition", *Neuropharmacology*, Vol. 139, pp. 163–172.

Bettelli, E., Pagany, M., Weiner, H.L., Linington, C., Sobel, R.A. and Kuchroo, V.K. (2003), "Myelin oligodendrocyte glycoprotein-specific T cell receptor transgenic mice develop spontaneous autoimmune optic neuritis", *The Journal of experimental medicine*, Vol. 197 No. 9, pp. 1073–1081.

Beynon, V., George, I.C., Elliott, C., Arnold, D.L., Ke, J., Chen, H., Zhu, L., Ke, C., Giovannoni, G., Scaramozza, M., Campbell, N., Bradley, D.P., Franchimont, N., Gafson, A. and Belachew, S. (2022), "Chronic lesion activity and disability progression in secondary progressive multiple sclerosis", *BMJ neurology open*, Vol. 4 No. 1, e000240.

Bill, C.A. and Vines, C.M. (2020), "Phospholipase C", *Advances in experimental medicine and biology*, Vol. 1131, pp. 215–242.

Billiau, A. and Matthys, P. (2001), “Modes of action of Freund's adjuvants in experimental models of autoimmune diseases”, *Journal of leukocyte biology*, Vol. 70 No. 6, pp. 849–860.

Bitsch, A., Schuchardt, J., Bunkowski, S., Kuhlmann, T. and Brück, W. (2000), “Acute axonal injury in multiple sclerosis. Correlation with demyelination and inflammation”, *Brain a journal of neurology*, 123 (Pt 6), pp. 1174–1183.

Bjartmar, C., Kidd, G., Mörk, S., Rudick, R. and Trapp, B.D. (2000), “Neurological disability correlates with spinal cord axonal loss and reduced N-acetyl aspartate in chronic multiple sclerosis patients”, *Annals of neurology*, Vol. 48 No. 6, pp. 893–901.

Bjartmar, C., Kinkel, R.P., Kidd, G., Rudick, R.A. and Trapp, B.D. (2001), “Axonal loss in normal-appearing white matter in a patient with acute MS”, *Neurology*, Vol. 57 No. 7, pp. 1248–1252.

Bjartmar, C., Wujek, J.R. and Trapp, B.D. (2003), “Axonal loss in the pathology of MS: consequences for understanding the progressive phase of the disease”, *Journal of the neurological sciences*, Vol. 206 No. 2, pp. 165–171.

Bjornevik, K., Cortese, M., Healy, B.C., Kuhle, J., Mina, M.J., Leng, Y., Elledge, S.J., Niebuhr, D.W., Scher, A.I., Munger, K.L. and Ascherio, A. (2022), “Longitudinal analysis reveals high prevalence of Epstein-Barr virus associated with multiple sclerosis”, *Science (New York, N.Y.)*, Vol. 375 No. 6578, pp. 296–301.

Bjornevik, K., Munger, K.L., Cortese, M., Barro, C., Healy, B.C., Niebuhr, D.W., Scher, A.I., Kuhle, J. and Ascherio, A. (2020), “Serum Neurofilament Light Chain Levels in Patients With Presymptomatic Multiple Sclerosis”, *JAMA neurology*, Vol. 77 No. 1, pp. 58–64.

Bonfoco, E., Krainc, D., Ankarcrona, M., Nicotera, P. and Lipton, S.A. (1995), “Apoptosis and necrosis: two distinct events induced, respectively, by mild and intense insults with N-methyl-D-aspartate or nitric oxide/superoxide in cortical cell cultures”, *Proceedings of the National Academy of Sciences*, Vol. 92 No. 16, pp. 7162–7166.

Bratkowski, M., Burdett, T.C., Danao, J., Wang, X., Mathur, P., Gu, W., Beckstead, J.A., Talreja, S., Yang, Y.-S., Danko, G., Park, J.H., Walton, M., Brown, S.P., Tegley, C.M., Joseph, P.R.B., Reynolds, C.H. and Sambashivan, S. (2022), “Uncompetitive, adduct-forming SARM1 inhibitors are neuroprotective in preclinical models of nerve injury and disease”, *Neuron*.

Brini, M., Calì, T., Ottolini, D. and Carafoli, E. (2014), “Neuronal calcium signaling: function and dysfunction”, *Cellular and molecular life sciences CMLS*, Vol. 71 No. 15, pp. 2787–2814.

Brini, M., Carafoli, E. and Calì, T. (2017), “The plasma membrane calcium pumps. Focus on the role in (neuro)pathology”, *Biochemical and biophysical research communications*, Vol. 483 No. 4, pp. 1116–1124.

Brini, M., Ottolini, D., Calì, T. and Carafoli, E. (2013), “Calcium in health and disease”, *Metal ions in life sciences*, Vol. 13, pp. 81–137.

Brookes, P.S., Yoon, Y., Robotham, J.L., Anders, M.W. and Sheu, S.-S. (2004), “Calcium, ATP, and ROS: a mitochondrial love-hate triangle”, *American journal of physiology. Cell physiology*, Vol. 287 No. 4, C817-33.

Brown, D., Altermatt, M., Dobreva, T., Chen, S., Wang, A., Thomson, M. and Gradinaru, V. (2021), “Deep Parallel Characterization of AAV Tropism and AAV-Mediated Transcriptional Changes via Single-Cell RNA Sequencing”, *Frontiers in immunology*, Vol. 12, p. 730825.

Brownell, B. and Hughes, J.T. (1962), “The distribution of plaques in the cerebrum in multiple sclerosis”, *Journal of neurology, neurosurgery, and psychiatry*, Vol. 25 No. 4, pp. 315–320.

Brownlee, W.J., Altmann, D.R., Da Alves Mota, P., Swanton, J.K., Miszkiel, K.A., Wheeler-Kingshott, C.G., Ciccarelli, O. and Miller, D.H. (2017), “Association of asymptomatic spinal cord lesions and atrophy with disability 5 years after a clinically isolated syndrome”, *Multiple sclerosis (Houndmills, Basingstoke, England)*, Vol. 23 No. 5, pp. 665–674.

Campbell, G.R., Ziabreva, I., Reeve, A.K., Krishnan, K.J., Reynolds, R., Howell, O., Lassmann, H., Turnbull, D.M. and Mahad, D.J. (2011), “Mitochondrial DNA deletions and neurodegeneration in multiple sclerosis”, *Annals of neurology*, Vol. 69 No. 3, pp. 481–492.

Carafoli, E. and Krebs, J. (2016), "Why Calcium? How Calcium Became the Best Communicator", *The Journal of biological chemistry*, Vol. 291 No. 40, pp. 20849–20857.

Carafoli, E., Santella, L., Branca, D. and Brini, M. (2001), "Generation, control, and processing of cellular calcium signals", *Critical reviews in biochemistry and molecular biology*, Vol. 36 No. 2, pp. 107–260.

Case, R.M., Eisner, D., Gurney, A., Jones, O., Muallem, S. and Verkhratsky, A. (2007), "Evolution of calcium homeostasis: from birth of the first cell to an omnipresent signalling system", *Cell calcium*, Vol. 42 No. 4-5, pp. 345–350.

Catterall, W.A. (2011), "Voltage-gated calcium channels", *Cold Spring Harbor perspectives in biology*, Vol. 3 No. 8, a003947.

Cencioni, M.T., Mattoscio, M., Magliozzi, R., Bar-Or, A. and Muraro, P.A. (2021), "B cells in multiple sclerosis - from targeted depletion to immune reconstitution therapies", *Nature Reviews Neurology*, Vol. 17 No. 7, pp. 399–414.

Cerullo, P., Brancaccio, P., Anzilotti, S., Vinciguerra, A., Cuomo, O., Fiorino, F., Severino, B., Di Vaio, P., Di Renzo, G., Annunziato, L. and Pignataro, G. (2018), "Acute and long-term NCX activation reduces brain injury and restores behavioral functions in mice subjected to neonatal brain ischemia", *Neuropharmacology*, Vol. 135, pp. 180–191.

Chan, K.Y., Jang, M.J., Yoo, B.B., Greenbaum, A., Ravi, N., Wu, W.-L., Sánchez-Guardado, L., Lois, C., Mazmanian, S.K., Deverman, B.E. and Gradinaru, V. (2017), "Engineered AAVs for efficient noninvasive gene delivery to the central and peripheral nervous systems", *Nature neuroscience*, Vol. 20 No. 8, pp. 1172–1179.

Chataway, J., Angelis, F. de, Connick, P., Parker, R.A., Plantone, D., Doshi, A., John, N., Stutters, J., MacManus, D., Prados Carrasco, F., Barkhof, F., Ourselin, S., Braisher, M., Ross, M., Cranswick, G., Pavitt, S.H., Giovannoni, G., Gandini Wheeler-Kingshott, C.A., Hawkins, C., Sharrack, B., Bastow, R., Weir, C.J., Stallard, N., Chandran, S., Gandini Wheeler-Kingshott, C.A., Williams, T., Beyene, T., Bassan, V., Zapata, A., Lyle, D., Cameron, J., Mollison, D., Colville, S., Dhillon, B., Gnanapavan, S., Nicholas, R., Rashid, W., Aram, J., Ford, H., Overell, J., Young, C., Arndt, H., Duddy, M., Guadagno, J., Evangelou, N., Craner, M., Palace, J., Hobart, J., Paling, D., Kalra, S. and McLean, B. (2020), "Efficacy of three neuroprotective drugs in secondary progressive multiple sclerosis (MS-SMART): a phase 2b, multiarm, double-blind, randomised placebo-controlled trial", *The Lancet Neurology*, Vol. 19 No. 3, pp. 214–225.

Chataway, J., Williams, T., Li, V., Marrie, R.A., Ontaneda, D. and Fox, R.J. (2024), "Clinical trials for progressive multiple sclerosis: progress, new lessons learned, and remaining challenges", *The Lancet. Neurology*, Vol. 23 No. 3, pp. 277–301.

Chen, X., He, W.-T., Hu, L., Li, J., Fang, Y., Wang, X., Xu, X., Wang, Z., Huang, K. and Han, J. (2016), "Pyroptosis is driven by non-selective gasdermin-D pore and its morphology is different from MLKL channel-mediated necroptosis", *Cell research*, Vol. 26 No. 9, pp. 1007–1020.

Chitnis, T., Imitola, J., Wang, Y., Elyaman, W., Chawla, P., Sharuk, M., Raddassi, K., Bronson, R.T. and Khoury, S.J. (2007), "Elevated neuronal expression of CD200 protects Wlds mice from inflammation-mediated neurodegeneration", *The American journal of pathology*, Vol. 170 No. 5, pp. 1695–1712.

Choi, S.R., Howell, O.W., Carassiti, D., Magliozzi, R., Gveric, D., Muraro, P.A., Nicholas, R., Roncaroli, F. and Reynolds, R. (2012), "Meningeal inflammation plays a role in the pathology of primary progressive multiple sclerosis", *Brain a journal of neurology*, Vol. 135 No. Pt 10, pp. 2925–2937.

Chu, F., Shi, M., Zheng, C., Shen, D., Zhu, J., Zheng, X. and Cui, L. (2018), "The roles of macrophages and microglia in multiple sclerosis and experimental autoimmune encephalomyelitis", *Journal of neuroimmunology*, Vol. 318, pp. 1–7.

Chyan, W., Kilgore, H.R., Gold, B. and Raines, R.T. (2017), "Electronic and Steric Optimization of Fluorogenic Probes for Biomolecular Imaging", *The Journal of organic chemistry*, Vol. 82 No. 8, pp. 4297–4304.

Coleman, M.P. and Freeman, M.R. (2010), "Wallerian degeneration, wld(s), and nmnat", *Annual review of neuroscience*, Vol. 33, pp. 245–267.

Coleman, M.P. and Höke, A. (2020), “Programmed axon degeneration: from mouse to mechanism to medicine”, *Nature reviews. Neuroscience*.

Coles, A.J., Wing, M.G., Molyneux, P., Paolillo, A., Davie, C.M., Hale, G., Miller, D., Waldmann, H. and Compston, A. (1999), “Monoclonal antibody treatment exposes three mechanisms underlying the clinical course of multiple sclerosis”, *Annals of Neurology*, Vol. 46 No. 3, pp. 296–304.

Compston, A. and Coles, A. (2008), “Multiple sclerosis”, *The Lancet*, Vol. 372 No. 9648, pp. 1502–1517.

Confavreux, C. and Vukusic, S. (2006), “Age at disability milestones in multiple sclerosis”, *Brain a journal of neurology*, Vol. 129 No. Pt 3, pp. 595–605.

Constantinescu, C.S., Farooqi, N., O'Brien, K. and Gran, B. (2011), “Experimental autoimmune encephalomyelitis (EAE) as a model for multiple sclerosis (MS)”, *British journal of pharmacology*, Vol. 164 No. 4, pp. 1079–1106.

Courjaret, R., Prakriya, M. and Machaca, K. (2024), “SOCE as a regulator of neuronal activity”, *The Journal of physiology*, Vol. 602 No. 8, pp. 1449–1462.

Craner, M.J., Newcombe, J., Black, J.A., Hartle, C., Cuzner, M.L. and Waxman, S.G. (2004), “Molecular changes in neurons in multiple sclerosis: altered axonal expression of Nav1.2 and Nav1.6 sodium channels and Na+/Ca2+ exchanger”, *Proceedings of the National Academy of Sciences of the United States of America*, Vol. 101 No. 21, pp. 8168–8173.

Cree, B.A.C., Cutter, G., Wolinsky, J.S., Freedman, M.S., Comi, G., Giovannoni, G., Hartung, H.-P., Arnold, D., Kuhle, J., Block, V., Munschauer, F.E., Sedel, F. and Lublin, F.D. (2020), “Safety and efficacy of MD1003 (high-dose biotin) in patients with progressive multiple sclerosis (SPI2): a randomised, double-blind, placebo-controlled, phase 3 trial”, *The Lancet. Neurology*, Vol. 19 No. 12, pp. 988–997.

Cree, B.A.C., Gourraud, P.-A., Oksenberg, J.R., Bevan, C., Crabtree-Hartman, E., Gelfand, J.M., Goodin, D.S., Graves, J., Green, A.J., Mowry, E., Okuda, D.T., Pelletier, D., Büdingen, H.-C. von, Zamvil, S.S., Agrawal, A., Caillier, S., Ciocca, C., Gomez, R., Kanner, R., Lincoln, R., Lizee, A., Qualley, P., Santaniello, A., Suleiman, L., Bucci, M., Panara, V., Papinutto, N., Stern, W.A., Zhu, A.H., Cutter, G.R., Baranzini, S., Henry, R.G. and Hauser, S.L. (2016), “Long-term evolution of multiple sclerosis disability in the treatment era”, *Annals of neurology*, Vol. 80 No. 4, pp. 499–510.

Csordás, G., Thomas, A.P. and Hajnóczky, G. (1999), “Quasi-synaptic calcium signal transmission between endoplasmic reticulum and mitochondria”, *The EMBO journal*, Vol. 18 No. 1, pp. 96–108.

Cunniffe, N. and Coles, A. (2021), “Promoting remyelination in multiple sclerosis”, *Journal of neurology*, Vol. 268 No. 1, pp. 30–44.

D’Orlando, C., Fellay, B., Schwaller, B., Salicio, V., Bloc, A., Gotzos, V. and Celio, M.R. (2001), “Calretinin and calbindin D-28k delay the onset of cell death after excitotoxic stimulation in transfected P19 cells”, *Brain Research*, Vol. 909 No. 1-2, pp. 145–158.

Dal-Bianco, A., Grabner, G., Kronnerwetter, C., Weber, M., Höftberger, R., Berger, T., Auff, E., Leutmezer, F., Trattnig, S., Lassmann, H., Bagnato, F. and Hametner, S. (2017), “Slow expansion of multiple sclerosis iron rim lesions: pathology and 7 T magnetic resonance imaging”, *Acta neuropathologica*, Vol. 133 No. 1, pp. 25–42.

Dalla Costa, G., Martinelli, V., Sangalli, F., Moiola, L., Colombo, B., Radaelli, M., Leocani, L., Furlan, R. and Comi, G. (2019), “Prognostic value of serum neurofilaments in patients with clinically isolated syndromes”, *Neurology*, Vol. 92 No. 7, e733-e741.

Davie, C.A., Hawkins, C.P., Barker, G.J., Brennan, A., Tofts, P.S., Miller, D.H. and McDonald, W.I. (1994), “Serial proton magnetic resonance spectroscopy in acute multiple sclerosis lesions”, *Brain a journal of neurology*, 117 (Pt 1), pp. 49–58.

DeBoy, C.A., Zhang, J., Dike, S., Shats, I., Jones, M., Reich, D.S., Mori, S., Nguyen, T., Rothstein, B., Miller, R.H., Griffin, J.T., Kerr, D.A. and Calabresi, P.A. (2007), “High resolution diffusion tensor imaging of axonal damage in focal inflammatory and demyelinating lesions in rat spinal cord”, *Brain a journal of neurology*, Vol. 130 No. Pt 8, pp. 2199–2210.

DeLuca, G.C., Ebers, G.C. and Esiri, M.M. (2004), "Axonal loss in multiple sclerosis: a pathological survey of the corticospinal and sensory tracts", *Brain a journal of neurology*, Vol. 127 No. Pt 5, pp. 1009–1018.

DeLuca, G.C., Williams, K., Evangelou, N., Ebers, G.C. and Esiri, M.M. (2006), "The contribution of demyelination to axonal loss in multiple sclerosis", *Brain a journal of neurology*, Vol. 129 No. Pt 6, pp. 1507–1516.

Dendrou, C.A., Fugger, L. and Friese, M.A. (2015), "Immunopathology of multiple sclerosis", *Nature reviews. Immunology*, Vol. 15 No. 9, pp. 545–558.

Denton, R.M. (2009), "Regulation of mitochondrial dehydrogenases by calcium ions", *Biochimica et biophysica acta*, Vol. 1787 No. 11, pp. 1309–1316.

Deutsche Gesellschaft für Neurologie e. V. (2022), *Leitlinie Leitlinie Multiple Sklerose für Patientinnen und Patienten*.

Deverman, B.E., Pravdo, P.L., Simpson, B.P., Kumar, S.R., Chan, K.Y., Banerjee, A., Wu, W.-L., Yang, B., Huber, N., Pasca, S.P. and Gradinaru, V. (2016), "Cre-dependent selection yields AAV variants for widespread gene transfer to the adult brain", *Nature biotechnology*, Vol. 34 No. 2, pp. 204–209.

Dhaouadi, N., Vitto, V.A.M., Pinton, P., Galluzzi, L. and Marchi, S. (2023), "Ca2+ signaling and cell death", *Cell calcium*, Vol. 113, p. 102759.

Diaz-Sanchez, M., Williams, K., Deluca, G.C. and Esiri, M.M. (2006), "Protein co-expression with axonal injury in multiple sclerosis plaques", *Acta neuropathologica*, Vol. 111 No. 4, pp. 289–299.

Dong, X., Wang, Y. and Qin, Z. (2009), "Molecular mechanisms of excitotoxicity and their relevance to pathogenesis of neurodegenerative diseases", *Acta pharmacologica Sinica*, Vol. 30 No. 4, pp. 379–387.

Dong, Y., D'Mello, C., Pinsky, W., Lozinski, B.M., Kaushik, D.K., Ghorbani, S., Moezzi, D., Brown, D., Melo, F.C., Zandee, S., Vo, T., Prat, A., Whitehead, S.N. and Yong, V.W. (2021), "Oxidized phosphatidylcholines found in multiple sclerosis lesions mediate neurodegeneration and are neutralized by microglia", *Nature neuroscience*.

D'Orlando, C., Celio, M.R. and Schwaller, B. (2002), "Calretinin and calbindin D-28k, but not parvalbumin protect against glutamate-induced delayed excitotoxicity in transfected N18-RE 105 neuroblastoma-retina hybrid cells", *Brain Research*, Vol. 945 No. 2, pp. 181–190.

Doura, T., Kamiya, M., Obata, F., Yamaguchi, Y., Hiyama, T.Y., Matsuda, T., Fukamizu, A., Noda, M., Miura, M. and Urano, Y. (2016), "Detection of LacZ-Positive Cells in Living Tissue with Single-Cell Resolution", *Angewandte Chemie (International ed. in English)*, Vol. 55 No. 33, pp. 9620–9624.

Duan, S., Lv, Z., Fan, X., Le Wang, Han, F., Wang, H. and Bi, S. (2014), "Vitamin D status and the risk of multiple sclerosis: a systematic review and meta-analysis", *Neuroscience letters*, Vol. 570, pp. 108–113.

Dziedzic, T., Metz, I., Dallenga, T., König, F.B., Müller, S., Stadelmann, C. and Brück, W. (2010), "Wallerian degeneration: a major component of early axonal pathology in multiple sclerosis", *Brain pathology (Zurich, Switzerland)*, Vol. 20 No. 5, pp. 976–985.

Evangelou, N., DeLuca, G.C., Owens, T. and Esiri, M.M. (2005), "Pathological study of spinal cord atrophy in multiple sclerosis suggests limited role of local lesions", *Brain a journal of neurology*, Vol. 128 No. Pt 1, pp. 29–34.

Evangelou, N., Esiri, M.M., Smith, S., Palace, J. and Matthews, P.M. (2000), "Quantitative pathological evidence for axonal loss in normal appearing white matter in multiple sclerosis", *Annals of Neurology*, Vol. 47 No. 3, pp. 391–395.

Fan, Y., Shi, L., Gu, Y., Zhao, Y., Xie, J., Qiao, J., Yang, G.-Y., Wang, Y. and Lu, C.-Z. (2007), "Pretreatment with PTD-calbindin D 28k alleviates rat brain injury induced by ischemia and reperfusion", *Journal of cerebral blood flow and metabolism official journal of the International Society of Cerebral Blood Flow and Metabolism*, Vol. 27 No. 4, pp. 719–728.

Ferguson, B., Matyszak, M.K., Esiri, M.M. and Perry, V.H. (1997), "Axonal damage in acute multiple sclerosis lesions", *Brain a journal of neurology*, 120 (Pt 3), pp. 393–399.

Filippi, M., Bozzali, M., Rovaris, M., Gonen, O., Kesavadas, C., Ghezzi, A., Martinelli, V., Grossman, R.I., Scotti, G., Comi, G. and Falini, A. (2003), "Evidence for widespread axonal damage at the earliest clinical stage of multiple sclerosis", *Brain a journal of neurology*, Vol. 126 No. Pt 2, pp. 433–437.

Fischer, M.T., Sharma, R., Lim, J.L., Haider, L., Frischer, J.M., Drexhage, J., Mahad, D., Bradl, M., van Horssen, J. and Lassmann, H. (2012), "NADPH oxidase expression in active multiple sclerosis lesions in relation to oxidative tissue damage and mitochondrial injury", *Brain a journal of neurology*, Vol. 135 No. Pt 3, pp. 886–899.

Forni, P.E., Scuoppo, C., Imayoshi, I., Taulli, R., Dastrù, W., Sala, V., Betz, U.A.K., Muzzi, P., Martinuzzi, D., Vercelli, A.E., Kageyama, R. and Ponzetto, C. (2006), "High levels of Cre expression in neuronal progenitors cause defects in brain development leading to microencephaly and hydrocephaly", *The Journal of Neuroscience*, Vol. 26 No. 37, pp. 9593–9602.

Forte, M., Gold, B.G., Marracci, G., Chaudhary, P., Basso, E., Johnsen, D., Yu, X., Fowlkes, J., Rahder, M., Stem, K., Bernardi, P. and Bourdette, D. (2007), "Cyclophilin D inactivation protects axons in experimental autoimmune encephalomyelitis, an animal model of multiple sclerosis", *Proceedings of the National Academy of Sciences of the United States of America*, Vol. 104 No. 18, pp. 7558–7563.

Freimann, F.B., Crome, O., Shevtsova, Z., Bähr, M. and Kügler, S. (2010), "Evaluation of long-term upregulation of Calbindin D28K as a preventive approach for ischaemic stroke", *International journal of stroke official journal of the International Stroke Society*, Vol. 5 No. 4, pp. 319–320.

Freund, T.F., Buzsáki, G., Leon, A., Baimbridge, K.G. and Somogyi, P. (1990), "Relationship of neuronal vulnerability and calcium binding protein immunoreactivity in ischemia", *Experimental brain research*, Vol. 83 No. 1, pp. 55–66.

Freund, T.F., Ylinen, A., Miettinen, R., Pitkänen, A., Lahtinen, H., Baimbridge, K.G. and Riekkinen, P.J. (1992), "Pattern of neuronal death in the rat hippocampus after status epilepticus. Relationship to calcium binding protein content and ischemic vulnerability", *Brain research bulletin*, Vol. 28 No. 1, pp. 27–38.

Friese, M.A., Schattling, B. and Fugger, L. (2014), "Mechanisms of neurodegeneration and axonal dysfunction in multiple sclerosis", *Nature reviews. Neurology*, Vol. 10 No. 4, pp. 225–238.

Frischer, J.M., Bramow, S., Dal-Bianco, A., Lucchinetti, C.F., Rauschka, H., Schmidbauer, M., Laursen, H., Sorensen, P.S. and Lassmann, H. (2009), "The relation between inflammation and neurodegeneration in multiple sclerosis brains", *Brain a journal of neurology*, Vol. 132 No. Pt 5, pp. 1175–1189.

Frischer, J.M., Weigand, S.D., Guo, Y., Kale, N., Parisi, J.E., Pirko, I., Mandrekar, J., Bramow, S., Metz, I., Brück, W., Lassmann, H. and Lucchinetti, C.F. (2015), "Clinical and pathological insights into the dynamic nature of the white matter multiple sclerosis plaque", *Annals of neurology*, Vol. 78 No. 5, pp. 710–721.

Fünfschilling, U., Supplie, L.M., Mahad, D., Boretius, S., Saab, A.S., Edgar, J., Brinkmann, B.G., Kassmann, C.M., Tzvetanova, I.D., Möbius, W., Diaz, F., Meijer, D., Suter, U., Hamprecht, B., Sereda, M.W., Moraes, C.T., Frahm, J., Goebbels, S. and Nave, K.-A. (2012), "Glycolytic oligodendrocytes maintain myelin and long-term axonal integrity", *Nature*, Vol. 485 No. 7399, pp. 517–521.

Galluzzi, L., Vitale, I., Aaronson, S.A., Abrams, J.M., Adam, D., Agostinis, P., Alnemri, E.S., Altucci, L., Amelio, I., Andrews, D.W., Annicchiarico-Petruzzelli, M., Antonov, A.V., Arama, E., Baehrecke, E.H., Barlev, N.A., Bazan, N.G., Bernassola, F., Bertrand, M.J.M., Bianchi, K., Blagosklonny, M.V., Blomgren, K., Borner, C., Boya, P., Brenner, C., Campanella, M., Candi, E., Carmona-Gutierrez, D., Cecconi, F., Chan, F.K.-M., Chandel, N.S., Cheng, E.H., Chipuk, J.E., Cidlowski, J.A., Ciechanover, A., Cohen, G.M., Conrad, M., Cubillos-Ruiz, J.R., Czabotar, P.E., D'Angiolella, V., Dawson, T.M., Dawson, V.L., Laurenzi, V. de, Maria, R. de, Debatin, K.-M., DeBerardinis, R.J., Deshmukh, M., Di Daniele, N., Di Virgilio, F., Dixit, V.M., Dixon, S.J., Duckett, C.S., Dynlacht, B.D., El-Deiry, W.S., Elrod, J.W., Fimia, G.M., Fulda, S., García-Sáez, A.J., Garg, A.D., Garrido, C., Gavathiotis, E., Golstein, P., Gottlieb, E., Green, D.R., Greene, L.A., Gronemeyer, H., Gross, A., Hajnoczky, G., Hardwick, J.M., Harris, I.S., Hengartner, M.O., Hetz, C., Ichijo, H., Jäättelä, M., Joseph, B., Jost, P.J., Juin, P.P., Kaiser, W.J., Karin, M., Kaufmann, T., Kepp, O., Kimchi, A., Kitsis, R.N., Klionsky, D.J., Knight, R.A., Kumar, S., Lee, S.W., Lemasters, J.J., Levine, B., Linkermann, A., Lipton, S.A., Lockshin, R.A., López-Otín, C., Lowe, S.W., Luedde, T., Lugli,

E., MacFarlane, M., Madeo, F., Malewicz, M., Malorni, W., Manic, G., Marine, J.-C., Martin, S.J., Martinou, J.-C., Medema, J.P., Mehlen, P., Meier, P., Melino, S., Miao, E.A., Molkentin, J.D., Moll, U.M., Muñoz-Pinedo, C., Nagata, S., Nuñez, G., Oberst, A., Oren, M., Overholtzer, M., Pagano, M., Panaretakis, T., Pasparakis, M., Penninger, J.M., Pereira, D.M., Pervaiz, S., Peter, M.E., Piacentini, M., Pinton, P., Prehn, J.H.M., Puthalakath, H., Rabinovich, G.A., Rehm, M., Rizzuto, R., Rodrigues, C.M.P., Rubinsztein, D.C., Rudel, T., Ryan, K.M., Sayan, E., Scorrano, L., Shao, F., Shi, Y., Silke, J., Simon, H.-U., Sistigu, A., Stockwell, B.R., Strasser, A., Szabadkai, G., Tait, S.W.G., Tang, D., Tavernarakis, N., Thorburn, A., Tsujimoto, Y., Turk, B., Vanden Berghe, T., Vandenabeele, P., Vander Heiden, M.G., Villunger, A., Virgin, H.W., Vousden, K.H., Vucic, D., Wagner, E.F., Walczak, H., Wallach, D., Wang, Y., Wells, J.A., Wood, W., Yuan, J., Zakeri, Z., Zhivotovsky, B., Zitvogel, L., Melino, G. and Kroemer, G. (2018), "Molecular mechanisms of cell death: recommendations of the Nomenclature Committee on Cell Death 2018", *Cell death and differentiation*, Vol. 25 No. 3, pp. 486–541.

Ge, Y., Grossman, R.I., Udupa, J.K., Wei, L., Mannon, L.J., Polansky, M. and Kolson, D.L. (2000), "Brain atrophy in relapsing-remitting multiple sclerosis and secondary progressive multiple sclerosis: longitudinal quantitative analysis", *Radiology*, Vol. 214 No. 3, pp. 665–670.

George, E.B., Glass, J.D. and Griffin, J.W. (1995), "Axotomy-induced axonal degeneration is mediated by calcium influx through ion-specific channels", *The Journal of Neuroscience*, Vol. 15 No. 10, pp. 6445–6452.

Gerdts, J., Brace, E.J., Sasaki, Y., DiAntonio, A. and Milbrandt, J. (2015), "SARM1 activation triggers axon degeneration locally via NAD^+ destruction", *Science (New York, N.Y.)*, Vol. 348 No. 6233, pp. 453–457.

Gilley, J., Ribchester, R.R. and Coleman, M.P. (2017), "Sarm1 Deletion, but Not WldS, Confers Lifelong Rescue in a Mouse Model of Severe Axonopathy", *Cell reports*, Vol. 21 No. 1, pp. 10–16.

Glock, C., Biever, A., Tushev, G., Nassim-Assir, B., Kao, A., Bartnik, I., Tom Dieck, S. and Schuman, E.M. (2021), "The translatome of neuronal cell bodies, dendrites, and axons", *Proceedings of the National Academy of Sciences*, Vol. 118 No. 43.

Gong, Y.-N., Guy, C., Olauson, H., Becker, J.U., Yang, M., Fitzgerald, P., Linkermann, A. and Green, D.R. (2017), "ESCRT-III Acts Downstream of MLKL to Regulate Necroptotic Cell Death and Its Consequences", *Cell*, Vol. 169 No. 2, 286-300.e16.

Gopal, S., Mikulskis, A., Gold, R., Fox, R.J., Dawson, K.T. and Amaravadi, L. (2017), "Evidence of activation of the Nrf2 pathway in multiple sclerosis patients treated with delayed-release dimethyl fumarate in the Phase 3 DEFINE and CONFIRM studies", *Multiple sclerosis (Houndmills, Basingstoke, England)*, Vol. 23 No. 14, pp. 1875–1883.

Green, A.J., Gelfand, J.M., Cree, B.A., Bevan, C., Boscardin, W.J., Mei, F., Inman, J., Arnow, S., Devereux, M., Abounasr, A., Nobuta, H., Zhu, A., Friessen, M., Gerona, R., Büdingen, H.C. von, Henry, R.G., Hauser, S.L. and Chan, J.R. (2017), "Clemastine fumarate as a remyelinating therapy for multiple sclerosis (ReBUILD): a randomised, controlled, double-blind, crossover trial", *Lancet (London, England)*, Vol. 390 No. 10111, pp. 2481–2489.

Guedes-Dias, P. and Holzbaur, E.L.F. (2019), "Axonal transport: Driving synaptic function", *Science (New York, N.Y.)*, Vol. 366 No. 6462.

Guo, Q., Christakos, S., Robinson, N. and Mattson, M.P. (1998), "Calbindin D28k blocks the proapoptotic actions of mutant presenilin 1: reduced oxidative stress and preserved mitochondrial function", *Proceedings of the National Academy of Sciences of the United States of America*, Vol. 95 No. 6, pp. 3227–3232.

Guthrie, J.P. (1978), "Hydrolysis of esters of oxy acids: p Ka values for strong acids; Brønsted relationship for attack of water at methyl; free energies of hydrolysis of esters of oxy acids; and a linear relationship between free energy of hydrolysis and p Ka holding over a range of 20 p K units", *Canadian Journal of Chemistry*, Vol. 56 No. 17, pp. 2342–2354.

Guyton, M.K., Das, A., Samantaray, S., Wallace, G.C., Butler, J.T., Ray, S.K. and Banik, N.L. (2010), "Calpeptin attenuated inflammation, cell death, and axonal damage in animal model of multiple sclerosis", *Journal of neuroscience research*, Vol. 88 No. 11, pp. 2398–2408.

Haas, J., Hug, A., Viehöver, A., Fritzsching, B., Falk, C.S., Filser, A., Vetter, T., Milkova, L., Korporal, M., Fritz, B., Storch-Hagenlocher, B., Krammer, P.H., Suri-Payer, E. and Wildemann, B. (2005), "Reduced

suppressive effect of CD4+CD25high regulatory T cells on the T cell immune response against myelin oligodendrocyte glycoprotein in patients with multiple sclerosis", *European journal of immunology*, Vol. 35 No. 11, pp. 3343–3352.

Hack, N.J., Wride, M.C., Charters, K.M., Kater, S.B. and Parks, T.N. (2000), "Developmental changes in the subcellular localization of calretinin", *The Journal of Neuroscience*, Vol. 20 No. 7, RC67.

Haider, L., Fischer, M.T., Frischer, J.M., Bauer, J., Höftberger, R., Botond, G., Esterbauer, H., Binder, C.J., Witztum, J.L. and Lassmann, H. (2011), "Oxidative damage in multiple sclerosis lesions", *Brain a journal of neurology*, Vol. 134 No. Pt 7, pp. 1914–1924.

Hansen, T., Skytthe, A., Stenager, E., Petersen, H.C., Brønnum-Hansen, H. and Kyvik, K.O. (2005), "Concordance for multiple sclerosis in Danish twins: an update of a nationwide study", *Multiple sclerosis (Houndmills, Basingstoke, England)*, Vol. 11 No. 5, pp. 504–510.

Harbauer, A.B., Hees, J.T., Wanderoy, S., Segura, I., Gibbs, W., Cheng, Y., Ordonez, M., Cai, Z., Cartoni, R., Ashrafi, G., Wang, C., Perocchi, F., He, Z. and Schwarz, T.L. (2022), "Neuronal mitochondria transport Pink1 mRNA via synaptojanin 2 to support local mitophagy", *Neuron*, Vol. 110 No. 9, 1516-1531.e9.

Hardingham, G.E., Arnold, F.J. and Bading, H. (2001), "Nuclear calcium signaling controls CREB-mediated gene expression triggered by synaptic activity", *Nature neuroscience*, Vol. 4 No. 3, pp. 261–267.

Hartley, D.M., Neve, R.L., Bryan, J., Ullrey, D.B., Bak, S.-Y., Lang, P. and Geller, A.I. (1996), "Expression of the calcium-binding protein, parvalbumin, in cultured cortical neurons using a HSV-1 vector system enhances NMDA neurotoxicity", *Molecular Brain Research*, Vol. 40 No. 2, pp. 285–296.

Hassen, G.W., Feliberti, J., Kesner, L., Stracher, A. and Mokhtarian, F. (2006), "A novel calpain inhibitor for the treatment of acute experimental autoimmune encephalomyelitis", *Journal of neuroimmunology*, Vol. 180 No. 1-2, pp. 135–146.

Healy, L.M., Stratton, J.A., Kuhlmann, T. and Antel, J. (2022), "The role of glial cells in multiple sclerosis disease progression", *Nature Reviews Neurology*, Vol. 18 No. 4, pp. 237–248.

Heim, N., Garaschuk, O., Friedrich, M.W., Mank, M., Milos, R.I., Kovalchuk, Y., Konnerth, A. and Griesbeck, O. (2007), "Improved calcium imaging in transgenic mice expressing a troponin C-based biosensor", *Nature methods*, Vol. 4 No. 2, pp. 127–129.

Henderson, A.P.D., Barnett, M.H., Parratt, J.D.E. and Prineas, J.W. (2009), "Multiple sclerosis: distribution of inflammatory cells in newly forming lesions", *Annals of neurology*, Vol. 66 No. 6, pp. 739–753.

Ho, B.K., Alexianu, M.E., Colom, L.V., Mohamed, A.H., Serrano, F. and Appel, S.H. (1996), "Expression of calbindin-D28K in motoneuron hybrid cells after retroviral infection with calbindin-D28K cDNA prevents amyotrophic lateral sclerosis IgG-mediated cytotoxicity", *Proceedings of the National Academy of Sciences of the United States of America*, Vol. 93 No. 13, pp. 6796–6801.

Hohlfeld, R., Dornmair, K., Meinl, E. and Wekerle, H. (2016a), "The search for the target antigens of multiple sclerosis, part 1: autoreactive CD4+ T lymphocytes as pathogenic effectors and therapeutic targets", *The Lancet. Neurology*, Vol. 15 No. 2, pp. 198–209.

Hohlfeld, R., Dornmair, K., Meinl, E. and Wekerle, H. (2016b), "The search for the target antigens of multiple sclerosis, part 2: CD8+ T cells, B cells, and antibodies in the focus of reverse-translational research", *The Lancet. Neurology*, Vol. 15 No. 3, pp. 317–331.

Holland, C.M., Charil, A., Csapo, I., Liptak, Z., Ichise, M., Khoury, S.J., Bakshi, R., Weiner, H.L. and Guttmann, C.R.G. (2012), "The relationship between normal cerebral perfusion patterns and white matter lesion distribution in 1,249 patients with multiple sclerosis", *Journal of neuroimaging official journal of the American Society of Neuroimaging*, Vol. 22 No. 2, pp. 129–136.

Holman, S.P., Lobo, A.S., Novorolsky, R.J., Nichols, M., Fiander, M.D.J., Konda, P., Kennedy, B.E., Gujar, S. and Robertson, G.S. (2020), "Neuronal mitochondrial calcium uniporter deficiency exacerbates axonal injury and suppresses remyelination in mice subjected to experimental autoimmune encephalomyelitis", *Experimental neurology*, Vol. 333, p. 113430.

Howard, M.J., David, G. and Barrett, J.N. (1999), "Resealing of transected myelinated mammalian axons in vivo: evidence for involvement of calpain", *Neuroscience*, Vol. 93 No. 2, pp. 807–815.

Howarth, C., Gleeson, P. and Attwell, D. (2012), "Updated energy budgets for neural computation in the neocortex and cerebellum", *Journal of cerebral blood flow and metabolism official journal of the International Society of Cerebral Blood Flow and Metabolism*, Vol. 32 No. 7, pp. 1222–1232.

Howell, O.W., Rundle, J.L., Garg, A., Komada, M., Brophy, P.J. and Reynolds, R. (2010), "Activated microglia mediate axoglial disruption that contributes to axonal injury in multiple sclerosis", *Journal of neuropathology and experimental neurology*, Vol. 69 No. 10, pp. 1017–1033.

Hu, C.-L., Nydes, M., Shanley, K.L., Morales Pantoja, I.E., Howard, T.A. and Bizzozero, O.A. (2019), "Reduced expression of the ferroptosis inhibitor glutathione peroxidase-4 in multiple sclerosis and experimental autoimmune encephalomyelitis", *Journal of neurochemistry*, Vol. 148 No. 3, pp. 426–439.

Hughes, R.O., Bosanac, T., Mao, X., Engber, T.M., DiAntonio, A., Milbrandt, J., Devraj, R. and Krauss, R. (2021), "Small Molecule SARM1 Inhibitors Recapitulate the SARM1-/- Phenotype and Allow Recovery of a Metastable Pool of Axons Fated to Degenerate", *Cell reports*, Vol. 34 No. 1, p. 108588.

Huxley A.F. and Stampfli, R. (1949), "Evidence for saltatory conduction in peripheral myelinated nerve fibres", *The Journal of physiology*, Vol. 108 No. 3, pp. 315–339.

Hwang, C., Sinskey, A.J. and Lodish, H.F. (1992), "Oxidized redox state of glutathione in the endoplasmic reticulum", *Science (New York, N.Y.)*, Vol. 257 No. 5076, pp. 1496–1502.

Hyrc, K., Handran, S.D., Rothman, S.M. and Goldberg, M.P. (1997), "Ionized intracellular calcium concentration predicts excitotoxic neuronal death: observations with low-affinity fluorescent calcium indicators", *The Journal of Neuroscience*, Vol. 17 No. 17, pp. 6669–6677.

Ibreljic, N., Draper, B.E. and Lawton, C.W. (2024), "Recombinant AAV genome size effect on viral vector production, purification, and thermostability", *Molecular therapy. Methods & clinical development*, Vol. 32 No. 1, p. 101188.

Inoue, K.-I., Miyachi, S., Nishi, K., Okado, H., Nagai, Y., Minamimoto, T., Nambu, A. and Takada, M. (2019), "Recruitment of calbindin into nigral dopamine neurons protects against MPTP-Induced parkinsonism", *Movement disorders official journal of the Movement Disorder Society*, Vol. 34 No. 2, pp. 200–209.

Jäckle, K., Zeis, T., Schaeren-Wiemers, N., Junker, A., van der Meer, F., Kramann, N., Stadelmann, C. and Brück, W. (2020), "Molecular signature of slowly expanding lesions in progressive multiple sclerosis", *Brain a journal of neurology*, Vol. 143 No. 7, pp. 2073–2088.

Jadiya, P., Garbincius, J.F. and Elrod, J.W. (2021), "Reappraisal of metabolic dysfunction in neurodegeneration: Focus on mitochondrial function and calcium signaling", *Acta Neuropathologica Communications*, Vol. 9 No. 1.

Jafari, M., Schumacher, A.-M., Snaidero, N., Ullrich Gavilanes, E.M., Neziraj, T., Kocsis-Jutka, V., Engels, D., Jürgens, T., Wagner, I., Weidinger, J.D.F., Schmidt, S.S., Beltrán, E., Hagan, N., Woodworth, L., Ofengeim, D., Gans, J., Wolf, F., Kreutzfeldt, M., Portugues, R., Merkler, D., Misgeld, T. and Kerschensteiner, M. (2021), "Phagocyte-mediated synapse removal in cortical neuroinflammation is promoted by local calcium accumulation", *Nature neuroscience*.

Jakimovski, D., Bittner, S., Zivadinov, R., Morrow, S.A., Benedict, R.H., Zipp, F. and Weinstock-Guttman, B. (2024), "Multiple sclerosis", *Lancet (London, England)*, Vol. 403 No. 10422, pp. 183–202.

Jakimovski, D., Kolb, C., Ramanathan, M., Zivadinov, R. and Weinstock-Guttman, B. (2018), "Interferon β for Multiple Sclerosis", *Cold Spring Harbor perspectives in medicine*, Vol. 8 No. 11.

Jeffery, N.D. and Blakemore, W.F. (1995), "Remyelination of mouse spinal cord axons demyelinated by local injection of lysolecithin", *Journal of neurocytology*, Vol. 24 No. 10, pp. 775–781.

Jordan, A.L., Yang, J., Fisher, C.J., Racke, M.K. and Mao-Draayer, Y. (2022), "Progressive multifocal leukoencephalopathy in dimethyl fumarate-treated multiple sclerosis patients", *Multiple sclerosis (Houndmills, Basingstoke, England)*, Vol. 28 No. 1, pp. 7–15.

Jung, H., Yoon, B.C. and Holt, C.E. (2012), "Axonal mRNA localization and local protein synthesis in nervous system assembly, maintenance and repair", *Nature reviews. Neuroscience*, Vol. 13 No. 5, pp. 308–324.

Jung, S., Chung, Y., Lee, Y., Lee, Y., Cho, J.W., Shin, E.-J., Kim, H.-C. and Oh, Y.J. (2019), "Buffering of cytosolic calcium plays a neuroprotective role by preserving the autophagy-lysosome pathway during MPP+-induced neuronal death", *Cell death discovery*, Vol. 5, p. 130.

Kadowaki, A. and Quintana, F.J. (2020), "The Gut-CNS Axis in Multiple Sclerosis", *Trends in neurosciences*, Vol. 43 No. 8, pp. 622–634.

Kaneko, S., Wang, J., Kaneko, M., Yiu, G., Hurrell, J.M., Chitnis, T., Khoury, S.J. and He, Z. (2006), "Protecting axonal degeneration by increasing nicotinamide adenine dinucleotide levels in experimental autoimmune encephalomyelitis models", *The Journal of neuroscience the official journal of the Society for Neuroscience*, Vol. 26 No. 38, pp. 9794–9804.

Kang, S., Dahl, R., Hsieh, W., Shin, A., Zsebo, K.M., Buettner, C., Hajjar, R.J. and Lebeche, D. (2016), "Small Molecular Allosteric Activator of the Sarco/Endoplasmic Reticulum Ca2+-ATPase (SERCA) Attenuates Diabetes and Metabolic Disorders", *The Journal of biological chemistry*, Vol. 291 No. 10, pp. 5185–5198.

Kapoor, R., Furby, J., Hayton, T., Smith, K.J., Altmann, D.R., Brenner, R., Chataway, J., Hughes, R.A.C. and Miller, D.H. (2010), "Lamotrigine for neuroprotection in secondary progressive multiple sclerosis: a randomised, double-blind, placebo-controlled, parallel-group trial", *The Lancet Neurology*, Vol. 9 No. 7, pp. 681–688.

Kappos, L., Edan, G., Freedman, M.S., Montalbán, X., Hartung, H.-P., Hemmer, B., Fox, E.J., Barkhof, F., Schippling, S., Schulze, A., Pleimes, D., Pohl, C., Sandbrink, R., Suarez, G. and Wicklein, E.-M. (2016), "The 11-year long-term follow-up study from the randomized BENEFIT CIS trial", *Neurology*, Vol. 87 No. 10, pp. 978–987.

Kerschensteiner, M., Bareyre, F.M., Buddeberg, B.S., Merkler, D., Stadelmann, C., Brück, W., Misgeld, T. and Schwab, M.E. (2004), "Remodeling of axonal connections contributes to recovery in an animal model of multiple sclerosis", *The Journal of experimental medicine*, Vol. 200 No. 8, pp. 1027–1038.

Kerschensteiner, M., Schwab, M.E., Lichtman, J.W. and Misgeld, T. (2005), "In vivo imaging of axonal degeneration and regeneration in the injured spinal cord", *Nature medicine*, Vol. 11 No. 5, pp. 572–577.

Klapstein, G.J., Vietla, S., Lieberman, D.N., Gray, P.A., Airaksinen, M.S., Thoenen, H., Meyer, M. and Mody, I. (1998), "Calbindin-D28k fails to protect hippocampal neurons against ischemia in spite of its cytoplasmic calcium buffering properties: evidence from calbindin-D28k knockout mice", *Neuroscience*, Vol. 85 No. 2, pp. 361–373.

Kneussel, M. and Friese, M.A. (2021), "SnapShot: Neuronal dysfunction in inflammation", *Neuron*, Vol. 109 No. 10, 1754-1754.e1.

Ko, K.W., Devault, L., Sasaki, Y., Milbrandt, J. and DiAntonio, A. (2021), "Live imaging reveals the cellular events downstream of SARM1 activation", *eLife*, Vol. 10.

Kook, S.-Y., Jeong, H., Kang, M.J., Park, R., Shin, H.J., Han, S.-H., Son, S.M., Song, H., Baik, S.H., Moon, M., Yi, E.C., Hwang, D. and Mook-Jung, I. (2014), "Crucial role of calbindin-D28k in the pathogenesis of Alzheimer's disease mouse model", *Cell death and differentiation*, Vol. 21 No. 10, pp. 1575–1587.

Kornek, B., Storch, M.K., Weissert, R., Wallstroem, E., Stefferl, A., Olsson, T., Linington, C., Schmidbauer, M. and Lassmann, H. (2000), "Multiple sclerosis and chronic autoimmune encephalomyelitis: a comparative quantitative study of axonal injury in active, inactive, and remyelinated lesions", *The American journal of pathology*, Vol. 157 No. 1, pp. 267–276.

Kosa, P., Wu, T., Phillips, J., Leinonen, M., Masvekar, R., Komori, M., Wichman, A., Sandford, M. and Bielekova, B. (2020), "Idebenone does not inhibit disability progression in primary progressive MS", *Multiple sclerosis and related disorders*, Vol. 45, p. 102434.

Krämer, J., Balloff, C., Weise, M., Koska, V., Uthmeier, Y., Esderts, I., Nguyen-Minh, M., Zimmerhof, M., Hartmann, A., Dietrich, M., Ingwersen, J., Lee, J.-I., Havla, J., Kümpfel, T., Kerschensteiner, M., Häußler, V., Heesen, C., Stellmann, J.-P., Zimmermann, H.G., Oertel, F.C., Ringelstein, M., Brandt, A.U., Paul, F., Aktas, O., Hartung, H.-P., Wiendl, H., Meuth, S.G. and Albrecht, P. (2024), "Evolution of retinal degeneration and prediction of disease activity in relapsing and progressive multiple sclerosis", *Nature Communications*, Vol. 15 No. 1, p. 5243.

Kuhlmann, T., Lingfeld, G., Bitsch, A., Schuchardt, J. and Brück, W. (2002), "Acute axonal damage in multiple sclerosis is most extensive in early disease stages and decreases over time", *Brain a journal of neurology*, Vol. 125 No. Pt 10, pp. 2202–2212.

Kuhlmann, T., Ludwin, S., Prat, A., Antel, J., Brück, W. and Lassmann, H. (2017), "An updated histological classification system for multiple sclerosis lesions", *Acta neuropathologica*, Vol. 133 No. 1, pp. 13–24.

Kuhlmann, T., Moccia, M., Coetzee, T., Cohen, J.A., Correale, J., Graves, J., Marrie, R.A., Montalban, X., Yong, V.W., Thompson, A.J. and Reich, D.S. (2023), "Multiple sclerosis progression: time for a new mechanism-driven framework", *The Lancet. Neurology*, Vol. 22 No. 1, pp. 78–88.

Kurtzke, J.F. (1983), "Rating neurologic impairment in multiple sclerosis: an expanded disability status scale (EDSS)", *Neurology*, Vol. 33 No. 11, pp. 1444–1452.

Kutzelnigg, A. and Lassmann, H. (2006), "Cortical demyelination in multiple sclerosis: a substrate for cognitive deficits?", *Journal of the neurological sciences*, Vol. 245 No. 1-2, pp. 123–126.

Kutzelnigg, A., Lucchinetti, C.F., Stadelmann, C., Brück, W., Rauschka, H., Bergmann, M., Schmidbauer, M., Parisi, J.E. and Lassmann, H. (2005), "Cortical demyelination and diffuse white matter injury in multiple sclerosis", *Brain a journal of neurology*, Vol. 128 No. Pt 11, pp. 2705–2712.

Kuusisto, H., Kaprio, J., Kinnunen, E., Luukkaala, T., Koskenvuo, M. and Elovaara, I. (2008), "Concordance and heritability of multiple sclerosis in Finland: study on a nationwide series of twins", *European journal of neurology*, Vol. 15 No. 10, pp. 1106–1110.

Kuźnicki, J., Isaacs, K.R. and Jacobowitz, D.M. (1996), "The expression of calretinin in transfected PC12 cells provides no protection against Ca(2+)-overload or trophic factor deprivation", *Biochimica et biophysica acta*, Vol. 1313 No. 3, pp. 194–200.

Lanz, T.V., Brewer, R.C., Ho, P.P., Moon, J.-S., Jude, K.M., Fernandez, D., Fernandes, R.A., Gomez, A.M., Nadj, G.-S., Bartley, C.M., Schubert, R.D., Hawes, I.A., Vazquez, S.E., Iyer, M., Zuchero, J.B., Teegen, B., Dunn, J.E., Lock, C.B., Kipp, L.B., Cotham, V.C., Ueberheide, B.M., Aftab, B.T., Anderson, M.S., DeRisi, J.L., Wilson, M.R., Bashford-Rogers, R.J.M., Platten, M., Garcia, K.C., Steinman, L. and Robinson, W.H. (2022), "Clonally expanded B cells in multiple sclerosis bind EBV EBNA1 and GlialCAM", *Nature*, Vol. 603 No. 7900, pp. 321–327.

Lappe-Siefke, C., Goebbels, S., Gravel, M., Nicksch, E., Lee, J., Braun, P.E., Griffiths, I.R. and Nave, K.-A. (2003), "Disruption of Cnp1 uncouples oligodendroglial functions in axonal support and myelination", *Nature genetics*, Vol. 33 No. 3, pp. 366–374.

Lassmann, H. (2018), "Multiple Sclerosis Pathology", *Cold Spring Harbor perspectives in medicine*, Vol. 8 No. 3.

Lassmann, H. and Bradl, M. (2017), "Multiple sclerosis: experimental models and reality", *Acta neuropathologica*, Vol. 133 No. 2, pp. 223–244.

Lassmann, H., van Horssen, J. and Mahad, D. (2012), "Progressive multiple sclerosis: pathology and pathogenesis", *Nature reviews. Neurology*, Vol. 8 No. 11, pp. 647–656.

Lee, M.A., Blamire, A.M., Pendlebury, S., Ho, K.H., Mills, K.R., Styles, P., Palace, J. and Matthews, P.M. (2000), "Axonal injury or loss in the internal capsule and motor impairment in multiple sclerosis", *Archives of neurology*, Vol. 57 No. 1, pp. 65–70.

Leloup, L., Shao, H., Bae, Y.H., Deasy, B., Stolz, D., Roy, P. and Wells, A. (2010), "m-Calpain activation is regulated by its membrane localization and by its binding to phosphatidylinositol 4,5-bisphosphate", *The Journal of biological chemistry*, Vol. 285 No. 43, pp. 33549–33566.

Leterrier, C., Dubey, P. and Roy, S. (2017), "The nano-architecture of the axonal cytoskeleton", *Nature reviews. Neuroscience*, Vol. 18 No. 12, pp. 713–726.

Levin, L.I., Munger, K.L., Rubertone, M.V., Peck, C.A., Lennette, E.T., Spiegelman, D. and Ascherio, A. (2005), "Temporal relationship between elevation of epstein-barr virus antibody titers and initial onset of neurological symptoms in multiple sclerosis", *JAMA*, Vol. 293 No. 20, pp. 2496–2500.

Li, C., Ma, Q., Toan, S., Wang, J., Zhou, H. and Liang, J. (2020), "SERCA overexpression reduces reperfusion-mediated cardiac microvascular damage through inhibition of the calcium/MCU/mPTP/necroptosis signaling pathways", *Redox biology*, Vol. 36, p. 101659.

Li, Y., Pazyra-Murphy, M.F., Avizonis, D., Sá Tavares Russo, M. de, Tang, S., Chen, C.-Y., Hsueh, Y.-P., Bergholz, J.S., Jiang, T., Zhao, J.J., Zhu, J., Ko, K.W., Milbrandt, J., DiAntonio, A. and Segal, R.A. (2022), "Sarm1 activation produces cADPR to increase intra-axonal Ca++ and promote axon degeneration in PIPN", *The Journal of cell biology*, Vol. 221 No. 2.

Lie, I.A., Weeda, M.M., Mattiesing, R.M., Mol, M.A.E., Pouwels, P.J.W., Barkhof, F., Torkildsen, Ø., Bø, L., Myhr, K.-M. and Vrenken, H. (2022), "Relationship Between White Matter Lesions and Gray Matter Atrophy in Multiple Sclerosis: A Systematic Review", *Neurology*, Vol. 98 No. 15, e1562-e1573.

Liu, C., Pan, J., Li, S., Zhao, Y., Wu, L.Y., Berkman, C.E., Whorton, A.R. and Xian, M. (2011), "Capture and visualization of hydrogen sulfide by a fluorescent probe", *Angewandte Chemie (International ed. in English)*, Vol. 50 No. 44, pp. 10327–10329.

Liu, G.-Y., Xie, W.-L., Wang, Y.-T., Chen, L., Xu, Z.-Z., Lv, Y. and Wu, Q.-P. (2023a), "Calpain: the regulatory point of myocardial ischemia-reperfusion injury", *Frontiers in cardiovascular medicine*, Vol. 10, p. 1194402.

Liu, P., Chen, W., Jiang, H., Huang, H., Liu, L., Fang, F., Li, L., Feng, X., Liu, D., Dalal, R., Sun, Y., Jafar-Nejad, P., Ling, K., Rigo, F., Ye, J. and Hu, Y. (2023b), "Differential effects of SARM1 inhibition in traumatic glaucoma and EAE optic neuropathies", *Molecular therapy. Nucleic acids*, Vol. 32, pp. 13–27.

Liu, Z., Chen, O., Wall, J.B.J., Zheng, M., Zhou, Y., Wang, L., Vaseghi, H.R., Qian, L. and Liu, J. (2017), "Systematic comparison of 2A peptides for cloning multi-genes in a polycistronic vector", *Scientific reports*, Vol. 7 No. 1, p. 2193.

Liu, Z., Zhang, T.-T., Yu, J., Liu, Y.-L., Qi, S.-F., Zhao, J.-J., Liu, D.-W. and Tian, Q.-B. (2016), "Excess Body Weight during Childhood and Adolescence Is Associated with the Risk of Multiple Sclerosis: A Meta-Analysis", *Neuroepidemiology*, Vol. 47 No. 2, pp. 103–108.

Lodygin, D., Hermann, M., Schweingruber, N., Flügel-Koch, C., Watanabe, T., Schlosser, C., Merlini, A., Körner, H., Chang, H.-F., Fischer, H.J., Reichardt, H.M., Zagrebelsky, M., Mollenhauer, B., Kügler, S., Fitzner, D., Frahm, J., Stadelmann, C., Haberl, M., Odoardi, F. and Flügel, A. (2019), "β-Synuclein-reactive T cells induce autoimmune CNS grey matter degeneration", *Nature*, Vol. 566 No. 7745, pp. 503–508.

Loreto, A., Di Stefano, M., Gering, M. and Conforti, L. (2015), "Wallerian Degeneration Is Executed by an NMN-SARM1-Dependent Late Ca(2+) Influx but Only Modestly Influenced by Mitochondria", *Cell reports*, Vol. 13 No. 11, pp. 2539–2552.

Los, G.V., Encell, L.P., McDougall, M.G., Hartzell, D.D., Karassina, N., Zimprich, C., Wood, M.G., Learish, R., Ohana, R.F., Urh, M., Simpson, D., Mendez, J., Zimmerman, K., Otto, P., Vidugiris, G., Zhu, J., Darzins, A., Klaubert, D.H., Bulleit, R.F. and Wood, K.V. (2008), "HaloTag: a novel protein labeling technology for cell imaging and protein analysis", *ACS chemical biology*, Vol. 3 No. 6, pp. 373–382.

Losseff, N.A., Webb, S.L., O'Riordan, J.I., Page, R., Wang, L., Barker, G.J., Tofts, P.S., McDonald, W.I., Miller, D.H. and Thompson, A.J. (1996), "Spinal cord atrophy and disability in multiple sclerosis. A new reproducible and sensitive MRI method with potential to monitor disease progression", *Brain a journal of neurology*, 119 (Pt 3), pp. 701–708.

Lovas, G., Szilágyi, N., Majtényi, K., Palkovits, M. and Komoly, S. (2000), "Axonal changes in chronic demyelinated cervical spinal cord plaques", *Brain a journal of neurology*, 123 (Pt 2), pp. 308–317.

Lublin, F.D., Häring, D.A., Ganjgahi, H., Ocampo, A., Hatami, F., Čuklina, J., Aarden, P., Dahlke, F., Arnold, D.L., Wiendl, H., Chitnis, T., Nichols, T.E., Kieseier, B.C. and Bermel, R.A. (2022), "How patients with multiple sclerosis acquire disability", *Brain a journal of neurology*, Vol. 145 No. 9, pp. 3147–3161.

Lucchinetti, C.F., Popescu, B.F.G., Bunyan, R.F., Moll, N.M., Roemer, S.F., Lassmann, H., Brück, W., Parisi, J.E., Scheithauer, B.W., Giannini, C., Weigand, S.D., Mandrekar, J. and Ransohoff, R.M. (2011), "Inflammatory cortical demyelination in early multiple sclerosis", *The New England journal of medicine*, Vol. 365 No. 23, pp. 2188–2197.

Lukinavičius, G., Umezawa, K., Olivier, N., Honigmann, A., Yang, G., Plass, T., Mueller, V., Reymond, L., Corrêa, I.R., Luo, Z.-G., Schultz, C., Lemke, E.A., Heppenstall, P., Eggeling, C., Manley, S. and Johnsson, K. (2013), "A near-infrared fluorophore for live-cell super-resolution microscopy of cellular proteins", *Nature chemistry*, Vol. 5 No. 2, pp. 132–139.

Luoqian, J., Yang, W., Ding, X., Tuo, Q.-Z., Xiang, Z., Zheng, Z., Guo, Y.-J., Li, L., Guan, P., Ayton, S., Dong, B., Zhang, H., Hu, H. and Lei, P. (2022), "Ferroptosis promotes T-cell activation-induced neurodegeneration in multiple sclerosis", *Cellular & molecular immunology*, Vol. 19 No. 8, pp. 913–924.

Lüscher, C. and Malenka, R.C. (2012), "NMDA receptor-dependent long-term potentiation and long-term depression (LTP/LTD)", *Cold Spring Harbor perspectives in biology*, Vol. 4 No. 6.

Lytton, J. (2007), "Na+/Ca2+ exchangers: three mammalian gene families control Ca2+ transport", *The Biochemical journal*, Vol. 406 No. 3, pp. 365–382.

Ma, M., Ferguson, T.A., Schoch, K.M., Li, J., Qian, Y., Shofer, F.S., Saatman, K.E. and Neumar, R.W. (2013), "Calpains mediate axonal cytoskeleton disintegration during Wallerian degeneration", *Neurobiology of disease*, Vol. 56, pp. 34–46.

Maday, S., Twelvetrees, A.E., Moughamian, A.J. and Holzbaur, E.L.F. (2014), "Axonal transport: cargo-specific mechanisms of motility and regulation", *Neuron*, Vol. 84 No. 2, pp. 292–309.

Maggi, P., Kuhle, J., Schädelin, S., van der Meer, F., Weigel, M., Galbusera, R., Mathias, A., Lu, P.-J., Rahmanzadeh, R., Benkert, P., La Rosa, F., Bach Cuadra, M., Sati, P., Théaudin, M., Pot, C., van Pesch, V., Leppert, D., Stadelmann, C., Kappos, L., Du Pasquier, R., Reich, D.S., Absinta, M. and Granziera, C. (2021), "Chronic White Matter Inflammation and Serum Neurofilament Levels in Multiple Sclerosis", *Neurology*, Vol. 97 No. 6, e543-e553.

Magliozzi, R., Howell, O., Vora, A., Serafini, B., Nicholas, R., Puopolo, M., Reynolds, R. and Aloisi, F. (2007), "Meningeal B-cell follicles in secondary progressive multiple sclerosis associate with early onset of disease and severe cortical pathology", *Brain a journal of neurology*, Vol. 130 No. Pt 4, pp. 1089–1104.

Magliozzi, R., Howell, O.W., Reeves, C., Roncaroli, F., Nicholas, R., Serafini, B., Aloisi, F. and Reynolds, R. (2010), "A Gradient of neuronal loss and meningeal inflammation in multiple sclerosis", *Annals of Neurology*, Vol. 68 No. 4, pp. 477–493.

Mahad, D., Ziabreva, I., Lassmann, H. and Turnbull, D. (2008), "Mitochondrial defects in acute multiple sclerosis lesions", *Brain a journal of neurology*, Vol. 131 No. Pt 7, pp. 1722–1735.

Mahad, D.J., Ziabreva, I., Campbell, G., Lax, N., White, K., Hanson, P.S., Lassmann, H. and Turnbull, D.M. (2009), "Mitochondrial changes within axons in multiple sclerosis", *Brain a journal of neurology*, Vol. 132 No. Pt 5, pp. 1161–1174.

Matsushima, G.K. and Morell, P. (2001), "The neurotoxicant, cuprizone, as a model to study demyelination and remyelination in the central nervous system", *Brain pathology (Zurich, Switzerland)*, Vol. 11 No. 1, pp. 107–116.

Mauker, P., Beckmann, D., Kitowski, A., Heise, C., Wientjens, C., Davidson, A.J., Wanderoy, S., Fabre, G., Harbauer, A.B., Wood, W., Wilhelm, C., Thorn-Seshold, J., Misgeld, T., Kerschensteiner, M. and Thorn-Seshold, O. (2024), "Fluorogenic Chemical Probes for Wash-free Imaging of Cell Membrane Damage in Ferroptosis, Necrosis, and Axon Injury", *Journal of the American Chemical Society*.

Meier, S., Willemse, E.A.J., Schaedelin, S., Oechtering, J., Lorscheider, J., Melie-Garcia, L., Cagol, A., Barakovic, M., Galbusera, R., Subramaniam, S., Barro, C., Abdelhak, A., Thebault, S., Achtnichts, L., Lalive, P., Müller, S., Pot, C., Salmen, A., Disanto, G., Zecca, C., D'Souza, M., Orleth, A., Khalil, M., Buchmann, A., Du Pasquier, R., Yaldizli, Ö., Derfuss, T., Berger, K., Hermesdorf, M., Wiendl, H., Piehl, F., Battaglini, M., Fischer, U., Kappos, L., Gobbi, C., Granziera, C., Bridel, C., Leppert, D., Maleska Maceski, A., Benkert, P. and Kuhle, J. (2023), "Serum Glial Fibrillary Acidic Protein Compared With Neurofilament Light Chain as a Biomarker for Disease Progression in Multiple Sclerosis", *JAMA neurology*, Vol. 80 No. 3, pp. 287–297.

Merkler, D., Ernsting, T., Kerschensteiner, M., Brück, W. and Stadelmann, C. (2006), "A new focal EAE model of cortical demyelination: multiple sclerosis-like lesions with rapid resolution of inflammation and extensive remyelination", *Brain a journal of neurology*, Vol. 129 No. Pt 8, pp. 1972–1983.

Mestas, J. and Hughes, C.C.W. (2004), "Of mice and not men: differences between mouse and human immunology", *Journal of immunology (Baltimore, Md. 1950)*, Vol. 172 No. 5, pp. 2731–2738.

Metwally, E., Zhao, G. and Zhang, Y.Q. (2021), "The calcium-dependent protease calpain in neuronal remodeling and neurodegeneration", *Trends in neurosciences*, Vol. 44 No. 9, pp. 741–752.

Miazek, A., Zalas, M., Skrzymowska, J., Bogin, B.A., Grzymajło, K., Goszczynski, T.M., Levine, Z.A., Morrow, J.S. and Stankewich, M.C. (2021), "Age-dependent ataxia and neurodegeneration caused by an αII spectrin mutation with impaired regulation of its calpain sensitivity", *Scientific reports*, Vol. 11 No. 1, p. 7312.

Miki, M., Tamai, H., Mino, M., Yamamoto, Y. and Niki, E. (1987), "Free-radical chain oxidation of rat red blood cells by molecular oxygen and its inhibition by alpha-tocopherol", *Archives of biochemistry and biophysics*, Vol. 258 No. 2, pp. 373–380.

Miller, D.H., Barkhof, F., Frank, J.A., Parker, G.J.M. and Thompson, A.J. (2002), "Measurement of atrophy in multiple sclerosis: pathological basis, methodological aspects and clinical relevance", *Brain a journal of neurology*, Vol. 125 No. Pt 8, pp. 1676–1695.

Molecular Probes, Thermo Fisher Scientific, *SYTOX® Dead Cell Stain Sampler Kit Manual*.

Monje, M.L., Phillips, R. and Sapolsky, R. (2001), "Calbindin overexpression buffers hippocampal cultures from the energetic impairments caused by glutamate", *Brain Research*, Vol. 911 No. 1, pp. 37–42.

Montalban, X., Hauser, S.L., Kappos, L., Arnold, D.L., Bar-Or, A., Comi, G., Seze, J. de, Giovannoni, G., Hartung, H.-P., Hemmer, B., Lublin, F., Rammohan, K.W., Selmaj, K., Traboulsee, A., Sauter, A., Masterman, D., Fontoura, P., Belachew, S., Garren, H., Mairon, N., Chin, P. and Wolinsky, J.S. (2017), "Ocrelizumab versus Placebo in Primary Progressive Multiple Sclerosis", *The New England journal of medicine*, Vol. 376 No. 3, pp. 209–220.

Moran, M.M. (2018), "TRP Channels as Potential Drug Targets", *Annual review of pharmacology and toxicology*, Vol. 58, pp. 309–330.

Moutsianas, L., Jostins, L., Beecham, A.H., Dilthey, A.T., Xifara, D.K., Ban, M., Shah, T.S., Patsopoulos, N.A., Alfredsson, L., Anderson, C.A., Attfield, K.E., Baranzini, S.E., Barrett, J., Binder, T.M.C., Booth, D., Buck, D., Celius, E.G., Cotsapas, C., D'Alfonso, S., Dendrou, C.A., Donnelly, P., Dubois, B., Fontaine, B., Fugger, L., Goris, A., Gourraud, P.-A., Graetz, C., Hemmer, B., Hillert, J., Kockum, I., Leslie, S., Lill, C.M., Martinelli-Boneschi, F., Oksenberg, J.R., Olsson, T., Oturai, A., Saarela, J., Søndergaard, H.B., Spurkland, A., Taylor, B., Winkelmann, J., Zipp, F., Haines, J.L., Pericak-Vance, M.A., Spencer, C.C.A., Stewart, G., Hafler, D.A., Ivinson, A.J., Harbo, H.F., Hauser, S.L., Jager, P.L. de, Compston, A., McCauley, J.L., Sawcer, S. and McVean, G. (2015), "Class II HLA interactions modulate genetic risk for multiple sclerosis", *Nature genetics*, Vol. 47 No. 10, pp. 1107–1113.

Murakami, M., Kano, F. and Murata, M. (2018), "LLO-mediated Cell Resealing System for Analyzing Intracellular Activity of Membrane-impermeable Biopharmaceuticals of Mid-sized Molecular Weight", *Scientific reports*, Vol. 8 No. 1, p. 1946.

Nakamura, K., Zuppini, A., Arnaudeau, S., Lynch, J., Ahsan, I., Krause, R., Papp, S., Smedt, H. de, Parys, J.B., Muller-Esterl, W., Lew, D.P., Krause, K.H., Demaurex, N., Opas, M. and Michalak, M. (2001), "Functional specialization of calreticulin domains", *The Journal of cell biology*, Vol. 154 No. 5, pp. 961–972.

Naraghi, M. and Neher, E. (1997), "Linearized buffered Ca2+ diffusion in microdomains and its implications for calculation of Ca2+ at the mouth of a calcium channel", *The Journal of Neuroscience*, Vol. 17 No. 18, pp. 6961–6973.

Nielsen, A.S., Kinkel, R.P., Madigan, N., Tinelli, E., Benner, T. and Mainero, C. (2013), "Contribution of cortical lesion subtypes at 7T MRI to physical and cognitive performance in MS", *Neurology*, Vol. 81 No. 7, pp. 641–649.

Nikić, I., Merkler, D., Sorbara, C., Brinkoetter, M., Kreutzfeldt, M., Bareyre, F.M., Brück, W., Bishop, D., Misgeld, T. and Kerschensteiner, M. (2011), "A reversible form of axon damage in experimental autoimmune encephalomyelitis and multiple sclerosis", *Nature medicine*, Vol. 17 No. 4, pp. 495–499.

Nikiforov, A., Kulikova, V. and Ziegler, M. (2015), "The human NAD metabolome: Functions, metabolism and compartmentalization", *Critical reviews in biochemistry and molecular biology*, Vol. 50 No. 4, pp. 284–297.

Ofengeim, D., Ito, Y., Najafov, A., Zhang, Y., Shan, B., DeWitt, J.P., Ye, J., Zhang, X., Chang, A., Vakifahmetoglu-Norberg, H., Geng, J., Py, B., Zhou, W., Amin, P., Berlink Lima, J., Qi, C., Yu, Q., Trapp, B. and Yuan, J. (2015), "Activation of necroptosis in multiple sclerosis", *Cell reports*, Vol. 10 No. 11, pp. 1836–1849.

Ontaneda, D., Tallantyre, E., Kalincik, T., Planchon, S.M. and Evangelou, N. (2019), "Early highly effective versus escalation treatment approaches in relapsing multiple sclerosis", *The Lancet. Neurology*, Vol. 18 No. 10, pp. 973–980.

Pandya, J.D., Nukala, V.N. and Sullivan, P.G. (2013), "Concentration dependent effect of calcium on brain mitochondrial bioenergetics and oxidative stress parameters", *Frontiers in neuroenergetics*, Vol. 5, p. 10.

Patrikios, P., Stadelmann, C., Kutzelnigg, A., Rauschka, H., Schmidbauer, M., Laursen, H., Sorensen, P.S., Brück, W., Lucchinetti, C. and Lassmann, H. (2006), "Remyelination is extensive in a subset of multiple sclerosis patients", *Brain a journal of neurology*, Vol. 129 No. Pt 12, pp. 3165–3172.

Patron, M., Granatiero, V., Espino, J., Rizzuto, R. and Stefani, D. de (2019), "MICU3 is a tissue-specific enhancer of mitochondrial calcium uptake", *Cell death and differentiation*, Vol. 26 No. 1, pp. 179–195.

Pedrera, L., Espiritu, R.A., Ros, U., Weber, J., Schmitt, A., Stroh, J., Hailfinger, S., Karstedt, S. von and García-Sáez, A.J. (2021), "Ferroptotic pores induce Ca2+ fluxes and ESCRT-III activation to modulate cell death kinetics", *Cell death and differentiation*, Vol. 28 No. 5, pp. 1644–1657.

Peng, T. and Yang, D. (2010), "Construction of a library of rhodol fluorophores for developing new fluorescent probes", *Organic letters*, Vol. 12 No. 3, pp. 496–499.

Perfetto, S.P., Chattopadhyay, P.K., Lamoreaux, L., Nguyen, R., Ambrozak, D., Koup, R.A. and Roederer, M. (2006), "Amine reactive dyes: an effective tool to discriminate live and dead cells in polychromatic flow cytometry", *Journal of immunological methods*, Vol. 313 No. 1-2, pp. 199–208.

Peterson, J.W., Bö, L., Mörk, S., Chang, A. and Trapp, B.D. (2001), "Transected neurites, apoptotic neurons, and reduced inflammation in cortical multiple sclerosis lesions", *Annals of Neurology*, Vol. 50 No. 3, pp. 389–400.

Petrova, N., Carassiti, D., Altmann, D.R., Baker, D. and Schmierer, K. (2018), "Axonal loss in the multiple sclerosis spinal cord revisited", *Brain pathology (Zurich, Switzerland)*, Vol. 28 No. 3, pp. 334–348.

Petzold, A., Boer, J.F. de, Schippling, S., Vermersch, P., Kardon, R., Green, A., Calabresi, P.A. and Polman, C. (2010), "Optical coherence tomography in multiple sclerosis: a systematic review and meta-analysis", *The Lancet. Neurology*, Vol. 9 No. 9, pp. 921–932.

Phillips, R.G., Meier, T.J., Giuli, L.C., McLaughlin, J.R., Ho, D.Y. and Sapolsky, R.M. (1999), "Calbindin D28K gene transfer via herpes simplex virus amplicon vector decreases hippocampal damage in vivo following neurotoxic insults", *Journal of neurochemistry*, Vol. 73 No. 3, pp. 1200–1205.

Picon, C., Jayaraman, A., James, R., Beck, C., Gallego, P., Witte, M.E., van Horssen, J., Mazarakis, N.D. and Reynolds, R. (2021), "Neuron-specific activation of necroptosis signaling in multiple sclerosis cortical grey matter", *Acta neuropathologica*.

Plucińska, G. and Misgeld, T. (2016), "Imaging of neuronal mitochondria in situ", *Current opinion in neurobiology*, Vol. 39, pp. 152–163.

Poorolajal, J., Bahrami, M., Karami, M. and Hooshmand, E. (2017), "Effect of smoking on multiple sclerosis: a meta-analysis", *Journal of public health (Oxford, England)*, Vol. 39 No. 2, pp. 312–320.

Preziosa, P., Pagani, E., Meani, A., Moiola, L., Rodegher, M., Filippi, M. and Rocca, M.A. (2022), "Slowly Expanding Lesions Predict 9-Year Multiple Sclerosis Disease Progression", *Neurology(R) neuroimmunology & neuroinflammation*, Vol. 9 No. 2.

Radhiyanti, P.T., Konno, A., Matsuzaki, Y. and Hirai, H. (2021), "Comparative study of neuron-specific promoters in mouse brain transduced by intravenously administered AAV-PHP.eB", *Neuroscience letters*, Vol. 756, p. 135956.

Ramos, S., Hartenian, E., Santos, J.C., Walch, P. and Broz, P. (2024), "NINJ1 induces plasma membrane rupture and release of damage-associated molecular pattern molecules during ferroptosis", *The EMBO journal*, Vol. 43 No. 7, pp. 1164–1186.

Rao, R., Shah, S., Bhattacharya, D., Toukam, D.K., Cáceres, R., Pomeranz Krummel, D.A. and Sengupta, S. (2022), "Ligand-Gated Ion Channels as Targets for Treatment and Management of Cancers", *Frontiers in Physiology*, Vol. 13, p. 839437.

Reali, C., Magliozzi, R., Roncaroli, F., Nicholas, R., Howell, O.W. and Reynolds, R. (2020), "B cell rich meningeal inflammation associates with increased spinal cord pathology in multiple sclerosis", *Brain pathology (Zurich, Switzerland)*, Vol. 30 No. 4, pp. 779–793.

Reddy, H., Narayanan, S., Arnoutelis, R., Jenkinson, M., Antel, J., Matthews, P.M. and Arnold, D.L. (2000), "Evidence for adaptive functional changes in the cerebral cortex with axonal injury from multiple sclerosis", *Brain a journal of neurology*, 123 (Pt 11), pp. 2314–2320.

Reich, D.S., Arnold, D.L., Vermersch, P., Bar-Or, A., Fox, R.J., Matta, A., Turner, T., Wallström, E., Zhang, X., Mareš, M., Khabirov, F.A. and Traboulsee, A. (2021), "Safety and efficacy of tolebrutinib, an oral brain-penetrant BTK inhibitor, in relapsing multiple sclerosis: a phase 2b, randomised, double-blind, placebo-controlled trial", *The Lancet. Neurology*, Vol. 20 No. 9, pp. 729–738.

Reiner, A. and Levitz, J. (2018), "Glutamatergic Signaling in the Central Nervous System: Ionotropic and Metabotropic Receptors in Concert", *Neuron*, Vol. 98 No. 6, pp. 1080–1098.

Rishal, I. and Fainzilber, M. (2014), "Axon-soma communication in neuronal injury", *Nature reviews. Neuroscience*, Vol. 15 No. 1, pp. 32–42.

Rocca, M.A., Valsasina, P., Meani, A., Gobbi, C., Zecca, C., Barkhof, F., Schoonheim, M.M., Strijbis, E.M., Vrenken, H., Gallo, A., Bisecco, A., Ciccarelli, O., Yiannakas, M., Rovira, A., Sastre-Garriga, J., Palace, J., Matthews, L., Gass, A., Eisele, P., Lukas, C., Bellenberg, B., Margoni, M., Preziosa, P. and Filippi, M. (2023), "Spinal cord lesions and brain grey matter atrophy independently predict clinical worsening in definite multiple sclerosis: a 5-year, multicentre study", *Journal of neurology, neurosurgery, and psychiatry*, Vol. 94 No. 1, pp. 10–18.

Rodríguez Murúa, S., Farez, M.F. and Quintana, F.J. (2022), "The Immune Response in Multiple Sclerosis", *Annual review of pathology*, Vol. 17, pp. 121–139.

Rosenkranz, S.C., Shaposhnykov, A.A., Träger, S., Engler, J.B., Witte, M.E., Roth, V., Vieira, V., Paauw, N., Bauer, S., Schwencke-Westphal, C., Schubert, C., Bal, L.C., Schattling, B., Pless, O., van Horssen, J., Freichel, M. and Friese, M.A. (2021), "Enhancing mitochondrial activity in neurons protects against neurodegeneration in a mouse model of multiple sclerosis", *eLife*, Vol. 10.

Rossi, A., Pizzo, P. and Filadi, R. (2019), "Calcium, mitochondria and cell metabolism: A functional triangle in bioenergetics", *Biochimica et biophysica acta. Molecular cell research*, Vol. 1866 No. 7, pp. 1068–1078.

Rothammer, N., Woo, M.S., Bauer, S., Binkle-Ladisch, L., Di Liberto, G., Egervari, K., Wagner, I., Haferkamp, U., Pless, O., Merkler, D., Engler, J.B. and Friese, M.A. (2022), "G9a dictates neuronal vulnerability to inflammatory stress via transcriptional control of ferroptosis", *Science advances*, Vol. 8 No. 31, eabm5500.

Rotman, B. and Papermaster, B.W. (1966), "Membrane properties of living mammalian cells as studied by enzymatic hydrolysis of fluorogenic esters", *Proceedings of the National Academy of Sciences*, Vol. 55 No. 1, pp. 134–141.

Rotman, B., Zderic, J.A. and Edelstein, M. (1963), "Fluorogenic substrates for beta-D-galactosidases and phosphatases derived from flurescein (3,6-dihydroxyfluoran) and its monomethylether", *Proceedings of the National Academy of Sciences*, Vol. 50 No. 1, pp. 1–6.

Rovaris, M., Gass, A., Bammer, R., Hickman, S.J., Ciccarelli, O., Miller, D.H. and Filippi, M. (2005), "Diffusion MRI in multiple sclerosis", *Neurology*, Vol. 65 No. 10, pp. 1526–1532.

Roy, J., Minotti, S., Dong, L., Figlewicz, D.A. and Durham, H.D. (1998), "Glutamate potentiates the toxicity of mutant Cu/Zn-superoxide dismutase in motor neurons by postsynaptic calcium-dependent mechanisms", *The Journal of Neuroscience*, Vol. 18 No. 23, pp. 9673–9684.

Sala, F. and Hernández-Cruz, A. (1990), "Calcium diffusion modeling in a spherical neuron. Relevance of buffering properties", *Biophysical journal*, Vol. 57 No. 2, pp. 313–324.

Salter, A., Kowalec, K., Fitzgerald, K.C., Cutter, G. and Marrie, R.A. (2020), "Comorbidity is associated with disease activity in MS: Findings from the CombiRx trial", *Neurology*, Vol. 95 No. 5, e446-e456.

Scalfari, A., Neuhaus, A., Daumer, M., Deluca, G.C., Muraro, P.A. and Ebers, G.C. (2013), "Early relapses, onset of progression, and late outcome in multiple sclerosis", *JAMA neurology*, Vol. 70 No. 2, pp. 214–222.

Scalfari, A., Neuhaus, A., Degenhardt, A., Rice, G.P., Muraro, P.A., Daumer, M. and Ebers, G.C. (2010), "The natural history of multiple sclerosis: a geographically based study 10: relapses and long-term disability", *Brain a journal of neurology*, Vol. 133 No. Pt 7, pp. 1914–1929.

Scalfari, A., Traboulsee, A., Oh, J., Airas, L., Bittner, S., Calabrese, M., Garcia Dominguez, J.M., Granziera, C., Greenberg, B., Hellwig, K., Illes, Z., Lycke, J., Popescu, V., Bagnato, F. and Giovannoni, G. (2024), "Smouldering-Associated Worsening in Multiple Sclerosis: An International Consensus Statement on Definition, Biology, Clinical Implications, and Future Directions", *Annals of Neurology*, Vol. 96 No. 5, pp. 826–845.

Schäffner, E., Bosch-Queralt, M., Edgar, J.M., Lehning, M., Strauß, J., Fleischer, N., Kungl, T., Wieghofer, P., Berghoff, S.A., Reinert, T., Krueger, M., Morawski, M., Möbius, W., Barrantes-Freer, A., Stieler, J., Sun, T., Saher, G., Schwab, M.H., Wrede, C., Frosch, M., Prinz, M., Reich, D.S., Flügel, A., Stadelmann, C., Fledrich, R., Nave, K.-A. and Stassart, R.M. (2023), "Myelin insulation as a risk factor for axonal degeneration in autoimmune demyelinating disease", *Nature neuroscience*, Vol. 26 No. 7, pp. 1218–1228.

Schiffmann, S.N., Cheron, G., Lohof, A., d'Alcantara, P., Meyer, M., Parmentier, M. and Schurmans, S. (1999), "Impaired motor coordination and Purkinje cell excitability in mice lacking calretinin", *Proceedings of the National Academy of Sciences*, Vol. 96 No. 9, pp. 5257–5262.

Schirmer, L., Antel, J.P., Brück, W. and Stadelmann, C. (2011), "Axonal loss and neurofilament phosphorylation changes accompany lesion development and clinical progression in multiple sclerosis", *Brain pathology (Zurich, Switzerland)*, Vol. 21 No. 4, pp. 428–440.

Schmidt, H. (2012), "Three functional facets of calbindin D-28k", *Frontiers in molecular neuroscience*, Vol. 5, p. 25.

Schmidt-Supprian, M. and Rajewsky, K. (2007), "Vagaries of conditional gene targeting", *Nature immunology*, Vol. 8 No. 7, pp. 665–668.

Schwaller, B. (2010), "Cytosolic Ca2+ buffers", *Cold Spring Harbor perspectives in biology*, Vol. 2 No. 11, a004051.

Schwaller, B. (2012), "The regulation of a cell's Ca(2+) signaling toolkit: the Ca (2+) homeostasome", *Advances in experimental medicine and biology*, Vol. 740, pp. 1–25.

Schwaller, B., Meyer, M. and Schiffmann, S. (2002), "'New' functions for 'old' proteins: the role of the calcium-binding proteins calbindin D-28k, calretinin and parvalbumin, in cerebellar physiology. Studies with knockout mice", *Cerebellum (London, England)*, Vol. 1 No. 4, pp. 241–258.

Schwaller, B., Tetko, I.V., Tandon, P., Silveira, D.C., Vreugdenhil, M., Henzi, T., Potier, M.-C., Celio, M.R. and Villa, A.E.P. (2004), "Parvalbumin deficiency affects network properties resulting in increased susceptibility to epileptic seizures", *Molecular and cellular neurosciences*, Vol. 25 No. 4, pp. 650–663.

Scorrano, L., Oakes, S.A., Opferman, J.T., Cheng, E.H., Sorcinelli, M.D., Pozzan, T. and Korsmeyer, S.J. (2003), "BAX and BAK regulation of endoplasmic reticulum Ca2+: a control point for apoptosis", *Science (New York, N.Y.)*, Vol. 300 No. 5616, pp. 135–139.

Serafini, B., Rosicarelli, B., Magliozzi, R., Stigliano, E. and Aloisi, F. (2004), "Detection of ectopic B-cell follicles with germinal centers in the meninges of patients with secondary progressive multiple sclerosis", *Brain pathology (Zurich, Switzerland)*, Vol. 14 No. 2, pp. 164–174.

Shields, D.C., Tyor, W.R., Deibler, G.E., Hogan, E.L. and Banik, N.L. (1998), "Increased calpain expression in activated glial and inflammatory cells in experimental allergic encephalomyelitis", *Proceedings of the National Academy of Sciences of the United States of America*, Vol. 95 No. 10, pp. 5768–5772.

Simmons, M.L., Frondoza, C.G. and Coyle, J.T. (1991), "Immunocytochemical localization of N-acetyl-aspartate with monoclonal antibodies", *Neuroscience*, Vol. 45 No. 1, pp. 37–45.

Simons, M. and Nave, K.-A. (2015), "Oligodendrocytes: Myelination and Axonal Support", *Cold Spring Harbor perspectives in biology*, Vol. 8 No. 1, a020479.

Singh, S., Dallenga, T., Winkler, A., Roemer, S., Maruschak, B., Siebert, H., Brück, W. and Stadelmann, C. (2017), "Relationship of acute axonal damage, Wallerian degeneration, and clinical disability in multiple sclerosis", *Journal of neuroinflammation*, Vol. 14 No. 1, p. 57.

Sleigh, J.N., Rossor, A.M., Fellows, A.D., Tosolini, A.P. and Schiavo, G. (2019), "Axonal transport and neurological disease", *Nature Reviews Neurology*, Vol. 15 No. 12, pp. 691–703.

Sorbara, C.D., Wagner, N.E., Ladwig, A., Nikić, I., Merkler, D., Kleele, T., Marinković, P., Naumann, R., Godinho, L., Bareyre, F.M., Bishop, D., Misgeld, T. and Kerschensteiner, M. (2014), "Pervasive axonal transport deficits in multiple sclerosis models", *Neuron*, Vol. 84 No. 6, pp. 1183–1190.

Spain, R., Powers, K., Murchison, C., Heriza, E., Winges, K., Yadav, V., Cameron, M., Kim, E., Horak, F., Simon, J. and Bourdette, D. (2017), "Lipoic acid in secondary progressive MS: A randomized controlled pilot trial", *Neurology(R) neuroimmunology & neuroinflammation*, Vol. 4 No. 5, e374.

Stadelmann, C., Timmler, S., Barrantes-Freer, A. and Simons, M. (2019), "Myelin in the Central Nervous System: Structure, Function, and Pathology", *Physiological reviews*, Vol. 99 No. 3, pp. 1381–1431.

Stefano, N. de, Matthews, P.M., Fu, L., Narayanan, S., Stanley, J., Francis, G.S., Antel, J.P. and Arnold, D.L. (1998), "Axonal damage correlates with disability in patients with relapsing-remitting multiple sclerosis. Results of a longitudinal magnetic resonance spectroscopy study", *Brain a journal of neurology*, 121 (Pt 8), pp. 1469–1477.

Stockwell, B.R. (2022), "Ferroptosis turns 10: Emerging mechanisms, physiological functions, and therapeutic applications", *Cell*, Vol. 185 No. 14, pp. 2401–2421.

Stout, A.K. and Reynolds, I.J. (1999), "High-affinity calcium indicators underestimate increases in intracellular calcium concentrations associated with excitotoxic glutamate stimulations", *Neuroscience*, Vol. 89 No. 1, pp. 91–100.

Strober, W. (2001), "Trypan blue exclusion test of cell viability", *Current protocols in immunology*, Appendix 3, Appendix 3B.

Sun, S., Li, F., Gao, X., Zhu, Y., Chen, J., Zhu, X., Yuan, H. and Gao, D. (2011), "Calbindin-D28K inhibits apoptosis in dopaminergic neurons by activation of the PI3-kinase-Akt signaling pathway", *Neuroscience*, Vol. 199, pp. 359–367.

Szabadkai, G., Bianchi, K., Várnai, P., Stefani, D. de, Wieckowski, M.R., Cavagna, D., Nagy, A.I., Balla, T. and Rizzuto, R. (2006), "Chaperone-mediated coupling of endoplasmic reticulum and mitochondrial Ca2+ channels", *The Journal of cell biology*, Vol. 175 No. 6, pp. 901–911.

Szabadkai, G. and Duchen, M.R. (2008), "Mitochondria. The hub of cellular Ca2+ signaling", *Physiology (Bethesda, Md.)*, Vol. 23, pp. 84–94.

Tai, Y.-H., Engels, D., Locatelli, G., Emmanouilidis, I., Fecher, C., Theodorou, D., Müller, S.A., Licht-Mayer, S., Kreutzfeldt, M., Wagner, I., Mello, N.P. de, Gkotzamani, S.-N., Trovò, L., Kendirli, A., Aljović, A., Breckwoldt, M.O., Naumann, R., Bareyre, F.M., Perocchi, F., Mahad, D., Merkler, D., Lichtenthaler, S.F., Kerschensteiner, M. and Misgeld, T. (2023), "Targeting the TCA cycle can ameliorate widespread axonal energy deficiency in neuroinflammatory lesions", *Nature metabolism*, Vol. 5 No. 8, pp. 1364–1381.

Tan, Y., Mui, D., Toan, S., Zhu, P., Li, R. and Zhou, H. (2020), "SERCA Overexpression Improves Mitochondrial Quality Control and Attenuates Cardiac Microvascular Ischemia-Reperfusion Injury", *Molecular therapy. Nucleic acids*, Vol. 22, pp. 696–707.

Tedeholm, H., Skoog, B., Lisovskaja, V., Runmarker, B., Nerman, O. and Andersen, O. (2015), "The outcome spectrum of multiple sclerosis: disability, mortality, and a cluster of predictors from onset", *Journal of neurology*, Vol. 262 No. 5, pp. 1148–1163.

Terry, R.L., Ifergan, I. and Miller, S.D. (2016), "Experimental Autoimmune Encephalomyelitis in Mice", *Methods in molecular biology (Clifton, N.J.)*, Vol. 1304, pp. 145–160.

Thacker, E.L., Mirzaei, F. and Ascherio, A. (2006), "Infectious mononucleosis and risk for multiple sclerosis: a meta-analysis", *Annals of neurology*, Vol. 59 No. 3, pp. 499–503.

The International Multiple Sclerosis Genetics Consortium (2019), "Multiple sclerosis genomic map implicates peripheral immune cells and microglia in susceptibility", *Science (New York, N.Y.)*, Vol. 365 No. 6460.

The International Multiple Sclerosis Genetics Consortium (2023), "Locus for severity implicates CNS resilience in progression of multiple sclerosis", *Nature*, Vol. 619 No. 7969, pp. 323–331.

The Multiple Sclerosis International Federation (2020), *Atlas of MS, 3rd Edition*.

Thestrup, T., Litzlbauer, J., Bartholomäus, I., Mues, M., Russo, L., Dana, H., Kovalchuk, Y., Liang, Y., Kalamakis, G., Laukat, Y., Becker, S., Witte, G., Geiger, A., Allen, T., Rome, L.C., Chen, T.-W., Kim, D.S., Garaschuk, O., Griesinger, C. and Griesbeck, O. (2014), "Optimized ratiometric calcium sensors for functional in vivo imaging of neurons and T lymphocytes", *Nature methods*, Vol. 11 No. 2, pp. 175–182.

Thieme Verlag (Ed.) (2010), *Duale Reihe Physiologie*, 2. Auflage.

Thompson, A.J., Banwell, B.L., Barkhof, F., Carroll, W.M., Coetzee, T., Comi, G., Correale, J., Fazekas, F., Filippi, M., Freedman, M.S., Fujihara, K., Galetta, S.L., Hartung, H.P., Kappos, L., Lublin, F.D., Marrie, R.A., Miller, A.E., Miller, D.H., Montalban, X., Mowry, E.M., Sorensen, P.S., Tintoré, M., Traboulsee, A.L., Trojano, M., Uitdehaag, B.M.J., Vukusic, S., Waubant, E., Weinshenker, B.G., Reingold, S.C. and Cohen, J.A. (2018), "Diagnosis of multiple sclerosis: 2017 revisions of the McDonald criteria", *The Lancet. Neurology*, Vol. 17 No. 2, pp. 162–173.

Thorley-Lawson, D.A. (2001), "Epstein-Barr virus: exploiting the immune system", *Nature reviews. Immunology*, Vol. 1 No. 1, pp. 75–82.

Tintore, M., Arrambide, G., Otero-Romero, S., Carbonell-Mirabent, P., Río, J., Tur, C., Comabella, M., Nos, C., Arévalo, M.J., Anglada, E., Menendez, R., Midaglia, L., Galán, I., Vidal-Jordana, A., Castilló, J., Mulero, P., Zabalza, A., Rodríguez-Acevedo, B., Rodriguez, M., Espejo, C., Sequeira, J., Mitjana, R., Barros, A. de, Pareto, D., Auger, C., Pérez-Hoyos, S., Sastre-Garriga, J., Rovira, A. and Montalban, X. (2020), "The long-term outcomes of CIS patients in the Barcelona inception cohort: Looking back to recognize aggressive MS", *Multiple sclerosis (Houndmills, Basingstoke, England)*, Vol. 26 No. 13, pp. 1658–1669.

Trager, N., Smith, A., Wallace Iv, G., Azuma, M., Inoue, J., Beeson, C., Haque, A. and Banik, N.L. (2014), "Effects of a novel orally administered calpain inhibitor SNJ-1945 on immunomodulation and neurodegeneration in a murine model of multiple sclerosis", *Journal of neurochemistry*, Vol. 130 No. 2, pp. 268–279.

Trapp, B.D., Peterson, J., Ransohoff, R.M., Rudick, R., Mörk, S. and Bö, L. (1998), "Axonal transection in the lesions of multiple sclerosis", *The New England journal of medicine*, Vol. 338 No. 5, pp. 278–285.

Trapp, B.D., Ransohoff, R. and Rudick, R. (1999), "Axonal pathology in multiple sclerosis: relationship to neurologic disability", *Current opinion in neurology*, Vol. 12 No. 3, pp. 295–302.

Tremlett, H., Yinshan, Z. and Devonshire, V. (2008), "Natural history of secondary-progressive multiple sclerosis", *Multiple sclerosis (Houndmills, Basingstoke, England)*, Vol. 14 No. 3, pp. 314–324.

Trip, S.A., Schlottmann, P.G., Jones, S.J., Altmann, D.R., Garway-Heath, D.F., Thompson, A.J., Plant, G.T. and Miller, D.H. (2005), "Retinal nerve fiber layer axonal loss and visual dysfunction in optic neuritis", *Annals of Neurology*, Vol. 58 No. 3, pp. 383–391.

Tur, C., Carbonell-Mirabent, P., Cobo-Calvo, Á., Otero-Romero, S., Arrambide, G., Midaglia, L., Castilló, J., Vidal-Jordana, Á., Rodríguez-Acevedo, B., Zabalza, A., Galán, I., Nos, C., Salerno, A., Auger, C., Pareto,

D., Comabella, M., Río, J., Sastre-Garriga, J., Rovira, À., Tintoré, M. and Montalban, X. (2023), "Association of Early Progression Independent of Relapse Activity With Long-term Disability After a First Demyelinating Event in Multiple Sclerosis", *JAMA neurology*, Vol. 80 No. 2, pp. 151–160.

Twyning, M.J., Tufi, R., Gleeson, T.P., Kolodziej, K.M., Campesan, S., Terriente-Felix, A., Collins, L., Lazzari, F. de, Giorgini, F. and Whitworth, A.J. (2024), "Partial loss of MCU mitigates pathology in vivo across a diverse range of neurodegenerative disease models", *Cell reports*, Vol. 43 No. 2, p. 113681.

Valiente-Gabioud, A.A., Garteizgogeascoa Suñer, I., Idziak, A., Fabritius, A., Basquin, J., Angibaud, J., Nägerl, U.V., Singh, S.P. and Griesbeck, O. (2023), "Fluorescent sensors for imaging of interstitial calcium", *Nature Communications*, Vol. 14 No. 1, p. 6220.

van den Berg, R., Hoogenraad, C.C. and Hintzen, R.Q. (2017), "Axonal transport deficits in multiple sclerosis: spiraling into the abyss", *Acta neuropathologica*, Vol. 134 No. 1, pp. 1–14.

van den Bosch, A.M.R., Hümmert, S., Steyer, A., Ruhwedel, T., Hamann, J., Smolders, J., Nave, K.-A., Stadelmann, C., Kole, M.H.P., Möbius, W. and Huitinga, I. (2023), "Ultrastructural Axon-Myelin Unit Alterations in Multiple Sclerosis Correlate with Inflammation", *Annals of Neurology*, Vol. 93 No. 4, pp. 856–870.

van den Bosch, L., Schwaller, B., Vleminckx, V., Meijers, B., Stork, S., Ruehlicke, T., van Houtte, E., Klaassen, H., Celio, M.R., Missiaen, L., Robberecht, W. and Berchtold, M.W. (2002), "Protective effect of parvalbumin on excitotoxic motor neuron death", *Experimental neurology*, Vol. 174 No. 2, pp. 150–161.

van San, E., Debruyne, A.C., Veeckmans, G., Tyurina, Y.Y., Tyurin, V.A., Zheng, H., Choi, S.M., Augustyns, K., van Loo, G., Michalke, B., Venkataramani, V., Toyokuni, S., Bayir, H., Vandenabeele, P., Hassannia, B. and Vanden Berghe, T. (2023), "Ferroptosis contributes to multiple sclerosis and its pharmacological targeting suppresses experimental disease progression", *Cell death and differentiation*, Vol. 30 No. 9, pp. 2092–2103.

Vandenabeele, P., Bultynck, G. and Savvides, S.N. (2023), "Pore-forming proteins as drivers of membrane permeabilization in cell death pathways", *Nature reviews. Molecular cell biology*, Vol. 24 No. 5, pp. 312–333.

Vargas, M.E., Yamagishi, Y., Tessier-Lavigne, M. and Sagasti, A. (2015), "Live Imaging of Calcium Dynamics during Axon Degeneration Reveals Two Functionally Distinct Phases of Calcium Influx", *The Journal of neuroscience the official journal of the Society for Neuroscience*, Vol. 35 No. 45, pp. 15026–15038.

Vercellino, M., Plano, F., Votta, B., Mutani, R., Giordana, M.T. and Cavalla, P. (2005), "Grey matter pathology in multiple sclerosis", *Journal of neuropathology and experimental neurology*, Vol. 64 No. 12, pp. 1101–1107.

Viar, K., Njoku, D., Secor McVoy, J. and Oh, U. (2020), "Sarm1 knockout protects against early but not late axonal degeneration in experimental allergic encephalomyelitis", *PloS one*, Vol. 15 No. 6, e0235110.

Viglietta, V., Baecher-Allan, C., Weiner, H.L. and Hafler, D.A. (2004), "Loss of functional suppression by CD4+CD25+ regulatory T cells in patients with multiple sclerosis", *The Journal of experimental medicine*, Vol. 199 No. 7, pp. 971–979.

Villegas, R., Martinez, N.W., Lillo, J., Pihan, P., Hernandez, D., Twiss, J.L. and Court, F.A. (2014), "Calcium release from intra-axonal endoplasmic reticulum leads to axon degeneration through mitochondrial dysfunction", *The Journal of neuroscience the official journal of the Society for Neuroscience*, Vol. 34 No. 21, pp. 7179–7189.

Waller, A. (1851), "Experiments on the Section of the Glosso-Pharyngeal and Hypoglossal Nerves of the Frog, and Observations of the Alterations Produced Thereby in the Structure of Their Primitive Fibres", *Edinburgh medical and surgical journal*, Vol. 76 No. 189, pp. 369–376.

Wang, H.G., Pathan, N., Ethell, I.M., Krajewski, S., Yamaguchi, Y., Shibasaki, F., McKeon, F., Bobo, T., Franke, T.F. and Reed, J.C. (1999), "Ca2+-induced apoptosis through calcineurin dephosphorylation of BAD", *Science (New York, N.Y.)*, Vol. 284 No. 5412, pp. 339–343.

Warne, J., Pryce, G., Hill, J.M., Shi, X., Lennerås, F., Puentes, F., Kip, M., Hilditch, L., Walker, P., Simone, M.I., Chan, A.W.E., Towers, G.J., Coker, A.R., Duchen, M.R., Szabadkai, G., Baker, D. and Selwood,

D.L. (2016), “Selective Inhibition of the Mitochondrial Permeability Transition Pore Protects against Neurodegeneration in Experimental Multiple Sclerosis”, *The Journal of biological chemistry*, Vol. 291 No. 9, pp. 4356–4373.

Waxman, S.G. (2006), “Axonal conduction and injury in multiple sclerosis: the role of sodium channels”, *Nature reviews. Neuroscience*, Vol. 7 No. 12, pp. 932–941.

Wegner, C., Esiri, M.M., Chance, S.A., Palace, J. and Matthews, P.M. (2006), “Neocortical neuronal, synaptic, and glial loss in multiple sclerosis”, *Neurology*, Vol. 67 No. 6, pp. 960–967.

Weideman, A.M., Tapia-Maltos, M.A., Johnson, K., Greenwood, M. and Bielekova, B. (2017), “Meta-analysis of the Age-Dependent Efficacy of Multiple Sclerosis Treatments”, *Frontiers in neurology*, Vol. 8, p. 577.

Wemmie, J.A., Taugher, R.J. and Kreple, C.J. (2013), “Acid-sensing ion channels in pain and disease”, *Nature reviews. Neuroscience*, Vol. 14 No. 7, pp. 461–471.

Wesolowski, M. (2018), “In vivo analysis of calcium-initiated axon degeneration in an animal model of MS in an animal model of MS”, Dissertation, Institute of Clinical Neuroimmunology, Ludwig-Maximilians-Universität, Munich, 24 May.

Wheeler, M.A., Clark, I.C., Tjon, E.C., Li, Z., Zandee, S.E.J., Couturier, C.P., Watson, B.R., Scalisi, G., Alkwai, S., Rothhammer, V., Rotem, A., Heyman, J.A., Thaploo, S., Sanmarco, L.M., Ragoussis, J., Weitz, D.A., Petrecca, K., Moffitt, J.R., Becher, B., Antel, J.P., Prat, A. and Quintana, F.J. (2020), “MAFG-driven astrocytes promote CNS inflammation”, *Nature*, Vol. 578 No. 7796, pp. 593–599.

Willer, C.J., Dyment, D.A., Risch, N.J., Sadovnick, A.D. and Ebers, G.C. (2003), “Twin concordance and sibling recurrence rates in multiple sclerosis”, *Proceedings of the National Academy of Sciences of the United States of America*, Vol. 100 No. 22, pp. 12877–12882.

Williams, P.R., Marincu, B.-N., Sorbara, C.D., Mahler, C.F., Schumacher, A.-M., Griesbeck, O., Kerschensteiner, M. and Misgeld, T. (2014), “A recoverable state of axon injury persists for hours after spinal cord contusion in vivo”, *Nature communications*, Vol. 5, p. 5683.

Winter, J.R., Jackson, C., Lewis, J.E., Taylor, G.S., Thomas, O.G. and Stagg, H.R. (2020), “Predictors of Epstein-Barr virus serostatus and implications for vaccine policy: A systematic review of the literature”, *Journal of global health*, Vol. 10 No. 1, p. 10404.

Witte, M.E., Nijland, P.G., Drexhage, J.A.R., Gerritsen, W., Geerts, D., van Het Hof, B., Reijerkerk, A., Vries, H.E. de, van der Valk, P. and van Horssen, J. (2013), “Reduced expression of PGC-1α partly underlies mitochondrial changes and correlates with neuronal loss in multiple sclerosis cortex”, *Acta neuropathologica*, Vol. 125 No. 2, pp. 231–243.

Witte, M.E., Schumacher, A.-M., Mahler, C.F., Bewersdorf, J.P., Lehmitz, J., Scheiter, A., Sánchez, P., Williams, P.R., Griesbeck, O., Naumann, R., Misgeld, T. and Kerschensteiner, M. (2019), “Calcium Influx through Plasma-Membrane Nanoruptures Drives Axon Degeneration in a Model of Multiple Sclerosis”, *Neuron*, Vol. 101 No. 4, 615-624.e5.

Wolswijk, G. (2000), “Oligodendrocyte survival, loss and birth in lesions of chronic-stage multiple sclerosis”, *Brain a journal of neurology*, 123 (Pt 1), pp. 105–115.

Woo, M.S., Engler, J.B. and Friese, M.A. (2024a), “The neuropathobiology of multiple sclerosis”, *Nature reviews. Neuroscience*.

Woo, M.S., Mayer, C., Binkle-Ladisch, L., Sonner, J.K., Rosenkranz, S.C., Shaposhnykov, A., Rothammer, N., Tsvilovskyy, V., Lorenz, S.M., Raich, L., Bal, L.C., Vieira, V., Wagner, I., Bauer, S., Glatzel, M., Conrad, M., Merkler, D., Freichel, M. and Friese, M.A. (2024b), “STING orchestrates the neuronal inflammatory stress response in multiple sclerosis”, *Cell*.

Wujek, J.R., Bjartmar, C., Richer, E., Ransohoff, R.M., Yu, M., Tuohy, V.K. and Trapp, B.D. (2002), “Axon loss in the spinal cord determines permanent neurological disability in an animal model of multiple sclerosis”, *Journal of neuropathology and experimental neurology*, Vol. 61 No. 1, pp. 23–32.

Würth, C., Grabolle, M., Pauli, J., Spieles, M. and Resch-Genger, U. (2013), “Relative and absolute determination of fluorescence quantum yields of transparent samples”, *Nature protocols*, Vol. 8 No. 8, pp. 1535–1550.

Xu, C., Nedergaard, M., Fowell, D.J., Friedl, P. and Ji, N. (2024), “Multiphoton fluorescence microscopy for in vivo imaging”, *Cell*, Vol. 187 No. 17, pp. 4458–4487.

Yang, J., Weimer, R.M., Kallop, D., Olsen, O., Wu, Z., Renier, N., Uryu, K. and Tessier-Lavigne, M. (2013), “Regulation of axon degeneration after injury and in development by the endogenous calpain inhibitor calpastatin”, *Neuron*, Vol. 80 No. 5, pp. 1175–1189.

Yang, J.H., Rempe, T., Whitmire, N., Dunn-Pirio, A. and Graves, J.S. (2022), “Therapeutic Advances in Multiple Sclerosis”, *Frontiers in neurology*, Vol. 13, p. 824926.

Yenari, M.A., Minami, M., Sun, G.H., Meier, T.J., Kunis, D.M., McLaughlin, J.R., Ho, D.Y., Sapolsky, R.M. and Steinberg, G.K. (2001), “Calbindin d28k overexpression protects striatal neurons from transient focal cerebral ischemia”, *Stroke*, Vol. 32 No. 4, pp. 1028–1035.

Yuan, A., Rao, M.V., Veeranna and Nixon, R.A. (2017), “Neurofilaments and Neurofilament Proteins in Health and Disease”, *Cold Spring Harbor perspectives in biology*, Vol. 9 No. 4.

Zeisel, L., Felber, J.G., Scholzen, K.C., Schmitt, C., Wiegand, A.J., Komissarov, L., Arnér, E.S.J. and Thorn-Seshold, O. (2024), “Piperazine-Fused Cyclic Disulfides Unlock High-Performance Bioreductive Probes of Thioredoxins and Bifunctional Reagents for Thiol Redox Biology”, *Journal of the American Chemical Society*, Vol. 146 No. 8, pp. 5204–5214.

Zhang, J., Jin, L., Hua, X., Wang, M., Wang, J., Xu, X., Liu, H., Qiu, H., Sun, H., Dong, T., Yang, D., Zhang, X., Wang, Y. and Huang, Z. (2023), “SARM1 promotes the neuroinflammation and demyelination through IGFBP2/NF-κB pathway in experimental autoimmune encephalomyelitis mice”, *Acta physiologica (Oxford, England)*, Vol. 238 No. 2, e13974.

Zhen, Y., Radulovic, M., Vietri, M. and Stenmark, H. (2021), “Sealing holes in cellular membranes”, *The EMBO journal*, e106922.

Zheng, X., Wu, B., Liu, Y., Simmons, S.K., Kim, K., Clarke, G.S., Ashiq, A., Park, J., Li, J., Wang, Z., Tong, L., Wang, Q., Rajamani, K.T., Muñoz-Castañeda, R., Mu, S., Qi, T., Zhang, Y., Ngiam, Z.C., Ohte, N., Hanashima, C., Wu, Z., Xu, X., Levin, J.Z. and Jin, X. (2024), “Massively parallel in vivo Perturb-seq reveals cell-type-specific transcriptional networks in cortical development”, *Cell*.

Zimmermann, H.G., Knier, B., Oberwahrenbrock, T., Behrens, J., Pfuhl, C., Aly, L., Kaminski, M., Hoshi, M.-M., Specovius, S., Giess, R.M., Scheel, M., Mühlau, M., Bellmann-Strobl, J., Ruprecht, K., Hemmer, B., Korn, T., Paul, F. and Brandt, A.U. (2018), “Association of Retinal Ganglion Cell Layer Thickness With Future Disease Activity in Patients With Clinically Isolated Syndrome”, *JAMA neurology*, Vol. 75 No. 9, pp. 1071–1079.

Zündorf, G. and Reiser, G. (2011), “Calcium dysregulation and homeostasis of neural calcium in the molecular mechanisms of neurodegenerative diseases provide multiple targets for neuroprotection”, *Antioxidants & redox signaling*, Vol. 14 No. 7, pp. 1275–1288.

Supplementary data

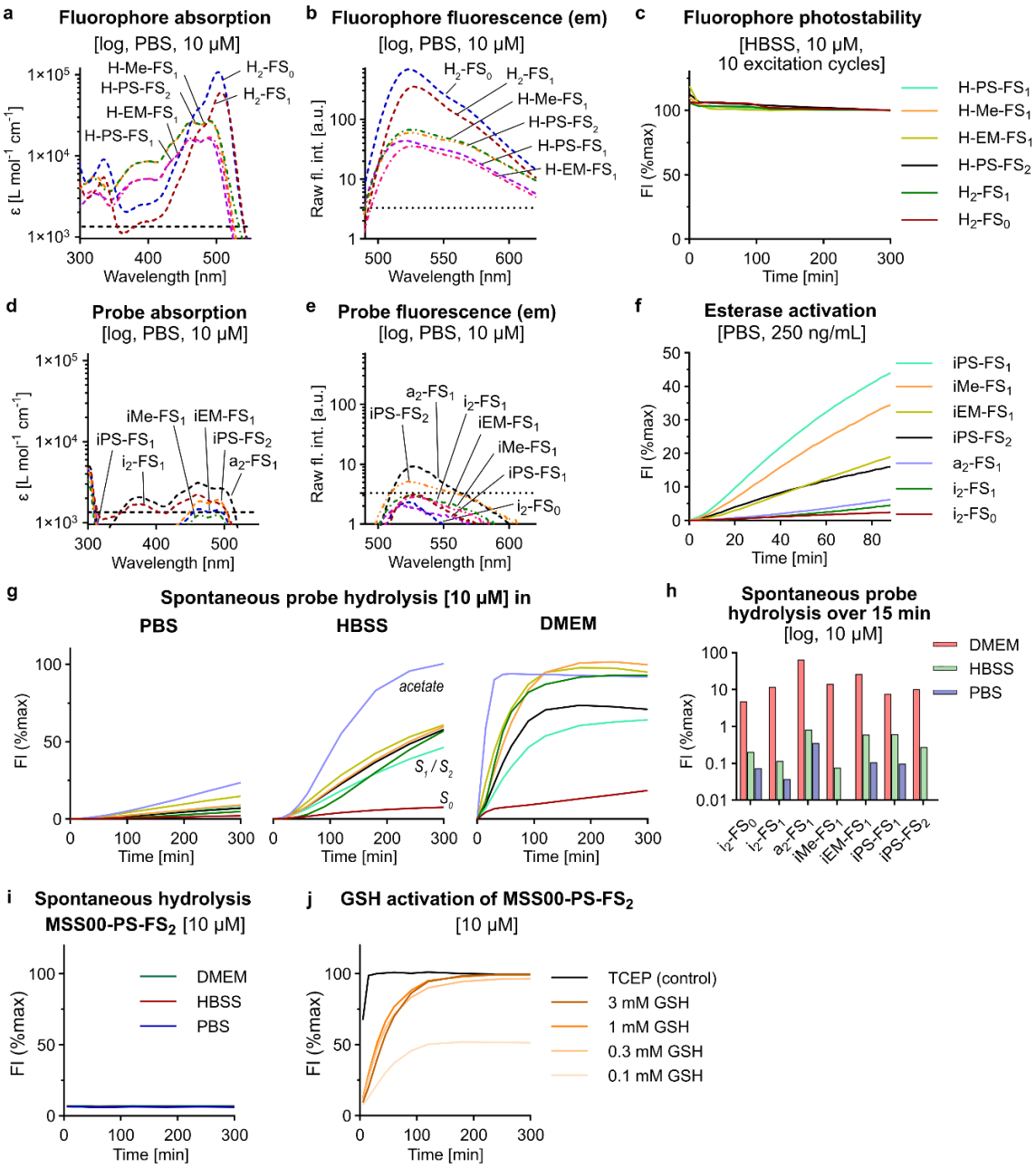

Supplementary Figure 1 – Photocharacterisation, stability towards hydrolysis and activation by esterase and GSH.

(a, d) Absorption spectra of fluorophores (a) and probes (d) at 10 µM in PBS. **(b, e)** Fluorescence emission spectra of the fluorophores (b) and probes (e) at 485 nm excitation, 10 µM in PBS. **(c)** Photostability of the fluorophores when excited 10 times over a timeframe of 6 h **(f)** Time course of probe activation by porcine liver esterase (probe 10 µM, esterase 250 ng/ml in PBS). **(g)** Time course of spontaneous probe hydrolysis in different media (probe 10 µM). **(h)** Summarised spontaneous hydrolysis data for 15 minute timepoint (= timescale of live cell imaging experiments, probe 10 µM). **(i)** Spontaneous hydrolysis of MSS00-PS-FS$_2$ (10 µM) in different media. **(j)** Time course of MSS00-PS-FS$_2$ activation by different concentrations of glutathione (GSH). Vertical dashed line in (a, b, d, e) indicates 5 % level of H-Me-FS1 extinction coefficient or fluorescence respectively. TCEP =(tris(2-carboxyethyl)phosphine (reducing agent). Data collected by Philipp Mauker.

Supplementary Table 1 – Quantum yields of novel fluorophores.

Fluorophore	Quantum yield
H_2-FS_0	0.78
H_2-FS_1	0.75
H-Me-FS_1	0.24
H-EM-FS_1	0.18
H-PS-FS_1	0.23
H-PS-FS_2	0.22

Figure licensing information

Figure 1, page 20

SPRINGER NATURE LICENSE
TERMS AND CONDITIONS

Nov 17, 2024

This Agreement between Daniela Beckmann ("You") and Springer Nature ("Springer Nature") consists of your license details and the terms and conditions provided by Springer Nature and Copyright Clearance Center.

License Number	5903681407878
License date	Nov 07, 2024
Licensed Content Publisher	Springer Nature
Licensed Content Publication	Nature Reviews Neuroscience
Licensed Content Title	The neuropathobiology of multiple sclerosis
Licensed Content Author	Marcel S. Woo et al
Licensed Content Date	May 24, 2024
Type of Use	Thesis/Dissertation
Requestor type	academic/university or research institute
Format	print and electronic
Portion	figures/tables/illustrations
Number of figures/tables/illustrations	1
Would you like a high resolution image with your order?	no
Will you be translating?	no
Circulation/distribution	1 - 29
Author of this Springer Nature content	no
Title of new work	In vivo analysis and therapeutic targeting of calcium-mediated axon degeneration in a multiple sclerosis model
Institution name	LMU Munich

Figure 2, page 22

CCC Marketplace

This is a License Agreement between Daniela Beckmann ("User") and Copyright Clearance Center, Inc. ("CCC") on behalf of the Rightsholder identified in the order details below. The license consists of the order details, the Marketplace Permissions General Terms and Conditions below, and any Rightsholder Terms and Conditions which are included below.

All payments must be made in full to CCC in accordance with the Marketplace Permissions General Terms and Conditions below.

Order Date	30-Oct-2024	Type of Use	Republish in a thesis/dissertation
Order License ID	1541345-1		
ISSN	1553-4014	Publisher	ANNUAL REVIEWS
		Portion	Image/photo/illustration

LICENSED CONTENT

Publication Title	Annual review of pathology	Publication Type	e-Journal
Article Title	The Immune Response in Multiple Sclerosis	Start Page	121
		End Page	139
Date	01/01/2006	Issue	1
Language	English	Volume	17
Country	United States of America	URL	http://arjournals.annualreviews.org/loi/pathmechdis
Rightsholder	Annual Reviews, Inc.		

REQUEST DETAILS

Portion Type	Image/photo/illustration	Distribution	Worldwide
Number of Images / Photos / Illustrations	1	Translation	Original language of publication
Format (select all that apply)	Print, Electronic	Copies for the Disabled?	No
Who Will Republish the Content?	Academic institution	Minor Editing Privileges?	Yes
		Incidental Promotional Use?	No
Duration of Use	Life of current and all future editions	Currency	EUR
Lifetime Unit Quantity	Up to 499		
Rights Requested	Main product		

NEW WORK DETAILS

Title	In vivo analysis and therapeutic targeting of calcium-mediated axon degeneration in a multiple sclerosis model	Institution Name	LMU Munich
		Expected Presentation Date	2024-12-06
Instructor Name	Daniela Beckmann		

ADDITIONAL DETAILS

Order Reference Number	N/A	The Requesting Person / Organization to Appear on the License	Daniela Beckmann

REQUESTED CONTENT DETAILS

Title, Description or Numeric Reference of the Portion(s)	Figure 4	Title of the Article / Chapter the Portion Is From	The Immune Response in Multiple Sclerosis
Editor of Portion(s)	Murúa, Sofía Rodríguez; Farez, Mauricio F.; Quintana, Francisco J.	Author of Portion(s)	Murúa, Sofía Rodríguez; Farez, Mauricio F.; Quintana, Francisco J.
Volume / Edition	17	Issue, if Republishing an Article From a Serial	1
Page or Page Range of Portion	121-139	Publication Date of Portion	2022-01-24

Figure 4, page 36

SPRINGER NATURE LICENSE
TERMS AND CONDITIONS

Nov 17, 2024

This Agreement between Daniela Beckmann ("You") and Springer Nature ("Springer Nature") consists of your license details and the terms and conditions provided by Springer Nature and Copyright Clearance Center.

License Number	5903661380948
License date	Nov 07, 2024
Licensed Content Publisher	Springer Nature
Licensed Content Publication	Nature Medicine
Licensed Content Title	A reversible form of axon damage in experimental autoimmune encephalomyelitis and multiple sclerosis
Licensed Content Author	Ivana Nikić et al
Licensed Content Date	Mar 27, 2011
Type of Use	Thesis/Dissertation
Requestor type	academic/university or research institute
Format	print and electronic
Portion	figures/tables/illustrations
Number of figures/tables/illustrations	1
Would you like a high resolution image with your order?	no
Will you be translating?	no
Circulation/distribution	1 - 29
Author of this Springer Nature content	no
Title of new work	In vivo analysis and therapeutic targeting of calcium-mediated axon degeneration in a multiple sclerosis model
Institution name	LMU Munich

Figure 5, page 39

SPRINGER NATURE LICENSE
TERMS AND CONDITIONS

Nov 17, 2024

This Agreement between Daniela Beckmann ("You") and Springer Nature ("Springer Nature") consists of your license details and the terms and conditions provided by Springer Nature and Copyright Clearance Center.

License Number	5903681032924
License date	Nov 07, 2024
Licensed Content Publisher	Springer Nature
Licensed Content Publication	Nature Reviews Neurology
Licensed Content Title	Mechanisms of neurodegeneration and axonal dysfunction in multiple sclerosis
Licensed Content Author	Manuel A. Friese et al
Licensed Content Date	Mar 18, 2014
Type of Use	Thesis/Dissertation
Requestor type	academic/university or research institute
Format	print and electronic
Portion	figures/tables/illustrations
Number of figures/tables/illustrations	1
Would you like a high resolution image with your order?	no
Will you be translating?	no
Circulation/distribution	1 - 29
Author of this Springer Nature content	no
Title of new work	In vivo analysis and therapeutic targeting of calcium-mediated axon degeneration in a multiple sclerosis model
Institution name	LMU Munich

Figure 6, page 44

SPRINGER NATURE LICENSE
TERMS AND CONDITIONS

Nov 17, 2024

This Agreement between Daniela Beckmann ("You") and Springer Nature ("Springer Nature") consists of your license details and the terms and conditions provided by Springer Nature and Copyright Clearance Center.

License Number	5905600126556
License date	Nov 10, 2024
Licensed Content Publisher	Springer Nature
Licensed Content Publication	Nature Reviews Molecular Cell Biology
Licensed Content Title	Calcium signalling: dynamics, homeostasis and remodelling
Licensed Content Author	Michael J. Berridge et al
Licensed Content Date	Jul 1, 2003
Type of Use	Thesis/Dissertation
Requestor type	academic/university or research institute
Format	print and electronic
Portion	figures/tables/illustrations
Number of figures/tables/illustrations	1
Would you like a high resolution image with your order?	no
Will you be translating?	no
Circulation/distribution	1 - 29
Author of this Springer Nature content	no
Title of new work	In vivo analysis and therapeutic targeting of calcium-mediated axon degeneration in a multiple sclerosis model
Institution name	LMU Munich

Acknowledgements

After five very intense years, a journey is finally coming to its end. Like for any good journey, it has been fun (mostly), I learned a lot and there are tons of images to document the process.

First and foremost, I would like to thank my supervisor, Prof. Martin Kerschensteiner. He has been supportive from day one, always motivating, always constructive. Whatever the experimental results, I could never be pessimistic for long, because his deep optimism about the axon project and clear pragmatic thinking always made me look ahead again. Second, I would like to thank Prof. Thomas Misgeld for co-supervising. His input, especially on everything microscopy and on the membrane damage sensor project has been very helpful, and it has been a privilege to have his expertise on board.

The people who got me started in the lab were Marta Wesolowski, who introduced me to *in vivo* imaging, and Paula Sanchez who taught me everything I needed to know about PC12 cells and membrane damage. I would have been completely lost without you, thank you!

Furthermore, I would like to thank Philipp Mauker for the great collaboration in developing a membrane damage sensor. It has been fun to learn about the chemistry and to deal with small amounts of white powders. Thank you also to Oliver Thorn-Seshold for supervising and supporting this project and to Angelika Harbauer and Simone Wanderoy, who saved us to in the fight against reviewer 3. I would also like to thank Andreas Thomae from the Core Facility Bioimaging, who helped me set up the live cell imaging approach and to the Core Facility Bioimaging team at large, including Mariano Gonzales Pisfil and Steffen Dietzel, for keeping the microscope running and the air objectives oil-free.

To all the other members of the Kerschensteiner lab past and present: I cannot recount here all the times you gave me useful advice, helped me out, or just generally made my day better. Thank you for making this lab the great collaborative and friendly place that it is, Emily Ullrich Gavilanes, Adinda Wens, Ioanna Emmanouilidis, Anastasiia Sydorenko, Clara de la Rosa del Val, Arek Kendirli, Yi-Heng Tai, Yves Carpentier Solorio, Veronika Pfaffenstaller, Carla Ares Carral, Paula Sanchez, Nils Treiber, Aleksandra Mezydlo and Daniel Engels.

Moreover, I would like to mention the students whom I had the privilege to supervise during my PhD. I have learned a lot from this experience, which has sometimes been a challenge, but overall, very nice and rewarding. Shout out to: Johanna Mathiszik, Katharina Langen, Aleksandar Markovski, Jonas Huber and Anastasiia Sydorenko.

Thank you to grINIM, the green initiative of the Institute of Clinical Neuroimmunology, for infusing my PhD with an extra dimension of sense and to the German Academic Scholarship Foundation (Studienstiftung des deutschen Volkes) for funding my PhD and for providing a network, in which inspiring and motivated people from very different fields come together.

On a more private note, I would like to thank Paul for being with me through all this time, for being there after a long stressful day, for supporting and for distracting me, because that is what you do best :) Last but not least, I would like to thank my parents, who have always believed in me and raised me to believe in my own abilities, too. I would never have made it this far without you.

Author contributions

Biosensor development / Publication Mauker, Beckmann et al., 2024
"Fluorogenic Chemical Probes for Wash-Free Imaging of Cell Membrane Damage in Ferroptosis, Necrosis, and Axon Injury", Journal of the American Chemical Society

- Oliver Thorn-Seshold, Martin Kerschensteiner and Thomas Misgeld conceived the study. Experiments were designed by them, Philipp Mauker and me.
- Candidate design, chemical synthesis, photocharacterisation, cell-free stability measurements, esterase and GSH activation assays (**Figure 7, Figure 8**, **Supplementary Figure 1**, **Supplementary Table 1, Figure 15a, b**) were performed by Philipp Mauker.
- The AAPH-mediated membrane damage assay was first established by Paula Sanchez for post-hoc analysis of fixed cells. The LLO-mediated membrane damage assay was first established by Ioanna Emmanouilidis for flow cytometry. Adaptation of these approaches into a live cell imaging-based compound screen was performed by me with microscopy advice from Andreas Thomae.
- All live cell imaging and quantification of live cell imaging data (**Figure 9, Figure 10, Figure 11, Figure 12, Figure 13, Figure 14, Figure 15c-f)** was performed by me
- Some preliminary quantification of live cell imaging data (determination of ideal loading time, data not shown) was performed by Katharina Langen.
- Use of MDG1 in detecting ferroptosis in ex vivo murine lung T cells (data not shown) was performed by Chantal Wientjens.
- Use of MDG1 in detecting necrotic damage to drosophila embryo epithelium (data not shown) was performed by Andrew J. Davidson.
- Use of MDG1 in detecting damage to axons growing in microfluidic chambers (**Figure 16**) was performed by Simone Wanderoy.

Calcium-binding protein overexpression

- Plasmids for rAAV production (cohorts 1 & 2) were cloned by me. cDNAs of murine calbindin and human calretinin were kindly provided by Professor Michael Meyer. A plasmid encoding Cre-T2A-KOFP was kindly provided by Adinda Wens. Likewise, rAAVs for cohorts 1 and 2 were produced by me. Plasmids and rAAVs of cohort 3 were ordered from VectorBuilder. (**Figure 17, Tabe 3**).
- Intravenous rAAV injections were performed by Clara de la Rosa del Val and me, EAE induction, *in vivo* two-photon imaging and subsequent perfusions were performed by me (**Figure 17, Figure 18a**)
- *In vivo* two-photon images were analysed by me (**Figure 18b, h, Figure 20**).
- Staining and confocal imaging of cortex and corresponding image analysis (**Figure 18c-e**) were performed by me. The tissue was dissected by Katharina Langen.
- For transfection of HEK cells and infection of HeLa cells (**Figure 18f, g**), samples were prepared by me and flow cytometry performed by Clara de la Rosa del Val.

- Overexpression analysis (staining, confocal imaging and image analysis) as presented in **Figure 19** was performed by me. Tissue was dissected by Katharina Langen and me. The antibodies used for staining were established by Jonas Huber. Spinal cord calbindin/calretinin stainings in general (decision for transverse cutting plane, testing of the analysis pipeline) were established by Johanna Mathiszik and Katharina Langen under my supervision.